ECOHYDROLOGICAL CONTROLS ON SOIL-MOISTURE FLUXES

IN ARID VADOSE ZONES

By

Renee Sandvig

Submitted in Partial Fulfillment

of the Requirements for the Degree of

Master of Science in Hydrology

New Mexico Institute of Mining and Technology

Socorro, New Mexico

May, 2005

ACKNOWLEDGEMENTS

TABLE OF CONTENTS

LIST OF FIGURES

LIST OF TABLES

CHAPTER 1

INTRODUCTION

1.1 Ecohydrological Relations of Vadose-Zone Moisture Fluxes to the Water Budget.

1.1.1. Study Motivation

In the arid, water-stressed American Southwest, the accurate assessment of the water resources for the area has become increasingly important, since the demands for water will increase with the rising population of this region. A water budget is typically used as an assessment of the water resources for a region. It estimates the amount of present and future water resources in an aquifer, catchments area, or a geographical region, which involves an evaluation of all the sources of water supply or recharge in comparison with all known discharges or extractions (USGS 2005).   The geographical region of interest in this study is the Río Grande Basin. The partitioning of precipitation into evaporation, runoff, and infiltration is an essential component to understanding the water budget. The infiltration component of the water budget can, in part, be quantified by determining the partitioning of the water that has infiltrated the soil subsurface between evapotranspiration (combination of evaporation and transpiration) and deep percolation, or recharge. Vadose-zone moisture fluxes are key to quantifying the recharge to the groundwater that supplies much of the Southwest with drinking water. See Figure 1.1 for a diagram of the elements of the water budget relevant to this study.
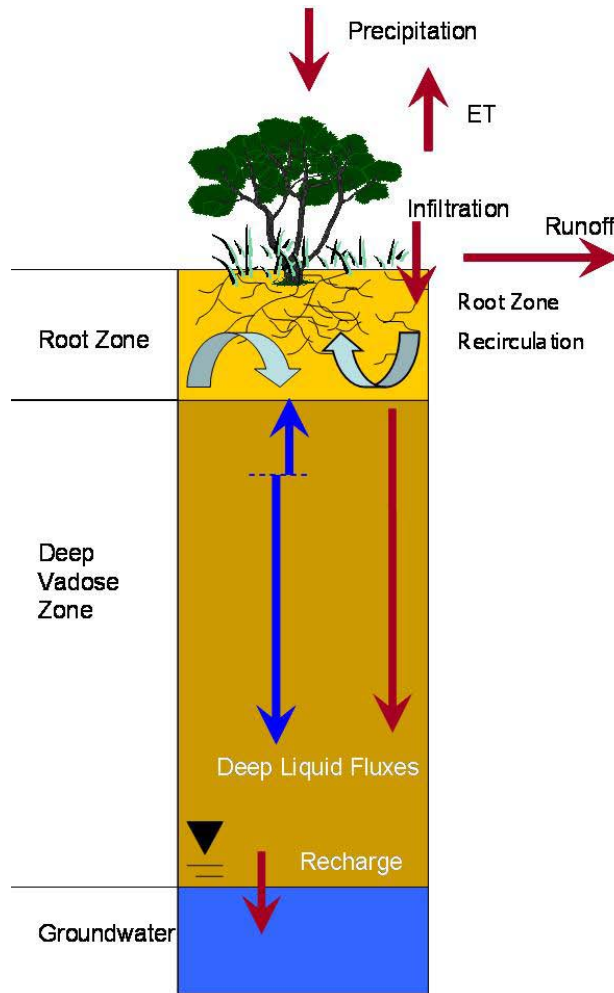
Figure 1.1. Water budget components important to vadose zone moisture fluxes. Water that has infiltrated the profile can recirculate in the root zone before either leaving the profile through evapotranspiration or percolating downward into the deep vadose zone. If liquid water reaches the deep vadose zone, it can percolate all the way to the groundwater table (red arrow) or it can it can be transported back upward through the profile, while the deeper vadose zone area still contains water that is draining to the groundwater table (blue arrows). Vadose-zone subdivisions are noted on the left side of diagram.

Groundwater tables in arid regions are typically very deep, often more than 100

meters (Anderholm 1987a, Anderholm 1987b, Myers 1994). Therefore, the

determination of actual groundwater recharge is difficult. Actual moisture fluxes in the

vadose zone can only be determined to the depth of sampling, with any estimated

downward flux at the greatest depth sampled referred to, in this study, as residual flux or

deep percolation. Since the groundwater table is often several tens of meters or more

below the deepest sampling depth, groundwater recharge from the residual flux cannot

necessarily be assumed. Alternatively, the groundwater recharge can be estimated

through computer modeling (Walvoord et al. 2002a).

Determination of these vadose-zone fluxes for an entire basin via individual

vadose-zone profiles is expensive and time consuming. Some of the problems that can

arise in obtaining field samples include access rights to the area of interest and the

accessibility of the area for drill rig. Accounting for the cost of the drill rig and the

extensive laboratory analysis of the soil samples that is required, the approximate price

per drill site in this study was $2,000 (US). Determination of the vadose zone fluxes of

the entire Río Grande Basin using these point measurements would require hundreds to

thousands of drilled soil cores, depending on the desired level of resolution. If a surface

feature that correlates to the vadose-zone-water fluxes could be found, this would

substantially reduce the cost and effort. This surface indicator must have a strong linkage

with deep vadose-zone moisture fluxes and be readily observable on the surface.

Vegetation type is an easily-observable surface-feature of the basin and can be

determined for a large area through remote sensing.

1.1.2. Vegetation as a Surface Indicator of Underlying Vadose-Zone Fluxes

Previous research results indicate vegetation as possibly a crucial component in

identifying the hydrological characteristics of arid vadose zones. Gee et al. (1994) has

demonstrated through the use of lysimeters at desert sites that the mere presence or

absence of vegetation greatly affects the underlying soil moisture fluxes. Significant

water accumulation in the subsurface was observed at all the sites in Gee's study when

the vegetation was removed. At two sites that each had bare soil, water accumulation and deep drainage accounted for 50 percent of the annual precipitation. At a third site with bare soil, elevated water storage persisted for more than three years even though rainfall during that time below average. When vegetation (a mix of desert shrubs and grasses) was present, water was quickly removed through evapotranspiration and no evidence of any water accumulation existed. Scanlon et al. (2003) found through long-term water-potential monitoring (5 -12 years) that, in response to seasonal fluctuations in precipitation, the penetration of wetting fronts under desert grass and shrub was restricted to the upper three meters of the profile. While the mere presence of vegetation affects the soil moisture of the vadose zone, to use vegetation as a surface indicator of underlying vadose-zone moisture fluxes, the vadose-zone moisture fluxes must be influenced differently by various vegetation types.

A close linkage between vegetation and vadose-zone dynamics was supported by Walvoord and Phillips (2004), who found that that areas with mixed shrub, creosote and grass vegetation had no groundwater recharge and actually supported a small net upward flux across the groundwater table. In contrast, they determined that there was appreciable recharge, about 3 mm yr^{-1}, under juniper sites; see Figure 1.2. In this study, Walvoord and Phillips used water-potential and chloride profiles to determine the vadose-zone fluxes and computer modeling to determine the groundwater recharge and equilibrium conditions. As shown in Figure 1.2, the water potential becomes less negative going from shrubs to grass to juniper trees. Chloride concentrations are greatest under the shrubs sites and become much less towards grass then juniper. Both water potential and chloride accumulation indicate that there is a greater downward liquid flux proceeding

from creosote to grass to juniper. Further, computer modeling determined that there was

no recharge under the shrub and grass sites and recharge only occurred under the juniper

sites (Walvoord and Phillips 2004).
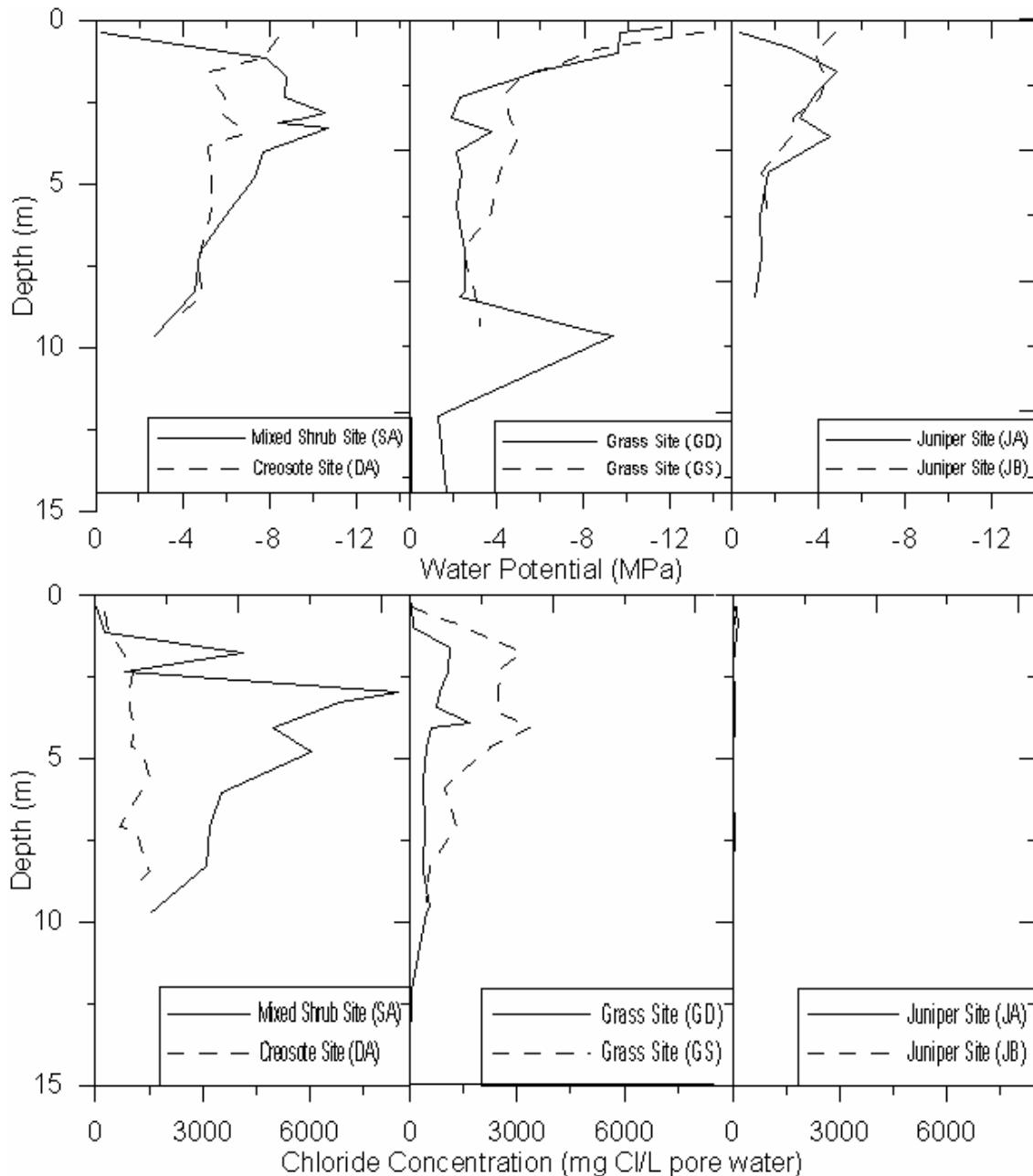
Figure 1.2. Water-potential and chloride-concentration profiles of the Trans-Pecos, TX study sites [from Walvoord (2002c)]. Data are grouped by vegetation type, with shrubs on left, then grass, then juniper on the right. Data plotted on same axes to demonstrate data trends.

All of the sites in their study, with the exception of the mixed shrub sites, were

relatively close together, negating the possibility that climate was the determining factor

for the differences seen in the soil moisture fluxes. The mixed shrub site was

approximately 200 km away, as shown in Figure 1.3, and it was cooler and wetter than

the other sites. If the more humid climate of the mixed shrub site did influence the

vadose zone moisture fluxes, then that site would be expected to have a greater amount of

recharge in comparison to the more arid sites, but the results demonstrated the reverse.
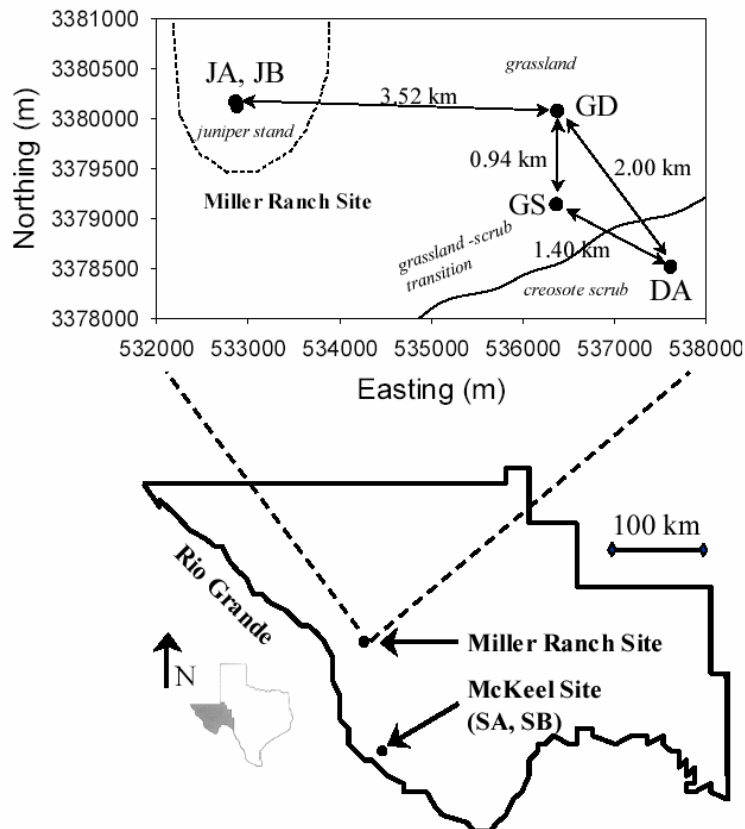
Figure 1.3. Location of study sites in the Trans-Pecos region, West Texas. Figure from Walvoord and Phillips (2004).

Newman et al. (1997) estimated deep downward fluxes under piñón-juniper

woodlands at an elevation of 2,140 meters in the northern Río Grande Valley. These

fluxes ranged from 0.02 to 1.1 cm yr^{-1} for the deepest sampled sections of the profiles.

They found lower downward fluxes under ponderosa pine, but this finding was attributed

to the effects of a thick clay layer in the profile that restricted downward flow rather than the differences in vegetation (Newman et al. 1997). This previous research indicates that vegetation community distributions may provide proxy information that will help to scale vadose-zone results from individual boreholes up to groundwater recharge estimates at the basin scale.

Based on these previous findings, we hypothesize that arid vegetation communities play a significant role in controlling the soil-moisture fluxes in arid vadose zones. Further investigation of the connection between vegetation type and the underlying vadose-zone fluxes is needed in order to test this hypothesized linkage more conclusively. To accomplish this, sampling should be conducted along a wider range of climatic conditions and with more sample sites within each vegetation type.

1.1.3. Influence of Climate and Vegetation on Groundwater Recharge Trends

If climate is the only control on vadose-zone moisture fluxes, then the aridity of an area could be expected to be inversely proportional to its underlying recharge. The more arid an area is the less recharge the underlying groundwater would receive. Conversely, the less arid an area is the more recharge the groundwater would receive. If differences in vegetation type do influence the underlying vadose-zone moisture fluxes and therefore the groundwater recharge of an area, then this effect might add additional structure to the simple correlation of aridity and groundwater recharge.

1.1.4. Ecohydrology Overview

Understanding the interactions and relations of vegetation and hydrology is now

classified under the term ecohydrology (Rodriguez-Iturbe 2000). For our purposes,

ecohydrology is best defined as a discipline that seeks to understand the interaction

between hydrological cycles and terrestrial ecosystems. This definition is consistent with

definitions of ecohydrology given by Rodriguez-Iturbe (2000) and Nuttle (2002). An

ecosystem consists of a dynamic set of living organisms (plants, animals, and

microorganisms) all interacting among themselves and with the environment in which

they live (soil, climate, water, and light) (Eco 2005). In this study, an ecosystem will be

referred to by its predominant vegetation type, with the acknowledgement that the

ecological community also contains many other plant species and that these other species,

as well as the burrowing animals of the ecosystem, can also affect the hydrology of the

area.

1.1.5. Vegetation and Soil Moisture Feedback

While the studies mentioned above can lead to the conclusion that

ecological factors may indicate the subsurface moisture fluxes, there is also a common

notion that soil moisture is the primary factor in determining vegetation spatial patterns

(Dick-Peddie 1993). Rodriguez-Iturbe (2000) stated that hydrologic mechanisms

underlie ecological patterns. He also asserts that soil moisture plays a dual role in being

both a cause and a consequence of the vegetation. The soil moisture of an area

determines the vegetation patterns yet the vegetation also affects the soil moisture of the

underlying vadose zone. Walvoord and Phillips (2004) attempted to reconciled these

positions by maintaining that the complex interactions and interconnectedness of ecologic

and hydrologic function allows for the validity of both perspectives, while

acknowledging that this view also makes the subject matter all the more confounding.

This interconnectedness of soil moisture and vegetation can be considered a feedback

loop with each element affecting the others. Therefore, vegetation can play a unique role

in being both a surface indicator of the underlying vadose-zone fluxes and also

influencing these fluxes.

1.1.6. Uptake of Nitrogen by Desert Ecosystems

Desert ecosystems have often been considered to be both water- and nutrient-

limited systems (Smith et al. 1997). However, Walvoord et al. (2003) recently

determined that a large reservoir of bioavailable nitrogen has been accumulating in

subsurface zones of arid regions throughout the Holocene. The presence of large

quantities of nitrogen sequestered below a depth of one meter demonstrates that not all of

the available nitrogen is consumed in the soil zone or returned to the atmosphere

(Walvoord et al. 2003). While the implications in relation to subsurface hydrology of this

nitrogen reservoir deep in the vadose zone are presently unclear, two possible

explanations exist. One explanation could be that desert plants are nitrogen limited but

are not efficiently capturing all of the available nitrogen. Another explanation could be

that desert plants are not nutrient limited as previously thought, but only water limited.

1.2. Determination of Vadose-Zone Moisture Fluxes

1.2.1. Introduction

One of most widely used means of determining deep percolation or groundwater

recharge is the water-balance method. In this method, recharge is calculated as a residual

in the soil-water budget equation (equation 1), with precipitation, evapotranspiration, and

change in water storage being independently determined quantities (Stephens 1996). The

soil-water-budget equation simply equates the difference between inputs and outputs to the change in water storage (S) of the soil. In the equation, infiltration (I) is the input and evaporation (E), transpiration (T), and recharge (R) are the outputs; shown in equation 1.

$$I - E - T - R = \Delta S \qquad\qquad (1)$$

The uncertainty of precipitation measurements is seldom less than ± five percent and the uncertainty for evapotranspiration is usually ± ten percent or more (Gee and Hillel 1988). A propagation of errors then occurs in using both terms in the water-balance equations to calculate the recharge. This is especially a concern when the recharge is a small fraction of precipitation, such as in arid areas; and the uncertainty in the recharge value calculated with this method generally exceeds the amount of the recharge itself (Gee and Hillel 1988). Therefore, another method of determining deep fluxes in arid vadose zones must be used and the one adopted in this study is a combination of environmental tracers and soil physical measurements. The accuracy of environmental tracers to determine these fluxes increases, not decreases, as soil-moisture content and soil-moisture fluxes decrease (Scanlon 1991).

1.2.2. Soil Physics

1.2.2.1. Soil-Water Potentials

Water moves in response to spatial differences in potential energy, also referred to as potential energy gradients. The types of potentials (Ψ) important for vadose zone are gravitational (z), water (w), matric (or pressure) (m), osmotic (o), and total (T) potential. The gravitational potential is the potential energy of the water determined by its position in a gravitational field in relation to a reference level or datum. Typically, this datum in soil science is usually either the soil surface or the groundwater table (Hillel 1998).

10

Water potential accounts for soil-water movement due to gradients in capillary pressure, chemical, temperature, and electrical potential and is a sum of both matric and osmotic potential (Stephens 1996). Water potential is determined from the relative humidity of the soil which is related to the water potential through the Kelvin equation, as shown in equation 2 (Hillel 1998, Stephens 1996).

$$\Psi_w = \Psi_m + \Psi_o = \frac{R * T}{M} * \ln\left(\frac{p}{p_o}\right)$$ (2)

where:

Ψ_w = water potential

Ψ_m = matric potential

Ψ_o = osmotic potential

p = vapor pressure of air

p_o = saturation vapor pressure at sample temperature

R = gas constant (8.31 J mol^{-1} K^{-1})

T = temperature (Kelvin)

M = molecular mass of water

$\left(\dfrac{p}{p_o}\right)$ = relative humidity of soil.

The matric potential describes the capillary and adsorptive forces that interact between the water, air, and the soil matrix. This interaction lowers the potential energy of the water. The water adheres to the soil matrix at tension, therefore the pressure of this water is lower than the atmospheric pressure (the reference pressure), and matric potential or pressure is negative in relation to the reference pressure (Hillel 1998). Osmotic potential describes the reduction of the soil-water potential energy due to the

presence of solutes. Solutes in the soil water reduce its vapor pressure and therefore affect vapor diffusion in the soil matrix (Hillel 1998). Osmotic potentials affect liquid water movement when diffusive barriers or semi-permeable membranes exist. While there are no know semi-permeable barriers at the sites, when soil wetness decreases and the water films shrink to a thickness on the same order as the diffuse layer of adsorbed cations, an appreciable degree of solute restriction can be expected to take place. This restriction could result in the soil exhibiting membrane-like properties of selective permeability when a solution is driven through a soil by a hydraulic gradient (Hillel 1998). Total potential is just the sum of all the potentials that pertain to the system of interest. This study mainly deals with the potential gradients that affect the flow of liquid water in the soil. Therefore, the effective total potential for this case is the sum of the matric and gravitational potentials, since no known diffusive barriers were present at the study areas. The total soil-water potential can be used to determine the direction of soil-water flow in relation to the chosen datum, with the water flowing from areas of high pressure to areas of low pressure (Hillel 1998).

To determine the unsaturated flow from the total potential, Darcy's Law (equation 3) can be used (Hillel 1998).

$$q = \frac{Q}{A} = -K\left(\theta \ or \ \Psi_m\right)\frac{d(\Psi_T)}{dz}$$

(3)

where:

q = Darcy Flux [L T^{-1}]

Q = flow volume [L^3]

A = area [L^2]

K (θ or Ψ) = unsaturated hydraulic conductivity which is dependent on the water content

(θ) or matric potential (Ψ_m) of the soil [L T^{-1}]

Ψ_m = matric potential of the soil water [L]

Ψ_T = total potential of the liquid soil water [L]

z = depth below the soil surface [L].

The unsaturated hydraulic conductivity is dependent on either water content or matric

potential. The two parameters are interrelated, so either can be used. This

interrelationship is quasi-exponential (Hillel 1998).

1.2.2.2. Interpretation of Matric Potential Profiles in Arid Regions

The matric potential profiles found in the arid American Southwest are typically

curved, with very negative matric potentials just below the surface and increasing

exponentially with depth, as seen in Figure 1.4.
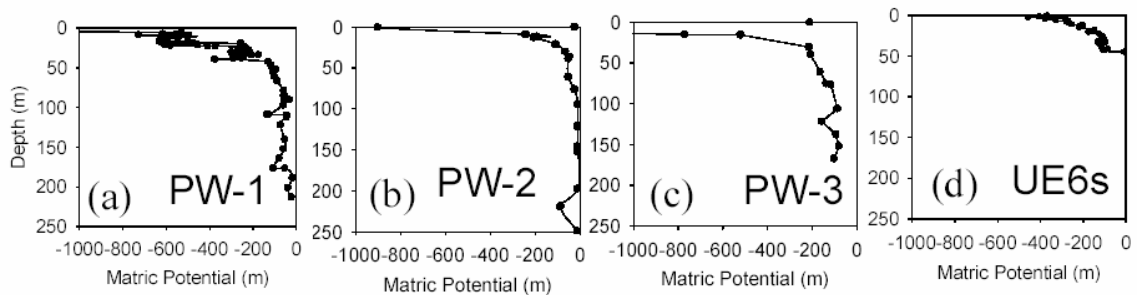
Figure 1.4. Measured matric potential profiles from a-c) Frenchman Flat and d) Yucca
Flat, Nevada. Data from Frenchman Flat from Estrella et al. (1993). Figure from
Walvoord et al. (2002b).

These profiles show an overall upward gradient of soil-water movement, with

high pressures at the base of the curves and low pressures near the top of the curves.

These gradients are typically steepest in the upper 50 meters of the profile. This steep

gradient near the surface is the result of evapotranspiration at the soil surface and in the

root zone of the vegetation. Scanlon et al. (1997) also reported that in interdrainage areas,

the water-potential measurements generally indicate an upward driving force in the top

20 to 40 meters of the profiles. However, below this depth the gradient reverses and the water drains downward by gravity (Scanlon et al. 1997).

1.2.3. Environmental Tracers

1.2.3.1. Chloride Deposition

The oceans are the largest single source of chloride aerosols. The chloride aerosol concentration is high near the coast and decreases rapidly with increasing distance inland (Feth 1981). The chloride aerosols result from the bursting of bubbles at the sea surface, which ejects salt particles or aerosols into the atmosphere (Feth, 1981). Chloride is deposited via dry fallout and through scavenging by precipitation, herein referred to as dry and wet deposition, respectively. The amount of dry deposition varies depending on distance from the ocean. While the amount of wet deposition varies with distance from the ocean, it also varies with precipitation amount, which is affected by topography. For a more detailed description of the processes of wet and dry deposition, see Sterling (2000). Once the chloride is deposited on the soil surface through dry deposition, it can be redistributed elsewhere by the wind. Dry deposition on the soil surface can also be translocated below the soil surface along with infiltrating precipitation carrying the wet chloride deposition. The rate of infiltration will affect the amount of chloride that enters the subsurface. The chloride concentration in the soil water is also affected by the amount of evaporation and transpiration of water at the surface and in the subsurface.

1.2.3.2. Chloride as an Environmental Tracer

Chloride is non-volatile and does not react with the soil matrix (conservative), making it an excellent tracer of water movement in the subsurface (Allison 1994). The

chloride will travel with the liquid water and also remain in the subsurface during evapotranspiration processes. If the amount of chloride input into the subsurface is known, then the amount of evapotranspiration and liquid movement through the soil matrix can be determined (Phillips 1994). The determination of chloride input is discussed in detail in Appendix A.

1.2.3.3. Chloride Mass-Balance Method

Chloride is used as a natural tracer to determine the flow of water through the vadose zone; it also quantifies the amount of groundwater recharging through the vadose zone. The amount of groundwater recharge can be estimated through the chloride mass-balance method (Cook et al. 1992). A mass-balance argument can be applied to the chloride ion to calculate the residual, or net, downward soil-water flux (Phillips 1994). Higher chloride values correspond to lower soil-water fluxes. Equation 4 is a simple mass balance equation for chloride (Walvoord 2002c).

$$C_p J_p + J_d = C_{Cl} J_R + C_{ET} J_{ET} \tag{4}$$

Where:

C_p = chloride concentration in precipitation $[M\ L^{-3}]$

J_p = precipitation rate $[L\ T^{-1}]$

J_d = chloride dry deposition rate $[M\ L^{-2}\ T^{-1}]$

C_{Cl} = chloride concentration in soil water $[M\ L^{-3}]$

J_R = residual soil-water flux $[L\ T^{-1}]$

C_{ET} = chloride concentration in evapotranspired water $[M\ L^{-3}]$

J_{ET} = evapotrapiration rate $[L\ T^{-1}]$.

The wet and the dry chloride mass fluxes are combined to form one chloride mass

flux term D_{Cl} [M L^{-2} T^{-1}]. Chloride concentration in evapotranspired water is considered negligible since chloride is non-volatile. With these two simplifications, equation 4 becomes:

$$J_R = \frac{D_{Cl}}{C_{Cl}} = \frac{C_P\, J_P + J_d}{C_{Cl}} \qquad (5)$$

where:

D_{Cl} = deposition rate of atmospheric chloride (both wet and dry) on the soil surface

[M L^{-2} T^{-1}]

The value of C_{Cl} is best determined by plotting the cumulative chloride content (mass per unit volume of soil) against the cumulative water content (volume of water per unit volume of soil) for the same depth interval (Phillips 1994). The data usually plot in straight line segments whose slopes corresponds to C_{Cl} for that depth interval. The assumptions inherent to the chloride mass-balance theory include: (1) the flow regime is one-dimensional vertically downward, piston-type flow, (2) the chloride is atmospherically derived, and the deposition rate is constant over time or can be averaged over the relevant time period, (3) steady-state flow conditions prevail, and (4) the chloride behaves conservatively (Phillips 1994).

Soil-water chloride values can also be used to determine the residence time of the chloride in the soil water by dividing the chloride inventory to the depth of interest by the chloride deposition rate, as shown equation 6 (Phillips 1994).

$$t_z = \frac{\int_0^z \theta\, C_{cl}\, dz}{D_{cl}} \qquad (6)$$

where:

t_z = transport time of the soil-water chloride to depth z [T]

θ = volumetric water content [$L^3 L^{-3}$].

1.2.3.4. Chloride/Bromide Ratios

Bromide is non-volatile and is non-reactive with the soil matrix, and is therefore a
conservative tracer. It behaves in a similar way to chloride, and it is also mainly derived
from atmospheric sources (Davis et al. 1998, Davis et al. 2004). The most significant
difference between bromide and chloride is their natural abundance, chloride is generally
40 to 80,000 times more abundant than bromide in natural waters. Therefore, small
changes in bromide will give rise to large variations in Cl^-/Br^- ratios (Davis et al. 1998).
If the chloride concentrations found in natural waters are low and the bromide
concentrations are near or below the detection limit, then the Cl^-/Br^- ratios will be altered
artificially by the detection limit of the instrument and not by any natural process. If the
level of bromide is near or below the detection limit, then Cl^-/Br^- ratios should not be
used to determine non-atmospheric sources of chloride.

Most shallow groundwater with chloride concentrations less than 5 mg L^{-1} have
ratios that reflect the local precipitation sources, with ratios generally between 80 and 160
(Davis et al. 1998, Davis et al. 2004). Small additions of water or chloride that did not
originate from precipitation or the atmosphere will alter these ratios. Therefore, Cl^-/Br^-
ratios can be employed to determine if the chloride tracer used for hydrological analyses
originated from sources other than the atmosphere. Connate waters, including oil field
waters, have ratios in the range of 200 to 400. Water affected by the dissolution of halite
will have much higher ratios in the range of 1,000 to 10,000 (Davis et al. 1998).

Some conditions in the subsurface may cause bromide to act nonconservatively, which affects the Cl^-/Br^- ratio. Ferrihydrite was shown to retard the transport of bromide, with ferrihydrite having an increasingly greater positive charge as the pH of the water decreases (Brooks et al. 1998). The presence of organic matter can alter the Cl^-/Br^- ratio, as a result of the cycling of bromide through the soil organic matter and biomass (Gerritse and George 1988). Bromide can be taken up by plant roots and subsequently released by the decaying soil organic matter (Kung 1990, Owens et al 1985). Approximately 50 percent of applied bromide was taken up by the vegetation in two studies, one conducted in a wetland (Whitmer et al. 2000) and the other in a potato field (Kung 1990). The accumulation of bromide in plant matter ranges from 7 kg ha^{-1} (700 mg m^{-2}) in ryegrass (Schnabel et al. 1995) to 54 kg ha^{-1} (5,400 mg m^{-2}) in orchardgrass (Owens et al.1985). The amount of bromide uptake and accumulation would vary with the amount and productivity of the vegetation (Owens et al. 1985). The uptake of bromide by vegetation may alter the ratios, as the uptake and release of bromide could vary throughout the year, depending on season and precipitation amounts.

1.2.3.5. Interpretations of Chloride Profiles

Measured chloride profiles from thick arid vadose zones often exhibit a bulge at shallow depths (1 to 3 meters) containing high chloride concentrations and relatively low, uniform concentrations at greater depth, as shown in Figure 1.5.
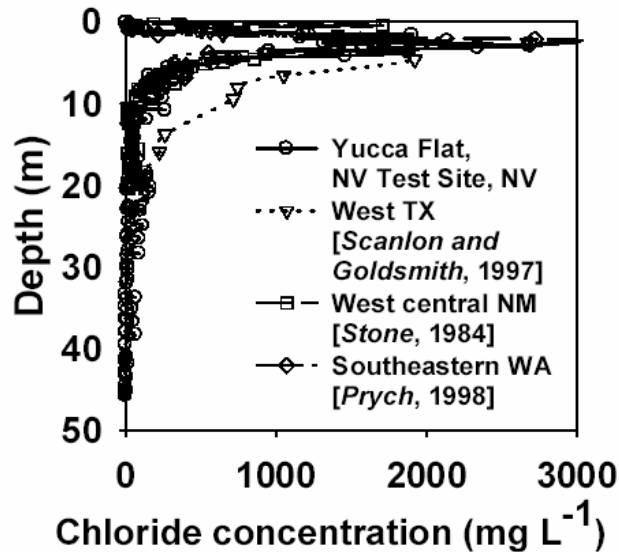
Figure 1.5. Vadose-zone chloride profiles under desert floor environments in the Western United States. Chloride values reported as pore water concentrations. Figure from Walvoord et al. (2002a).

Chloride bulges are common in arid environments and form when the infiltrating water that contains atmospherically-derived chloride enters the subsurface but does not infiltrate below the root zone. The bulge then results from the accumulation of concentrated chloride in the soil water through evapotranspiration (Peck et al. 1981). Phillips (1994) compared several chloride profiles from the American Southwest, all of which demonstrated relatively uniform chloride accumulation intervals of 13 to 16 kyr, which the author argued coincides with the Pleistocene – Holocene climate shift which took place around that time period.

1.2.4. Discrepancy Between Matric Potential and Chloride Profiles

There is a discrepancy between the conceptual model used to interpret chloride profiles and the implications of the hydrodynamics of the matric potential profiles found in desert vadose zones. While the use of the chloride mass balance method discussed above assumes a one-dimensional downward liquid flux, the matric potential profiles

19

indicate upward flux throughout most of the profile. Walvoord et al. (2002a) attempted to reconciled this discrepancy. They determined that, with time, the upward thermal vapor flux driven by the geothermal gradient dominates the hydrodynamics of the deep vadose zone. The gravitationally-driven return of the liquid water resulting from the cooling and condensation of upward vapor fluxes produces the nearly uniform matric-potential profile of the deep vadose zone. Desert vadose zones are locked in long-term drying transients that are so gradual that they appear to be in a steady-state condition. Current net moisture fluxes in desert vadose zones are generally upward, groundwater recharge is extremely small, and the net moisture flux below the root zone is not equivalent in magnitude or frequently even direction to the flux across the water table (Walvoord et al. 2002a). Therefore, the chloride mass balance method for determining residual fluxes in vadose zones should not be employed unless there is downward flux below the root zone; otherwise, one of the essential assumptions of the model will be violated. The presence of downward fluxes in the profile can be determined through total potential gradients.

1.2.5. Indication of Response to Climate Shift

Matric potential and chloride profiles with large bulges of low potential and high concentration, respectively, are the result of long-term drying, as demonstrated by Walvoord and Phillips (2004). As seen in Figure 1.6, model-generated profiles that were simulated as a transition from a 10 mm yr^{-1} flux to a 0 mm yr^{-1} flux at 16 ka (thousand years ago) matched the data measured at a mixed desert shrub site in Texas (Walvoord and Phillips 2004). The profiles did not show a response to the drying condition until 6 ka, which concurs well with the timing of desert scrub establishment in the area

constrained to between 8 and 4 ka by packrat midden data. The model-simulated

moisture fluxes for the profile data from Figure 1.6. are shown in Figure 1.7. Upward

liquid and vapor fluxes driven by large matric-potential gradients are important from

below the root zone to about 32 meters depth. From 18 to 32 meters depth, the moisture

flux is mainly in the liquid phase, while the gradient is still upward. Below 32 meters,

the gravity driven downward liquid flux is similar magnitude but opposite in direction to

the geothermally driven upward vapor flux (Walvoord and Phillips 2004).
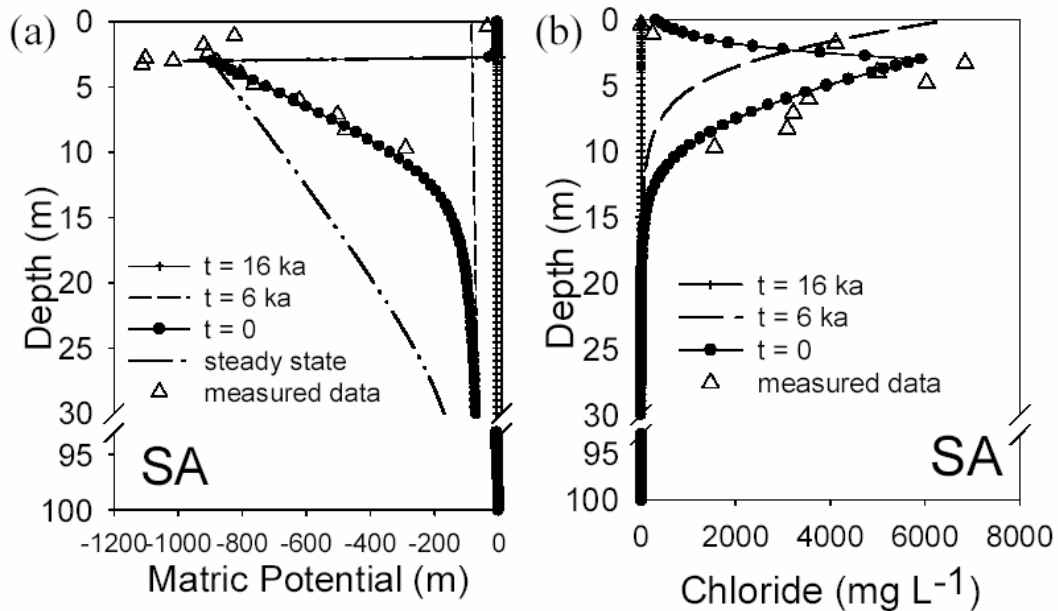
Figure 1.6. (a) Modeled matric-potential profiles and (b) modeled chloride profiles from desert scrub area. Measured data for a desert scrub site are shown for comparison. Chloride values are in pore water concentrations. SA refers to the source of the measured data, desert scrub site A. Figure from Walvoord and Phillips (2004).

21
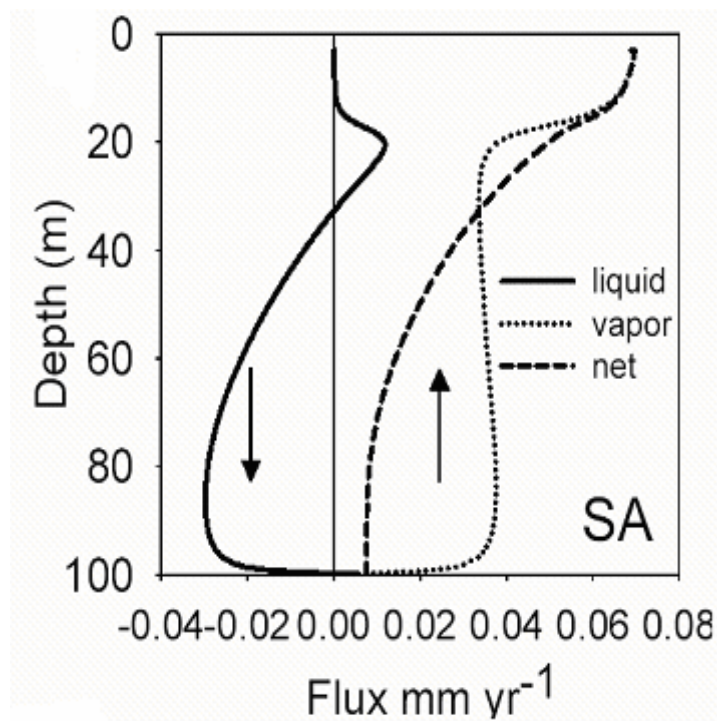
Figure 1.7. Modeled current moisture flux profiles at desert scrub site. SA refers to the source of the measured data, desert scrub site A. Figure from Walvoord and Phillips (2004).

1.3. Moisture Fluxes in Arid Vadose Zones and Groundwater Recharge

1.3.1. Introduction

There are two types of groundwater recharge: diffuse and localized recharge. Diffuse recharge results from widespread infiltration of precipitation at the point of impact (Hendrickx and Walker 1997). Localized recharge occurs when overland flow is funneled into a topographic depression or into a preferential flow path (Hendrickx and Walker 1997). For semiarid and arid areas, localized recharge is considered at least as significant, or more significant, then diffuse recharge (Stephens 1994). In this study, a flushing event will refer to the complete vertical saturation and subsequent drainage of the entire profile by liquid water, which will essentially reduce the chloride concentration and increase the matric potential to near zero. Preferential, focused, and lateral flow refer

22

to the movement of liquid water through specific sections of the profile, therefore reducing the chloride concentrations and increasing the matric potentials of this specific area only.

1.3.2. Recharge from Topographic Depressions

Topographic depressions and arroyos can cause recharge that exceeds the amount caused by only diffuse recharge. Water ponds in topographic lows and this increase in pressure head will cause the water to enter the subsurface more readily and flow through the subsurface more quickly, than nearby flatter areas receiving the same amount of precipitation. Scanlon et al. (1999) conducted a study comparing the interdrainage areas of a basin to areas of localized topographic depressions, mainly fissures, gulleys and borrow pits. The study found low fluxes of 0.02 to 0.04 mm yr^{-1} at the interdrainage sites, compared to high fluxes of 10 mm yr^{-1} in the localized depressions. The topographic depressions occupied less than one percent of the basin area, but they contributed more to the subsurface moisture flux than the interdrainage areas (Scanlon et al. 1999).

1.3.3. Recharge from Preferential Pathways

One type of preferential flow path is a macropore, which is a pore with a diameter greater than 3 millimeters (Germann 1990). Root channels, animal burrows, fractures, faults, bedding planes, karst topography, and unstable wetting fronts resulting from water-repellent or heterogeneous soils are also preferential flow paths. Since preferential pathways bypass sections of the soil matrix, they may cause groundwater recharge estimates from the chloride tracer and matric-potential profiles to be inaccurate, mainly underestimating potential recharge. Preferential pathways can funnel water to the

groundwater table much faster than if it traveled as a distributed flux through the soil matrix (Hendrickx and Walker 1997).

This study mainly deals with the determination of diffuse recharge, but evidence of preferential pathways can sometimes be seen in chloride and matric-potential profiles. It is difficult to distinguish between preferential pathways and periodic flushing events using only chloride and matric-potential profiles. Walvoord and Phillips (2004) attributed unusually low chloride concentrations and relatively average, negative matric potential profiles at one site investigated to the flushing of an isolated flow conduit. During a flushing event, both the chloride concentrations and matric potentials would be reset to near zero. Subsequent drying and lateral redistribution of water in the profile would have caused this isolated area to reequilibrate with the water potential in the surrounding soil, which was unaffected by the isolated flushing event. The reestablishment of the matric potential profile to the condition prior to the flushing event would take much less time then the reestablishment of chloride concentrations to the concentrations that existed before the flushing event. This difference in response times is because water moves in response to changes in potential energy gradients much faster than chloride diffuses in response to changes in concentration gradients. The amount of chloride accumulation in the profile could then indicate the approximate time since the last flushing event. This is of course not the only possible scenario that may explain the combination of negative matric potentials and very low chloride concentrations, but it does seem the most plausible (Walvoord and Phillips 2004).

1.3.4. Preferential Pathways and Chloride and Matric-Potential Bulges

The flow through a preferential flow path originates from an area located away

from the profile area sampled, bypassing the surface of this sampled profile and flowing only through specific and isolated profile sections. Chloride bulges, discussed above in Section 1.2.3.5, may be used to identify profiles that have undergone flow through preferential pathways. Flow through preferential pathways may reduce the chloride concentrations in some sections of the profile, but not the entire profile, as occurs with complete, one-dimensional flushing of the profile from the soil surface. The mere presence of a chloride bulge need not indicate preferential or by-pass flow. Other evidence to coincide with the chloride bulge must be present to indicate that preferential flow is occurring beneath the bulge.

Preferential flow is possible in areas with vegetation that contains fairly large roots or areas that have soils that are heterogeneous with depth, causing lateral flow. Peck et al. (1981) concluded that chloride bulges found at his study sites were the result of water movement at greater depths through root channels. Johnson (1987) found a localized area of recharge in a piezometer field, where he also measured chloride concentration profiles. From the chloride profiles, he determined that in a small area the recharge rates were 50 to 100 mm yr^{-1} as opposed to the 2.2 to 7.2 mm yr^{-1} rate found elsewhere in the study area. This small area also coincided with a localized increase in groundwater levels. Johnson concluded that this was an area of preferential water flow that was likely associated with a quartz layer and finer textured materials found in nearby cores. Some of the other chloride profiles show steep concentration gradients with depth that coincide with strata of differing hydraulic properties (Johnston 1987). Therefore, some of the chloride bulges may have been caused by this preferential flow path created from flow through the more conductive strata.

Neither of these studies measured the matric potential of the profiles. While other
external evidence was used in these studies to determine preferential flow, another way to
determine preferential flow is to use matric potential profiles coincident with chloride
profiles. If the chloride concentrations are low, as is usually seen below the bulges, and
matric potentials are much less negative in these same areas compared with other areas of
the profile, then this would be a possible indicator of a preferential flow that has bypassed
the surface of the profile. Figure 1.8 shows idealized matric-potential and chloride-
concentration profiles that indicate an area of possible preferential flow.
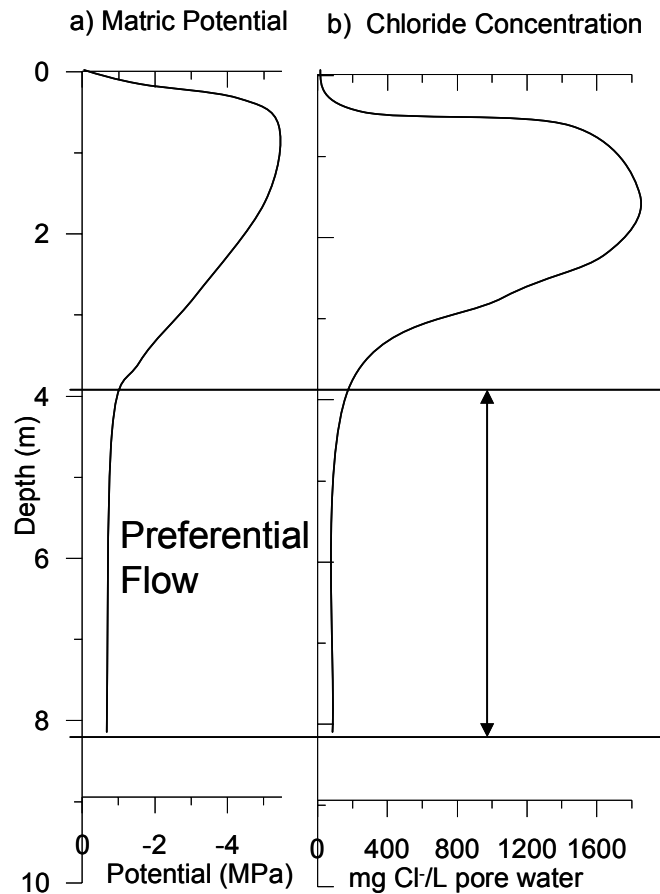
Figure 1.8. Idealized a) matric-potential and b) chloride-concentration profiles
indicating an area of possible preferential flow. Arrow and lines note area of possible
preferential flow. MPa = mega Pascals.

Comparing these profiles with those normally found in desert vadose zones, as

26

shown in Figures 1.5 for matric potential and Figure 1.6 chloride concentration, it can be seen that the bottom of the bulge is much deeper in those profiles, then the bottom of the bulge seen in Figure 1.8. The bottom of the bulge is also deeper in profiles that are recovering from previous flushing events, as shown in Figure 1.6. This could be the result of the reduction of the bottom of the bulge by the water flow through the preferential flow area.

1.3.5. Influences on Soil-Moisture Fluxes

In addition to the factors that influence soil-moisture fluxes in the vadose zone, climate, vegetation, topography and preferential flow, which were already discussed, many other secondary factors that can influences these fluxes also exists.

1.3.5.1. Plant Roots

Roots have already been mentioned as being potential preferential flow paths, both when they die and decay, leaving a macropore, or along the live root. Roots can also affect the matric potential of the profile through the process of transpiration. Gradients in hydrostatic pressure cause water to move from the soil and into the plant root (Steudle 2000). Desert shrubs have the ability to sustain more negative matric potentials before wilting than more mesic species. Desert species have been found to sustain matric potentials as low as -4 to -10 MPa (mega Pascals) (Pokeman and Sperry 2000, Seyfried et al. 2005). This ability to sustain such negative matric potentials not only increases the survival rate of these species in desert environments, but the plants are also able to dry out the soil in their root zones close to these matric potential limits.

1.3.5.2. Soil Texture

The hydraulic conductivity of a soil greatly affects the movement of liquid water through the subsurface. Hydraulic conductivity can vary greatly depending on the texture of the soil.   The saturated hydraulic conductivity of a soil is considered constant if the porosity is assumed to be constant. Table 1.1 presents default saturated hydraulic conductivity values by soil texture and demonstrates that the values can range by several orders of magnitude.

Soil Texture	Saturated Hydraulic Conductivity	% Clay Content Range for Textural Class
Silty Clay	0.02 ± 0.11	40 to 60
Silty Clay Loam	0.07 ± 0.19	27.5 to 40
Sandy Clay	0.12 ± 0.28	35 to 45
Clay	0.20 ± 0.42	55 to 100
Silt	0.25 ± 0.33	0 to 11
Clay Loam	0.26 ± 0.70	27.5 to 40
Silty Loam	0.45 ± 1.2	0 to 27.5
Loam	1.0 ± 1.8	9 to 27.5
Sandy Clay Loam	1.3 ± 2.7	20 to 35
Sandy Loam	4.4 ± 5.6	0 to 20
Loamy Sand	14.6 ± 11.4	0 to 15
Sand	29.7 ± 0.18	0 to 10

Table 1.1. Default saturated hydraulic conductivity values for each textual class. Soil texture listed in order of increasing saturated hydraulic conductivity values. Saturated hydraulic conductivity values taken from Carsel and Parrish (1988). Clay percentage (by weight) for each soil textural class from USDA textural triangle, with clay being defined as particles less than 2 μm diameter (Soil Survey Staff 1993).

As shown in the Table 1.1, soils with the lowest hydraulic conductivity have low levels of sand and high levels of silt and clay. The conductivity does not increase substantially until higher levels of sand are present in the loam and sand soils. Loam is a soil that is a mixture of sand, clay, and silt. Unsaturated hydraulic conductivity varies exponentially depending on the water content and matric suction of the soil, with high suction and low water content corresponding with low unsaturated hydraulic conductivity (Hillel 1998). Even though saturated hydraulic conductivity of sandy soils is typically

greater than that of clay soils, the unsaturated conductivity of the sandy soil decreases more steeply with increasing matric suction, eventually becoming lower than the unsaturated conductivity of clay at the same matric-suction levels (Hillel 1998).

Newman et al. (1997) found that high clay contents in the subsurface can greatly affect chloride concentrations and therefore soil moisture fluxes. They found the downward fluxes to be an order of magnitude lower under ponderosa pine than under piñón-juniper woodlands, even though the precipitation was 4 cm yr^{-1} higher in the ponderosa pine areas. This difference was related not to the differences in plant cover but to the difference in subsurface soil texture. The soils under the ponderosa pines contained clay-rich layers that restricted the downward movement of the soil moisture, whereas the soils under the piñón-juniper had a much lower clay content (Newman et al. 1997).

1.3.5.3. Temporal Variability of Precipitation

Precipitation in the American Southwest is characterized by intense but short rainfall events in the summer as a result of monsoonal weather patterns and longer, less intense rainfall events in the winter. This, combined with the extremely reduced evapotranspiration demand in the winter usually results in increased infiltration and decreased runoff during these months. Therefore, winter would seem to be the most likely time for groundwater recharge. As shown in the studies discussed above, most areas on the basin floor (with mainly creosote and grass vegetation) do not undergo any infiltration past the first few meters. While the winter rainfall may infiltrate a few meters into the subsurface, during the following summer this moisture is then taken out of the profile due to the increased evapotranspiration demand. A five-year monitoring study

reported that matric potentials under creosote sites in the Mojave Desert remained

between -5.5 and -7.5 Mpa at a 1.55 to 4.5 meter depth (Andraski 1997). At these sites,

soil below a few meters appeared to be buffered from diurnal and seasonal changes in

rainfall, at least on a decadal time scale. In areas with some downward moisture fluxes,

such as higher-elevation areas with juniper and ponderosa pine vegetation, winter is most

likely when majority of the recharge takes place.

1.3.5.4. Infiltration of Water Into the Subsurface

The infiltration of precipitation into the subsurface is dependent on many factors,

including the reduction of infiltration capacity with time from the onset of the

precipitation event, the initial water content, and the surface conditions (including surface

soil crusts), shallow layers of low permeability, and the saturated hydraulic conductivity

of the soil at the surface (Hillel 1998). Of these, only factors unrelated to precipitation

events will be discussed, as others are beyond the scope of this study. These factors

include surface soil crusts and the saturated hydraulic conductivity of surface soils. The

higher the saturated hydraulic conductivity of the surface soil, the higher the infiltration

rate (Hillel 1998). The default saturated hydraulic conductivity rates by soil texture are

listed in Table 1.1. In regards to infiltration, the slope of the soil surface can decrease the

infiltration rate of the surface. As the slope of an area increases, the runoff also increases

therefore decreasing the overall infiltration (Hillel 1998).

Surface soil crusts are typically less permeable than a surface soil of the same

texture without a crust. These crusts form in the desert because the soils are often devoid

of protection from vegetation cover during rainstorms or flood events and this results in

spontaneous slacking and breakdown of soil aggregates (Hillel 1998). Another type of

crust that can form in desert environments are microbiotic crusts. These crusts are formed by living organisms and their by-products, creating a surface crust of soil particles bound together by organic materials (Johnson 1997). Above ground crust thickness can reach up to 10 centimeters. The presence or absence of a crust is partly determined by soil texture and conductivity, pH, moisture, and possibly temperature. Cyanobacteria or green algae make up a large component of microbiotic crusts in semiarid and arid regions of the United States (Johnson 1997). Microbiotic crusts can alter infiltration, as Loope and Gifford (1972) have shown increases in infiltration in the presence of crusts. This increase in infiltration was attributed to increased aggregate stability. Another study by Williams et al. (1995) found either decreases in infiltration or no effect. Differences in findings seemed to be site specific and were often related to soil texture and chemical properties of the soil.

1.3.5.5. Lateral flow

Soils with layers of differing textures and hydraulic properties are common. They are the result of different depositional events and geomorphological processes as the soil weathers and ages. Lateral flow is caused by perched water that develops at the interface between two layers of contrasting hydraulic conductivities (Hendrickx and Walker 1997). Once the water begins to pond on top of the impeding layer of low conductivity, it can begin to flow laterally, since this is the path of least resistance to flow. Sloping layers of differing hydraulic conductivities will increase the amount of lateral flow. Water will not flow downward again until enough water has ponded on top of the less conductive layer and increased the pressure head, overcoming the pore pressure of the less conductive layer (Hendrickx and Walker 1997). In unsaturated lateral flow, coarse-textured soils

become an impeding layer to flow, because under unsaturated conditions small pores in fine-textured soils transmit water more readily than the large pores in coarse-textured soils. Conversely, in saturated lateral flow, fine-textured soils become the layer that impedes flow (Hendrickx and Walker 1997). Lateral flow may occur at the soil-bedrock interface, as the bedrock will most likely have a different conductivity than the overlying soil.

1.3.5.6. Carbonate Deposition

Layers of precipitated calcium carbonate commonly form in the subsurface of the American Southwest. Most of the precipitated calcium carbonate in these layers originates from aeolian dusts and in rainfall (Birkeland 1999). Carbonate development in soil profiles is classified into stages, from stage I to VI. The carbonate in stage I is present in thin, discontinuous clast coatings. In stage II the carbonate is also present in the soil matrix and increases in amount with each increasing stage. K horizons contain at least stage III carbonate development, and laminar carbonate deposits are classified as stage IV through stage VI (Birkeland 1999). With increasing time, the calcium-carbonate dominated soil layers or horizons become increasingly impregnated by carbonate precipitation onto the soil matrix until the voids become constricted and eventually plugged, greatly restricting water percolation through the horizon (Birkeland 1999). At this point, water tends to collect periodically over the plugged horizon. The resulting dissolution and re-precipitation of this carbonate produce a laminated section of the upper K horizon (Birkeland, 1999). Carbonate dissolution pipes and fractures can create preferential pathways for water flow that can bypass the indurated calcite layers, allowing water to infiltrate below the indurated layer.

Infiltration of water through calcium carbonate deposits is greatly dependent on its level of development and stage of induration. Table 1.2 lists infiltration rates of differing levels of carbonate development.

Induration Grade	Carbonate Content (%)	Infiltration Rate (m s^{-1})	Source
Very Strong	75 to 90	$< 7.06 \times 10^{-7}$	(Gile 1961)
Strong	50 to 75	7.06×10^{-7} to 4.23×10^{-6}	(Gile 1961)
Moderate	30 to 50	4.23×10^{-6} to 1.06×10^{-5}	(Gile 1961)
Slight	10 to 30	1.06×10^{-5} to 2.82×10^{-5}	(Gile 1961)
Not indurated	< 30	1.06×10^{-5} to 3.52×10^{-5}	(Gile 1961)
Not indurated	unknown	6.9×10^{-4} (after 10 days)	(Aronovici 1972)
Not indurated	unknown	2.5×10^{-5} (after 42 days)	(Aronovici 1972)
Moderate	30	8.7×10^{-6}	(Baumhardt 1993)
None (well sorted gravel)	0	10^{-4} to 10^{-2}	(Fetter 1994)
None (well sorted sand)	0	10^{-3} to 10^{-5}	(Fetter 1994)
None (silty sands)	0	10^{-5} to 10^{-7}	(Fetter 1994)
None (silts)	0	10^{-6} to 10^{-8}	(Fetter 1994)

Table 1.2. Infiltration rates of various levels of calcium carbonate indurations. Calcium carbonate percent by weight. Default infiltration rates for gravel, sand, and silt soils added for comparison.

Infiltration rates from these sources are relatively consistent by induration grade. Calcium carbonate can deposit in sandy and gravelly soil horizons, so a comparison of the infiltration rates of these soils with the infiltration rates of the calcium-carbonate deposits is useful. For calcium-carbonate-dominated horizons that are at least moderately indurated, the infiltration rates are several orders of magnitude less than the gravelly or sandy soils that the carbonate has deposited within. The infiltration rates of the well-indurated areas are more similar to silty sands and silt than to the sands and gravels they originally deposited within. This demonstrates that even though the textural analysis may

indicate a sandy soil, the hydraulic properties of the soil may more closely resemble a silty soil if the soil has significant carbonate deposition.

1.3.5.7. Rocky Subsurface Soils

Vadose zones do not usually consist of uniform soils; rocks and boulders are often found in the subsurface. Whether or not these rocks affect the flow of water in the vadose zone was considered by Bouwer and Rice (1983). They conducted an experiment in which columns were filled with sand-gravel and sand-boulders. Tensiometers were used to monitor pressure head, and a neutron probe monitored soil-water content. Outflow from the columns was also collected. For the sand-gravel columns, the sand had an average diameter of 0.27 millimeters and the gravel had an average diameter of 1.5 centimeters, with the gravel consisting of 70 percent of the total weight of the column. For the sand-boulder columns, the same sand was used, and the average dimensions of the boulders were 20 centimeters length, 14.8 centimeters width, and 6.2 centimeters height, with the boulders laid on their flat side and a 2.4 centimeter depth spacing between the boulders. The results showed that for these stony soils, both the saturated and unsaturated conductivities for downward flow could be determined from the soil (in this case sand) fraction alone. The presence of gravel and boulders did significantly increase the solute dispersivity of the soil medium (Bouwer and Rice 1983).

The flow of water through stony soils was further investigated by Hendrickx et al. (1991), who determined the travel times through a 100 meter deep, stony vadose zone in Pakistan through numerical analysis. The yearly net infiltration by an artificial recharge of 40 centimeters was found to take 35 years to reach the groundwater table, which was at a depth of 100 meters, in a sandy loam soil without stones. Comparatively, the travel

time was only 17 years in the same soil with 60 percent stones. Therefore, stony soils shorten recharge travel times considerably. The presence of stones would also increase the advection of the solutes in the vadose zone. It was also determined that stony soils reduced the water retention and hydraulic conductivity of the soil (Hendrickx et al. 1991).

1.3.5.8. Vapor Movement and Water-Table Depth

Through the use of computer modeling, Walvoord et al. (2002a) found a divergence in liquid and net moisture fluxes with vapor fluxes in deep vadose zones. To simulate the climate shift of approximately 15 ka, a wet environment was simulated using an initial downward flux condition, and then the transition to a drier, hotter climate was simulated as a fixed sub-root-zone matric potential condition for 15 kyr. The results of the simulations showed an upward isothermal vapor flux that contributes significantly to the drying of the of the upper 25 meters of the vadose zone, as seen in Figure 1.9. Between the bottom of the root zone and 25 meters depth, vapor fluxes were found to exceed the liquid fluxes by at least one order of magnitude, as a result of the dry conditions and low unsaturated permeability. Liquid flows upward above 25 meters and downward below it, increasing with depth as a result of divergent drying processes. The net moisture flux determined in this study illustrated that the net moisture flux below the root zone is not equivalent in magnitude or direction to the flux across the underlying water table (Walvoord et al. 2002a). This demonstrates that vapor fluxes can play a significant role in the movement of moisture in arid vadose zones.
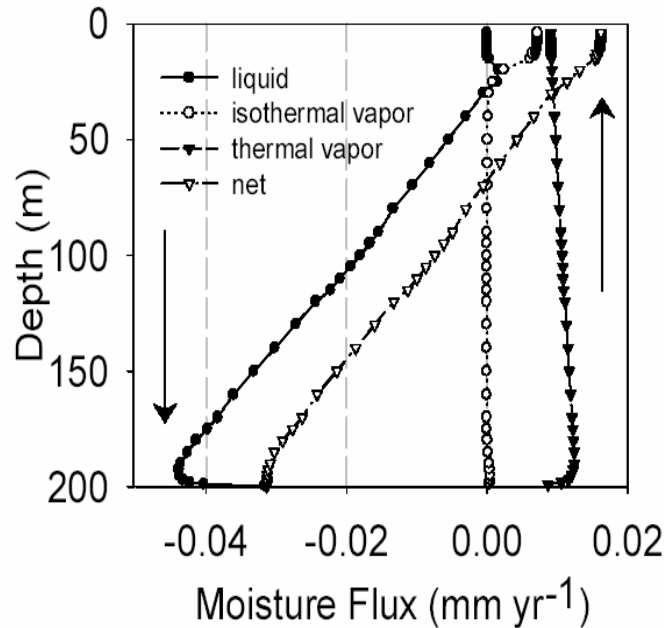
Figure 1.9. Moisture-flux profile (below 4 meters depth) 15 kyr after a climate shift from downward flux conditions to a fixed sub-root-zone matric potential condition. Negative values indicate downward fluxes. Vapor flux gradients are upward, while liquid and net flux gradients are downward. Figure from Walvoord et al. (2002a).

The depth of the groundwater table was found to affect the flow of liquid and vapor through desert vadose zones. Walvoord et al. (2002a) determined that the upward vapor flux exceeded the upward liquid flux by a least one order of magnitude for thick vadose zones greater than 25 meters depth. In contrast, it was found that the upward liquid flux exceeded the upward vapor flux below 10 meters depth when the vadose zones were shallower than 25 meters depth. Capillarity draws enough water upward from the water table of shallow vadose zones to significantly increase the unsaturated permeability and consequently increase the net upward moisture flux. Vadose zones with thicknesses greater than 100 meters show little sensitivity to increases in water table depth, as demonstrated by their overlapping profiles in Figure 1.10 (Walvoord et al. 2002a).
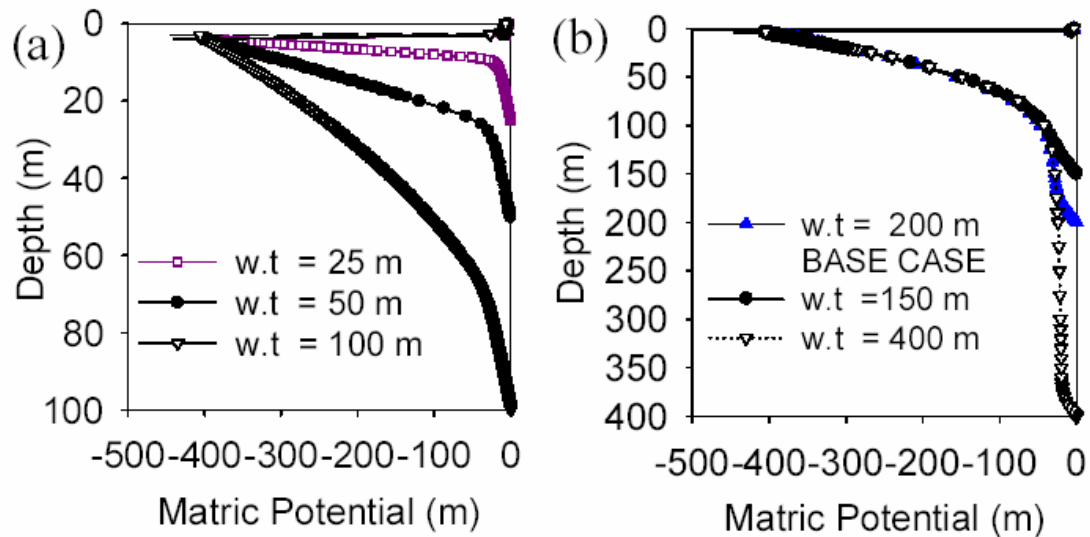
Figure 1.10. Steady-state matric potential profiles for variable water table depths of (a) 25 to 100 meters and (b) 150 to 400 meters. The profiles show a decrease in curvature with increasing vadose zone thickness, reflecting a decrease in the overall matric-potential gradient. Figure from Walvoord et al. (2002a).

1.4. Electrical Conductivity

The electrical resitivity/conductivity of a substance is a measure of the difficulty/ease with which an electrical current can be made to flow through a substance. Most soil and rock minerals are electrical insulators of very high resitivity (McNeil 1980). In general, the conductivity of soils and rocks is electrolytic and takes place through moisture filled pores and passageways contained in the matrix. The conductivity of both rocks and soils is determined by the following: (1) the shape and size of the pores or passageways and number of pores or passageways present in the matrix, (2) the water content of the pores, (3) the concentration of dissolved electrolytes in the pore water, (4) the temperature and phase state of the pore water and (5) the amount and composition of colloids (McNeil 1980). Therefore, since the constituents, structure, and moisture content of different soils and rocks can vary greatly, differences in subsurface electrical conductivity can be an indicator of subsurface heterogeneity.

CHAPTER 2

STUDY AREA

2.1. Site Selection Parameters

The objective of this research was to determine the relative degree to which ecology and climate influence the hydrodynamics of the underlying vadose zone. In order to demonstrate the influences of climate and ecology on soil-moisture fluxes, study sites were chosen that had varying climatic and vegetation parameters, while other parameters were held as constant as feasible. Parameters, other than ecology and climate, that could affect the vadose zone moisture fluxes are topography, surface soil texture, and heterogeneous subsurface soils.

The experimental design started with the determination of a transect area along which the climate changed gradually and that also included all the ecosystems to be tested. After this transect area was established, sites within this area where chosen based on the following criteria, which were aimed at holding all non-climatic and non-ecological influences on soil-moisture fluxes as constant as possible. These criteria were that the site have sandy soils, relatively flat topography and relatively homogenous subsurface soils. In order to have access to the land and the site, additional criteria were that the site was located close to an established road and that the land owners or managers were amenable to drilling on their lands.

As a result of feasibility, time and money constraints, the ecosystems to be tested

were narrowed down to creosote, grass, juniper, and ponderosa pine. These ecosystems are prevalent in the area and constitute of 55 percent of the total vegetation cover of New Mexico, as shown in Table 2.1 (Dick-Peddie 1993).

	Acres	% of Total State Area
Total NM State Area	78,000,000	-
Total Vegetated Area	71,000,000	91
Vegetation	**Acres**	**% of Vegetated Area**
Creosote	4,600,000	6.5
Grassland	21,000,00	29
Juniper	7,700,00	11
Ponderosa Pine	6,000,000	8.4
Total	39,000,000	55

Table 2.1. Total vegetated area of New Mexico broken down into the vegetation of interest in this study. Data from Dick-Peddie (1993).

These ecosystems also tend to exist in flat areas with sandy soils. The piñón-juniper mixed woodland ecosystem was considered, but most of the area this ecosystem occupied along the transect was rocky and on steep slopes. The sites needed to be free of large rocks and boulders in order to make the drilling more feasible; a core depth of five to ten meters was desired. Electromagnetic (EM) measurements of the proposed sites were taken in order to determine if there were any boulders under the surface and to verify that the subsurface soils were relatively homogenous. Other practical considerations were land ownership, presence of an access road, and that accessibility of the site itself to the drill rig.

In order to determine possible drill sites, temperature, precipitation, potential evaporation, and vegetation maps were obtained. Maps of annual average parameters were used since the expected chloride-accumulation and water-potential equilibrium times would be over much longer time periods, likely in the thousands of years.

2.2. Transect Area

The area of the state of New Mexico in which the transect was located in is shown in Figure 2.1. Figure 2.2 depicts a more detailed view of this transect area. Figure 2.1 denotes the relation of the transect line to the Río Grande, topography and towns. As seen in this figure, elevation increases going from east to west along the transect, away from the Río Grande.
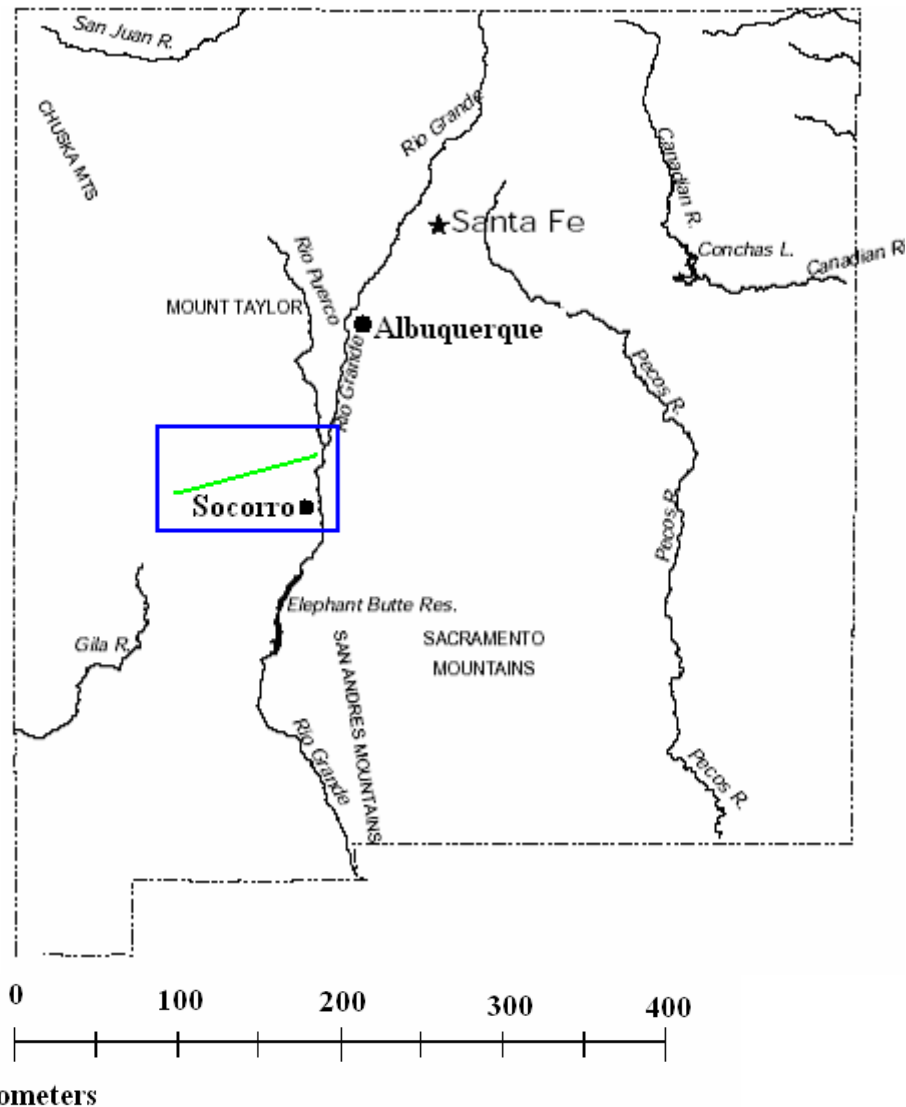
Figure 2.1. Transect area in relation to the state of New Mexico, outlined by rectangular area; transect line located just north of Socorro. Major rivers, mountains, and cities noted. Map modified from original (State 2005).
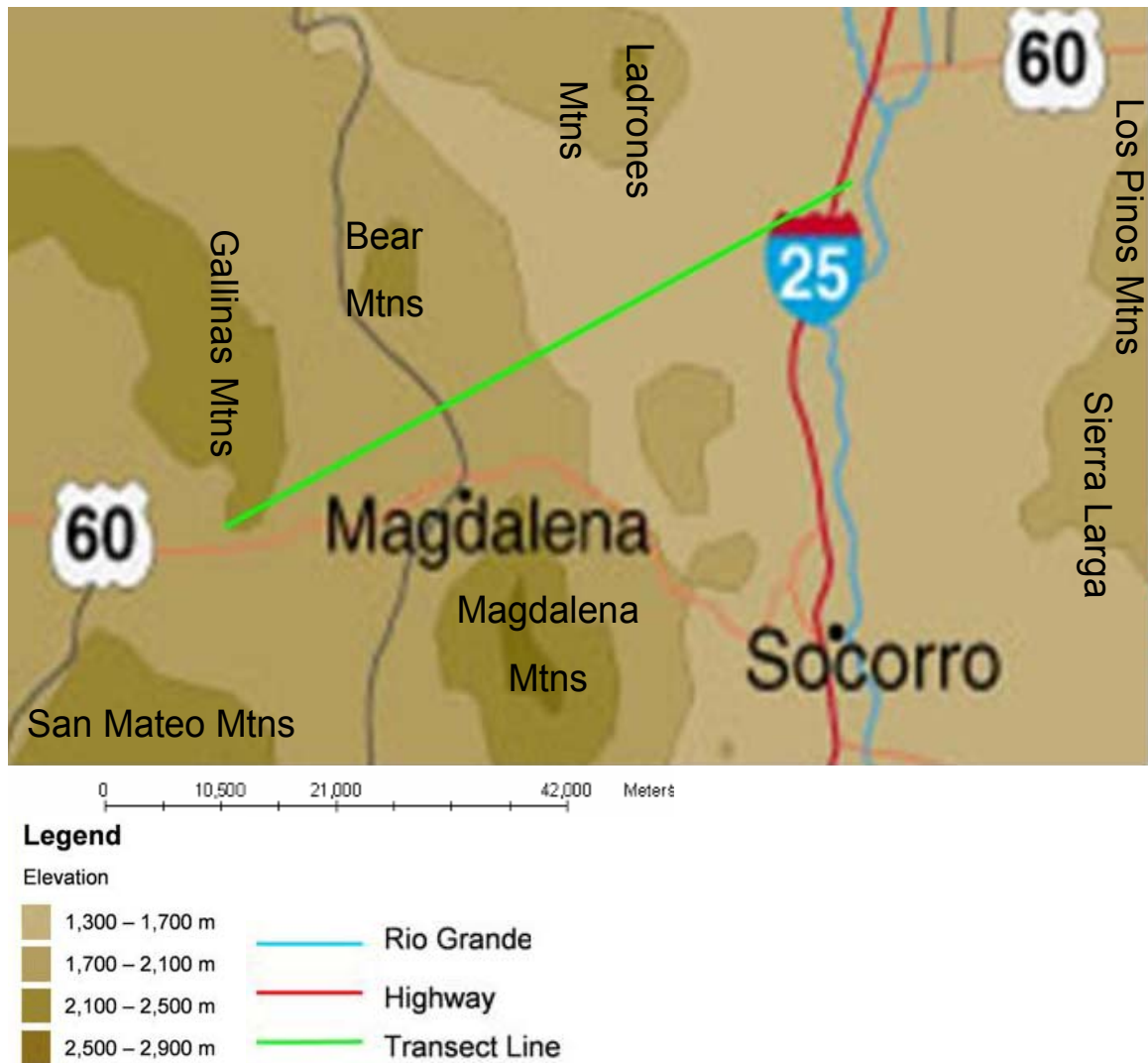
Figure 2.2. Detailed view of transect area outlined in Figure 2.1. The transect line is shown in relationship to surrounding towns, Río Grande and topography. Map modified from original. (Purdue 2005)

2.3. GIS Maps

Maps of the transect area were developed using Geographic Information System (GIS) software. The software used was Esri® Arc Map™ and Esri® Arc Toolbox™, Version 8.3. All obtained data maps were converted to the GCS North American 1983 coordinate system and datum. These GIS maps were necessary to select possible drilling locations along the transect. Temperature, precipitation, potential evaporation, and

vegetation maps were obtained for this selection process.

2.3.1. Average Annual Temperature Map

The average annual temperature map in Figure 2.3 was obtained from the Spatial Climate Analysis Service at Oregon State University (SCAS/OSU). This data set contains spatially gridded average annual temperatures for the climatological period 1961-1990. The temperature was calculated as the mean of monthly minimum and maximum temperature grids developed. Distribution of the point measurements to a spatial grid for minimum and maximum temperature was accomplished using PRISM (Parameter-elevation Regressions on Independent Slopes Model), developed by Chris Daly of SCAS/OSU (PRISM 2004).

PRISM is an analytical model that uses point data and a digital elevation model (DEM) to generate gridded estimates of monthly and annual mean temperature (as well as other climatic parameters). PRISM is well suited to regions with mountainous terrain, because it incorporates a conceptual framework that addresses the spatial scale and pattern of orographic processes (PRISM 2004). Temperature was modeled monthly, and an annual grid was produced by averaging the monthly grids. A Gaussian filter was applied to increase the resolution of the grids from the base resolution 2.5 arc-minutes (~4 km) to 1.25 arc-minutes (~2 km). This filter is a modification of the Barnes filter, originally adapted by Dr. Stephen Esbensen of Oregon State University, and it was later modified for use by Wayne P. Gibson, also of Oregon State University (Climate Source 2004). Point estimates of climate originated from the following sources: 1) National Weather Service Cooperative (COOP) stations, 2) Natural Resources Conservation Service (NRCS) SNOTEL, and 3) local networks. All COOP station data were subjected

to quality control checks by the National Climatic Data Center (NCDC) and Spatial

Climate Analysis Service (Climate Source 2004).
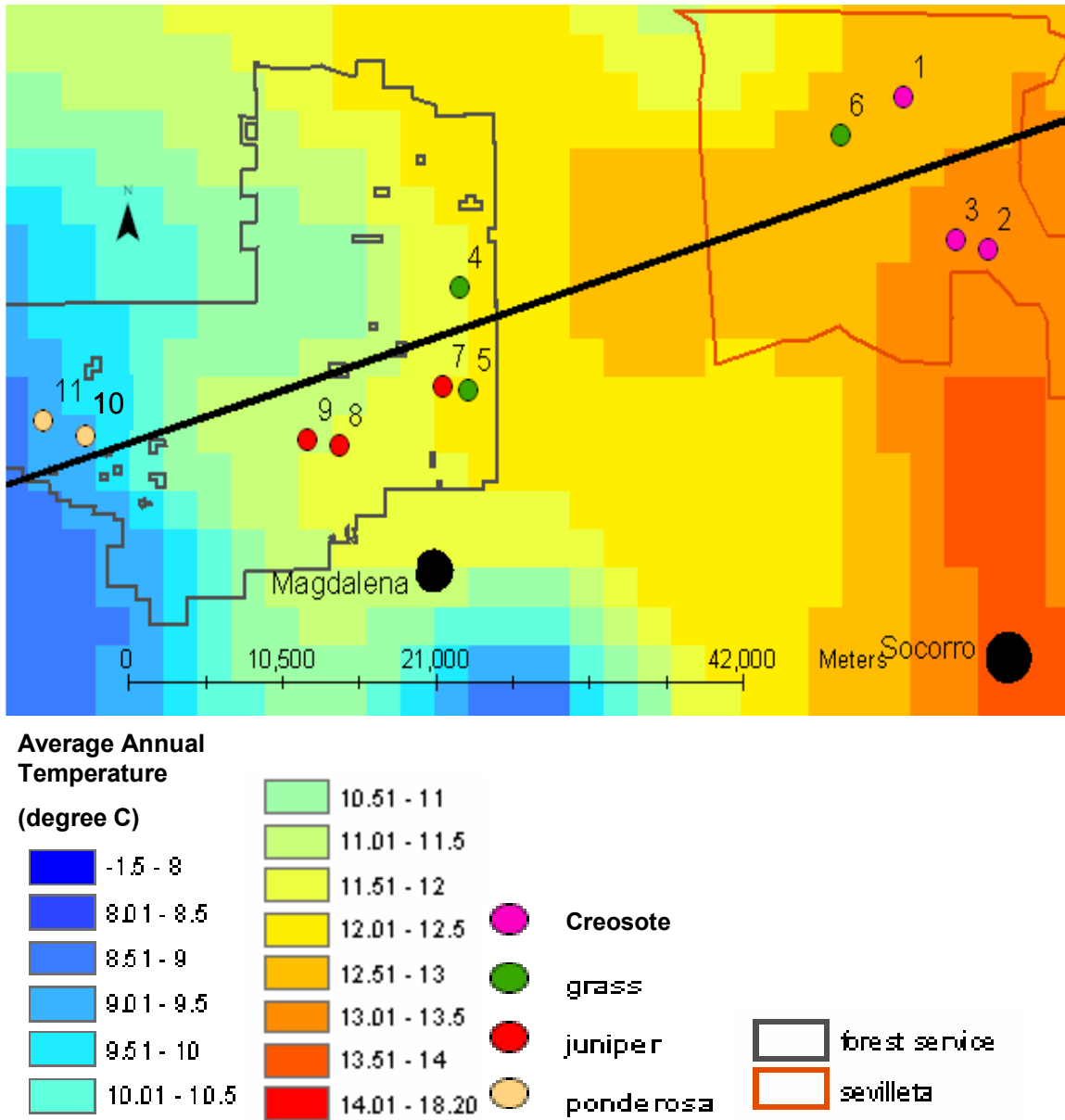
Figure 2.3. Average annual temperature in degrees Celsius for transect area. Transect line, land ownership, and drill sites are also shown. The temperature along the transect varies gradually from warmer in the east to cooler in the west.

2.3.2 Average Annual Precipitation Map

The precipitation map in Figure 2.4, obtained through the Resource Geographic

Information System (RGIS) Clearinghouse (RGIS 2004), contains the spatially gridded

average annual precipitation for the climatological period 1961 - 1990. Interpolation

between the point measurements onto a spatial grid was accomplished using the PRISM

model, as described in the above section. The precipitation estimated for each grid cell is

an average over the cell area; thus, point precipitation can be estimated at a spatial

resolution no better than half the dimension of a cell (2 km) (Precipitation Map 2004).

The point estimates of precipitation originated from the same sources as those for the

previous map. All COOP station data were subjected to quality control checks by the

National Climatic Data Center (NCDC) (Precipitation Map 2004).
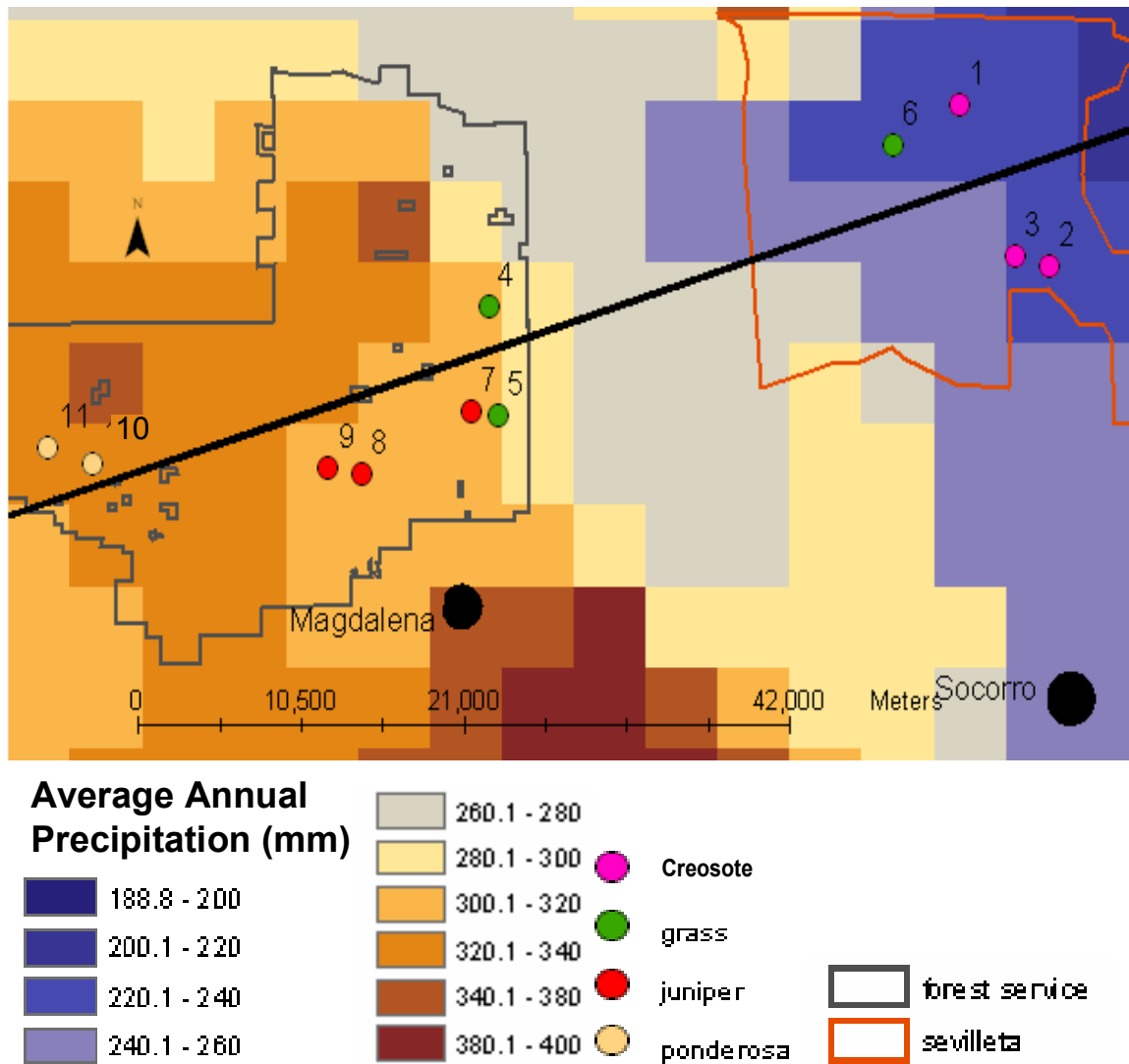
Figure 2.4. Average annual precipitation in millimeters for the transect area. Transect line, land ownership, and drill sites are also shown. The precipitation along the transect varies from lower amounts of precipitation in the east to higher amounts of precipitation in the west.

2.3.3. Potential Evaporation GIS Map.

Potential evaporation (PE) is the amount of water that would be removed from a surface by evaporation processes if sufficient water were available to completely meet the atmospheric demand (Thornthwaite 1948). The PE values in the obtained data layer were based on annual free-water surface evaporation, which is the rate of evaporation from a shallow lake for a year. The data upon which the map is based are for the period 1956 to

45

1970. The original digital ArcGIS PE map was obtained from Earth Data Analysis

Center through the Resource Geographic Information System Clearinghouse in

Albuquerque New Mexico (RGIS 2004). The exact projection of the original map was

somewhat uncertain. The map was digitized from a Mylar original and then transformed

repeatedly into Albers coordinates until a fit was achieved (Evaporation Map 2004). A

state boundary line runs down the digital map as it does on the Mylar original. Each half

was a separate data set; the two were joined using MAPJOIN in ArcMap (Evaporation

Map 2004).

This original digital PE map contained PE isopleths. A unique PE value for each

point on the map was necessary for the determination of a specific site's climate. The

original paper version of the digital map was obtained from New Mexico in Maps

(Williams 1986). Using the paper map and the digital isopleth map mentioned above, a

contour map of the PE values was created for the transect area. A surface map of

continuous PE values was then created through the kriging function in ArcMap. The

resultant map is shown below in Figure 2.5.

Use of the kriging function to obtain point PE data between PE contour line poses

some uncertainty in this parameter. Also, because of the sparse network of weather

stations that measure this parameter and the highly irregular terrain of New Mexico, it is

difficult to determine climatic conditions between stations. As a result, the isopleths of

the original paper map and the resultant digital map are to be considered approximations

(Williams 1986). PE is greatly controlled by solar radiation, as is air temperature. Since

the PE map in Figure 2.5 is fairly similar to the temperature map shown in Figure 2.3

above, the PE map is considered to be the best estimate possible for this parameter. Out

of all the climatic parameter data obtained, the PE data are considered to have the most

uncertainty.
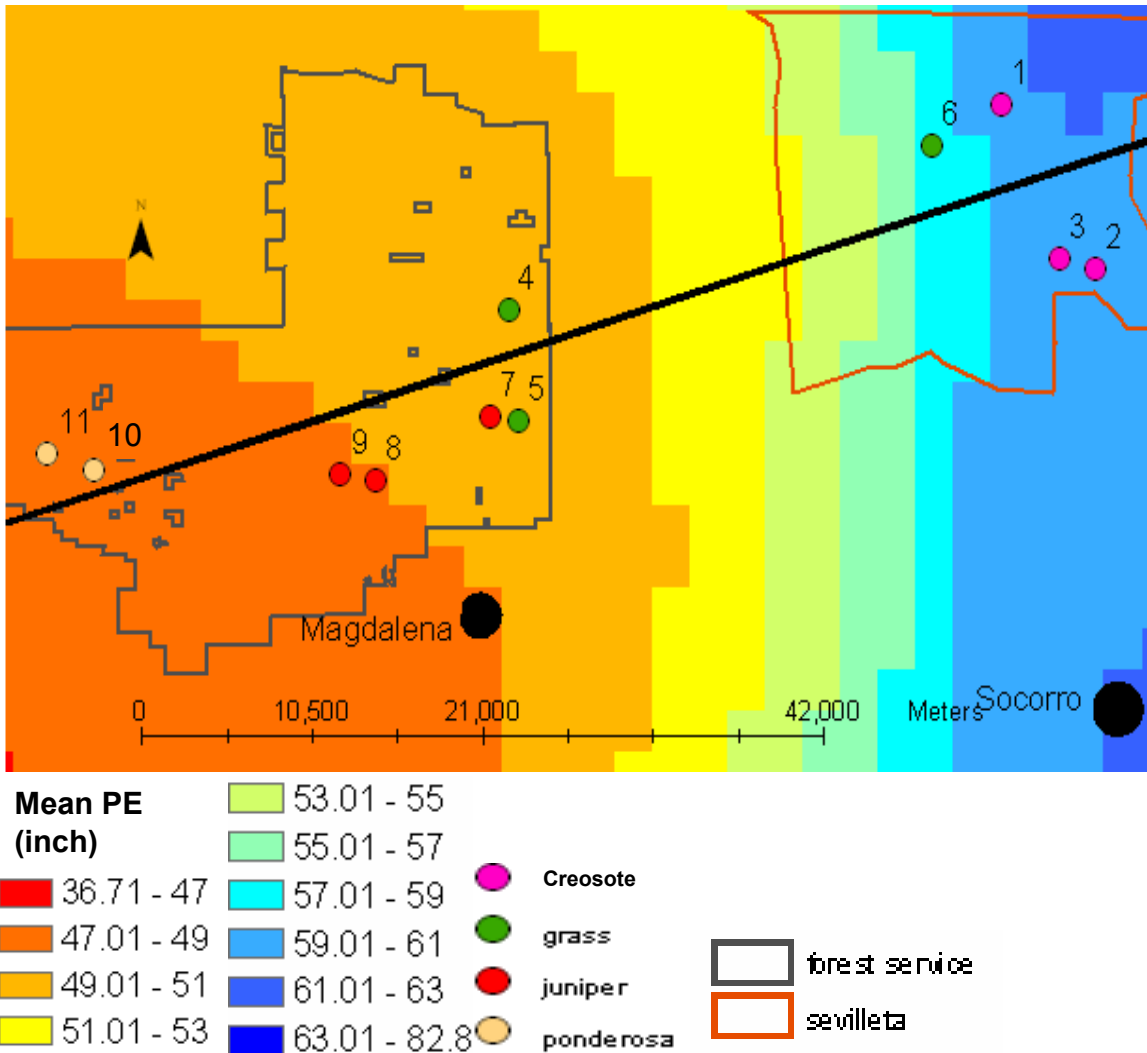
Figure 2.5. Average annual potential evaporation in inches for the transect area. Transect line, land ownership, and drill sites are also shown. The potential evaporation along the transect varies from high potential evaporation demand on the east side of the transect to low evaporation demand on the west side of the transect.

2.3.4. Aridity Index Map

Whether or not a climate is moist or dry cannot be determined from the

precipitation alone. Additionally, if the precipitation exceeds the demand for evaporation

and transpiration must be determined to characterize the climate, since both precipitation

and evapotranspiration are equally important climatic factors (Thornthwaite 1948).

47

Where precipitation exceeds the water need, the climate is moist, and where the water need exceeds the precipitation, the climate is dry (Thornthwaite 1948). The aridity index (AI) determines the degree to which a climate is wet or dry and is a function of the ratio of potential evaporation to precipitation (Budyko 1974), as shown in equation 7.

$$Aridity\ Index = \frac{Average\ Annual\ Potential\ Evaporation\ (mm)}{Average\ Annual\ Precipitation\ (mm)} \quad (7)$$

The aridity index is used in this study to determine the extent to which climate controls the vadose zone moisture fluxes. To accomplish this, the potential evaporation, which was interpolated from pan evaporation data, was used to determine the aridity index. Regions where the AI is greater than one are broadly classified as dry since the evaporative demand cannot be met by precipitation; regions with an AI of less than one are classified as wet (Arora 2002). Ponce et al. (2000) further divided the AI values into the following climatic categories, 0.375 to 0.75 as humid, 0.75 to 2 as sub-humid, 2 to 5 as semiarid, and 5 to 12 as arid.

To determine the AI of the transect area, the average annual precipitation and PE maps shown above in Figures 2.4 and 2.5, respectively, were converted to the same units of millimeters and overlaid in GIS using the raster calculator. The resultant map is shown below in Figure 2.6. The transect area contains aridity values from 3 to 7, falling within the semiarid to arid region of Ponce's climatic subdivisions. These divisions may correspond to changes in the vadose-zone dynamics, since the division between basin-floor non-recharge areas and recharge areas presumably lies somewhere along an arid-semiarid gradient (Walvoord and Phillips 2004). Therefore, if climate were the main determinant of recharge, then the arid Sites of 1, 2, 3 and 6 would be non-recharge areas

and the semiarid Sites of 4, 5, 7, 8, 9, 10, and 11 would be recharge areas.
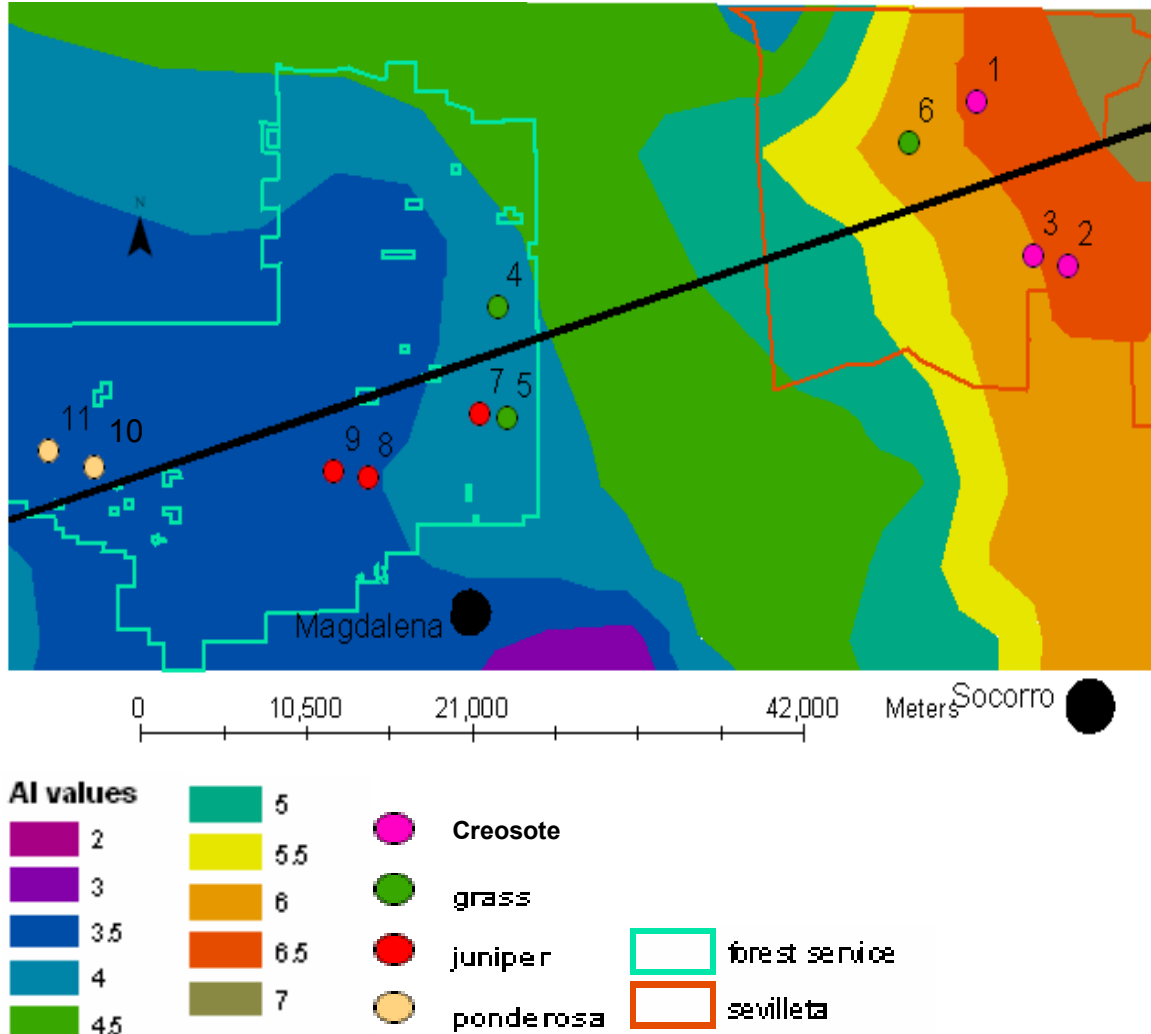
Figure 2.6. Aridity index of the transect area. Transect line, land ownership, and drill sites are also shown. The AI values on the transect vary from high values in the east to low values in the west.

2.3.5. Vegetation Map

The vegetation map was obtained from Earth Data Analysis Center through the

Resource Geographic Information System Clearinghouse in Albuquerque New Mexico

(RGIS 2004). The data originated from a 1:1,000,000 scale paper map by Dick-Peddie

(1993). Only vegetation type areas were extracted from the source map. The data

contains all lines and polygons representing the vegetation types and the outline of the

State of New Mexico. Attribute accuracy was tested by manual overlaying with the

original; no errors were detected. All lines and polygons were inspected, verified, and

corrected by performing a "clean" routine using ARC/Edit in ARC/INFO 5.0.1.

Cartographic and spatial topology accuracy are 100%. Horizontal accuracy was tested by

visual comparison of digital data with the source data using check plots (Vegetation Map

2004).

The categories, originally specified by Dick-Peddie, were reclassified as follows:

Chihuahuan Desert Scrub to Creosote, Desert Grassland to Grass, Juniper Savanna to

Juniper, Coniferous Mixed Woodlands to Piñón-Juniper, and Montane Coniferous Forest

to Ponderosa Pine. This reclassification was done for the purpose of simplicity and

clarity and was based on the category's description and field observations. The resultant

map, Figure 2.7, is a simplification of the actual vegetation pattern of the area,

demonstrating overall ecological trends.
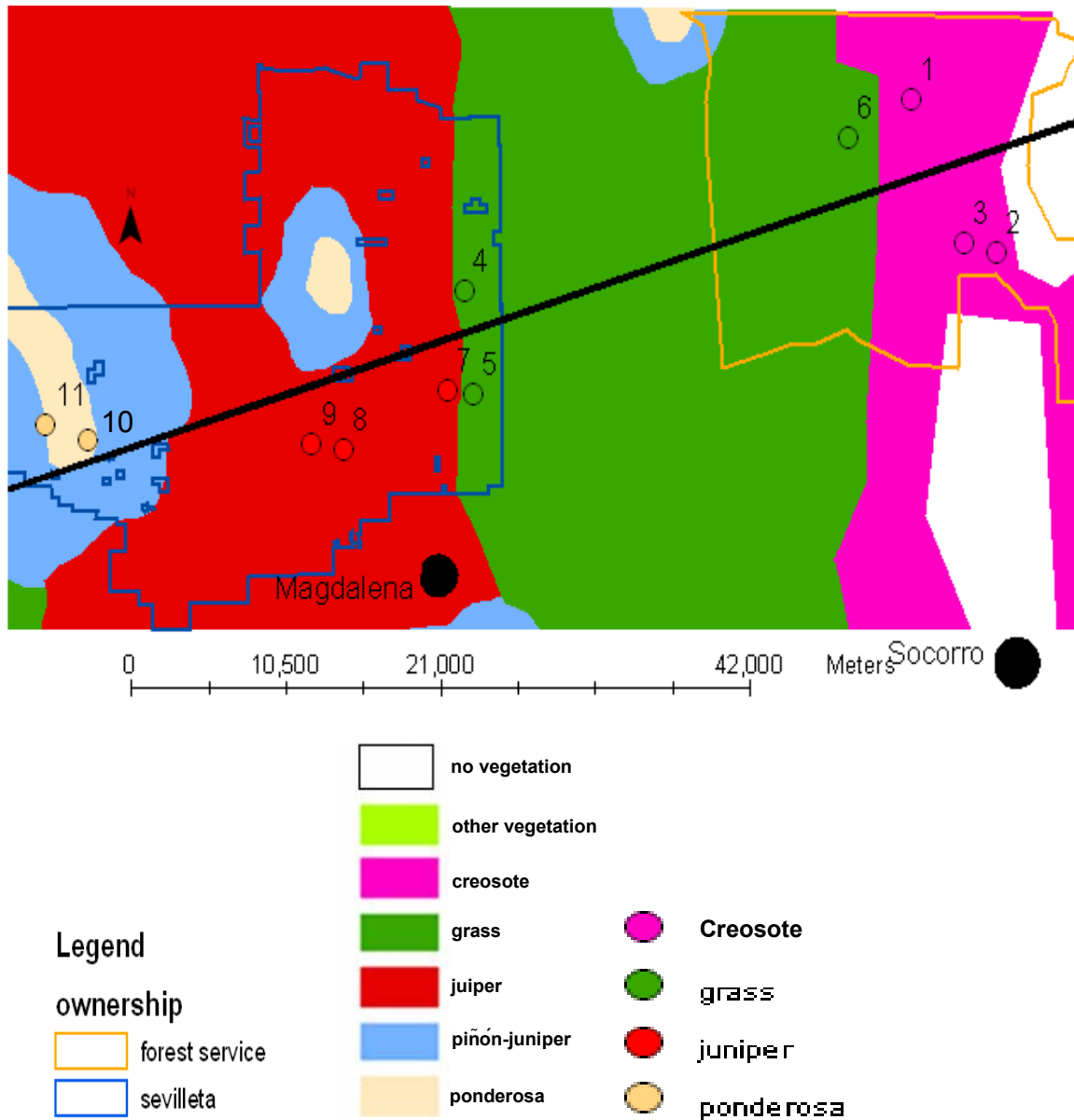
Figure 2.7. Vegetation of the transect area. Transect line, land ownership, and drill sites are also shown. Vegetation changes from creosote to grass to juniper to piñón-juniper mixed woodland to ponderosa pine going from east to west along the transect. This map is a simplification of the vegetation communities in order to demonstrate overall trends.

2.3.6. Site Location Map

After field-checking possible sites, the sites shown on the map below (Figure 2.8) were chosen. Eleven sites were chosen altogether. The land-ownership map was obtained from Earth Data Analysis Center through the Resource Geographic Information System Clearinghouse in Albuquerque New Mexico (RGIS 2004). The data were

51

scanned from the original BLM 1:100k map plates, which were used to produce the
1:100k color land status maps. 586 plates were scanned, edited with LT4X (a raster data
editing package), and converted to the Map Overlay Statistical System (MOSS). In
MOSS the individual files were merged into statewide coverages, generalized by
dissolving polygons less than 158 acres, and then used to produce the plates for the
1:500K NM Surface Ownership Map. The individual coverages were then converted to
ARC Map, re-verified for completeness, and checked for locational accuracy. This was
done by the verification of polygon identities, the validity of polygon locations was
checked against the reference data sets and other ownership coverages, and an exhaustive
inspection of the map plates that were produced with the data (Land 2004).

The roads of the transect area were obtained from the U.S. Department of
Commerce, Bureau of the Census, Geography Division. The Redistricting Census 2000
TIGER/Line files are an extract of selected geographic and cartographic information
from the Census TIGER data base. The geographic coverage for a single TIGER/Line
file is a county or statistical equivalent entity, with the coverage area based on January 1,
2000 legal boundaries (Roads 2004).
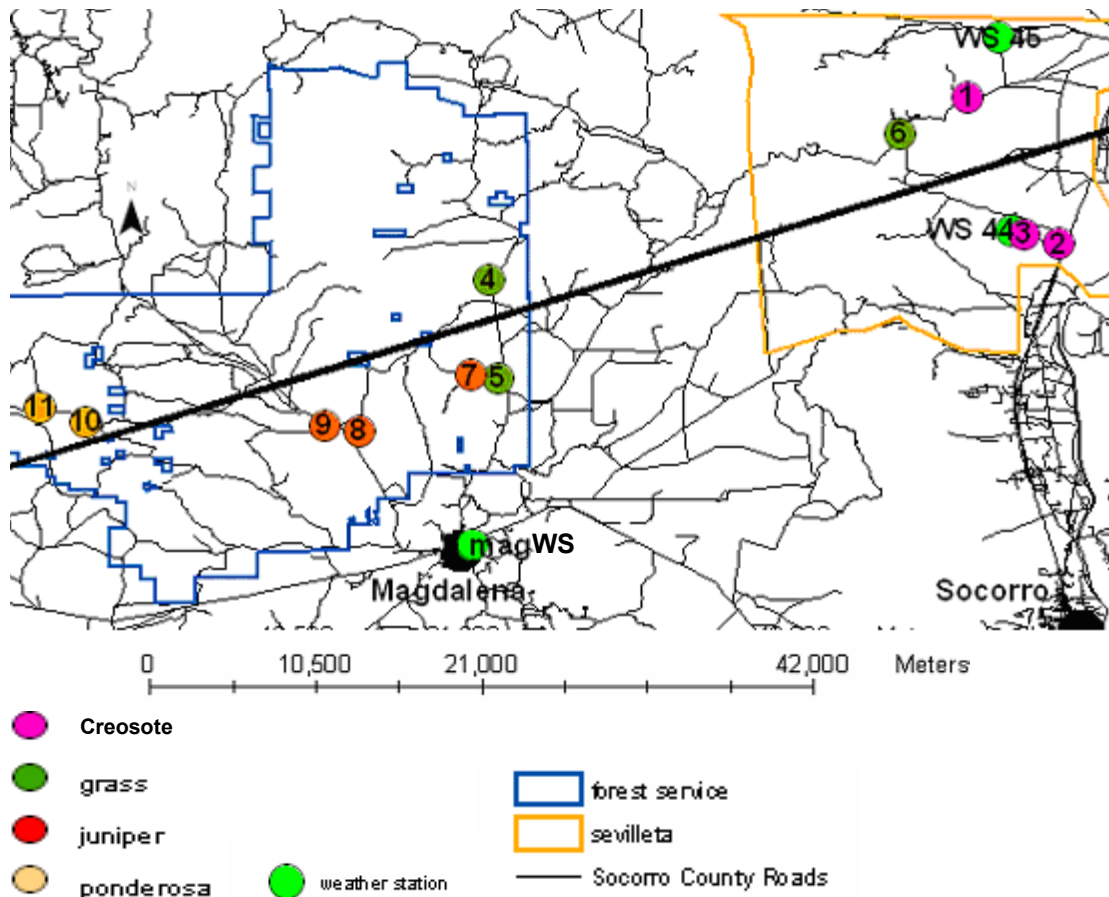
Figure 2.8. Sites, roads, and land ownership of the transect area. Transect line and weather stations are also shown. WS = weather station. Weather stations discussed in next section.

2.4. Climate

Data for the present climate of the study area were obtained from the following weather stations. Data for Sites 1 and 6 were obtained from Sevilleta Long Term Ecological Research (LTER) station number 45, Bronco. The latitude and longitude of this station are 34.406 N, 106.934 W decimal degrees, respectively; the elevation is 1,547 meters. This station came online in 1989. Sites 1 and 6 are located 4.1 and 7.7 kilometers, respectively, southwest from this weather station. Data for Sites 2 and 3 were obtained from the Sevilleta LTER station number 44, Río Salado. The latitude and longitude of this station are 34.296 N, 106.927 W decimal degrees, respectively; the

53

elevation is 1,503 meters. This station came online in 1990. Sites 2 and 3 are respectively located 2.7 and 0.76 kilometers to the east of this weather station. Data from both LTER stations were obtained from the LTER website (LTER 2004).

Three weather stations exist or existed near Magdalena Sites 4,5, and 7 to 11. One weather station was operated by the LTER near the Langmuir observatory. This station's elevation of 3,243 meters was much higher than any of the sites, and the data set was very limited. Another weather station is called a Magdalena station, but it is 43 kilometers away from the town of Magdalena. Data from this station were used to obtain the weather near the time of drilling, with the caveat that it is 43 kilometers from the town of Magdalena. A final station within the town of Magdalena was found, but it had ceased operations in 1993. Since this station had data for a longer period (from January 1, 1914 to October 31, 1993), was much closer to the sites, and was in the elevation range of the study sites, it was used for the area's overall climate determination. These data were obtained off the internet from the National Climatic Data Center Station's Historical Listing for the National Weather Service's Cooperative Network (NCDC 2004). The station's number in the network was 295353. The latitude and longitude were 34.117 N, 107.233 W decimal degrees, respectively. The elevation was 1,996 meters, which is within the elevational range (1,876 to 2,381 meters) of the study sites. This weather station is 9.3 kilometers southwest from the closest site, Site 8, and 24 kilometers southwest from the furthest site, Site 11.

For the Magdalena and Sevilleta Weather Stations, the highest amounts of rain occur during the months of July, August, and September, a result of the summer monsoonal rains. See Figure 2.9 for the data from all three weather stations. The

Magdalena Station had consistently more rain then the Sevilleta Stations, but all stations

followed the same pattern. The Magdalena Weather Station is expected to have higher

precipitation totals since that station was higher in elevation than the Sevilleta Station.
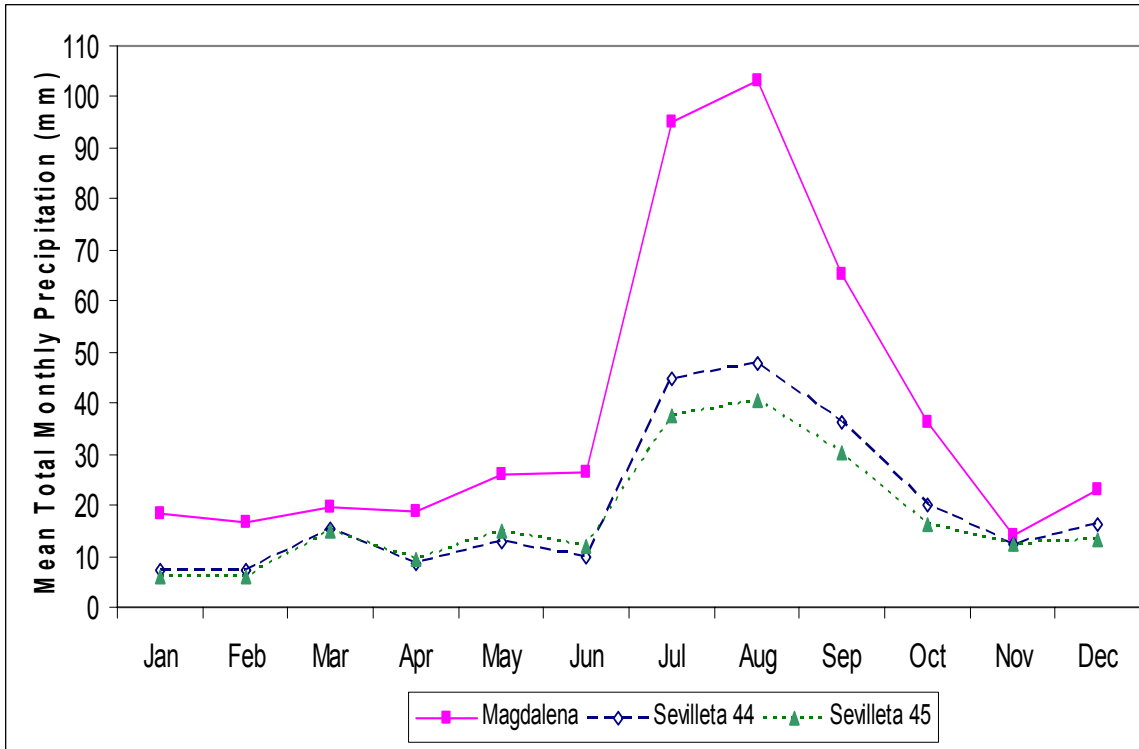
Figure 2.9. Mean Total Monthly Precipitation in millimeters of the three weather
stations near the transect. The higher amount of precipitation seen in the Sevilleta
weather stations is probably the result of the different operational lengths of the stations.

The temperature trends of the three weather stations are very similar. The

Magdalena station had a consistently lower mean monthly temperature, as expected due

to its higher elevation. See Figure 2.10 for the mean monthly temperature data for each

weather station.
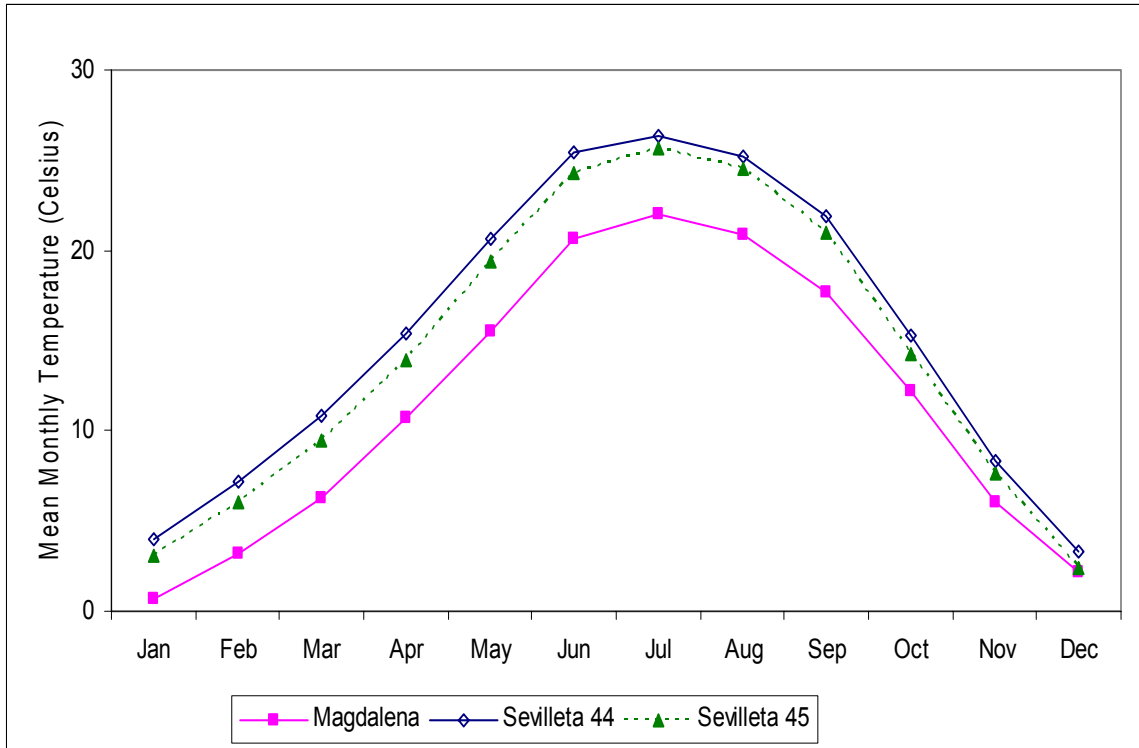
Figure 2.10. Mean monthly temperature in degrees Celsius of the three weather stations near the transect.

2.5. Climate Conditions Prior to and During Drilling

Table 2.2 lists the climate data for the period prior to and during the drilling, which took place from March 15 to 18, 2004. Data are shown daily during drilling, weekly for the six weeks prior to drilling, and monthly for the remainder of the previous year. The Sevilleta Weather Stations used were the same as listed in the previous section. The data from another Magdalena station were used, as mentioned above. These data were obtained off the internet from the Remote Automated Weather Station Listing for the National Weather Service's Cooperative Network (RAWS 2004). The station has operated since the year 2000. Its latitude and longitude are 33° 51' N, 107° 33' W, respectively, and it has an elevation of 2,591 meters. This weather station is 38 kilometers south from Site 10, the closest site, and 55 kilometers south from Site 4, the furthest site. This station is higher than the study sites, which have elevations ranging

from 1,876 to 2,381 meters. The higher elevation of this weather station may result in precipitation measurements exceeding precipitation amounts that actually occurred at the sites. The station is also 43 kilometers from the town of Magdalena.

No rain was observed during the drilling period; see Table 2.2 below. The only significant rainfall before drilling occurred in the second and third weeks of February. These rainfall events were not great enough to expect much impact on the soils of the study sites, with the rainfall probably not infiltrating more than several centimeters.

		Total Precipitation (mm)			Average Temperature (deg C)		
		Magdalena	Sevilleta 44	Sevilleta 45	Magdalena	Sevilleta 44	Sevilleta 45
February	2003	27.6	10.9	9.9	1.7	5.9	5.2
March	2003	66.9	6.1	6.3	2.9	9.9	9.0
April	2003	3.2	1.9	0.3	7.3	14.8	13.8
May	2003	0.0	0.0	0.0	14.3	21.0	20.3
June	2003	0.5	1.2	8.7	17.4	24.1	23.7
July	2003	0.1	0.6	6.6	21.1	28.8	28.4
August	2003	10.3	28.8	15.9	17.5	25.9	25.4
September	2003	2.7	14.5	24.3	15.7	22.2	21.6
October	2003	43.6	48.6	49.3	12.1	17.5	16.5
November	2003	18.8	14.8	20.1	4.5	8.5	7.8
December	2003	56.7	0.0	0.0	2.1	3.5	2.7
January	2004	25.4	4.5	4.2	0.5	3.8	3.2
31-Jan-04	6-Feb-04	0.0	0.0	0.0	-2.4	1.9	0.8
7-Feb-04	13-Feb-04	3.7	2.9	0.9	-7.5	-0.1	-0.7
14-Feb-04	20-Feb-04	0.0	0.0	0.0	0.0	6.6	5.6
21-Feb-04	27-Feb-04	50.7	4.2	5.1	-1.2	6.8	6.2
28-Feb-04	5-Mar-04	3.1	18.3	28.0	-0.1	5.4	5.1
6-Mar-04	12-Mar-04	0.7	2.6	0.6	0.4	11.4	11.2
	13-Mar-04	0.0	0.0	0.0	3.6	11.5	12.1
	14-Mar-04	0.0	0.0	0.0	1.2	12.9	13.4
	15-Mar-04	0.0	0.0	0.0	3.0	15.5	14.0
	16-Mar-04	0.0	0.0	0.0	2.1	14.6	12.4
	17-Mar-04	0.0	0.0	0.0	2.3	14.8	13.7
	18-Mar-04	0.0	0.0	0.0	3.1	15.1	13.4
	19-Mar-04	0.0	0.0	0.0	4.4	16.4	14.8

Table 2.2. Average temperature in degrees Celsius and total precipitation in millimeters. Daily time period used just before and during drilling, weekly used for two months prior to drilling and monthly used for remainder of year prior to drilling.

2.6. Regional Vegetation

The four ecosystems of interest contained in the transect area are described below.

2.6.1. Creosote Bush Ecosystem

In the creosote ecosystem, the creosote bush (*Larrea tridentata*) predominates strongly, with the bushes ranging in height from 1 to 1.5 meters tall. The ecosystem is densely populated with around forty bushes in a ten meter radius. The spacing of the bushes vary from one to three meters, on average. The main grasses of this ecosystem are western wheatgrass (*Pascopyrum smithii*) and bush muhla (*Muhlenbergia porteri*), with broom snakeweed (*Gutierre sarothrae*) being the predominant weed. The underbrush plant clusters are spaced 0.3 to 1.5 meters apart, with well connected interspaces. The ecosystem contains less than one percent four-winged saltbush (*Atriplex canescens*) (near Site 1) or one-seed juniper (*Juniperus monosperma*) and honey mesquite (*Prosopis glandulosa*) (near Sites 2 and 3).

2.6.2. Grassland Ecosystem

The principal grasses in the grassland ecosystem are blue grama (*Bouteloua gracilis*) (Sites 4 and 5), black grama (*Bouteloua eriopoda*), (Sites 4 and 5), bush muhla (*Muhlenbergia porteri*) (Site 4 and 6) and tobosa (*Hilaria mutica*) (Site 5). The grass interspaces range from 15 to 30 centimeters across and are not connected. The average height of the grasses is 30 centimeters. Tree cholla (*Opuntia imbricata*) and purple prickly pear (*Opuntia macrocentra*) are common cacti. Several types of weeds are present, depending on the site, with desert zinnia (*Zinnia acerosa*), hairy golden aster (*Heterotheca villosa*), Russian thistle (*Salsola iberica*), banana yucca (*Yucca baccata*),

squawbush (*Rhus trilobata*), and broom snakeweed (*Gutierre sarothrae*) being common.

2.6.3. Juniper Ecosystem

In the juniper ecosystem, the predominant juniper species is the one-seed juniper (*Juniperus monosperma*), with less than five percent piñón pine (*Pinus edulis*) and less than one percent Mexican piñón pine (*Pinus cembroides*) and Utah juniper (*Juniperus osteosperma*). The junipers tend to grow about five meters apart, with approximately six junipers in a ten meter radius. The juniper and piñón trees are around three meters tall. The prevalent grass is black grama (*Bouteloua eriopoda*). Other important plants in the ecosystem are squawbush (*Rhus trilobata*), banana yucca (*Yucca baccata*), hairy golden aster (*Heterotheca villosa*), broom snakeweed (*Gutierre sarothrae*), desert zinnia (*Zinnia acerosa*), and yellow toadflax (*Linaria vulgaris*). The spacing of the under-story plants are approximately one meter across on average and the interspaces are well connected.

2.6.4. Ponderosa Pine Ecosystem

The trees in the ponderosa ecosystem consist of approximately seventy percent ponderosa pine (*Pinus ponderosa*), twenty percent juniper, and ten percent piñón pine (*Pinus edulis*). Three types of juniper exist in this area: Utah juniper (*Juniperus osteosperma*), alligator juniper (*Juniperus deppeana*), and one-seed juniper (*Juniperus monosperma*), with one-seed juniper being predominant. The density of ponderosa pines are approximately six in a ten meter radius, having a one to five meter spacing, depending on maturity. The mature ponderosa pine trees are over thirty meters tall, and the juniper and piñón pine trees are around three meters tall. The predominant grass is black grama (*Bouteloua eriopoda*), and broom snakeweed (*Gutierre sarothrae*) and hairy

golden aster (*Heterotheca villosa*) are the predominant weeds. The under story plant
clusters are approximately 30 centimeters across and the interspaces are somewhat
interconnected. Depending on the distance from a ponderosa pine tree, pine needle
ground cover ranges from no cover to a depth of several centimeters.

2.6.5. Ecotone distance

An ecotone is the portion of the landscape where two ecosystems meet, creating
an area that contain characteristics of both ecosystems. The change in soil moisture
fluxes across ecotones is important when characterizing the effects of vegetation on these
fluxes, since the climate is nearly the same across ecotones. Sites along the transect were
also chosen for their proximity to an ecotone. There are two ecotones of particular
interest on the transect. One ecotone of interest on the transect is the grass-and-creosote
ecotone; this ecotone is diffuse, and the ecology changes from grass to creosote patches
several times between Drill Sites 1 and 6, which are four kilometers apart. Grass Site 6 is
around 120 meters from the closest creosote-dominated area, and Creosote Site 1 is
around 330 meters from the closest grass-dominated area.

The second ecotone of particular interest is the grass-and-juniper ecotone. This is
a fairly sharp ecotone and is approximately 340 meters from Grass Site 5 and 1,140
meters from Juniper Site 7. Sites 5 and 7 are approximately 1,480 meters apart from each
other. Grass Site 4 is also about 300 meters from a juniper-dominated area. The piñón-
juniper mix ecosystem was not sampled and there was not a juniper-and-ponderosa-pine
ecotone along the transect.

2.7. Paleoclimate and Paleoecology

A major change in the climate of a region affects its water balance and ecology. Paleoclimatic and paleoecological reconstructions determine the changes that have occurred as a result of a major climate change. Paleoenvironmental reconstructions were performed at paleolake San Agustin which is located near the Magdalena Sites. One study employed the oxygen isotope content of ostracode valves in order to achieve a high-resolution reconstruction of the time interval from 36 to 15 ka (thousand calendar years before the present time) (Phillips et al. 1992). The oxygen isotopic content of the valves varied depending on depth in the core and this reconstruction indicated that climate typical of full glacial period at the San Agustin Site began about 26 ka and ended about 20.6 ka (Phillips et al. 1992). The end of the full glacial climate marked the transition from a climate colder and wetter climate to that of today's warm and dry climate. Based on regional evidence, temperatures during the last glacial maximum were approximately six degrees Celsius less than in the present and precipitation was 20 to 40 percent greater than present (Plummer 2002). Following the last glacial maximum, temperatures increased by about four degrees Celsius between 18 and 12 ka, with the most dramatic warming occurring at around 15 ka (Plummer 2002).

Another study in the San Agustin plains was conducted using pollen, diatom, ostracode, and radiocarbon analyses to reconstruct paleoclimates. Four major paleoenvironmental phases were found: Between 18 and 15 ka, open *Pinus/Picea* woodland existed with abundant *Artemisia, Gramineae,* and *Compositae ubuliflorae,* which indicates the climate must have been cooler than today's, with predominately winter precipitation and dry summers (Markgraf et al. 1984). The next phase, between

15 and 10 ka, was not very different, with *Pinus, Artemisia,* and *Gramineae* showing a decrease and Juniper showing an increase in number. This demonstrates that the climate had not changed significantly (Markgraf et al. 1984). A major change occurred in the third phase, 10 to 5 ka, reflected by the disappearance of *Picea, Artemisia,* and *Compositae tubuliforae,* which left only *Pinus, Juniperus,* and *Gramineae* as the major components of the vegetation. This suggests that the temperature had increased and that the quantity of the precipitation decreased and/or the seasonality of the precipitation increased (Markgraf et al. 1984). The fourth phase, 5 ka to present, has high amounts of *Chenopodiineae* and *Sarcobatus* in addition to the pine, juniper, and grasslands previously found, indicating that the area has become even more arid, with similar vegetation as exists today (Markgraf et al. 1984).

The Sevilleta sites are located in the northernmost extent of the Chihuahuan desert. According to Van Devender (1990), during the late Wisconsin stage (20 to 10 ka) a piñón-juniper-oak woodland covered the rocky slopes of the entire elevational gradient of what is now occupied by the Chihuahuan Desert. Xeric desert scrub communities formed in the early Holocene epoch (10 to 8 ka) after piñón and juniper departed (Van Devender 1990). This was determined through the analysis of preserved packrat middens. Determination of paleovegetation using present packrat middens tends to bias the vegetation sampling to that of cave areas, where the middens are most likely to be preserved. Caves are usually found in areas of steep, rocky slopes, and thus the vegetation around a cave may not be the same as in the basin floor areas. Therefore, the packrat midden data for these areas should be interpreted with caution.

2.8. Disturbances of Plant Regimes.

At least since the arrival in the late 16th century of the Spanish in what was to become the state of New Mexico, people have been impacting the vegetation of the state through grazing, recreation, and fire suppression. Native Americans likely also influenced the environment, mainly through the setting of fires and engaging in agriculture along the Río Grande, which included water diversion (Scurlock 1998). Recent extensive droughts have also affected the present climate regimes.

2.8.1. Grazing

All areas of the transect have been grazed, mainly by cattle and sheep. Cattle have recently become the predominate grazing animal in the region, since they are less labor intensive than sheep (Scurlock 1998). The effects of grazing by cattle can cause the disappearance of valuable forage grasses, an increase in the amount of shrubs over large areas, and an acceleration of soil erosion (Hernandez et al. 1971). Overgrazing, which was common by the Spanish colonial and Mexican periods, and started in the late sixteenth century, became more intense and widespread with the arrival of the Anglo Americans (Scurlock 1998). Grazing mainly occurred in the Río Grande Valley area, where most of the early settlers lived. Large amounts of grazing did not occur in the forested areas of the mountains until the early 20th century (Scurlock 1998).

The Sevilleta National Wildlife Refuge is in the Río Grande Valley, but it has not been grazed at least since the Campbell family donated the land to the Nature Conservancy in early 1973. The Refuge was officially established on December 28th, 1973 (SNWR 2005). The process of desertification was thought to be well advanced when the Refuge was established, and vegetation recovery was predicted to take decades

or more (Hernandez et al. 1971). The Forest Service attempted to control grazing on its lands through strict law enforcement and the issuance of grazing permits beginning in 1912 (Scurlock 1998). Grazing presently continues in the Forest Service areas of the transect.

Several plants that were found at the study sites also indicate the ecosystems have been stressed by grazing. If a significant amount of poisonous plants are present, this demonstrates overgrazing of the grass to such an extent that the poisonous plant populations increase preferentially since they are not eaten by cattle. Broom snakeweed (*Gutierre sarothrae*) was the most extensively found weed throughout the transect. It was found in all but three sites, Sites 2, 6, and 8. Broom snakeweed plant is poisonous to cattle, causing calf abortions. The presence of this weed intermixed with grass indicates an improper utilization of pastures (Whitson 2001). Other plants identified at the sites, field pennycress (*Thlaspi arvense*), fringed sagebrush (*Artemisia frigida*), woolly plantain (*Plantago patagonica*), yellow toadflax (*Linaria vulgaris*) and Russian thistle (*Salsola iberica*), were all found in disturbed grasslands and wastelands (Whitson 2001). Silverleaf nightshade (*Solanum elaeagnifolium*) and twogrooved milkvetch (*Astragalus bisulcatus*) are both poisonous to livestock (Whitson 2001). The presence of these plants indicates that the study areas have been affected by grazing. Many of these plant are even found in the Sevilleta, which indicates that the area has not yet fully recovered from the grazing that ceased over thirty years ago.

2.8.2. Recreation

The Magdalena area sites within the Cibola Forest Service are used for recreation, mainly hunting, off-road vehicles, snow mobiles, and wood collection; trucks are also

commonly driven off of the established dirt roads. The effects of these activities on the vegetation is most likely similar to those found with grazing, but to a lesser degree. The Sevilleta Refuge is fenced in and locked to the general public; the only use of the Refuge is by researchers, wildlife managers, and utility workers. Their impact on the vegetation of the Sevilleta sites is much less than the impact of people on the Magdalena area sites.

2.8.3. Fires

Since the last ice age, lower-elevation forest lands have evolved with the influence of relatively frequent, episodic fires that were generally of low intensity. Fire frequency is correlated with the presence of fuel sufficient to effectively spread the fire over the landscape (Scurlock 1998). This frequency, for pre–1900 fires, varied from every two to ten years for ponderosa and mixed conifer forests. Fires in the higher spruce-fir and lower piñón-juniper forests had a frequency between 50 and 300 years and were of high intensity (Scurlock 1998).

Fire frequency in New Mexico generally declined sharply after 1880 (Scurlock 1998). This decline was initially the result of grazing that began in the area, which decreased the ground fuels. Fire suppression became common in the 1920s, mainly in the ponderosa pine areas. The decline in forest fires through artificial suppression changed the ecology, causing an increased growth of underbrush. This increase in underbrush also increases the intensity of any fires that do occur, resulting in significant damage to the forest.

2.8.4. Drought

Drought can alter the water balance and ecology of an area. At least 52 droughts

lasting one year or more, totaling about 238 years, occurred in the Middle Río Grande

Basin in a 448 year historic period. Droughts, therefore, have had a mean occurrence of

8.6 years, and a mean length of 4.6 years (Scurlock 1998). The most extreme drought in

the past century occurred in the early 1950s (Scurlock 1998). There is also widespread

agreement that a severe drought was in progress in New Mexico at the time of drilling

(Booker et al. 2005). While these droughts have a natural and regular cycle, they will

have a temporal effect on the vegetation.

2.9. Hydrogeology of the Transect Area

There are three major groundwater basins in the transect area, as shown in Figure

2.11. These basins are the La Jencia Basin, the Albuquerque-Belen Basin, and the San

Agustin Basin. The La Jencia Basin, a partly-closed basin, is bounded on the west by the

Bear Mountains, on the south and west by the Magdalena Mountains, and the north by

the Ladron Mountains. The principal aquifer system in the La Jencia Basin is composed

of Quaternary and Tertiary Santa Fe Group deposits. This principal aquifer system can

be divided into the shallow aquifer, the Popotosa confining bed, and the Popotosa aquifer

(Anderholm 1987a).

The San Agustin Basin is a closed basin thus is bounded on the west and south by

the Continental Divide, on the north by the Datil and Gallinas Mountains, and on the east

by the Gallinas and San Mateo Mountains. The San Agustin Basin aquifer consists of

alluvial and bolson-fill deposits and the Gila Conglomerate in the San Agustin Graben

(Myers et al. 1994).

The Albuquerque-Belen Basin is an open basin, which is drained by the Río

Grande. The basin is bounded on the east by the Sandia, Manzanita, Manzano, and Los

Piños Mountains. The Joyita Hills, Socorro Basin, and Ladron peak border the basin on

the south. The western basin boundary consists of the Lucero uplift and the Río Puerco

fault zone. The Nacimiento uplift, Jemez volcanic complex, and Santo Domingo basin

border the basin on the north. The Albuquerque-Belen Basin aquifer consists of basin-fill

deposits of interbedded gravel, sand, silt, and clay and are of late Oligocene to Holocene

in age (Anderholm 1987b).
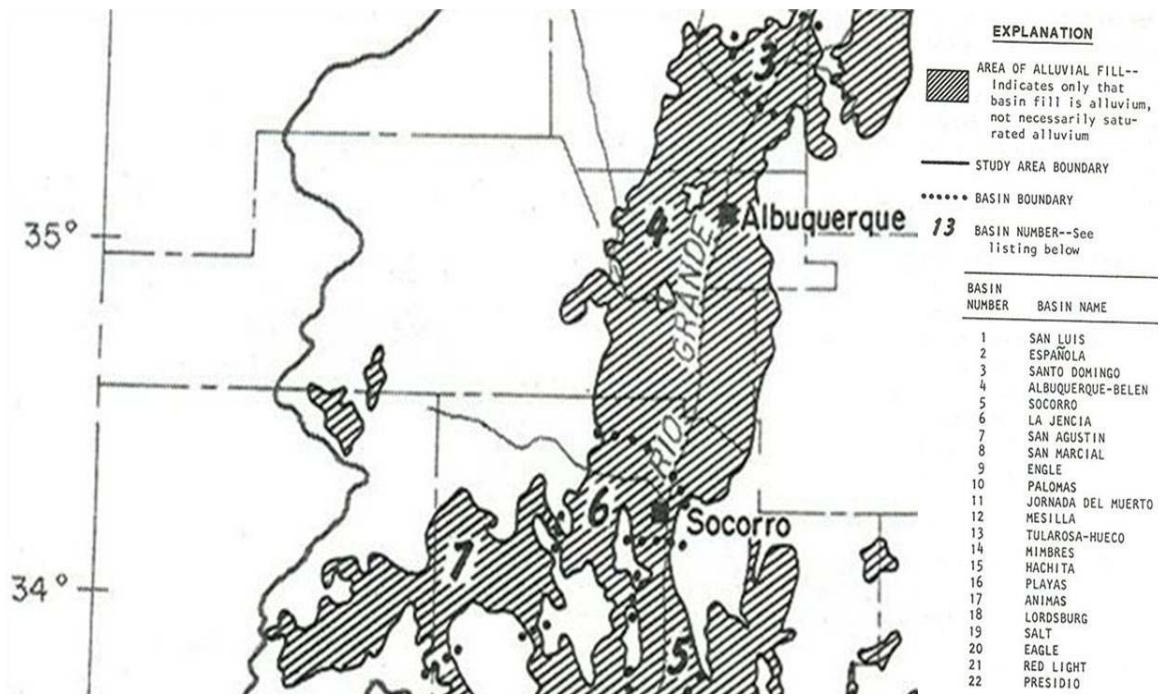
Figure 2.11. The three basins of the study area, La Jencia Basin (6), Albuquerque-Belen Basin (4), and the San Agustin Basin (7). Modified from Anderholm (1987a). Not all basins listed are shown, only those pertinent to this study.

CHAPTER 3

MATERIALS AND METHODS

3.1. Drilling Method

A hollow-stem auger drill rig with a split-spoon sampler was utilized to obtain the soil cores at the sites. No fluids were used in the drilling. Hammer percussion advanced the sampler ahead of the rotating auger so that mixing of the soil sample did not occur. The soil samples can become compacted using this method, but not mixed. The split-spoon sampler was five feet long with a two inch inner diameter and a three inch outer diameter. It included a trap at the end to prevent the soil from falling out of the sampler during removal from the auger hole; see Figure 3.1. Immediately after the sampler was removed, it was opened and the soil was placed into plastic, sealable freezer bags, removing as much air from the bag as possible. The samples were taken in approximately 15 centimeters long sections. These bagged samples were then placed into another bag, then into a cooler to prevent sun exposure and tearing. The sample bags were taken to the lab at the end of each field day. To prevent water loss, these bags were not reopened until the water potential and water content were to be determined for that sample.
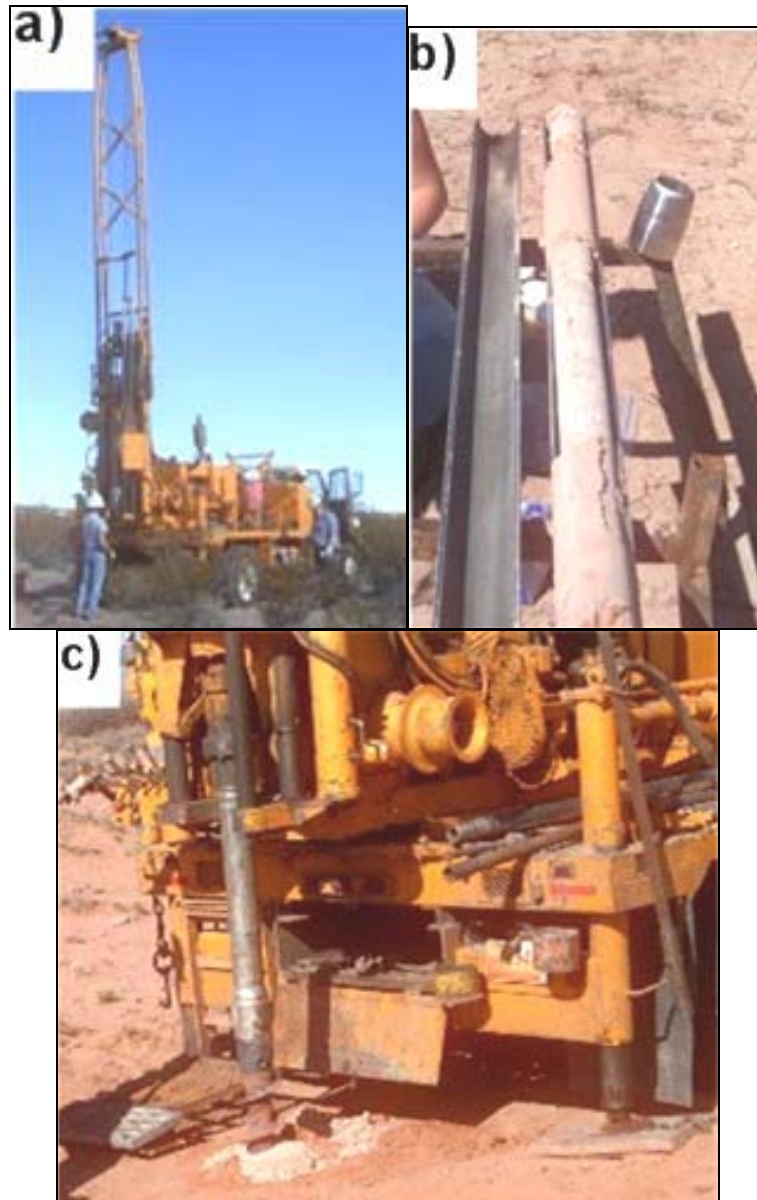
Figure 3.1. Pictures of core drilling. a) Hollow stem auger drill rig. b) Open split spoon sampler with soil recovery. c) Rotating hollow stem auger.

3.2. Subsurface Electrical Conductivity

An EM31 meter was used to determine the electrical conductivity of the subsurface soil of the drill sites. This meter can determine the conductivity to a depth of six meters in the vertical dipole position, as shown in Figure 3.2. A grid of measurements was taken in four twenty meter long transects that ran through the proposed site, as shown Figure 3.3. Measurements were taken in this pattern to sample

69

more intensively the area closest to the proposed site versus areas further away. The

conductivity values are in milliSiemens per meter (μS m^{-1}) units. The EM31 dial reading

multiplied by the range setting determines the conductivity in mS m^{-1}. The EM31 meter

was not calibrated for individual readings. The homogeneity of the soil is determined by

difference between the readings, not the absolute measurements. To make sure the

subsurface was relatively homogenous and there were no large rocks or boulders to

impede drilling, the measurements were taken before drilling took place. If the

conductivity values near the site varied by more than 15 mS m^{-1}, then another site was

surveyed. Soil conductivity values that varied less than 6 mS m^{-1} near the site were

considered homogenous.

Figure 3.2. The EM31 meter in use, with the EM the pole being 3.7 meters long, worn at hip level in the vertical dipole position.
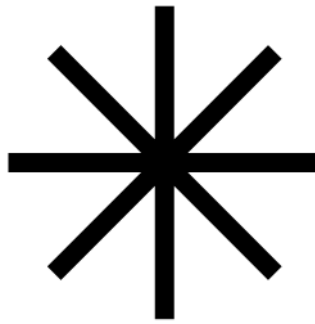
Figure 3.3. Pattern of EM31 measurements. Each transect line was 20 meters long. The center was the proposed site location.

3.3. Soil Tests

Several tests were performed on the soil taken from the drill cores.

3.3.1. Anions

Soil samples were leached to extract all water soluble anions. This was done by placing approximately 100 grams of soil and 100 grams of 18 Ω de-ionized water into a cup that was then sealed. These cups were then slowly rotated, head over heels, for at least 24 hours. McGurk and Stone (1985) demonstrated that the adequate shaking time for leaching soil of chloride is eight hours, regardless of soil type. Therefore, 24 hours of slow rotation is considered more than sufficient to leach all the chloride and other anions from the soil sample. After allowing the soil in the samples to settle, water was removed for analysis. The concentrations of the anions were determined by means of ion chromatography. The anions concentrations were determined for chloride, bromide, fluoride, nitrate, nitrite, phosphate, and sulfate.

3.3.2. Water Potential

The water-potential values for the samples were measured by the use of a water-potential meter, as shown in Figure 3.4. The value obtained using this method is a

measure of both matric and osmotic potential since the method measures water vapor pressure, not the liquid water (WP4 1998). The meter was calibrated before each use with a manufacturer-prepared standard. The meter used was a WP4 Dewpoint PotentiaMeter, made by Decagon Devices, Inc., and it has a measurement range of -60 to 0 MPa (megaPascals). It has an accuracy of ± 0.1 MPa from 0 to – 10 MPa and an accuracy of ± 0.01 from -10 to -60 MPa (WP4 1998). The method of determining soil water potential and a description of the meter's operation are outlined by Gee et al. (1992).

Figure 3.4. The water potential meter used in this study, with the sample placement drawer open.

3.3.3. Bulk Density

The bulk density of the soil cores were necessary to determine the volumetric water content and integrated soil profile parameters such as total chloride deposition or matric potential. The bulk density was determined by using the paraffin-clod method, as outlined by Singer (1986). For this method, a structured aggregate of soil (also referred to as a clod or ped) is oven dried, a string is added around the ped, and the ped is weighed. All weight measurements for this method used the same triple-beam balance. This ped is

then dipped into paraffin wax and weighed again. The wax-covered ped was then suspended in water and weighed again. The wax-coated ped was then broken open and any particles greater than 2 millimeters were removed from the ped and weighed separately. The calculation of the bulk density from these measurements is also outlined in the Singer method (Singer 1986). For each sampled depth interval, bulk-density measurements were taken for two peds, which were then averaged.

Peds were taken from the core samples. Not all of these core samples contained usable peds; therefore, peds were not available for all core sections. The bulk-density values were extrapolated to missing core sections according to their soil textures and sample sites. The use of hammer percussion to obtain the soil samples decreases the possibility of sample mixing, but it increases the possibility of soil compaction. In the field, soil compaction occurred for the split-spoon sampling cores. Since the entire sample was present, this was not a concern for most parameters determined for the soil sample; compaction was a concern only for bulk-density measurements. To determine whether or not the peds taken from the core were compacted, the bulk-density measurements of peds from soil pits dug near the drill site were used included for comparison.

3.3.4. Water Content

The soil-water content was determined by weighing a small aluminum pan, placing the soil sample in the pan, and then weighing it again. The samples were dried in an oven at least 105 degrees Celsius for at least 24 hours. The samples with obviously high clay contents were dried for another few days to make sure all water was released. The dried soil and pan were then weighed again. The weight of the water in that sample

73

was determined by taking the difference between the dry and wet weights. A water density of one gram per milliliter was assumed to determine the pore water volume of the soil sample. The gravimetric water content and pore-water volume were calculated using the following formulas:

$$Gravimetric\ Water\ Content = \frac{water\ weight\ (g)}{dry\ soil\ weight\ (g)}$$

$$Pore\ Water\ (L) = \frac{water\ weight\ (g)}{dry\ soil\ weight\ (g)} * \frac{0.001\ L\ water}{1\ g\ water} * dry\ soil\ sampled\ (g)$$

3.3.5. Particle Size and Soil Texture

Particle sizes were determined for sections of the soil profile. Continuous sections of similar soil type in the soil profile were determined by appearance and texture. The particle size was determined via sieving soil samples and observing the settling time of the soil particles in water according to the method outlined by Janitzky (1986). This method results in a percentage by weight of sand, silt, and clay in the soil sample. Sand particles are considered greater than 50 μm, clay less than 2 μm, and silt between 2 and 50 μm, following the United State's Department of Agriculture (USDA) scheme for the classification of soil fractions according to particle diameter ranges. The soil textural class was determined for each sample based on the mass percentages of sand, silt, and clay. These textural classes were determined based on the USDA textural triangle (Soil Survey Staff 1999).

3.3.6. Calcium Carbonate

The calcium carbonate content was also determined for continuous sections of the soil profiles. These sections were determined based on the color and bubbling intensity

of acid dropped on the sample. The carbonate content was determined by drying the soil sample and placing a known amount of sample into a sealed chamber, then placing a predetermined amount of acid on it in order to convert the carbonate into carbon dioxide gas. The amount of carbon dioxide gas produced was measured by recording the water level change of the attached tube. The amount of generated carbon dioxide gas was then converted to the percentage of carbonate in the sample. This was done according to the method outlined by Machette (1986).

3.3.7. Leachate Electrical Conductivity and Osmotic Potential

The electrical conductivity of the soil leachates was determined through the use of a portable electrical conductivity (EC) probe. The probe was calibrated before use and every 20 readings thereafter. The EC probe was an Oakton 35607-20, con-200 series probe. All EC values were taken in microSiemens per centimeter ($\mu S\ cm^{-1}$). Since the presence of anions increases the conductivity of water, the electrical conductivity of the leachate can be converted into a rough estimate of the osmotic potential by the following two methods.

Since the EC value of the soil leachate, and not the pore water, was taken, the EC value was corrected to that of the pore water with the use of the EC correction factor, as shown in equation 8.

$$EC\ Correction\ Factor = \frac{Volume\ of\ Leachate + Volume\ of\ Pore\ Water}{Volume\ of\ Pore\ Water} \tag{8}$$

The first method converts EC directly to osmotic potential. According to the United Nations Food and Agriculture Organization (FAO) (Abrol et al. 1988), the conversion directly osmotic potential directly from EC is as shown in equation 9.

$$EC\ (\mu S\ cm^{-1}) * 0.36 = Osmotic\ Potential\ (kPa) \hspace{2cm} (9)$$

The second method converts the EC value to parts per million of salt (ppm, or mg L^{-1}), assuming the salt was either all NaCl or $CaCO_3$, then it converts the EC value to osmotic potential using equations 10 and 11.

$$EC\ (\mu S\ cm^{-1}) * 640 = ppm\ concentration\ (Abrol\ et\ al.\ 1988) \hspace{1cm} (10)$$

$$Osmotic\ Potential\ (kPa) = n * C * R * T \hspace{2cm} (11)$$

where:

n = number of dissociable particles per molecules (2 for both salts)

C = concentration (moles L^{-1}), assuming all the salt was either all NaCl or all $CaCO_3$

R = ideal gas constant, 0.08205 L atm mol^{-1} K^{-1}

T = temperature (assumed to be 293 Kelvin).

Because the amount of either salt in the sample is unknown, this method produces two values for osmotic potential. Since the first method of using the direct conversion from EC to osmotic potential yielded values between the two extremes of assuming the salts consisted entirely of either NaCl or $CaCO_3$, this method was considered to result in the most reasonable estimate of osmotic potential for this application.

As described in Section 3.3.2, the measured water potential values include both matric and osmotic potentials (WP4 1998). Therefore, to obtain matric potential, the estimated osmotic potential values can be subtracted out of the measured water potential values for that sample to determine its matric potential. Since no known semi-permeable membrane was present in the study, the matric potential and the gravity potential constitute the total potential of the liquid soil water (Hillel 1998). The gravitational potential was determined from the depth of the soil sample from the soil surface.

Therefore, the gravitational potential of the soil-water is negative since the samples were below the datum. The soil surface was chosen as the datum, since the depth to the groundwater tables were estimated for each site from a map that interpolated the groundwater levels between well measurements and therefore contain some uncertainty. The direction of water movement in the depth profile can be determined from the gradient of the total potential (Hillel 1998). Since the datum was chosen as the soil surface, negative total potential gradients are downward in direction and positive are upward.

3.4. Rock Identification

Rocks found in the soil cores were identified. The amount of a certain type of rock or the position of the rock in the core were not determined, with the exception of Sites 10 and 11, where important depth patterns were noticed during drilling. The presence of calcium carbonate, as a weathering product within or coating the rocks, was determined using carbonic acid. When possible, the mineral crystals within the rocks were determined.

3.5. Soil Pit Characterization

After drilling had taken place, soil pits were dug at the four sites. These pits were dug to determine root density and distribution as well as ped compaction. The pits were dug to a depth between 77 and 135 centimeters. Soil horizons were determine by appearance and texture. Peds were taken for each identified soil horizon. Each soil horizon was described using the descriptive terminology developed for use by soil scientists (Soil Survey Staff 1993). For each horizon, dry and wet Munsell color,

structure, gravel percentage, consistence, texture, clay films, pores, carbonates, and boundaries were described.

3.6. Root Density and Distribution Analysis

A soil pit was dug at four sites, to determine the root distribution and density of each vegetation type. Soil pits were dug at Site 1 for creosote, Site 5 for grass, Site 8 for juniper, and Site 11 for ponderosa pine. The roots in a 10 by 10 centimeter square, as in Figure 3.5, were counted according to size classes with a diameter of less than one millimeter, between one and ten millimeters and greater than ten millimeters, noting any very large roots. Three replicates were performed per 20 millimeter depth increment and averaged by size class, then by number-per-depth increment for root density.

Figure 3.5. The 10 by 10 centimeter square used to count roots in the soil pits.

3.7. Infiltrometer

A tension infiltrometer, manufactured by Soil Measurement Systems and described in Ankeny et al. (1991), was used to determine the surface saturated hydraulic conductivity of each surface soil type found at the sites where textural analysis was preformed; this is described in Section 3.3.5. Surface saturated hydraulic conductivity determines the maximum infiltration rate possible into a specific soil type. To set up the infiltrometer at the site, rocks and plant material were cleared from a small area. A level

ring of pure sand was placed on the surface of the soil. Both tubes of the infiltrometer were filled with water. The infiltrometer disc containing a membrane was soaked in a bucket of water and all air bubbles were removed; the disc was then placed on the ring of sand. The system was checked for air bubbles, then all clamps were opened. The tension stick was raised and lowered until a steady stream of about one bubble per two seconds was exiting the tension stick. See Figure 3.6 for pictures of the infiltrometer setup.

The infiltrometer was left flowing at the site for about two hours. Readings were then taken every five minutes and once they decreased at a constant rate three consecutive intervals, they were no longer taken. The tension stick was then raised up, and readings were again taken until equilibrium was reached. Three measurements were taken per infiltrometer, and there were two infiltrometers per site. If all six measurements were successfully taken, this would result in six saturated hydraulic conductivity values per surface soil type; these values were then averaged. Hydraulic conductivity was determined using equations 12, 13 and 14.

$$Q = \pi\, r^2\, v \tag{12}$$

$$\alpha = \frac{\ln\left[Q(h_2)/Q(h_1)\right]}{h_2 - h_1} \tag{13}$$

$$Q(h) = \pi\, r^2\, K_{sat}\, \exp(\alpha\, h)\left[1 + \frac{4}{\pi\, r\, \alpha}\right] \tag{14}$$

where:

Q = volume of water entering the soil per unit time ($cm^3\ hr^{-1}$)

r = radius of water supply tube of the tension infiltrometer (2.225 cm)

v = rate of decrease of the water level in the water supply tube ($cm\ hr^{-1}$)

h = tension (cm)

K_{sat} = saturated hydraulic conductivity ($cm\ hr^{-1}$)

α = Van Genuchten parameter.

Equation 14 is then solved for saturated hydraulic conductivity. That value is used in equation 15 to obtain unsaturated hydraulic conductivity.

$$K(h) = K_{sat} \exp(\alpha\, h) \tag{15}$$

The relationship between the tension and the unsaturated hydraulic conductivity is non-linear. This method follows that outlined for tension infiltrometers by Ankeny et al. (1991).
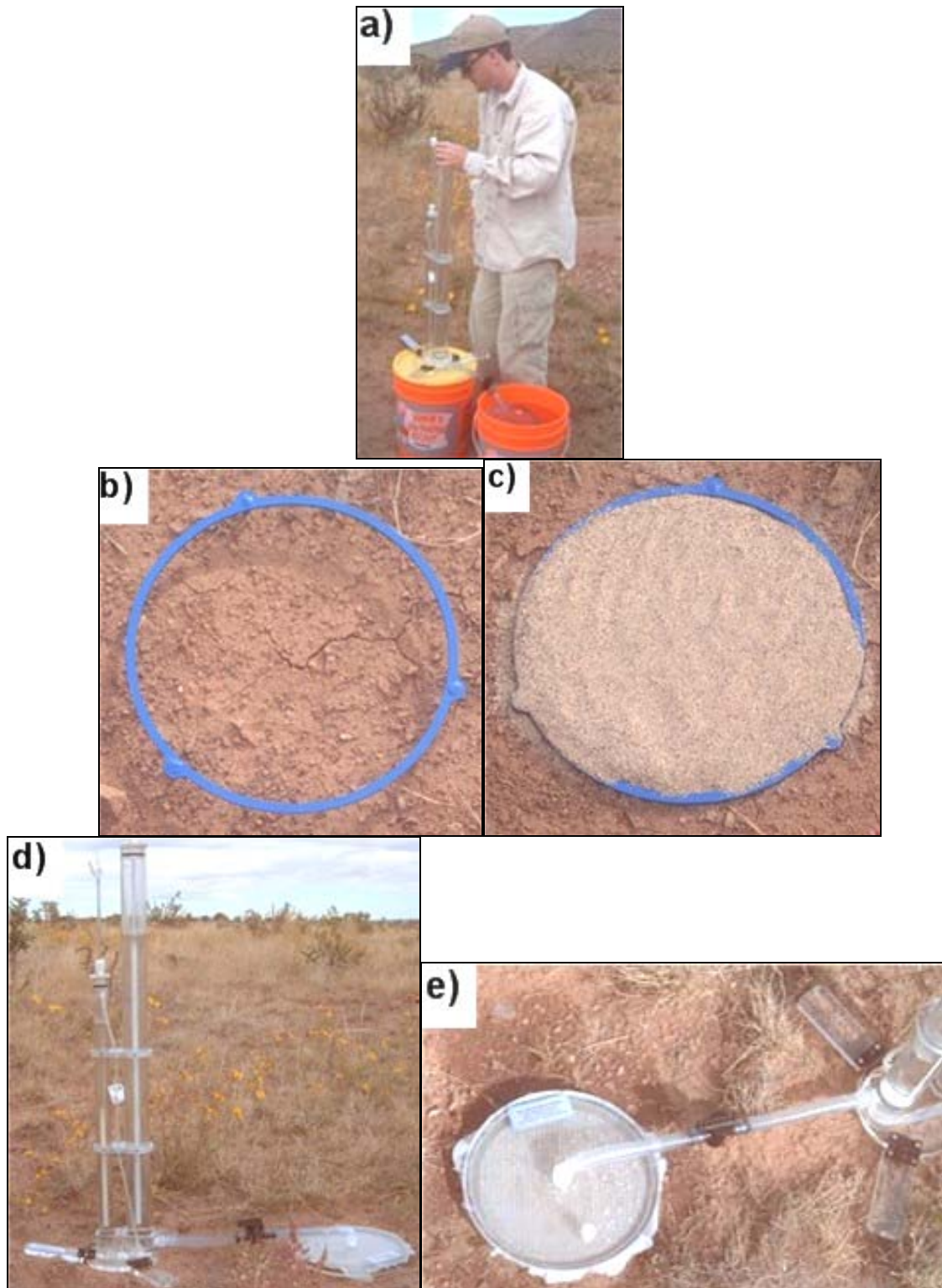
Figure 3.6. Tension infiltrometer pictures. a) The infiltrometer being setup in the field.
b) Ring around area that has been prepared, free of rock and plants. c) Ring area filled
with pure sand and leveled. d) Infiltrometer in use. e) Infiltrometer disc in use.

CHAPTER 4

RESULTS

4.1. Introduction

The results of all experimental measurements are contained in this chapter, either in graphical or written form. A listing of the individual data points are located in Appendix B. Table 4.1 summarizes the precipitation, potential evaporation, aridity index, and temperature parameters for each site, as obtained from the GIS data maps discussed in Section 2.2. Table 4.2 summarizes key site parameters, such as vegetation, latitude and longitude coordinates, elevation, slope and aspect, and groundwater table depths for each site. With the exception of these summary tables, all other data are organized on a site-by-site basis.

Site #	Average Annual Temperature (° C)	Average Annual Precipitation (mm)	Average Annual PE (mm)	Aridity Index (-)
1	12.8	231	1,530	6.70
2	13.3	235	1,530	6.67
3	13.3	230	1,530	6.67
4	12.0	302	1,280	4.21
5	12.2	306	1,270	4.13
6	12.8	230	1,460	6.34
7	12.1	306	1,270	4.13
8	11.7	308	1,240	3.92
9	11.5	316	1,240	3.92
10	9.5	336	1,220	3.64
11	9.2	327	1,220	3.72

Table 4.1. Summary of the climatic parameters for each site as obtained from the GIS data maps discussed in Section 2.2. PE refers to potential evaporation. Temperature and PE values were averaged daily, then yearly. These yearly values were then averaged with the data for the other years. Precipitation values were totaled for each year and then averaged with the data for other years.

Site #	Vegetation	Latitude	Longitude	Elevation (m)	Slope (°)	aspect (°)	Depth of Drill Hole (m) (depth to rock)	Groundwater Table depth from surface (m)	Alluvial Basins
		(decimal degrees)							
1	creosote	34.371417	106.950967	1,590	2.0	320	8.95	> 91[b]	ABQ-Belen
2	creosote	34.288150	106.899600	1,470	1.5	270	7.50	40[b]	ABQ-Belen
3	creosote	34.294183	106.919083	1,500	1.5	0	8.70	40[b]	ABQ-Belen
4	grass	34.267817	107.224167	1,880	1.5	40	9.00	47[a]	La Jencia
5	grass	34.211783	107.218917	1,900	2.0	50	5.25	57[a]	La Jencia
6	grass	34.355217	106.990383	1,560	1.0	60	4.50	> 91[b]	ABQ-Belen
7	juniper	34.213550	107.234967	1,930	1.5	140	9.00	68[a]	La Jencia
8	juniper	34.181417	107.297700	2,040	1.5	180	5.40	115[a]	La Jencia
9	juniper	34.184467	107.317183	2,050	1.0	180	8.70	107[a]	La Jencia
10	ponderosa	34.187367	107.453500	2,300	6.0	20	4.80 (2.70)	113[c]	San Agustin
11	ponderosa	34.195067	107.479750	2,380	2.5	10	4.80 (2.85)	122[c]	San Agustin

Table 4.2. Summary of the physical parameters of the sites. "Groundwater Table depth from surface" column footnotes refer to the source for that data, as listed below.

a. Anderholm 1987a
b. Anderholm 1987b
c. Myers et al. 1994

4.2. Data Extrapolation

Soil parameters for some of the depth intervals were estimated to economize on the time and funding. These parameters were bulk density, particle size, and calcium carbonate content. For the bulk-density measurements, peds were taken from the core samples, but not all core samples contained usable peds. They were also taken from soil pits dug at some of the drill sites. Even with these two sources, peds were not available for all depth intervals. The bulk-density values were extended to missing depth intervals according to their respective soil textures and sample sites. In order to extrapolate the calcium carbonate values, the calcium carbonate content was determined for continuous sections of each soil profile, where sections were identified according to color and bubbling intensity of acid dropped on the sample. Similarly for particles size extrapolation, measured particle size was extended over sections of the soil profile. Continuous sections of similar soil type in a soil profile were determined by appearance and texture.

4.3. Site 1 – Creosote – Sevilleta Site

Figure 4.1. Picture of Site 1, looking west. Sierra Ladrones in the right, top of picture.

4.3.1. Site Description

Site 1 (Figure 4.1) is located in the Sevilleta National Wildlife Refuge. The latitude and longitude of the site are 34.371417 and 106.950967 decimal degrees, respectively. The elevation is 1,590 meters above sea level, and the slope and aspect of the site are 2 and 320 degrees, respectively. The depth of the drill hole at this site was 8.95 meters. The depth of the groundwater table below the surface is estimated to be at least 91 meters. This site lies within the Albuquerque-Belen alluvial groundwater basin (Anderholm 1987b). The soil at this site is classified as a Torrifluvent Entisol. This classification was obtained from a map of soil taxonomy that was based on data from the Natural Resources Conservation Service (Soil Map 2005, Soil Survey Staff 1999).

The average annual temperature for this site is 12.8°C (Celsius), the average annual precipitation for this site in 231 millimeters and the average annual potential evaporation is 1,530 millimeters; this yields an aridity index of 6.70. These data were obtained from the GIS maps presented in Section 2.2; they demonstrate that this site is

the warmest and most arid of the transect. The predominant vegetation of this site is creosote bush. The Sevilleta has not been grazed at least since the Campbell family donated the land to the Nature Conservancy in early 1973. The refuge was officially established on December 28, 1973 (SNWR 2005).

4.3.2. EM31 Data

The subsurface electrical-conductivity data were measured using an EM31. Just before drilling took place, Site 1 had to be moved from its proposed location due to problems with drill rig access. This new location placed Site 1 outside of the area assessed using the EM31. Therefore, no EM31 data exists for the actual Site 1 drilling location.

4.3.3. Plant Identification and Density

Site 1 contains approximately forty-five creosote bushes (*Larrea tridentata*) within a ten meters radius of the drill site. The bushes are 60 to 150 centimeters tall and are spaced 30 to 90 centimeters apart. All of the grass was senescent when the area was sampled, but bush muhla (*Muhlenbergia porteri*) grass was found nearby. Broom snakeweed (*Gutierre sarothrae*) and purple prickly pear (*Opuntia macrocentra*) were also found on the site. The underbrush clumps are spaced about 30 to 150 centimeters apart and the interspaces are connected. Creosote almost completely dominates the area's ecosystem, which consisted of less than one percent four-winged saltbush (*Atriplex canescens*). Approximately 90 meters from the site, grass (bush muhla) areas predominant.

4.3.4. Site Distance from Ecotone

Site 1 is located near a grass and creosote ecotone. This ecotone is diffuse, and the ecology changes from grass to creosote patches several times between the two closest grass and creosote drill sites, Sites 1 and 6, which are four kilometers apart. This site is around 330 meters from the closest grass-dominated area.

4.3.5. Geology

This site is on an alluvial fan originating from the Sierra Ladrones to the west. Most of the rocks that were in the soil core of Site 1 were igneous rocks. Chert, a sedimentary rock, was also present. Basalt was the dominant rock, containing noticeable biotite, olivine, and feldspar crystals. Rhyolite, containing feldspar, biotite, and sanidine crystals, and granite were also found in this core. Most rocks were coated with calcium carbonate.

4.3.6. Graphical Summary of Major Parameters

The major parameters associated with depth are shown in Figure 4.2; each parameter is placed side by side for comparison.
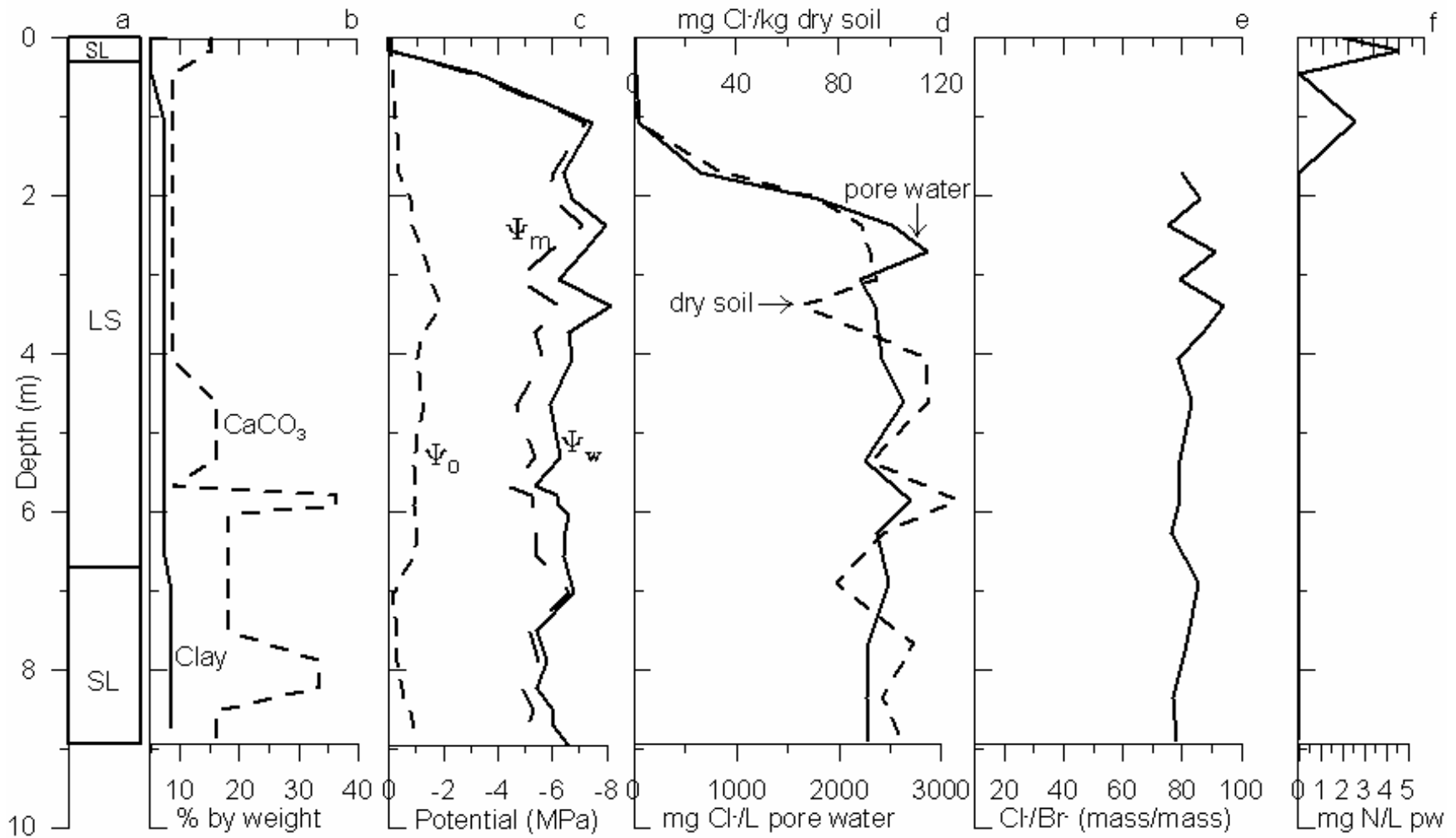
Figure 4.2. Profiles for Site 1 of a) soil texture, b) % CaCO3 and clay by weight, c) osmotic (Ψ_o), matric (Ψ_m), and water (Ψ_w) potential, d) mg Cl- per Liter of pore water (pw) or per kg dry soil, e) Cl-/Br- ratio, does not include ratios with non-detect bromide levels, f), and mg total Nitrogen/Liter pw. SL = Sandy Loam, LS = Loamy Sand Soil. $\Psi_o + \Psi_m = \Psi_w$

88

4.3.7. Soil Pit Characterization

A 135 centimeter-deep soil pit was dug approximately two meters from drill Site 1. The soil profile is shown in Figure 4.3; Tables 4.3 and 4.4 show the soil description.
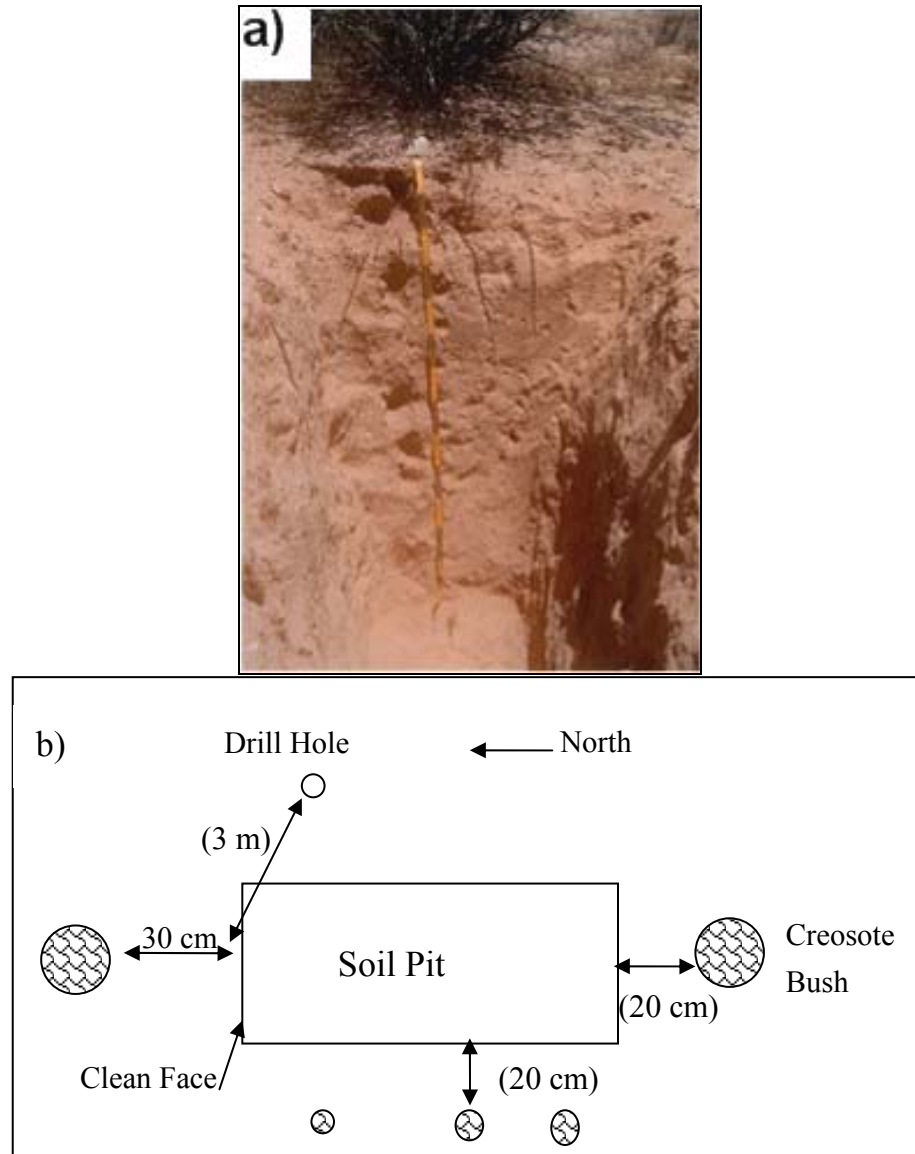
Figure 4.3. Soil pit at Site 1. This pit was dug to a depth of 135 cm. a) The clean face is shown, and each black and yellow stripe on the measuring tape denotes 1 meter. The bottom of a creosote bush can be seen at the top of the picture. b) A plan-view diagram of the soil pit in relation to nearby creosote bushes trees and drill site. This diagram is not to scale. Lengths in parentheses are estimated.

| | | | | Structure | | | | Consistence | | | |
| | | | | | | | | wet | | | |
Horizon	Depth (cm)	dry color	moist color	ped grade	ped size	ped shape	% gravel	sticky	plasticity	dry	Texture
A	0 to 7	7.5 YR 6/4	7.5 YR 4/4	1	f	sbk	<10	ss	ps	so	SL
A/B	7 to 20	7.5 YR 7/4	7.5 YR 4/4	2	c	sbk	<10	ss	ps	H	L
Bk1	20 to 60	7.5 YR 6/3	7.5 YR 4/4	2	m - c	sbk	<10	ss	ps	so	SL
Bk2	60 to 75	7.5 YR 7/4	7.5 YR 4/6	2	f	sbk	20	ss	ps	so	SL
Bk3	75 to 100	7.5 YR 7/4	7.5 YR 5/4	2	m	sbk	<10	ss	ps	so	SL
Bk4	100 to 135	7.5 YR 7/3	7.5 YR 4/4	2	m	sbk	<10	ss	ps	sh	SL

Location: Site 1, Sevilleta
Aspect: North
Vegetation: Creosote
Date/time: 6/23/2004 10 am

Table 4.3. Soil pit characterization at Site 1. The soil description method used follows the procedure outlined by the Soil Survey Staff (1993). f = fine, m = medium, c = coarse, sbk = subangular blocky, ss = slightly sticky, ps = slightly plastic, so = soft, sh = slightly hard, h = hard, SL = sandy loam, L = loam.

| | | Roots | | | Pores | | Boundary | | |
	Clay films	frequency class	size	nature	frequency class	size	distinctness	topography	Carbonate
A	none	2 (common)	vf – f	woody	none		clear	smooth	stage 1
A/B	none	2 (common)	vf - c	woody	1 (few)	fine	clear	wavy	stage 1
Bk1	none	1 (few)	vf – f	woody	1 (few)	m	clear	wavy	stage 1
Bk2	none	1 (few)	vf – f	woody	1 (few)	fine	clear	wavy	stage 1+
Bk3	none	1 (few)	vf	woody	1 (few)	fine	clear	wavy	stage 1
Bk4	none	1 (few)	vf	woody	1 (few)	fine	buried	buried	stage 1+

Table 4.4. Soil pit characterization at Site 1 (continued). The soil description method used follows the procedure outlined by the Soil Survey Staff (1993). vf = very fine, f = fine, m = medium, c = coarse.

4.3.8. Root Density Analysis

A root density analysis for a creosote bush, which was 31 centimeters from the clean face of the soil pit at Site 1, was performed using a ten by ten centimeter square for sampling. There was some grass underneath the shrub; if they were located within the sampling area, the roots of this grass were also included in this analysis. The results of this analysis are shown in Table 4.5. All roots with a diameter greater than 1 millimeter were located at a depth of twenty centimeters, spreading laterally as shown in Figure 4.4.

A close-up of these larger roots is also shown in this Figure. Roots less than 1 millimeter in diameter were found throughout the profile, with only a few in the bottom of the pit.

Depth (cm)	Average # of Roots with noted Diameter			Total	%	Notes
	< 1 mm	1 - 10 mm	> 10 mm			
0 to 20	55	0.67	0	55	27	
20 to 40	55	4.3	0	59	29	All larger creosote roots were located at 20 cm depth, laterally spread and having diameters from 0.25 to 1 cm.
40 to 60	25	0.67	0	26	12	
60 to 80	23	0.67	0	24	12	
80 to 100	21	0	0	21	10	
100 to 130	22	0	0	22	10	
			Total	207		Very few roots at bottom of pit.

Table 4.5. Root density analysis of creosote bush at Site 1. Values shown are the average number of roots of that diameter of the three replicates taken at each depth interval. A 10 by 10 cm square was used to count the roots. The majority of the roots were located in the upper two measured intervals.
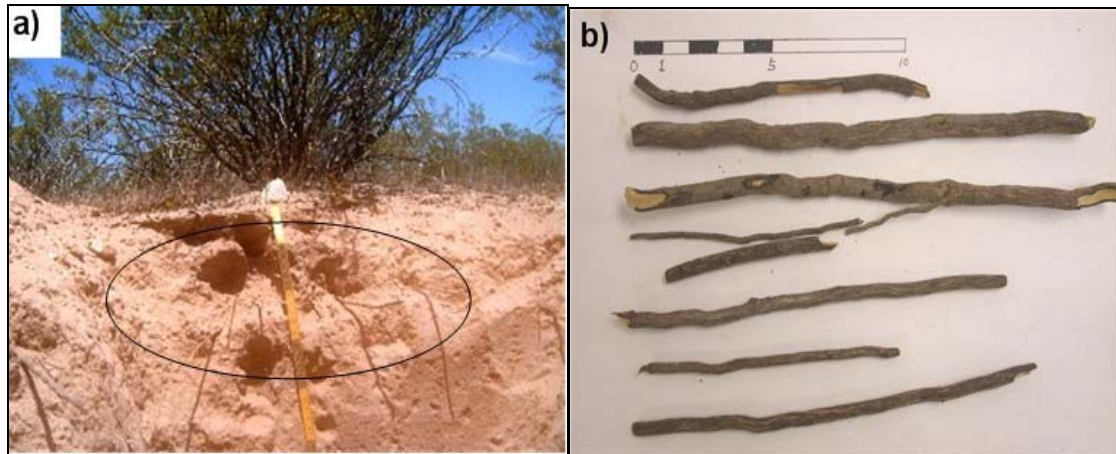
Figure 4.4. Root density analysis of creosote bush at Site 1. a) The larger roots of the creosote bush, as indicated by the black oval, spreading laterally at 20 cm depth. The creosote bush is located in the top half of the picture. The black and yellow sections of the measuring tape are 1 meter. b) These same large roots are shown in a close up laboratory picture. The ruler shown is in centimeters. The diameters of the larger roots ranged from 0.25 to 1 cm.

4.3.9. Bulk Density from Soil Pit and Soil Core

The bulk density of the peds found in the core and soil pit are shown in Table 4.6.

Since peds originated from both the wall of the soil pit and the core, any possible

compaction of the peds in the soil core can be determined. When comparing the averages

of the bulk densities of both the core and the pit peds, there is no significant difference

between them, demonstrating that there was slight-to-no compaction of the peds in this

soil core.

Site 1 – Pit Source of Peds		
Bulk Density (g cm^{-3})	Depth (m)	Soil Texture
1.77	0.09	SL
1.38	0.34	LS
1.61	1.02	LS
1.69	1.71	LS
1.34	2.22	LS
1.61	2.98	LS
Average Bulk Density (g cm^{-3})		# Samples
1.57 ± 0.17		6
Site 1 – Core Source of Peds		
Bulk Density (g cm^{-3})	Depth (m)	Soil Texture
1.67	0.23	SL
1.58	1.95	LS
1.72	3.34	LS
Average Bulk Density (g cm^{-3})		# Samples
1.66 ± 0.07		3

Table 4.6. Bulk density values of peds from soil pit and soil core of Site 1. Peds from
soil pit were taken from the wall of the clean face. SL = sandy loam, LS = loamy sand.

4.3.10. Infiltrometer Data

No infiltrometer measurements were taken at this site. The surface soil of this site

is sandy loam, and the infiltrometer measurements for Site 3 on sandy loam soil are

considered to be representative for this site as well.

4.4. Site 2 – Creosote – Sevilleta Site

Figure 4.5. Picture of Site 2, facing south.

4.4.1. Site Description

Site 2 (Figure 4.5) is located in the Sevilleta National Wildlife Refuge. The latitude and longitude of the site are 34.288150 and 106.899600 decimal degrees, respectively. The elevation is 1,470 meters above sea level, and the slope and aspect of the site are 1.5 and 270 degrees, respectively. The depth of the drill hole at this site was 7.5 meters. The depth of the groundwater table below the surface is estimated to be approximately 40 meters. This site lies within the Albuquerque-Belen alluvial groundwater basin (Anderholm 1987b). The soil at this site is classified as a Torrifluvent Entisol. This classification was obtained from a map of soil taxonomy that was based on data from the Natural Resources Conservation Service (Soil Map 2005, Soil Survey Staff 1999).

The average annual temperature for this site is 13.3°C, the average annual precipitation for this site is 235 millimeters, and the average annual potential evaporation

is 1,530 millimeters; yielding an aridity index of 6.67. These data were obtained from the

GIS maps in Section 2.2. The predominant vegetation of this site is creosote bush. The

Sevilleta has not been grazed at least since the Campbell family donated the land to the

Nature Conservancy in early 1973 (SNWR 2005).

4.4.2. EM31 Data

EM31 subsurface conductivity values were taken at Site 2. Figure 4.6 shows the

results of this survey. The difference in the electrical conductivity (EC) values, not the

absolute values of the measurements, is the important indicator of soil heterogeneity.

This site is considered relatively homogenous, since the EC values near the site

(intersection of transects) vary by only 5 mS m^{-1} (milliSiemens per meter).
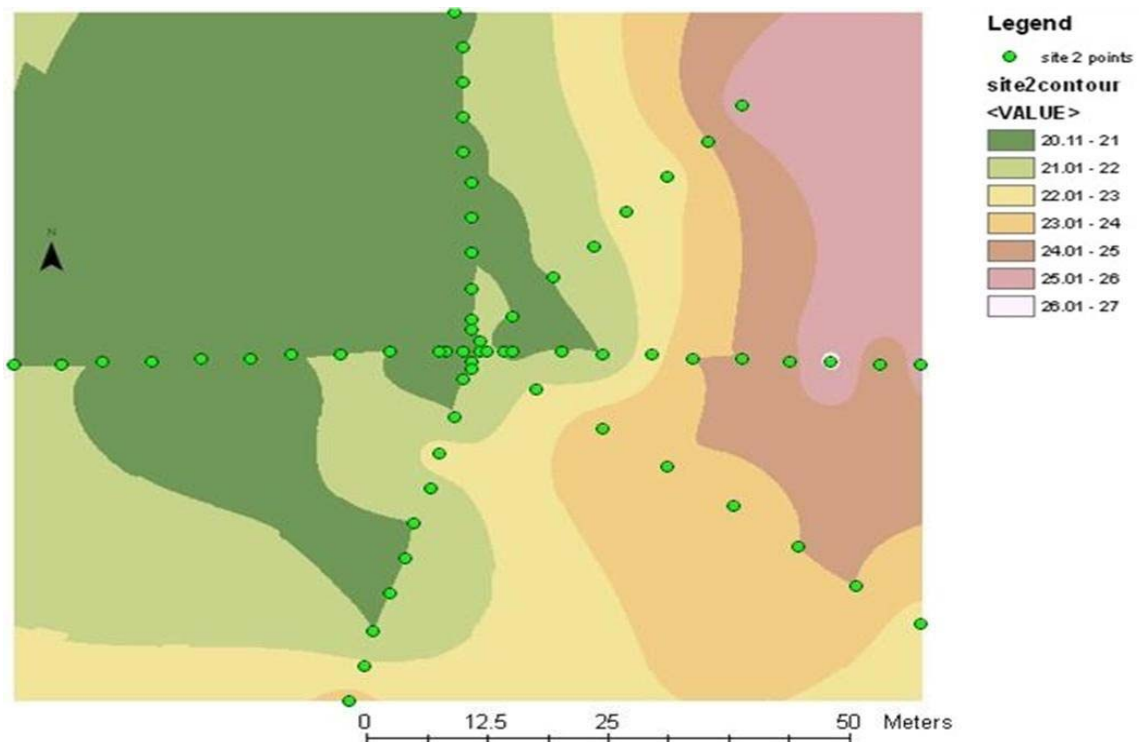
Figure 4.6. Contour of Site 2 conductivity values based on the measurements (green circles) along the transects. Conductivity values in legend in mS m^{-1} units. Site located at intersection of transects. Contours were determined through kriging the EC measurements. The contour interval is 1 mS m^{-1}.

4.4.3. Plant Identification and Density

Site 2 contains approximately forty creosote bushes (*Larrea tridentata*) within a ten meter radius of the drill site. The height of the bushes range from 90 to 120 centimeters tall, and the bushes are spaced between 30 and 90 centimeters apart. The grasses at the site are western wheatgrass (*Pascopyrum smithii*) and bush muhla (*Muhlenbergia porteri*). Other plants near the site are squawbush (*Rhus trilobata*), purple prickly pear (*Opuntia macrocentra*), and hairy golden aster (*Heterotheca villosa*). The underbrush clumps are about 30 to 150 centimeters apart and cover about three percent of the area, with the interspaces are connected. The ecosystem of the area is almost completely dominated by creosote, and it consists of less than one percent one-seed juniper (*Juniperus monosperma*) and honey mesquite (*Prosopis glandulosa*).

4.4.4. Site Distance from Ecotone

Site 2 is within a fairly continuous, large section of creosote bush and is not considered near an ecotone.

4.4.5. Geology

The site is on an alluvial fan originating from the Sierra Ladrones to the west. Most of the rocks that were in the soil core of Site 2 were igneous rocks. Chert was also present. Basalt was the dominant rock. The basalt rocks contained noticeable biotite, olivine, quartz, and feldspar crystals. Rhyolite containing feldspar, biotite, and sanidine crystals; granite with biotite crystals; and a few solid quartz pieces were also found in this core. Most rocks were coated with calcium carbonate.

4.4.6. Graphical Summary of Major Parameters

The major parameters that are associated with depth are shown in Figure 4.7.
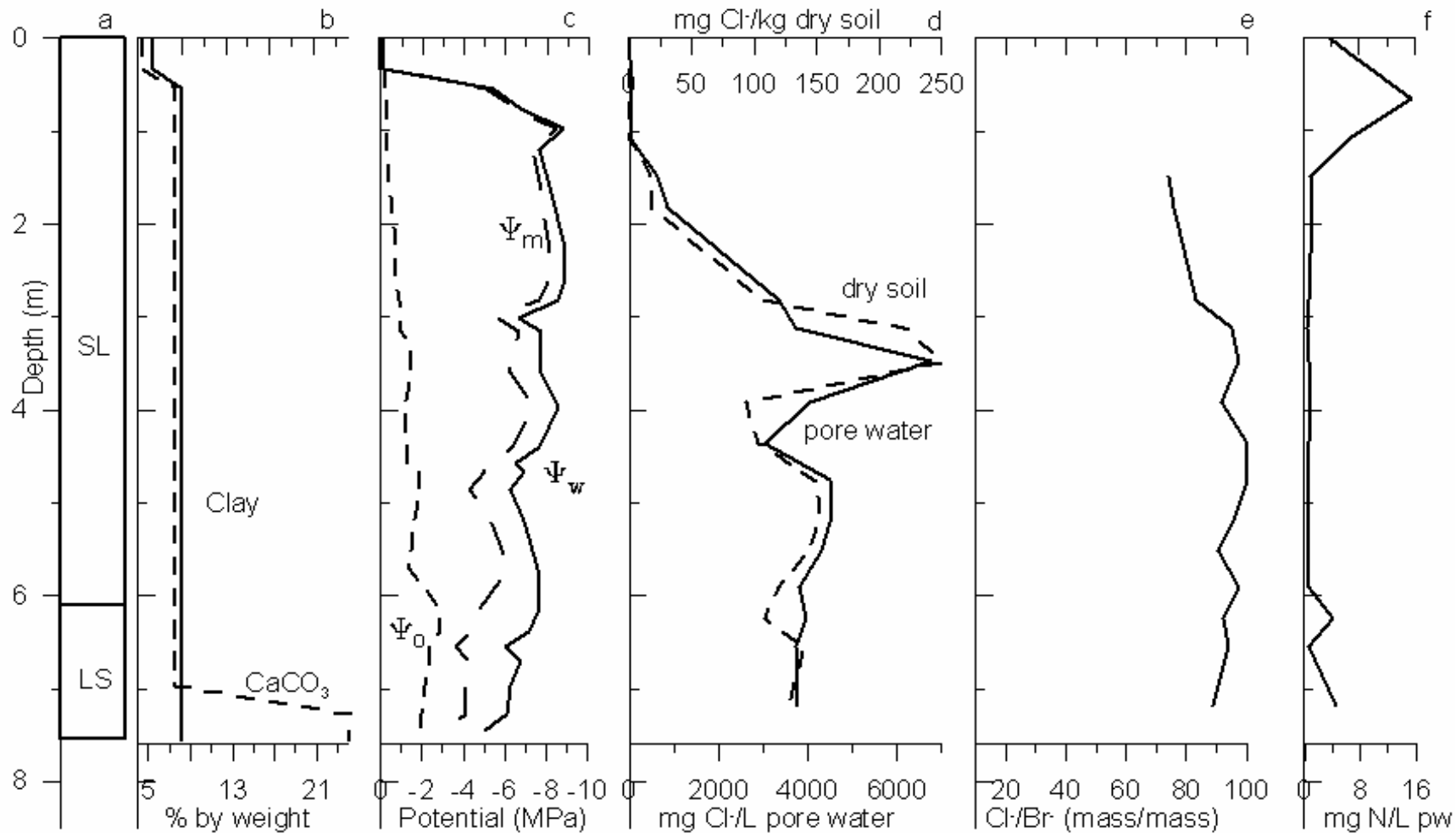
Figure 4.7. Profiles for Site 2 of a) soil texture, b) % CaCO3 and clay by weight, c) osmotic (Ψo), matric (Ψm), and water (Ψw) potential, d) mg Cl- per Liter of pore water (pw) or per kg dry soil, e) Cl-/Br- ratio, does not include ratios with non-detect bromide levels, f), and mg total Nitrogen/Liter pw. SL = Sandy Loam, LS = Loamy Sand Soil. $\Psi_o + \Psi_m = \Psi_w$

4.4.7. Soil Pit Characterization

No soil pit was dug at this site.

4.4.8. Root Density Analysis

No soil pit was dug at this site. The soil pit for determining creosote bush root properties was dug at Site 1, and the root density analysis for that site is considered to be representative of this site as well.

4.4.9. Bulk Density From Soil Core

Bulk density values from the soil core are shown in Table 4.7.

Site 2 – Core Ped Source		
Bulk Density (g cm^{-3})	Depth (m)	Texture
1.74	1.85	SL
1.47	3.16	SL
1.55	4.86	SL

Table 4.7. Bulk Density values from the soil core taken at Site 2. SL = sandy loam soil.

4.4.10. Infiltrometer Data

No infiltrometer measurements were taken at this site. The surface soil of this site is sandy loam, and the infiltrometer measurements for Site 3 on sandy loam soil are considered valid for this site as well.

4.5. Site 3 – Creosote – Sevilleta Site

Figure 4.8. Picture of Site 3, facing west.

4.5.1. Site Description

Site 3 (Figure 4.8) is located in the Sevilleta National Wildlife Refuge. The

latitude and longitude of the site are 34.294183 and 106.919083 decimal degrees,

respectively. The elevation is 1,500 meters above sea level, and the slope and aspect of

the site are 1.5 and 0 degrees, respectively. The depth of the drill hole at this site was 8.7

meters. Based on data in Anderholm (1987b), the depth of the groundwater table below

the surface is estimated to be approximately 40 meters. This site lies within the

Albuquerque-Belen alluvial groundwater basin (Anderholm 1987b). The soil at this site

is classified as a Torrifluvent Entisol. This classification was obtained from a map of soil

taxonomy that was based on data from the Natural Resources Conservation Service (Soil

Map 2005, Soil Survey Staff 1999).

The average annual temperature for this site is 13.3°C, the average annual

precipitation for this site is 230 millimeters, and the average annual potential evaporation

is 1,530 mm; yielding an aridity index of 6.67. These data were obtained from the GIS

maps in Section 2.2. The predominant vegetation of this site is creosote bush. The

Sevilleta has not been grazed at least since the Campbell family donated the land to the

Nature Conservancy in early 1973 (SNWR 2005).

4.3.2. EM31 data

EM31 conductivity values were taken at Site 3. Figure 4.9 illustrates the results

of this survey. The difference in the EC values, not the absolute values of the

measurements, is the important indicator of soil heterogeneity. This site is considered

fairly homogenous, since the EC values near the site vary by only 5 mS m^{-1}.
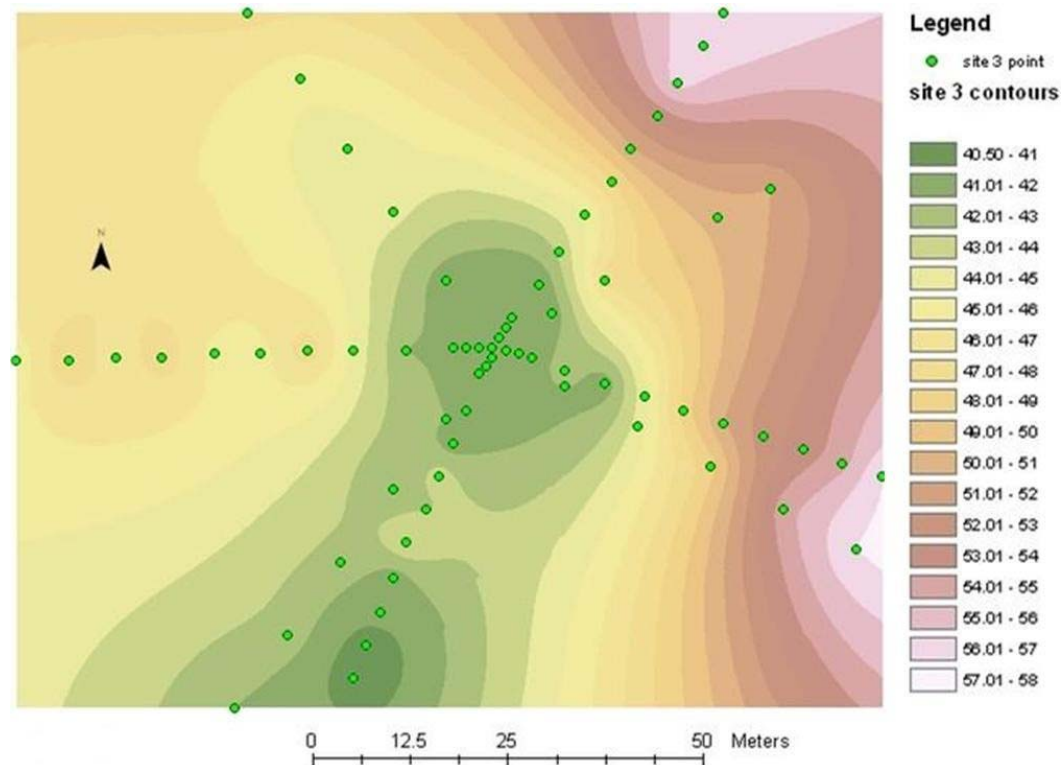
Figure 4.9. Contour of Site 3 conductivity values based on the measurements (green circles) along the transects. Conductivity values in legend in mS m^{-1} units. Site located at intersection of transects. Contours were determined through kriging the EC measurements. The contour interval is 1 mS m^{-1}.

4.5.3. Plant Identification and Density

Site 3 contains approximately thirty creosote bushes (*Larrea tridentata*) within a ten meter radius of the drill site. The bushes are 90 to 150 centimeters tall and are spaced between 30 and 60 centimeters apart. This site contains a significant amount of broom snakeweed (*Gutierre sarothrae*), which makes up at least five percent of the cover and is the only weed. The only grass, western wheatgrass (*Pascopyrum smithii*), covers about five to ten percent of the area. The grass/weed clumps are about 30 to 150 centimeters across and are connected. The area's ecosystem is almost completely dominated by creosote, and it consists of less than one percent one-seed juniper (*Juniperus monosperma*) and honey mesquite (*Prosopis glandulosa*).

4.5.4. Site Distance From Ecotone

Site 3 is within a fairly continuous, large section of creosote bush and is not considered to be near an ecotone.

4.5.5. Geology

The site is on an alluvial fan originating from the Sierra Ladrones to the west. Most of the rocks that were in the soil core of Site 3 were igneous rocks; chert was also present. Basalt was the dominant rock, containing noticeable biotite and feldspar crystals. Rhyolite containing biotite, feldspar, and sanidine crystals, and granite were also found in this core. Most rocks were coated with calcium carbonate.

4.5.6. Graphical Summary of Major Parameters

The major parameters that are associated with depth are shown in Figure 4.10.
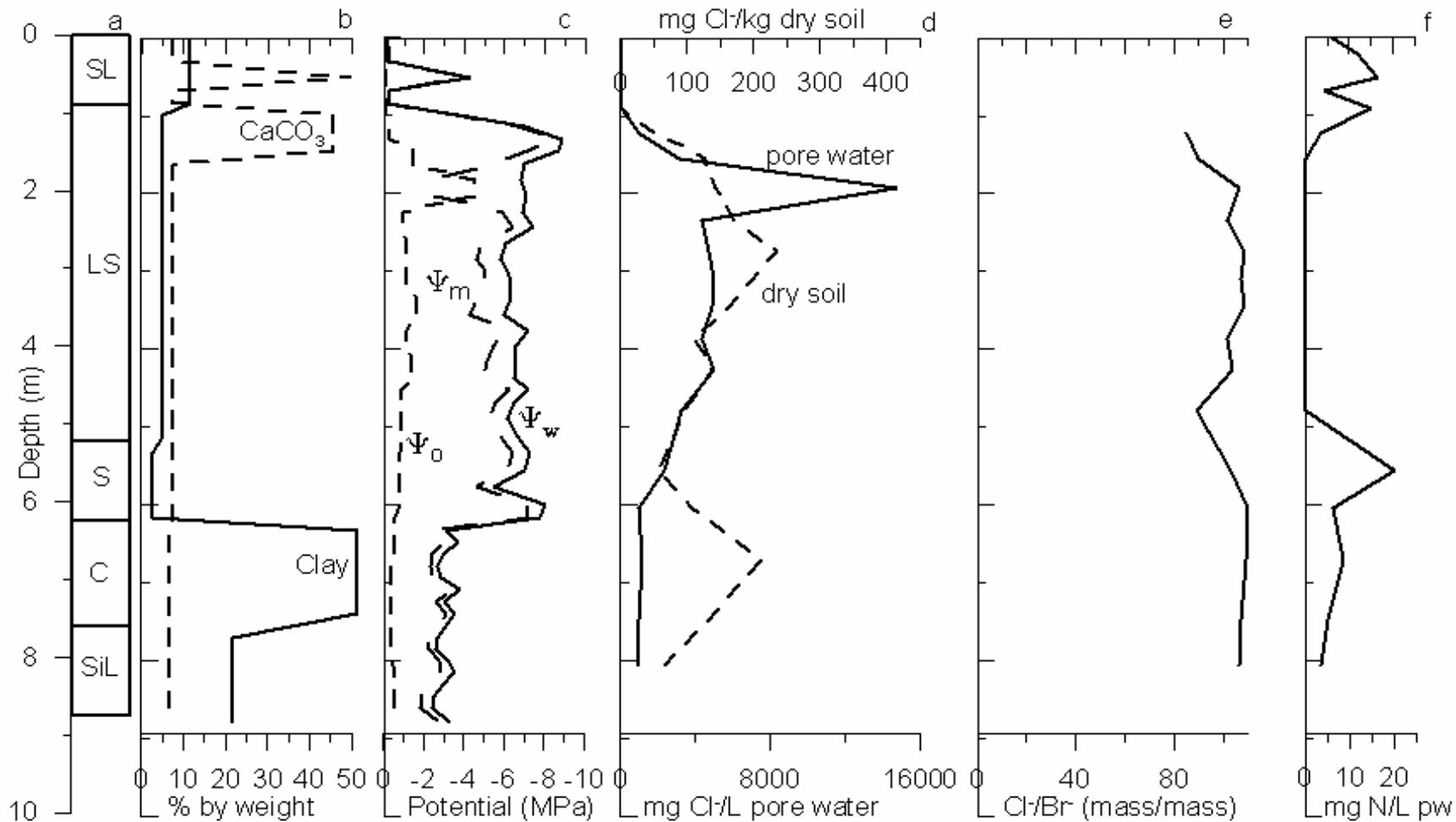
Figure 4.10. Profiles for Site 3 of a) soil texture, b) % CaCO3 and clay by weight, c) osmotic (Ψo), matric (Ψm), and water (Ψw) potential, d) mg Cl- per Liter of pore water (pw) or per kg dry soil, e) Cl-/Br- ratio, does not include ratios with non-detect bromide levels, f), and mg total Nitrogen/Liter pw. SL = Sandy Loam, LS = Loam Sand, C = Clay, SiL = Silty Loam, S = Sand Soil.
$\Psi_o + \Psi_m = \Psi_w$

102

4.5.7 Soil Pit Characterization

No soil pit was dug at this site.

4.5.8. Root Density Analysis

No soil pit was dug at this site. The soil pit for determining creosote properties was dug at Site 1 and the root density analysis for that site is considered to be representative of this site as well.

4.5.9. Bulk Density From Soil Core

Bulk density values from the soil core are shown in Table 4.8.

Site 3 – Core Ped Source		
Bulk Density (g cm^{-3})	Depth (m)	Texture
1.66	0.30	SL
1.53	0.51	SL
1.58	3.35	LS
1.68	5.55	S
2.04	7.71	SiL

Table 4.8. Bulk density values from the Site 3 soil core. SL = sandy loam, LS = loamy sand, S = sand, and SiL = silty loam soil.

4.5.10. Infiltrometer Data

The infiltrometer data measured at Site 3 are summarized in Table 4.9. Three infiltrometer measurements were taken at each of the two sites, resulting in six saturated conductivity (Ksat) calculated values. The average Ksat value calculated from the data was somewhat lower than the default value for this soil type. The soil crust was not removed from the area so that the measurement would represent actual field infiltration conditions. This could explain the measured value having a lower value than the default value. Figure 4.11 shows the two surface areas, before surface preparation, where the

infiltrometer measurements were taken.

Site 3 – Sandy Loam Soil					
Surface Soil Texture	Default K sat (cm hr⁻¹)	Average K sat (cm hr⁻¹)	# of measurements	Alpha	% Clay in Surface Soil
SL	4.42	3.27 ± 2.69	6	0.24	11.6

Table 4.9. Infiltrometer data from Site 3. Default Ksat (saturated hydraulic conductivity) for sandy loam soil from Carsel and Parrish (1988). Ksat value an average of calculated Ksat values from six measured infiltration values. Alpha is a Van Genuchten parameter. SL = sandy loam soil.
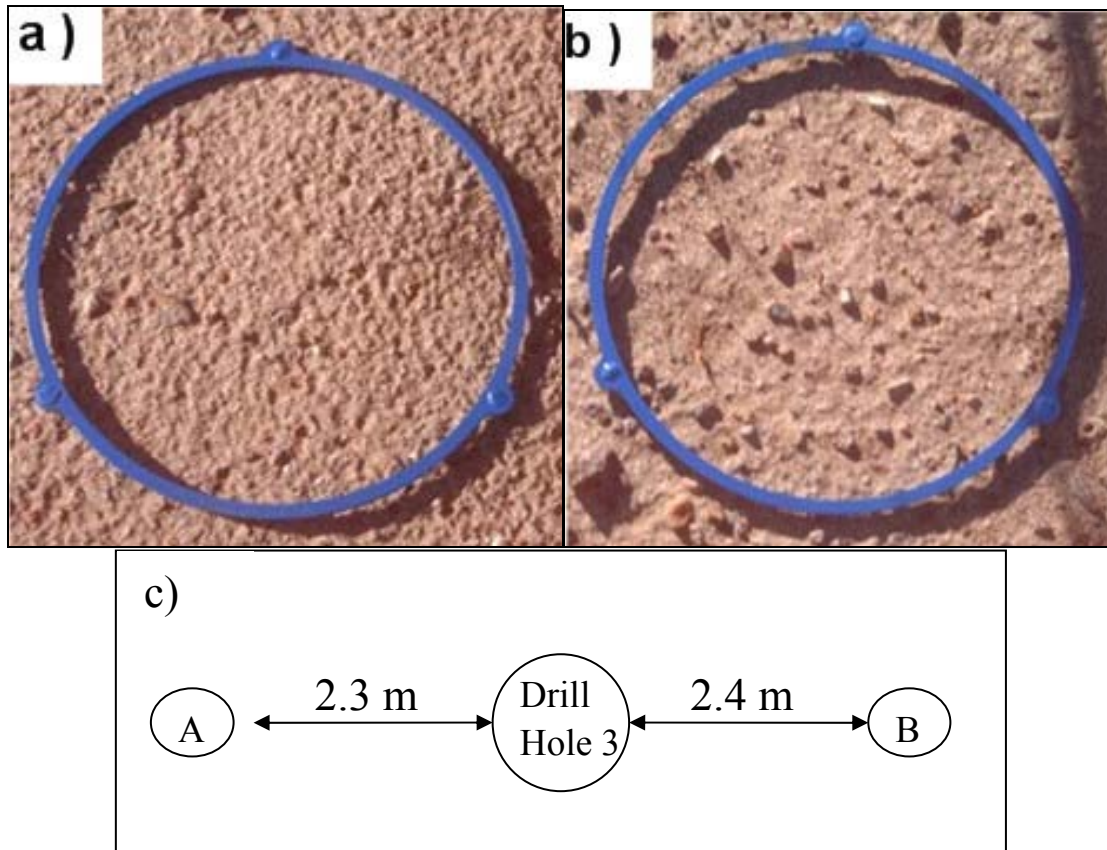
Figure 4.11. a) and b) Surface areas (areas inside rings) where infiltrometer measurements were taken before surface preparation in the top two pictures. Rings have a 20 cm diameter. c) Plan-view diagram of the infiltrometer setup with A = infiltrometer A and B = infiltrometer B and distances between infiltrometers and sites noted. Diagram is not to scale.

4.6. Site 4 – Grassland – Forest Service Site

Figure 4.12. Picture of Site 4 facing west.

4.6.1. Site Description

Site 4 (Figure 4.12) is located in Cibola National Forest, north of Magdalena, NM.

The latitude and longitude of the site are 34.267817 and 107.224167 decimal degrees,

respectively. The elevation is 1,880 meters above sea level, and the slope and aspect of

the site are 1.5 and 40 degrees, respectively. The depth of the drill hole at this site was

9.0 meters. The depth of the groundwater table below the surface is estimated at 47

meters. This site lies within the La Jencia alluvial groundwater basin (Anderholm 1987a).

The soil at this site is classified as a Haplargid Aridisol. This classification was obtained

from a map of soil taxonomy that was based on data from the Natural Resources

Conservation Service (Soil Map 2005, Soil Survey Staff 1999).

The average annual temperature for this site is 12.0 ° C, the average annual

precipitation for this site is 302 millimeters, and the average annual potential evaporation

is 1,280 millimeters; yielding an aridity index of 4.21. These data were obtained from the

GIS maps in Section 2.2. Grass is the predominant vegetation of this site. The Forest

Service attempted to control grazing on its lands through strict law enforcement and the

issuance of grazing permits beginning in 1912 (Scurlock 1998). Cattle grazing presently

continues in this area.

4.6.2. EM31 Data

EM31 subsurface conductivity values were taken at Site 4. The results of this

survey are shown in Figure 4.6. The difference in the EC values, not the absolute values

of the measurements, is the important indicator of soil heterogeneity. This site is

considered very homogenous, since the EC values near the site (intersection of transects)

vary by only 2 mS m^{-1}.
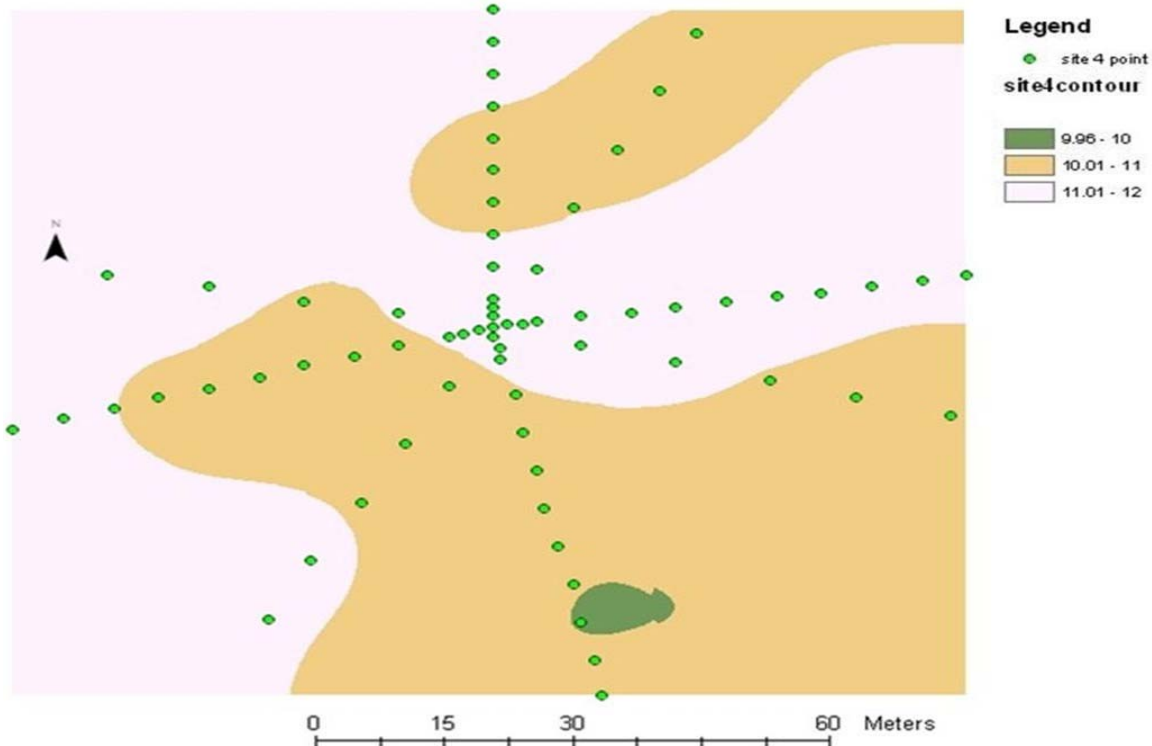
Figure 4.13. Contour of Site 4 conductivity values based on the transects. Conductivity values in legend in mS m^{-1} units. Site contours were determined through kriging the EC measurements. The contour interval is 1 mS m^{-1}.

4.6.3. Plant Identification and Density

The predominant grasses at Site 4 are blue grama (*Bouteloua gracilis*), black grama (*Bouteloua eriopoda*), and bush muhla (*Muhlenbergia porteri*); the site also contains tobosa (*Hilaria mutica*) grass. Other plants within a ten meter radius of the drill site are desert zinnia (*Zinnia acerosa*), hairy golden aster (*Heterotheca villosa*), tree cholla (*Opuntia imbricata*), broom snakeweed (*Gutierre sarothrae*), twogrooved milkvetch (*Astragalus bisulcatus*), silverleaf nightshade (*Solanum elaeagnifolium*), and netseed lambsquaters (*Chenopodium berlandieri*). The interspaces of the plants are approximately 15 to 30 centimeters across and are not connected.

4.6.4. Site Distance From Ecotone

Grass Site 4 is also about 300 meters away from a juniper-dominated area.

4.6.5. Geology

All of the rocks found in the soil core of Site 4 were igneous. The basalt rocks were vesicular and contained observable olivine and augite crystals. Rhyolite containing feldspar, biotite, and quartz crystals; granite containing olivine and quartz crystals; and tuff containing feldspar and biotite crystals were also found in this core.

4.6.6. Graphical Summary of Major Parameters

The major parameters that are associated with depth are shown in Figure 4.14.
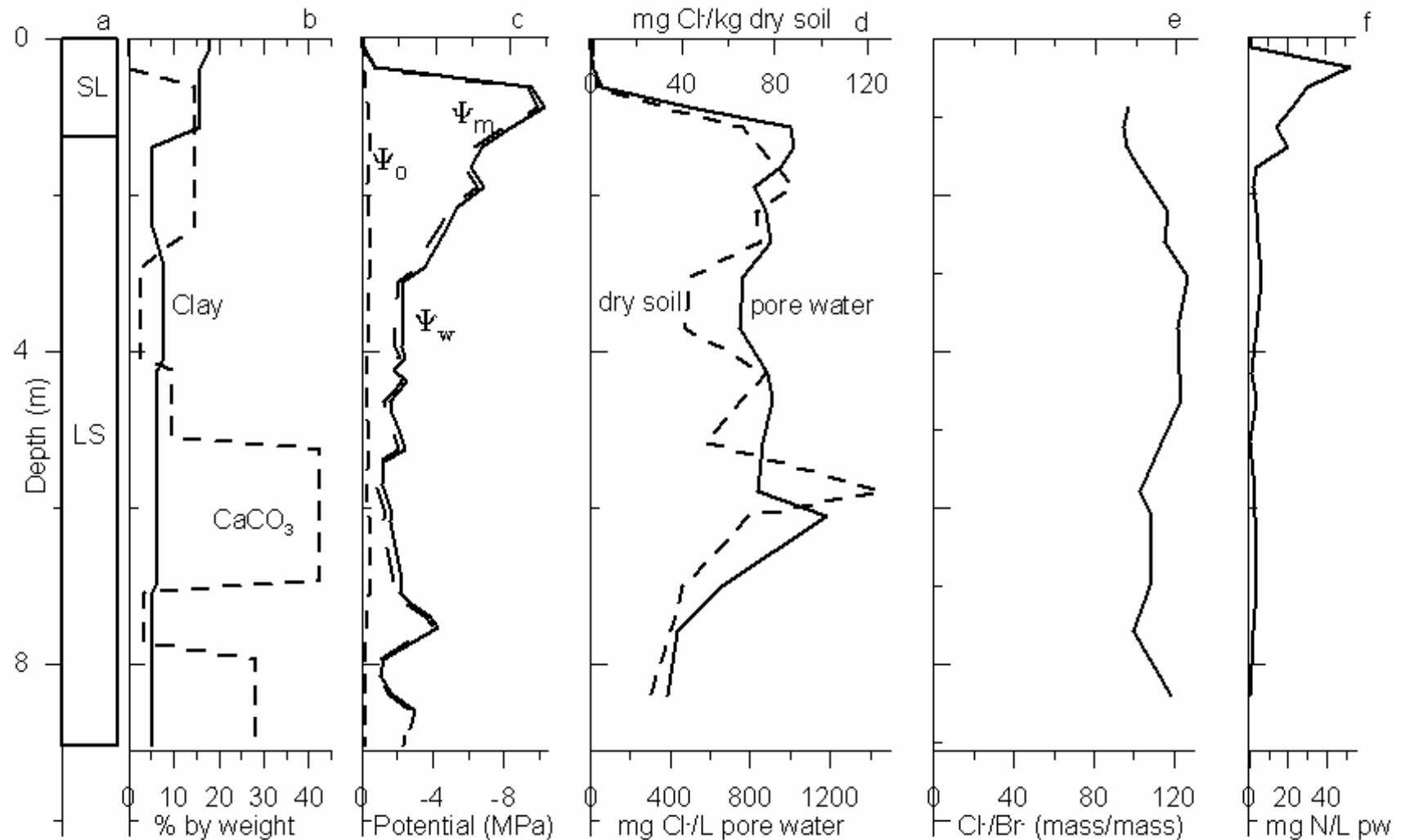
Figure 4.14. Profiles for Site 4 of a) soil texture, b) % CaCO3 and clay by weight, c) osmotic (Ψo), matric (Ψm), and water (Ψw) potential, d) mg Cl- per Liter of pore water (pw) or per kg dry soil, e) Cl-/Br- ratio, does not include ratios with non-detect bromide levels, f), and mg total Nitrogen/Liter pw. SL = Sandy Loam, LS = Loamy Sand Soil. $\Psi_o + \Psi_m = \Psi_w$

4.6.7. Soil Pit Characterization

No soil pit was dug at this site.

4.6.8. Root Density Analysis

No soil pit was dug at this site. The soil pit for determining grass root properties was dug at Site 5, and the root density analysis for that site is considered representative of this site as well.

4.6.9. Bulk Density From Soil Core

Bulk density values from the soil core are shown in Table 4.10.

Site 4 – Core Ped Source		
Bulk Density (g cm^{-3})	Depth (m)	Texture
1.60	1.14	SL
1.57	2.41	LS
1.74	4.80	LS
1.96	7.95	LS

Table 4.10. Bulk Density values from Site 4 soil core. SL = sandy loam and LS = loamy sand soil.

4.6.10. Infiltrometer Data

No infiltrometer measurements were taken at this site. The surface soil of this site is sandy loam, and the infiltrometer measurements for Site 3 on sandy loam soil are considered valid for this site as well.

4.7. Site 5 – Grassland – Forest Service Site

Figure 4.15. Picture of Site 5, facing north.

4.7.1. Site Description

Site 5 (Figure 4.15) is located in Cibola National Forest, north of Magdalena, NM.

Its latitude and longitude are 34.211783 and 107.218917 decimal degrees, respectively.

The elevation is 1,900 meters above sea level, and the slope and aspect of the site are 2

and 50 degrees, respectively. The depth of the drill hole at this site was 5.25 meters, and

the depth of the groundwater table below the surface is estimated at around 57 meters.

This site lies within the La Jencia alluvial groundwater basin (Anderholm 1987a). The

soil at this site is classified as a Haplargid Aridisol. This classification was obtained from

a map of soil taxonomy that was based on data from the Natural Resources Conservation

Service (Soil Map 2005, Soil Survey Staff 1999).

The average annual temperature for this site is 12.2°C, the average annual

precipitation for this site is 306 millimeters, and the average annual potential evaporation

is 1,270 millimeters; this yields an aridity index of 4.13. These data were obtained from

the GIS maps in Section 2.2. The predominant vegetation of this site is grass. The Forest

Service attempted to control grazing on its lands through strict law enforcement and the issuance of grazing permits beginning in 1912 (Scurlock 1998). Cattle grazing presently continues in this area.

4.7.2. EM31 Data

EM31 subsurface conductivity values were taken at Site 5. The results of this survey are shown in Figure 4.6. The difference in the EC values, not the absolute values of the measurements, is the important indicator of soil heterogeneity. This site is considered relatively homogenous, since the EC values near the site (intersection of transects) vary by only 2 mS m^{-1}.
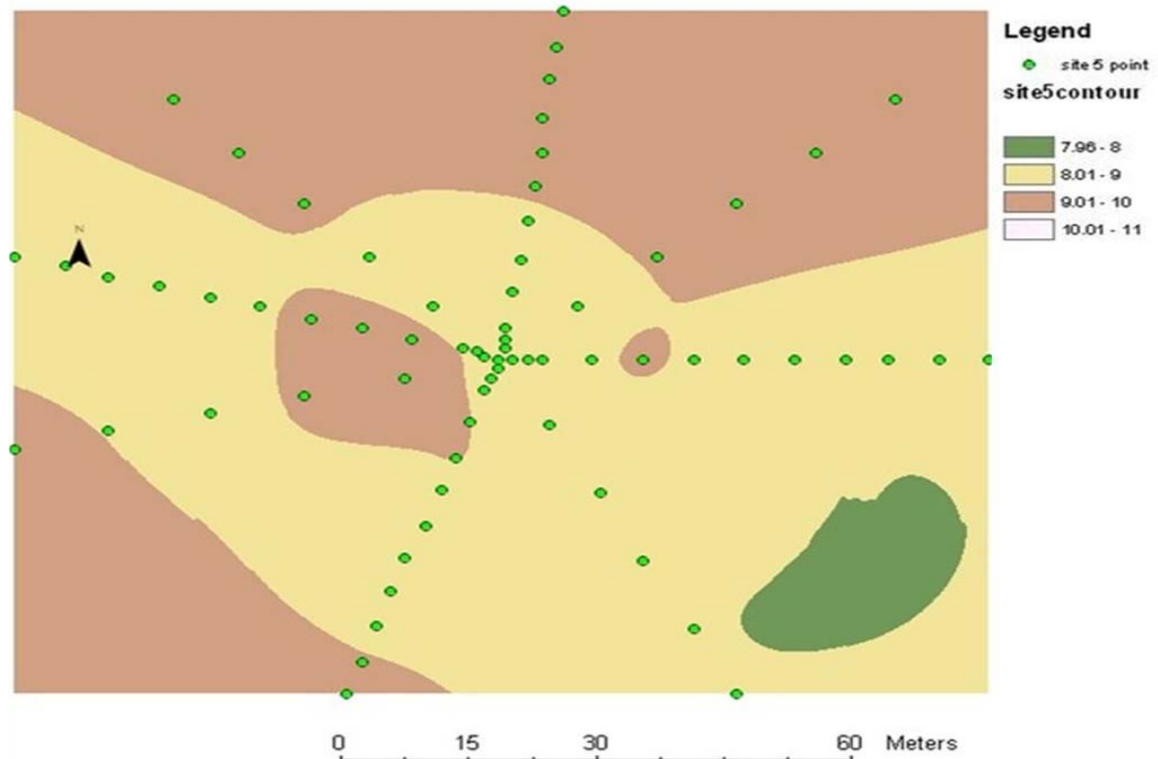
Figure 4.16. Contour of Site 5 conductivity values based on the measurements (green circles) along the transects. Conductivity values in legend in mS m^{-1} units. Contours were determined through kriging the EC measurements. The contour interval is 1 mS m^{-1}.

4.7.3. Plant Identification and Density

The predominant grasses of Site 5 are blue grama (*Bouteloua gracilis*), black grama (*Bouteloua eriopoda*), and tobosa (*Hilaria mutica*). Other plants within a ten meter radius of the drill site are tree cholla (*Opuntia imbricata*), spurge (*Chamaesyce maculata*), purple prickly pear (*Opuntia macrocentra*), hairy golden aster (*Heterotheca villosa*), silverleaf nightshade (*Solanum elaeagnifolium*), banana yucca (*Yucca baccata*), Russian thistle (*Salsola iberica*), whitethorn acacia (*Acacia constricta*), broom snakeweed (*Gutierre sarothrae*), yellow toadflax (*Linaria vulgaris*), netseed lambsquaters (*Chenopodium berlandieri*), and cudweed (*Gnaphalium spp.*). The interspaces of the plants are approximately 15 to 30 centimeters across and are not connected.

4.7.4. Site Distance From Ecotone

A grass and juniper ecotone is located near this site. This is a fairly sharp ecotone that is approximately 340 meters from Grass Site 5 and 1,140 meters from Juniper Site 7. Sites 5 and 7 are approximately 1,480 meters apart.

4.7.5. Geology

Most of the rocks that were in the soil core of Site 5 were igneous rocks; chert a sedimentary rock, was also present. Rhyolite was the dominant rock, containing noticeable feldspar crystals. Welded tuff with feldspar and sanidine crystals, vesicular basalt, and granite containing muscovite and biotite crystals were also found in this core.

4.7.6. Graphical Summary of Major Parameters

The major parameters that are associated with depth are shown in Figure 4.17.
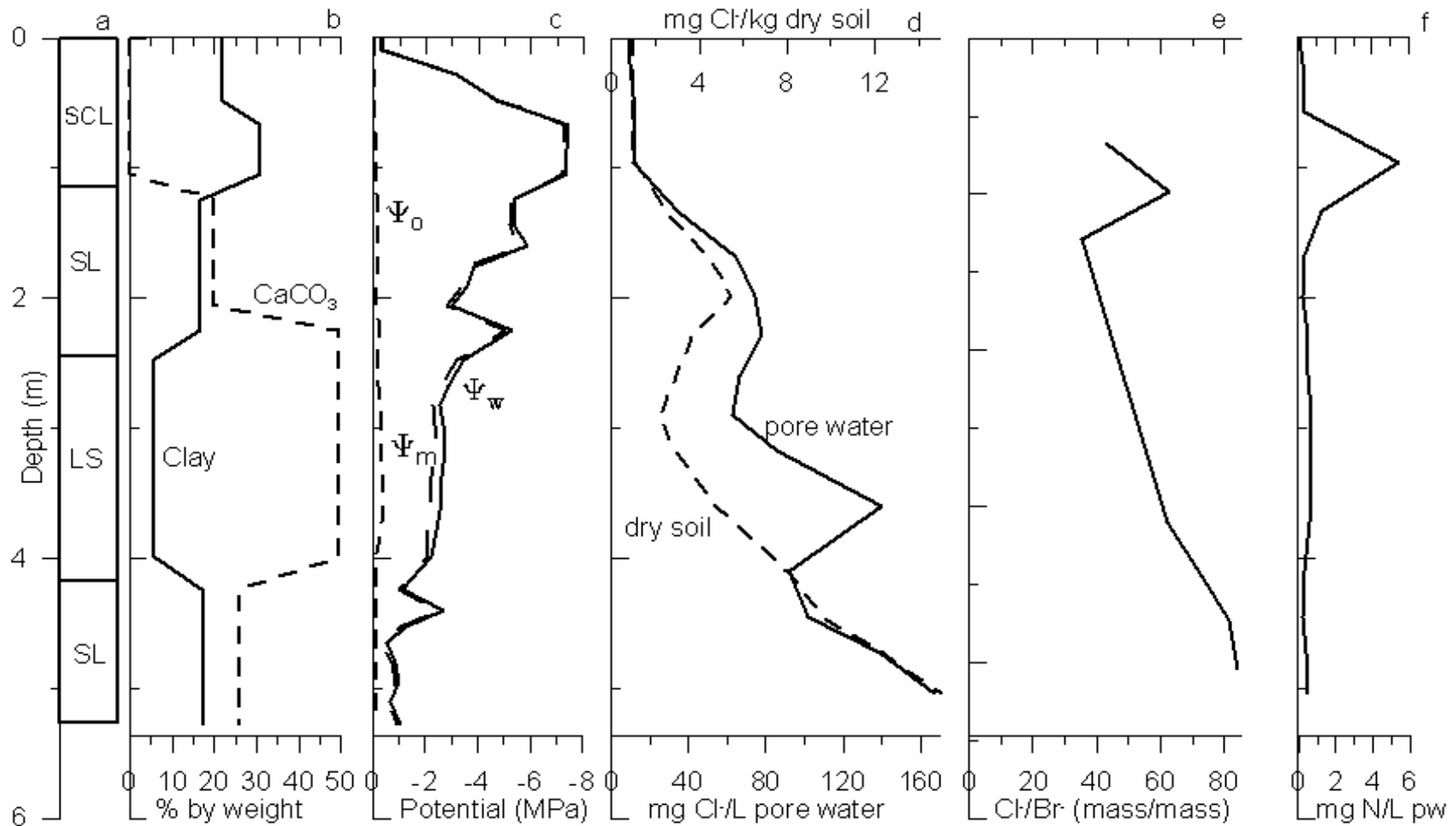
Figure 4.17. Profiles for Site 5 of a) soil texture, b) % CaCO3 and clay by weight, c) osmotic (Ψo), matric (Ψm), and water (Ψw) potential, d) mg Cl- per Liter of pore water (pw) or per kg dry soil, e) Cl-/Br- ratio, does not include ratios with non-detect bromide levels, f), and mg total Nitrogen/Liter pw. SL = Sandy Loam, LS = Loamy Sand, SCL = Sandy Clay Loam Soil. $\Psi_o + \Psi_m = \Psi_w$

4.7.7. Soil Pit Characterization

A 77-centimeter soil pit was dug near drill Site 5. The soil profile is shown in Figure 4.18 and the soil description is shown in Tables 4.11 and 4.12 The clean face of the soil pit was placed facing the opposite direction of the drill hole, since drilling destroyed most of the grass near the drill hole.
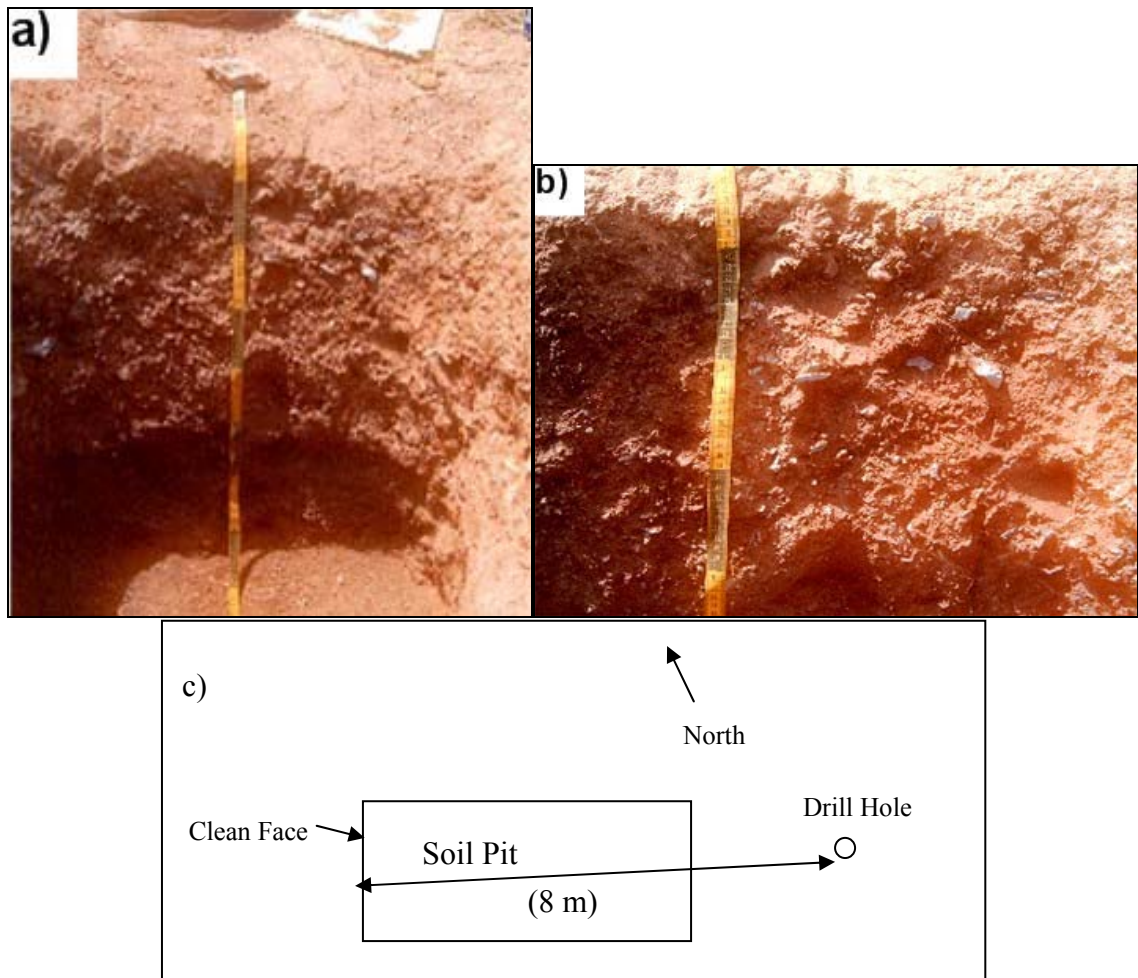
Figure 4.18. Soil pit at Site 5. This pit was dug to a depth of 77 cm. a) The clean face of the entire profile is shown, and each black and yellow stripe on the measuring tape denotes 1 meter. Before digging, grass was present on the edge of the clean face. b) A close-up of the upper part of the profile to show the large amount and size of rocks imbedded in the clay soil. c) A plan-view diagram of the soil pit in relation to the drill site. Lengths in parentheses are estimated. Diagram is not to scale.

Location: Site 5, Forest Service											
Aspect: West Northwest											
Vegetation: Grass											
Date/time: 6/26/2004 2:30 pm											
					Structure				Consistence		
									wet		
Horizon	Depth (cm)	Dry Color	Moist Color	Ped Grade	Ped Size	Ped Shape	% gravel	sticky	plasticity	dry	Texture
A	0 to 15	7.5 YR 4/3	7.5 YR 2.5/3	1	m	sbk	10	ss	ps	h	SC
Bt	15 to 52	7.5 YR 3/4	7.5 YR 3/2	1	m	sbk	50	ss	ps	h	C
B	52 to 77	7.5 YR 4/4	7.5 YR 3/4	1	m	sbk	20	ss	ps	h	SCL

Table 4.11. Soil pit characterization at Site 5. The soil description method used follows the procedure outlined by the Soil Survey Staff (1993). m = medium, sbk = subangular blocky, ss = slightly sticky, ps = slightly plastic, h = hard, SC = sandy clay, C = clay, SCL = sandy clay loam soil.

		Roots			Pores		Boundary			
Horizon	Clay films	frequency class	size	nature	frequency class	size	distinctness	topography		Carbonate
A	none	2 (common)	vf	woody	2 (common)	fine	clear	smooth		none
Bt	none	3 (many)	vf	woody	2 (common)	fine	clear	smooth		none
B	none	1 (few)	vf - f	woody	3 (many)	fine	buried	buried		none

Table 4.12. Soil pit characterization at Site 5 (continued). The soil description method used follows the procedure outlined by the Soil Survey Staff (1993). vf = very fine, f = fine.

4.7.8. Root Density Analysis

A root density analysis of the grass growing on the edge of the clean face of the soil pit at Site 5 was performed using a 10 by 10 centimeter square. The results of this analysis are shown in Table 4.13. Almost all of the grass roots were less than one millimeter in diameter. There were no roots in the bottom of pit, so one meter is the estimate for the full extent of the grass roots.

Depth (cm)	Average # of Roots with Noted Diameter			Total	%	Notes
	< 1 mm	1 - 10 mm	> 10 mm			
0 to 20	24	0.0	0.0	24	28	
20 to 40	41	0.0	0.0	41	**47**	
40 to 60	16	0.0	0.0	16	18	
60 to 80	5.7	1.0	0.0	6.7	8	only 3 roots in entire pit larger than 1 mm, and they are just barely larger.
			Total	87		no roots at bottom of pit

Table 4.13. Root density analysis of grass at Site 5. Values shown are the average number of roots of that diameter of the three replicates taken at each depth interval. A 10 by 10 cm square was used to count the roots. The majority of the roots were located between 20 and 40 cm depth.

4.7.9. Bulk Density from Soil Pit and Soil Core

The bulk density of peds found in the core and soil pit are shown in Table 4.14.

Since peds from both the wall of the soil pit and the core were taken, any possible

compaction of the peds in the soil core can be determined. When comparing the averages

of the bulk densities of both the core and the pit peds, there is no significant difference

between them, demonstrating that slight-to-no compaction of the peds occurred in this

soil core.

Site 5 – Pit Ped Source		
Bulk Density (g cm^{-3})	Depth (m)	Texture
1.44	0.19	SCL
1.45	0.85	SL
1.62	1.64	SCL
Average Bulk Density (g cm^{-3})		# Samples
1.50 ± 0.10		3
Site 5 – Core Ped Source		
Bulk Density (g cm^{-3})	Depth (m)	Texture
1.48	0.05	SCL
1.55	1.60	SL
1.63	4.65	SL
Average Bulk Density (g cm^{-3})		# Samples
1.56 ± 0.08		3

Table 4.14. Bulk density values of peds from both the core and soil pit from Site 5. SCL = sandy clay loam, SL = sandy loam soil.

4.7.10. Infiltrometer Data

The infiltrometer data measured at Site 5 are summarized in Table 4.15. Three

infiltrometer measurements were taken at two sites, resulting in six saturated conductivity

values. The average Ksat value calculated from the data was half the default value for

this soil type. The soil crust was not removed from the area so that the measurement

would represent actual field infiltration conditions. This could explain the measured

value having a value lower than the default value. Figure 4.19 shows the two surface

areas of which infiltrometer measurements were taken before surface preparation. As a

result of the extremely low saturated conductivity of the soil surface at this site, there was

significant lateral spreading of the water from the infiltration disc. This spreading is

shown in Figure 4.19.

Site 5 – Sandy Clay Loam Soil					
Surface Soil Texture	Default K sat (cm hr^{-1})	Average K sat (cm hr^{-1})	# of Measurements	Alpha	% Clay in Surface Soil
SCL	1.3	0.58 ± 0.48	6	0.10	21.84

Table 4.15. Infiltrometer data from Site 5. Default Ksat for sandy clay loam soil from Carsel and Parrish (1988). Ksat value an average of calculated Ksat values from the six measured infiltration values taken at two sites. Alpha is a Van Genuchten parameter. SCL = sandy clay loam soil.
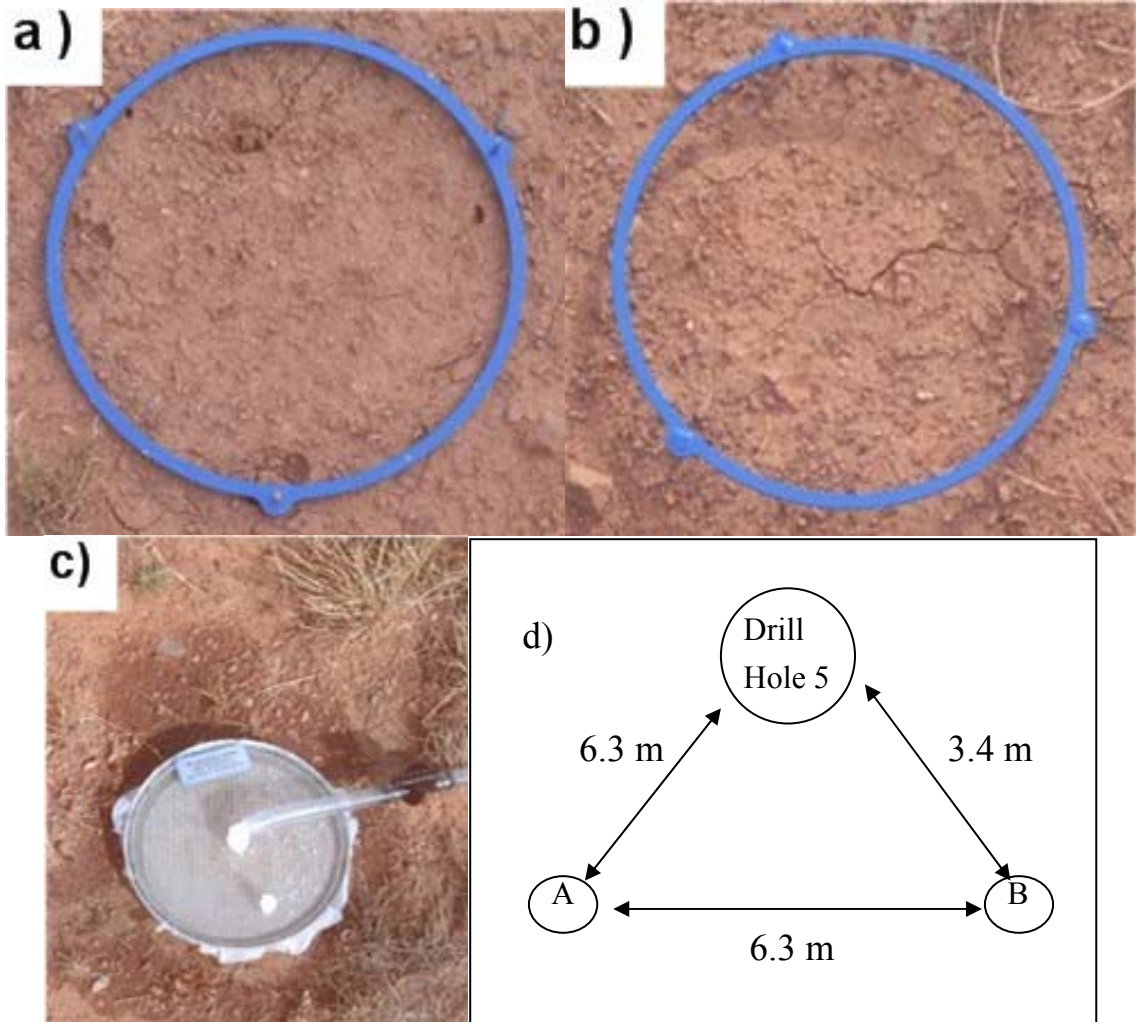
Figure 4.19. a) and b) Surface areas (area inside rings) where infiltrometer measurements were taken before surface preparation in the top two pictures. The rings have a 20 cm diameter. c) The lateral spreading of water from the disc. The water saturated soil is the darker area of the soil around the infiltrometer disc. d) A plan-view diagram of infiltrometer setup with A = infiltrometer A and B = Infiltrometer B and distances between infiltrometers and sites noted. Diagram is not to scale.

4.8. Site 6 – Grassland – Sevilleta Site

Figure 4.20. Picture of Site 6, facing west.

4.8.1. Site Description

Site 6 (Figure 4.20.) is located in the Sevilleta National Wildlife Refuge. The latitude and longitude of the site are 34.355217 and 106.990383 decimal degrees, respectively. The elevation is 1,560 meters above sea level, and the slope and aspect of the site are 1 and 60 degrees, respectively. The depth of the drill hole at this site was 4.50 meters. The depth of the groundwater table below the surface is estimated to be greater than 91 meters. This site lies within the Albuquerque-Belen alluvial groundwater basin (Anderholm 1987b). The soil at this site is classified as a Haplargid Aridisol. This classification was obtained from a map of soil taxonomy that was based on data from the Natural Resources Conservation Service (Soil Map 2005, Soil Survey Staff 1999).

The average annual temperature for this site is 12.8 ° C, the average annual precipitation for this site is 230 millimeters, and the average annual potential evaporation is 1,460 millimeters; this yields an aridity index of 6.34. These data were obtained from

the GIS maps in Section 2.2. Grass is the main vegetation of this site. The Sevilleta has not been grazed at least since the Campbell family donated the land to the Nature Conservancy in early 1973. The Refuge was officially established on December 28th, 1973 (SNWR 2005).

4.8.2. EM31 Data

The subsurface electrical conductivity data were obtained using the EM31 meter, before drilling. Site 6 had to be moved from its proposed location just before the actual drilling took place as a result of problems with drill rig access. This new location placed Site 6 outside of the area originally assessed using the EM31. Therefore, no EM31 data exists for the actual Site 6 drilling location.

4.8.3. Plant Identification and Density

The predominant grass of Site 6 was bush muhla (*Muhlenbergia porteri*). Other plants within a ten meter radius of the drill site are hairy golden aster (*Heterotheca villosa*), Russian thistle (*Salsola iberica*), sulfurflower (*Eriogonum umbellatum*), four large squawbushes (*Rhus trilobata*), tree cholla (*Opuntia imbricata*), and desert zinnia (*Zinnia acerosa*). The interspaces of the plants vary widely from 15 to 150 centimeters across and are not well connected.

4.8.4. Site Distance from Ecotone

Site 6 is near a grass and creosote ecotone. This ecotone is diffuse, and the ecology changes from grass to creosote patches several times between drill Sites 1 and 6, which are four kilometers apart. Grass Site 6 is approximately 120 meters from the closest creosote-dominated area, and Creosote Site 1 is around 330 meters from the

121

closest grass-dominated area.

4.8.5. Geology

This site is on an alluvial fan originating from the Sierra Ladrones to the east. Most of the rocks that were in the soil core of Site 6 were igneous rocks. The sedimentary rock, chert, and the metamorphic rock, epidote with quartz crystals, were also found. Basalt was the dominant rock, containing observable orthoclase and olivine crystals. Rhyolite, containing sanidine and muscovite crystals; granite with orthoclase and quartz crystals; and granodiorite were also present in this core. Most rocks were coated with calcium carbonate.

4.8.6. Graphical Summary of Major Parameters

The major parameters that are associated with depth are shown in Figure 4.21.
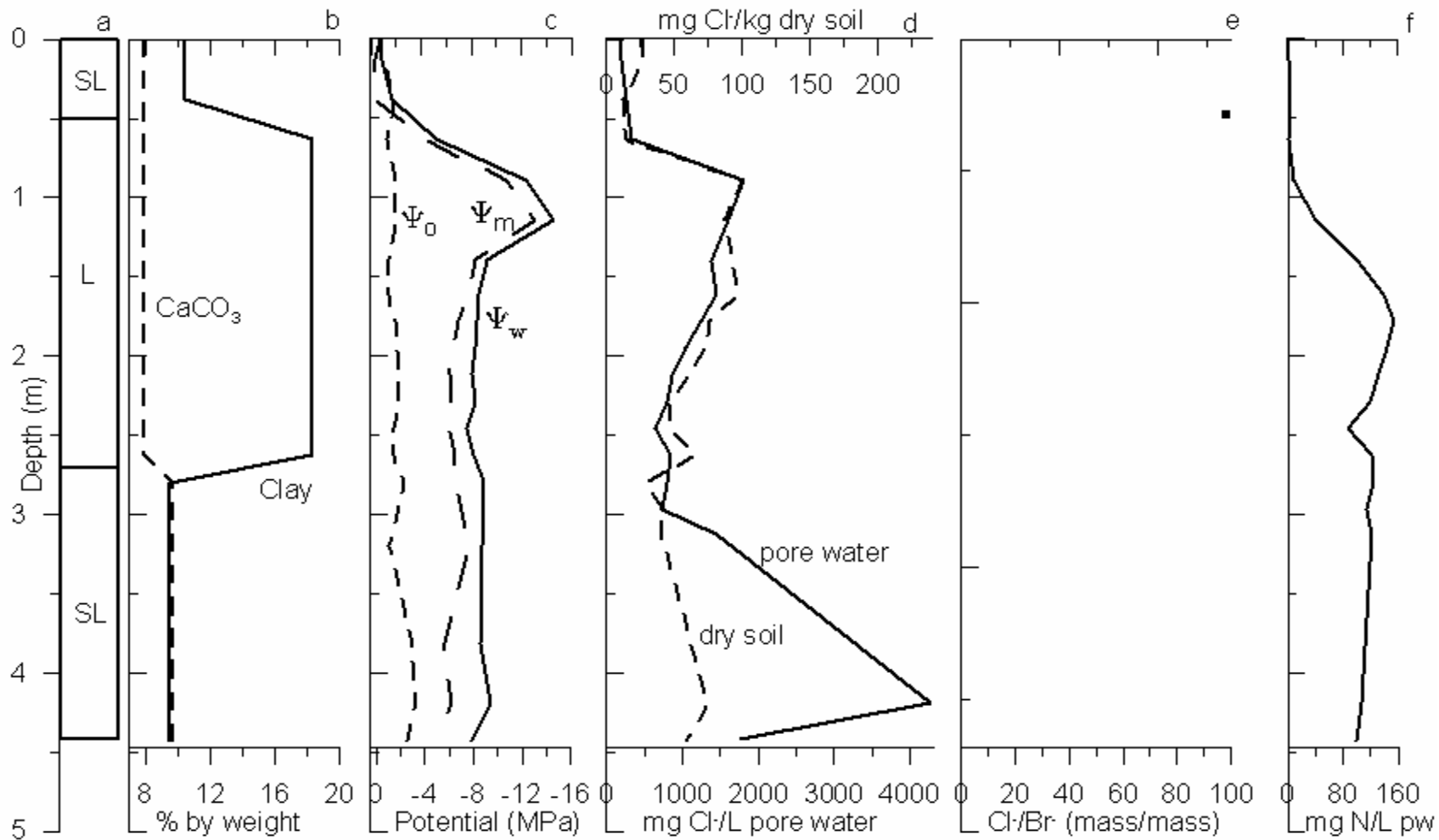
Figure 4.21. Profiles for Site 6 of a) soil texture, b) % CaCO3 and clay by weight, c) osmotic (Ψ_o), matric (Ψ_m), and water (Ψ_w) potential, d) mg Cl- per Liter of pore water (pw) or per kg dry soil, e) Cl-/Br- ratio, does not include ratios with non-detect bromide levels, f), and mg total Nitrogen/Liter pw. SL = Sandy Loam, L = Loam Soil. $\Psi_o + \Psi_m = \Psi_w$

123

4.8.7. Soil Pit Characterization

No soil pit was dug at this site.

4.8.8. Root Density Analysis

No soil pit was dug at this site. The soil pit for determining grass root properties was dug at Site 5 and the root density analysis for that site is considered representative of this site as well.

4.8.9. Bulk Density Data from Soil Core

Bulk density values from the soil core are shown in Table 4.16.

Site 6 – Core Ped Source		
Bulk Density (g cm^{-3})	Depth (m)	Texture
1.37	0.89	L

Table 4.16. Bulk Density values from Site 6 soil core. L = loam soil.

4.6.10. Infiltrometer Data

No infiltrometer measurements were taken at this site. The surface soil of this site is sandy loam, and the infiltrometer measurements for Site 3 on sandy loam soil are considered valid at this site as well.

4.9. Site 7 – Juniper - Forest Service Site

Figure 4.22. Picture of Site 7, facing north.

4.9.1. Site Description

Site 7 (Figure 4.22) is located in Cibola National Forest, just north of Magdalena, NM. The latitude and longitude of the site are 34.213550 and 107.234967 decimal degrees, respectively. The elevation is 1,930 meters above sea level, and the slope and aspect of the site are 1.5 and 140 degrees, respectively. The depth of the drill hole at this site was 9.0 meters. The depth of the groundwater table below the surface is estimated at around 68 meters. This site lies within the La Jencia alluvial groundwater basin (Anderholm 1987a). The soil at this site is classified as a Haplargid Aridisol. This classification was obtained from a map of soil taxonomy that was based on data from the Natural Resources Conservation Service (Soil Map 2005, Soil Survey Staff 1999).

The average annual temperature for this site is 12.1°C, the average annual precipitation is 306 millimeters, and the average annual potential evaporation is 1,270 millimeters; yielding an aridity index of 4.13. These data were obtained from the GIS maps in Section 2.2. Juniper is the predominant vegetation of this site. The Forest

Service attempted to control grazing on its lands through strict law enforcement law and the issuance of grazing permits beginning in 1912 (Scurlock 1998). Cattle grazing presently continues in this area.

4.9.2. EM31 Data

EM31 subsurface conductivity values were taken at Site 7. The results of this survey are shown in Figure 4.23. The difference in the EC values, not the absolute values of the measurements, is the important indicator of soil heterogeneity. This site is considered relatively homogenous, since the EC values near the site (intersection of transects) vary by only 3 mS m^{-1}.
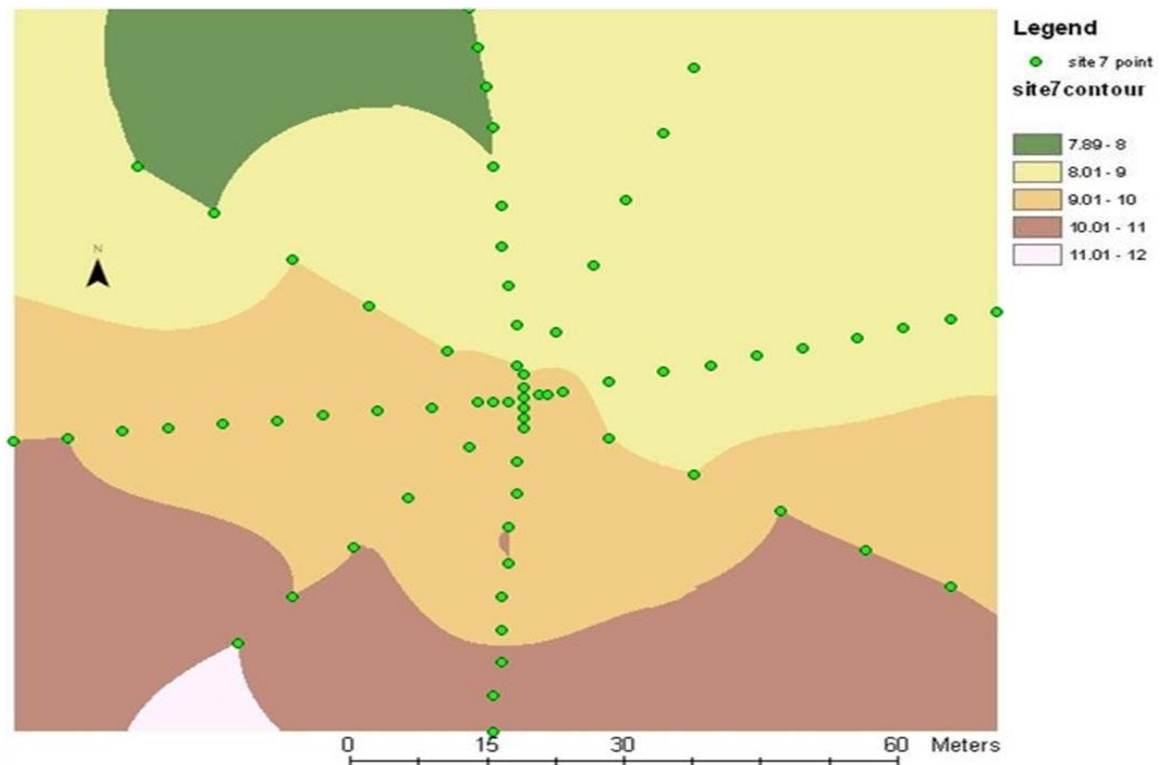
Figure 4.23. Contour of Site 7 conductivity values based on the measurements (green circles) along the transects. Conductivity values in legend in mS m^{-1} units. Contours were determined through kriging the EC measurements. The contour interval is 1 mS m^{-1}.

4.9.3. Plant Identification and Density

Site 7 contains eight one-seed junipers (*Juniperus monosperma*), within a ten meter radius of the drill site, which are approximately 3 meters tall, on average. One Mexican piñón (*Pinus cembroides*) on the site is approximately two meters tall, and one piñón pine (*Pinus edulis*) is approximately three meters tall. The predominant grasses of the site are blue grama (*Bouteloua gracilis*), black grama (*Bouteloua eriopoda*), and tobosa (*Hilaria mutica*). The site also contains silverleaf nightshade (*Solanum elaeagnifolium*), whitethorn acacia (*Acacia constricta*), hairy golden aster (*Heterotheca villosa*), two banana yuccas (*Yucca baccata*), one squawbush (*Rhus trilobata*), desert zinnia (*Zinnia acerosa*), broom snakeweed (*Gutierre sarothrae*), yellow toadflax (*Linaria vulgaris*), and fireweed (*Epilobium angustifolium*). The understory plant interspaces are about 60 to 90 centimeters across and are well connected.

4.9.4. Site Distance from Ecotone

A fairly sharp grass and juniper ecotone exists near Site 7. This ecotone is approximately 340 meters from Grass Site 5 and 1,140 meters from Juniper Site 7. Sites 5 and 7 are approximately 1,480 meters apart.

4.9.5. Geology

The majority of the rocks found in the soil core of Site 7 were igneous rocks; chert was also present. Rhyolite was the dominant rock and it contained noticeable muscovite, sanidine, biotite, and feldspar crystals. These rhyolite rocks were very large, possibly boulder sized, as they were significantly larger than the sampler, which had a 7.6 centimeter outer diameter. Vesicular basalt with olivine and biotite crystals was also

present in this core.

4.9.6. Graphical Summary of Major Parameters

The major parameters that are associated with depth are shown in Figure 4.24.
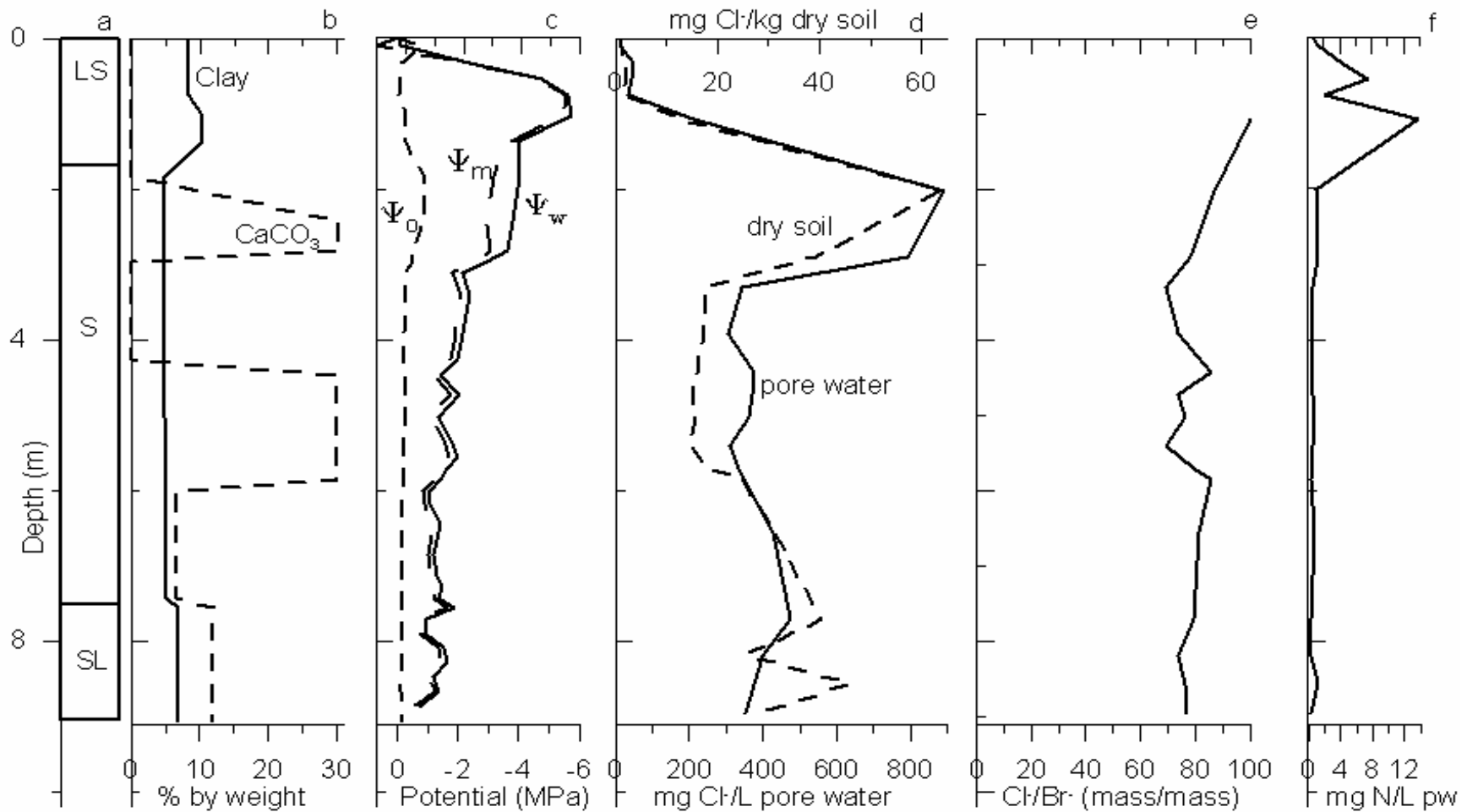
Figure 4.24. Profiles for Site 7 of a) soil texture, b) % CaCO3 and clay by weight, c) osmotic (Ψ_o), matric (Ψ_m), and water (Ψ_w) potential, d) mg Cl- per Liter of pore water (pw) or per kg dry soil, e) Cl-/Br- ratio, does not include ratios with non-detect bromide levels, f), and mg total Nitrogen/Liter pw. SL = Sandy Loam, LS = Loamy Sand, S= Sand Soil. $\Psi_o + \Psi_m = \Psi_w$

129

4.9.7. Soil Pit Characterization

No soil pit was dug at this site.

4.9.8. Root Density Analysis

No soil pit was dug at this site. The soil pit for determining juniper root

properties was dug at Site 8 and the root density analysis for that site is also considered

to be representative of this site as well

4.9.9. Bulk Density Data from Soil Core

Bulk density values from the soil core are shown in Table 4.17.

Site 7 – Core Ped Source		
Bulk Density (g cm^{-3})	Depth (m)	Texture
1.52	0.11	LS
1.73	1.83	S
1.65	5.33	S
2.30	6.45	SL
1.47	7.72	SL

Table 4.17. Bulk Density values from Site 7 soil core. LS = loamy sand, S = sand, and SL = sandy loam soil.

4.9.10. Infiltrometer Data

No infiltrometer measurements were taken at this site. The surface soil of this site

is loamy sand, and the infiltrometer measurements for Site 8 on loamy sand soil are

considered to be valid at this site as well.

4.10. Site 8 – Juniper - Forest Service Site

Figure 4.25. Picture of Site 8, facing east.

4.10.1. Site Description

Site 8 (Figure 4.25.) is located in Cibola National Forest, north of Magdalena, NM. The latitude and longitude of the site are 34.181417 and 107.297700 decimal degrees, respectively. The elevation is 2,040 meters above sea level, and the slope and aspect of the site are 1.5 and 180 degrees, respectively. The depth of the drill hole at this site was 5.4 meters. The depth of the groundwater table below the surface is estimated at around 115 meters. This site lies within the La Jencia alluvial groundwater basin (Anderholm 1987a). The soil at this site is classified as a Haplargid Aridisol. This classification was obtained from a map of soil taxonomy that was based on data from the Natural Resources Conservation Service (Soil Map 2005, Soil Survey Staff 1999).

The average annual temperature for this site is 11.7 ° C, the average annual precipitation is 308 millimeters, and the average annual potential evaporation is 1,240 millimeters; yielding an aridity index of 3.92. These data were obtained from the GIS maps in Section 2.2. The predominant vegetation of this site is juniper. The Forest

Service attempted to control grazing on its lands through strict law enforcement and the issuance of grazing permits beginning in 1912 (Scurlock 1998). Cattle grazing presently continues in this area.

4.10.2. EM31 Data

EM31 subsurface conductivity values were taken at Site 8. The results of this survey are shown in Figure 4.26. The difference in the EC values, not the absolute values of the measurements, is the important indicator of soil heterogeneity. This site is considered relatively homogenous, since the EC values near the site (intersection of transects) vary by only 3 mS m^{-1}.
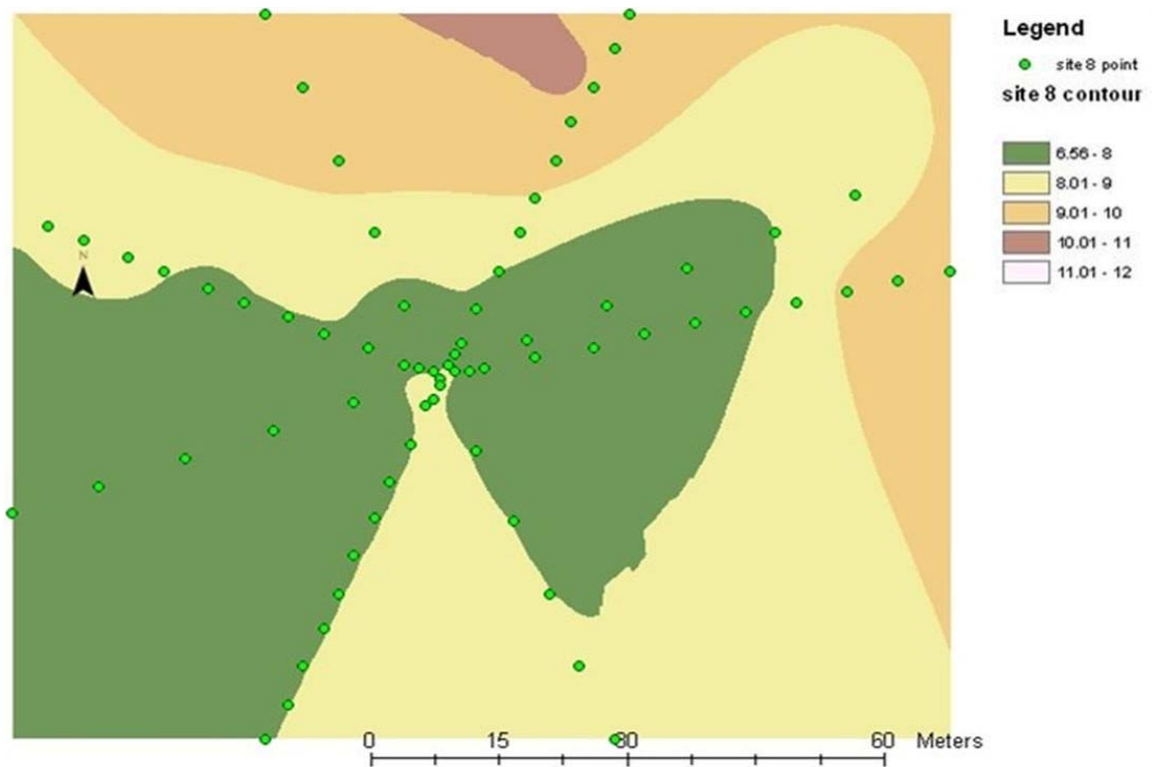
Figure 4.26. Contour of Site 8 conductivity values based on the measurements (green circles) along the transects. Conductivity values in legend in mS m^{-1} units. Contours were determined through kriging the EC measurements. The contour interval is 1 mS m^{-1}.

4.10.3. Plant Identification and Density

Within a ten meter radius of the site, Site 8 contains five one-seed junipers (*Juniperus monosperma*) which are approximately three meters tall, on average. The site also contains one piñón pine (*Pinus edulis*) and a few Utah junipers (*Juniperus osteosperma*) are nearby. The predominant grasses are blue grama (*Bouteloua gracilis*) and black grama (*Bouteloua eriopoda*). The grass bush muhla (*Muhlenbergia porteri*) is also present at the site. Other plants at the site are desert zinnia (*Zinnia acerosa*), yellow toadflax (*Linaria vulgaris*), purple prickly pear (*Opuntia macrocentra*), purple aster (*Machaeranthera canescens*), hairy golden aster (*Heterotheca villosa*), squawbush (*Rhus trilobata*), wavyleaf oak (*Quercus undulata*), netseed lambsquaters (*Chenopodium berlandieri*), and fringed sagebrush (*Artemisia frigida*). The understory plant interspaces are about 60 to 120 centimeters across and are well connected.

4.10.4. Site Distance from Ecotone

Site 8 is within a fairly continuous, large section of juniper and is not considered to be near an ecotone.

4.10.5. Geology

All of the rocks that were in the soil core of Site 8 were igneous rocks. The rocks from this core were highly weathered, therefore their individual crystalline minerals were difficult to determine, especially for the basalt and tuff rocks. The basalt rocks were highly vesicular, with some of the vesicles filled with various weathering products. Because these weathering products did not react with carbonic acid, they were not calcium carbonate. Rhyolite containing muscovite, feldspar, and olivine crystals; granite

with quartz and feldspar crystals; and tuff were also found in this core.

4.10.6. Graphical Summary of Major Parameters

The major parameters that are associated with depth are shown in Figure 4.27.
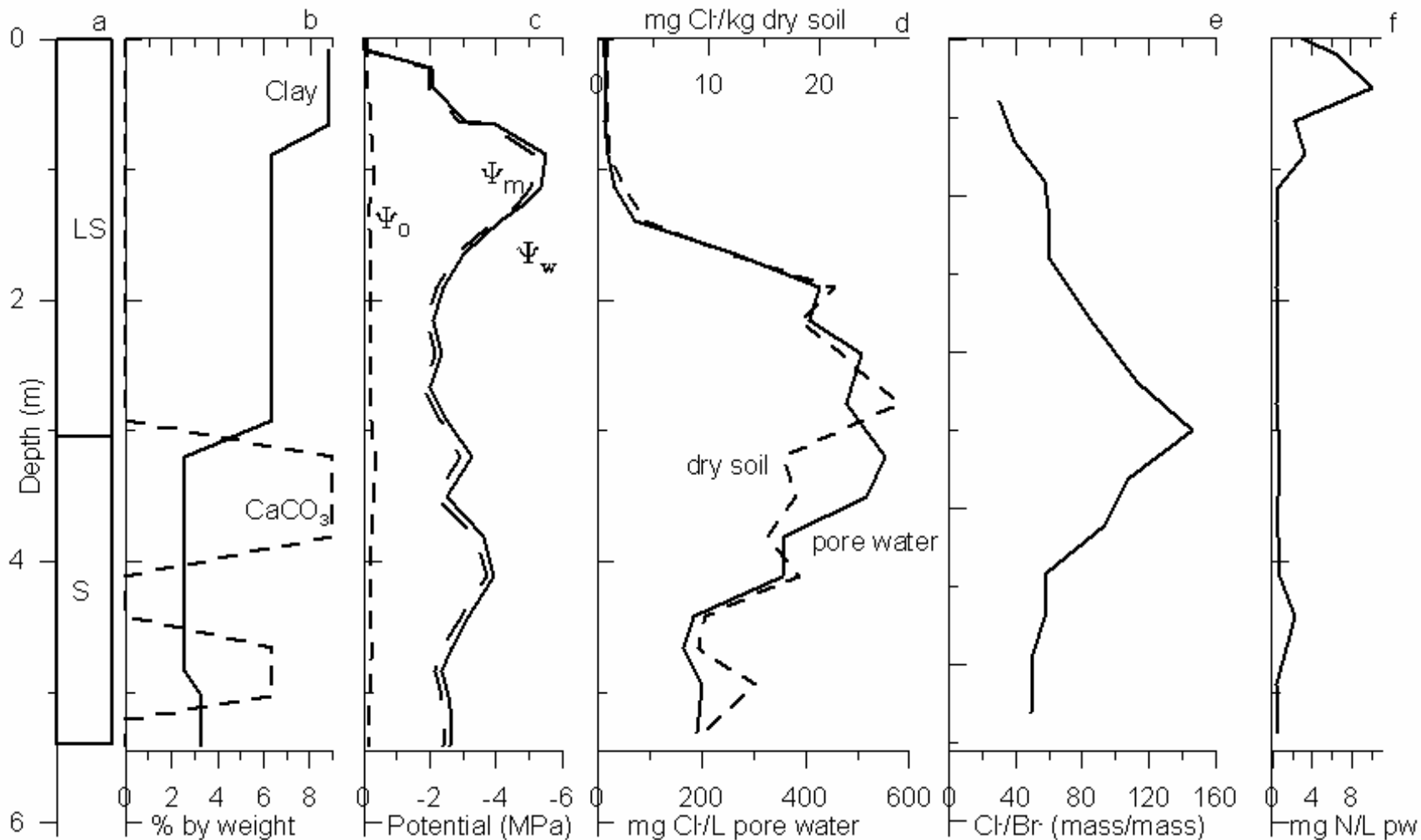
Figure 4.27. Profiles for Site 8 of a) soil texture, b) % CaCO3 and clay by weight, c) osmotic (Ψo), matric (Ψm), and water (Ψw) potential, d) mg Cl- per Liter of pore water (pw) or per kg dry soil, e) Cl-/Br- ratio, does not include ratios with non-detect bromide levels, f), and mg total Nitrogen/Liter pw. LS = Loamy Sand, S= Sand Soil. $\Psi_o + \Psi_m = \Psi_w$

4.10.7. Soil Pit Characterization

A 104-centimeter soil pit was dug near Drill Site 8. The soil profile is shown in Figure 4.28, and the soil description is shown in Tables 4.18 and 4.19. The clean face of the soil pit was placed near a juniper tree in order to perform a root density analysis. This placement oriented the clean face away from the drill hole.

d)

Clean Face

North

Juniper
Tree

3.72 m

Soil Pit

(4 m)

(8 m)

Drill Hole
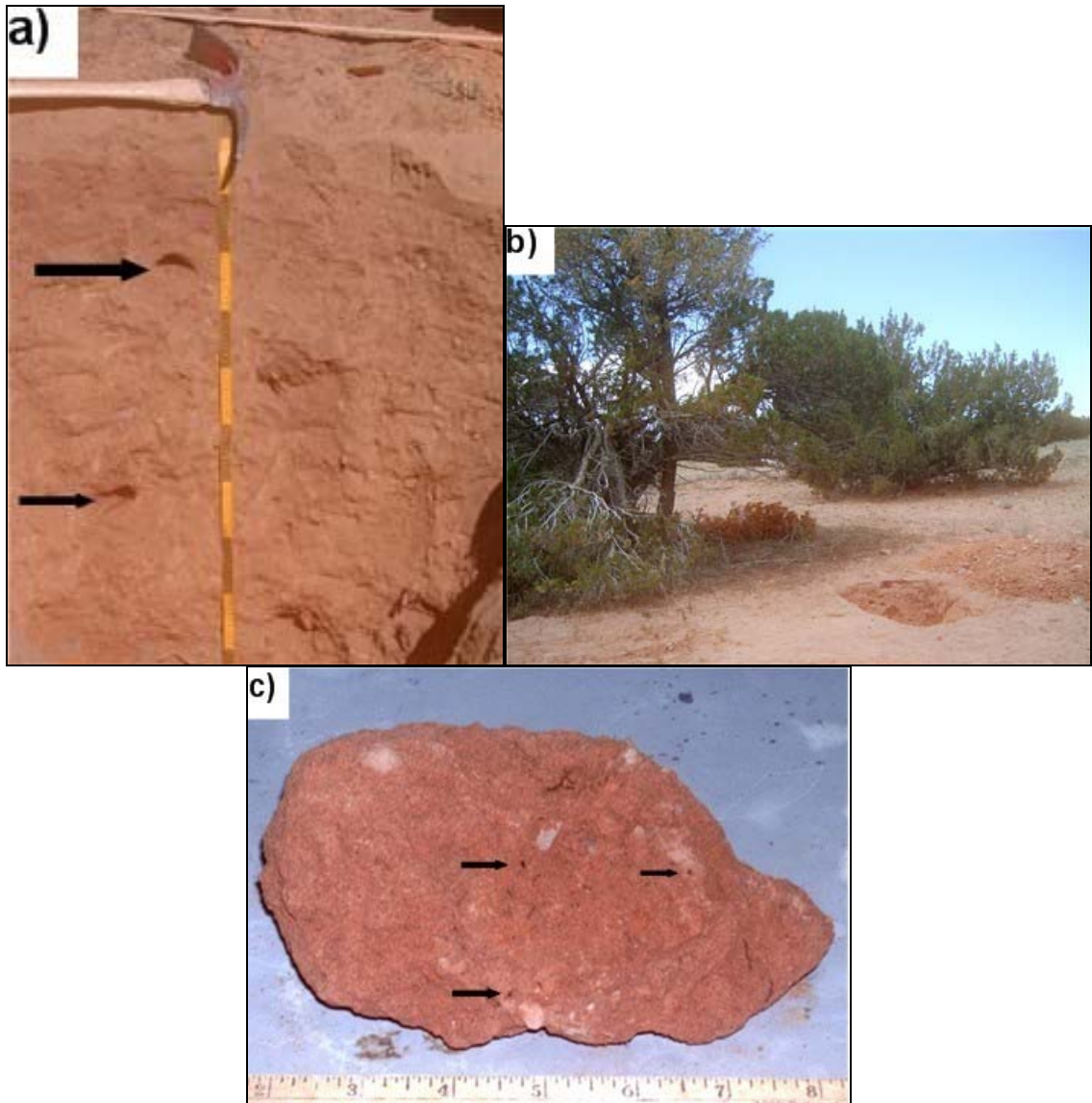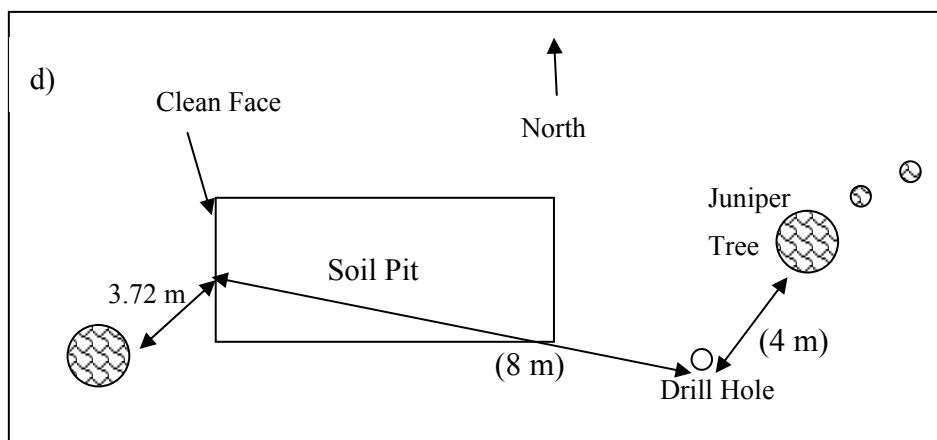
Figure 4.28. Soil pit at Site 8. This pit was dug to a depth of 104 cm. a) The clean face is shown and each black and yellow stripe on the measuring tape denotes 1 meter. The arrows denote decayed root holes. b) The soil pit in relation to the surrounding juniper trees. The closest juniper tree (left side of picture) was 3.72 meters from the soil pit, oriented at a 45 angle from the clean face. c) Ped taken from pit wall. Ruler shown in inches. The ped was 6 inches (15 cm) in length, and contained many visible pores, which are indicated by arrows. This soil pit contained many large ped aggregations, indicating that the soil is highly structured. d) Plan-view diagram of the soil pit in relation to nearby juniper trees and drill site. Lengths in parentheses are estimated. Diagram not to scale.

Location: Site 8, Forest Service											
Aspect: West											
Vegetation: Juniper											
Date/time: 6/22/2004 10:30 am											
				Structure				Consistence			
								Wet			
Horizon	Depth (cm)	Dry Color	Moist Color	Ped Grade	Ped Size	Ped Shape	% Gravel	Sticky	Plasticity	dry	Texture
A	0 to 10	7.5 YR 2.5/3	7.5 YR 4/3	1	f	sbk	10	ss	po	so	SL
B	10 to 50	7.5 YR 2.5/3	7.5 YR 4/4	3	m	sbk	10	ss	po	h	SL
Bt1	50 to 69	7.5 YR 3/4	7.5 YR 4/4	2	m	sbk	20	ss	po	h	SCL
Bt2	69 to 95	7.5 YR 3/4	7.5 YR 5/4	2	m	sbk	50	s	ps	h	SiCL
Bt3	95 to 104	7.5 YR 4/4	7.5 YR 4/6	1	m	sbk	20	ss	ps	h	SC

Table 4.18. Soil pit characterization at Site 8. The soil description method used follows the procedure outlined by the Soil Survey Staff (1993). f = fine, m = medium, sbk = subangular blocky, ss = slightly sticky, s = sticky, po = non-plastic, ps = slightly plastic, so = soft, h = hard, SL = sandy loam, SC = sandy clay, SiCL = silty clay loam, SCL = sandy clay loam soil.

Horizon	Clay Films	Roots Frequency Class	Size	Nature	Pores Frequency Class	Size	Boundary Distinctness	Topography	Calcium Carbonate
A	none	3 (many)	vf - m	woody	2 (common)	m	clear	smooth	none
B	none	2 (common)	vf - m	woody	3 (many)	f - c	gradual	wavy	none
Bt1	none	2 (common)	vf - c	woody	3 (many)	f - c	gradual	wavy	none
Bt2	none	1 (few)	vf - c	woody	2 (common)	f	clear	wavy	none
Bt3	none	1 (few)	m - c	woody	1 (few)	f	buried	buried	none

Table 4.19. Soil pit characterization at Site 8 (continued). The soil description method used follows the procedure outlined by the Soil Survey Staff (1993). vf = very fine, f = fine, m = medium, c = course.

4.10.8. Root Density Analysis

A root density analysis of the juniper trees growing near the soil pit at Site 8 was performed using a ten by ten centimeter square. Some grass was present underneath the juniper; if they were located within the sampling square, the grass roots were also included in this analysis. The results of the analysis are shown in Table 4.20

Depth (cm)	Average # of Roots with Noted Diameter < 1 mm	1 - 10 mm	> 10 mm	total	%	Notes
0 to 20	28	1.3	0	30	38	
20 to 40	17	1.3	0	18	23	Decayed root holes – at 22 cm depth and 19 cm deep, at 30 cm depth and 38 cm deep (left wall of pit), at 30 cm depth and 38 cm deep.
40 to 60	18	2.3	0.33	21	27	Decayed root hole with root still in it at 58 cm profile depth, 9 cm deep.
60 to 80	6.7	2.0	0.33	9	11	Largest root here – 9 cm circumference.
80 to 105	0	0.67	0.33	1	1	
			Total	79		Roots present at bottom of pit.

Table 4.20. Root density analysis of juniper at Site 8. Values shown are the average number of roots for that diameter of the three replicates taken at each depth interval. A 10 by 10 cm square was used to count the roots. The majority of the roots were located between 0 and 20 cm depth.

Figure 4.29. Root density analysis of juniper at Site 8. a) Decaying juniper root on side of soil pit. b) Hole formed by decayed juniper root, 48 centimeters deep. c) Another hole formed by decayed root, 97 centimeters deep. d) Large roots are shown in a close up laboratory picture. The ruler shown here is in centimeters. The diameters of the larger roots ranged from 1 to 2.5 cm. e) Juniper tree on edge of arroyo, with washed out roots. The arrow points to main tap root. Large roots also extend to the left of the tree.

4.10.9. Bulk Density from Soil Pit and Soil Core

The bulk density of peds found in the core and soil pit are shown in Table 4.21. Since peds were taken from both the wall of the soil pit and the core, any possible compaction of the peds in the soil core can be determined. When comparing the averages of the bulk densities of both the core and the pit peds, no significant difference between them exists, demonstrating slight to-no-compaction of the peds in this soil core.

Site 8 – Pit Ped Source		
Bulk Density (g cm^{-3})	Depth (m)	Texture
1.70	0.06	LS
1.42	1.78	LS
1.63	1.99	LS
1.63	2.08	LS
1.18	2.76	LS
Average Bulk Density (g cm^{-3})		# Samples
1.51 ± 0.21		5
Site 8 – Core Ped Source		
Bulk Density (g cm^{-3})	Depth (m)	Texture
1.65	0.08	LS
1.59	1.27	LS
Average Bulk Density (g cm^{-3})		# Samples
1.62 ± 0.04		2

Table 4.21. Bulk density values of peds from soil pit and soil core of Site 8. Peds from soil pit were taken from the wall of the clean face. LS = loamy sand.

4.10.10. Infiltrometer Data

The infiltrometer data measured at Site 8 are summarized in Table 4.22. Three infiltrometer measurements were taken at two sites, resulting in six Ksat values. One of the Ksat values, 52.8 cm hr^{-1}, was ten times higher than all of the other values; this value was considered an outlier and was not used in determining the average Ksat. The average Ksat value calculated from the data was one-third the default value for this soil type. The soil crust was not removed from the area so that the measurement would represent actual field infiltration conditions. This could be the reason for the measured value being lower than the default value. Figure 4.30. shows the two surface areas that infiltrometer

measurements were taken at before surface preparation.

Site 8 – Loamy Sand Soil					
Surface Soil Texture	Default Ksat (cm hr^{-1})	Average K sat (cm hr^{-1})	# of Measurements	Alpha	% Clay in Surface Soil
LS	15	4.59 ± 1.64	5	0.15	8.85

Table 4.22. Infiltrometer data from Site 8. Default Ksat for loamy sand soil from Carsel and Parrish (1988). Ksat value an average of the five calculated Ksat values from the five measured infiltration values taken at two sites. Alpha is a Van Genuchten parameter. LS = loamy sand soil.
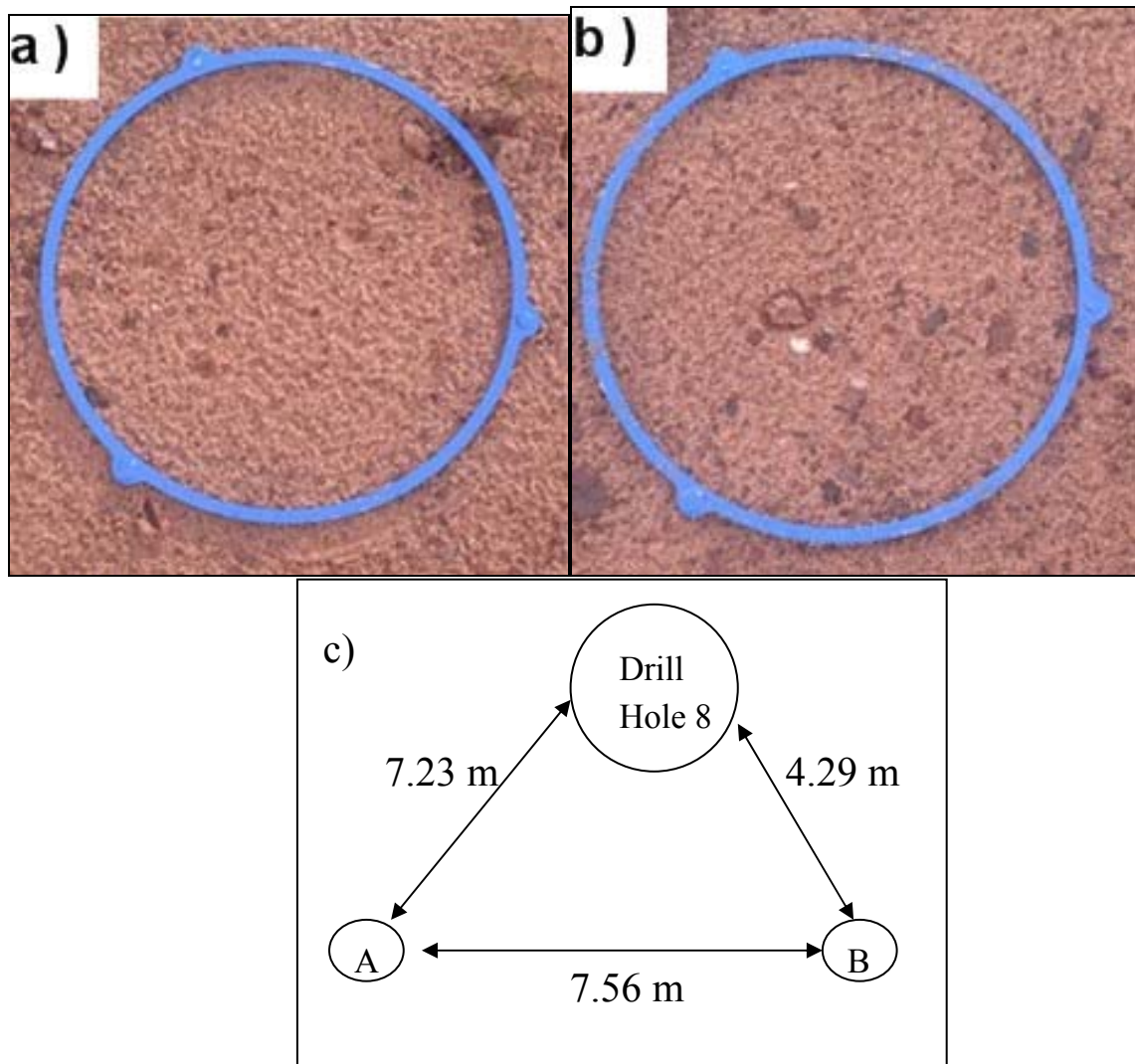
Figure 4.30. a) and b) Surface areas (area inside rings) where infiltrometer measurements were taken before surface preparation in the top two pictures. The rings have a 20 cm diameter. c) Plan-view diagram of the infiltrometer setup with A = infiltrometer A and B = infiltrometer B and distances between infiltrometers and sites noted. Diagram is not to scale.

4.11. Site 9 – Juniper - Forest Service Site

Figure 4.31. Picture of Site 9, facing north.

4.11.1. Site Description

Site 9 (Figure 4.31) is located in Cibola National Forest, just north of Magdalena, NM. The latitude and longitude of the site are 34.184467 and 107.317183 decimal degrees, respectively. The elevation is 2,050 meters above sea level, and the slope and aspect of the site are 1 and 180 degrees, respectively. The depth of the drill hole at this site was 5.4 meters. The depth of the groundwater table below the surface is estimated to be around 107 meters. This site lies within the La Jencia alluvial groundwater basin (Anderholm 1987a). The soil at this site is classified as a Haplargid Aridisol. This classification was obtained from a map of soil taxonomy that was based on data from the Natural Resources Conservation Service (Soil Map 2005, Soil Survey Staff 1999).

The average annual temperature for this site is 11.5 ° C, the average annual precipitation is 316 millimeters, and the average annual potential evaporation is 1,240 mm; this yields an aridity index of 3.92. These data were obtained from the GIS maps in section 2.2. Juniper is the predominant vegetation of this site. The Forest Service attempted to control grazing on its lands through strict law enforcement and the issuance

of grazing permits beginning in 1912 (Scurlock 1998). Cattle grazing presently continues in this area.

4.11.2. EM31 Data

EM31 subsurface conductivity values were taken at Site 9. The results of this survey are shown in Figures 4.32 and 4.33. The difference in the EC values, not the absolute values of the measurements, is the important indicator of soil heterogeneity. Figure 4.32 shows the first EC survey taken of the area; since this survey demonstrated some heterogeneity in the area's soil, another site was surveyed. This second was located 101 meters to the south of the original survey, and survey is shown in Figure 4.33. While this second site still shows significant variation in the conductivity measurements, variation was much less than that in the first site chosen. Both figures have the identical contour interval of 1 mS m^{-1}. At the second site, which was chosen for drilling, the electrical conductivity measurements differ by 6 mS m^{-1} near the site.
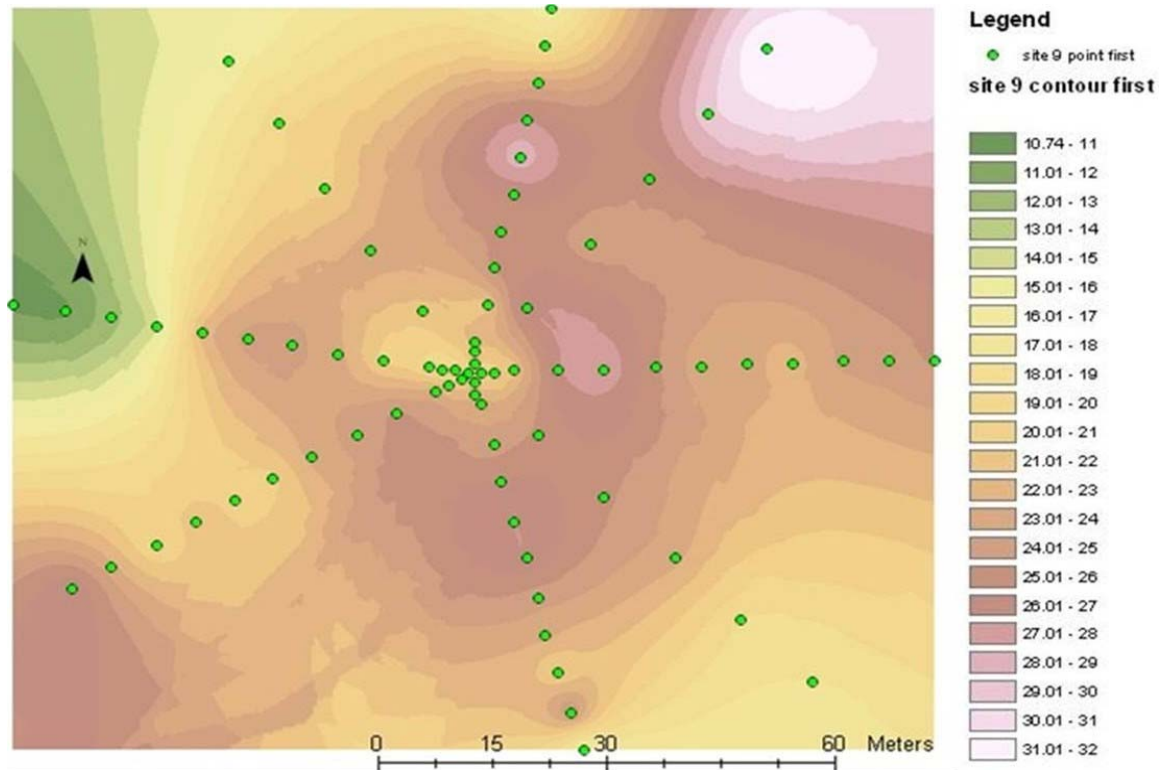
Figure 4.32. Contour of Site 9 conductivity values based on the measurements (green circles) along the transects. Conductivity values in legend in mS m^{-1} units. Site located at intersection of transects. This was the first survey of the Site 9 area. Because of the soil heterogeneities demonstrated in this survey, this site was not chosen for drilling. The latitude and longitude of the site were 34.18538 and 107.317167 decimal degrees, respectively. Contours were determined through kriging the EC measurements. The contour interval is 1 mS m^{-1}.

144
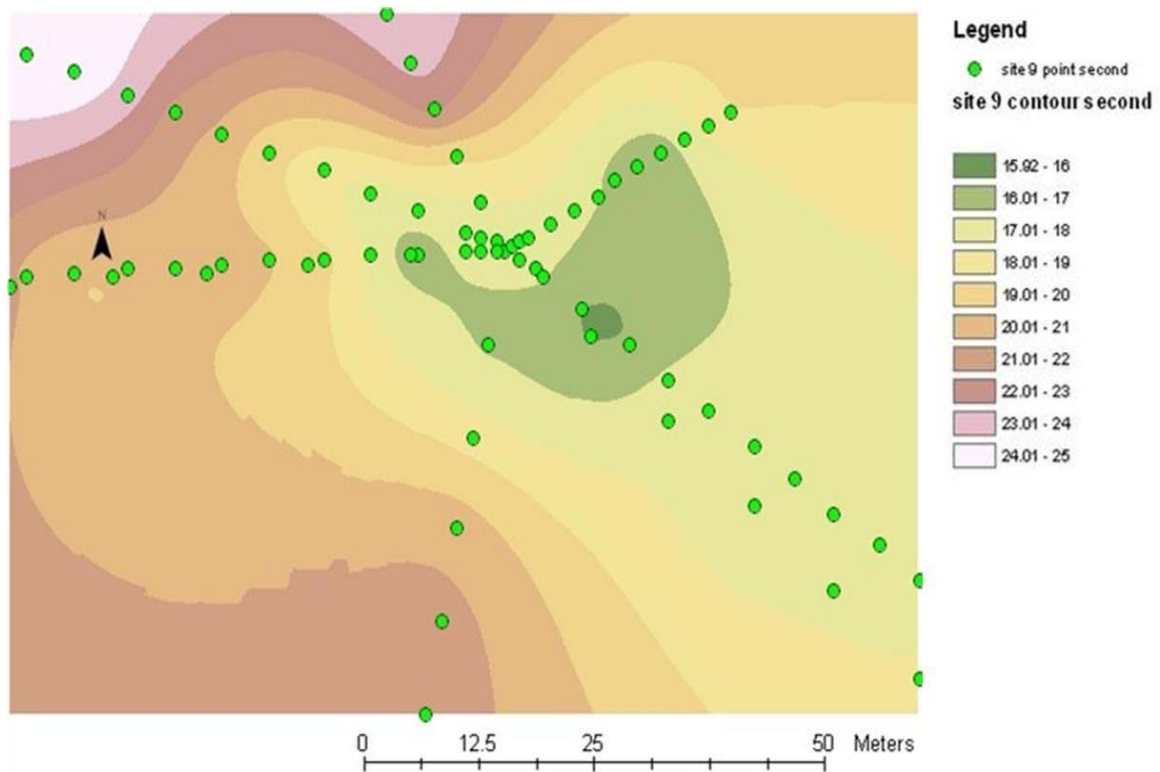
Figure 4.33. Contour of Site 9 conductivity values based on the measurements (green circles) along the transects. Conductivity values in legend in mS m^{-1} units. Site located at intersection of transects. This was the second survey of the Site 9 area. Since it had much less heterogeneity than the first survey, this site was chosen for drilling the soil core. Contours were determined through kriging the EC measurements. The contour interval is 1 mS m^{-1}.

4.11.3. Plant Identification and Density

Within a ten meter radius of the drill site, Site 9 contains six one-seed junipers (*Juniperus monosperma*) that are approximately 3 meters tall, on average. The predominant grasses are blue grama (*Bouteloua gracilis*), black grama (*Bouteloua eriopoda*), and bush muhla (*Muhlenbergia porteri*). Gyp threeawn (*Aristida gypsophila*) grass is also present the site. Other plants at the site are desert zinnia (*Zinnia acerosa*), broom snakeweed (*Gutierre sarothrae*), yellow toadflax (*Linaria vulgaris*), squawbush (*Rhus trilobata*), hairy golden aster (*Heterotheca villosa*), broom snakeweed (*Gutierre sarothrae*), purple aster (*Machaeranthera canescens*), and fringed sagebrush (*Artemisia frigida*). The understory plant interspaces are about 15 to 30 centimeters across and are

145

not well connected.

4.11.4. Site Distance from Ecotone

Site 9 is within a fairly continuous, large section of juniper and is not considered to be near an ecotone.

4.11.5. Geology

All of the rocks that were in the soil core of Site 9 were igneous rocks where basalt was the dominant rock. The basalt rock was vesicular and contained observable biotite, olivine and feldspar crystals. Tuff with olivine and biotite crystals and granodiorite were also found in this core. Most rocks were coated with calcium carbonate.

4.11.6. Graphical Summary of Major Parameters

The major parameters that are associated with depth are shown in Figure 4.34.
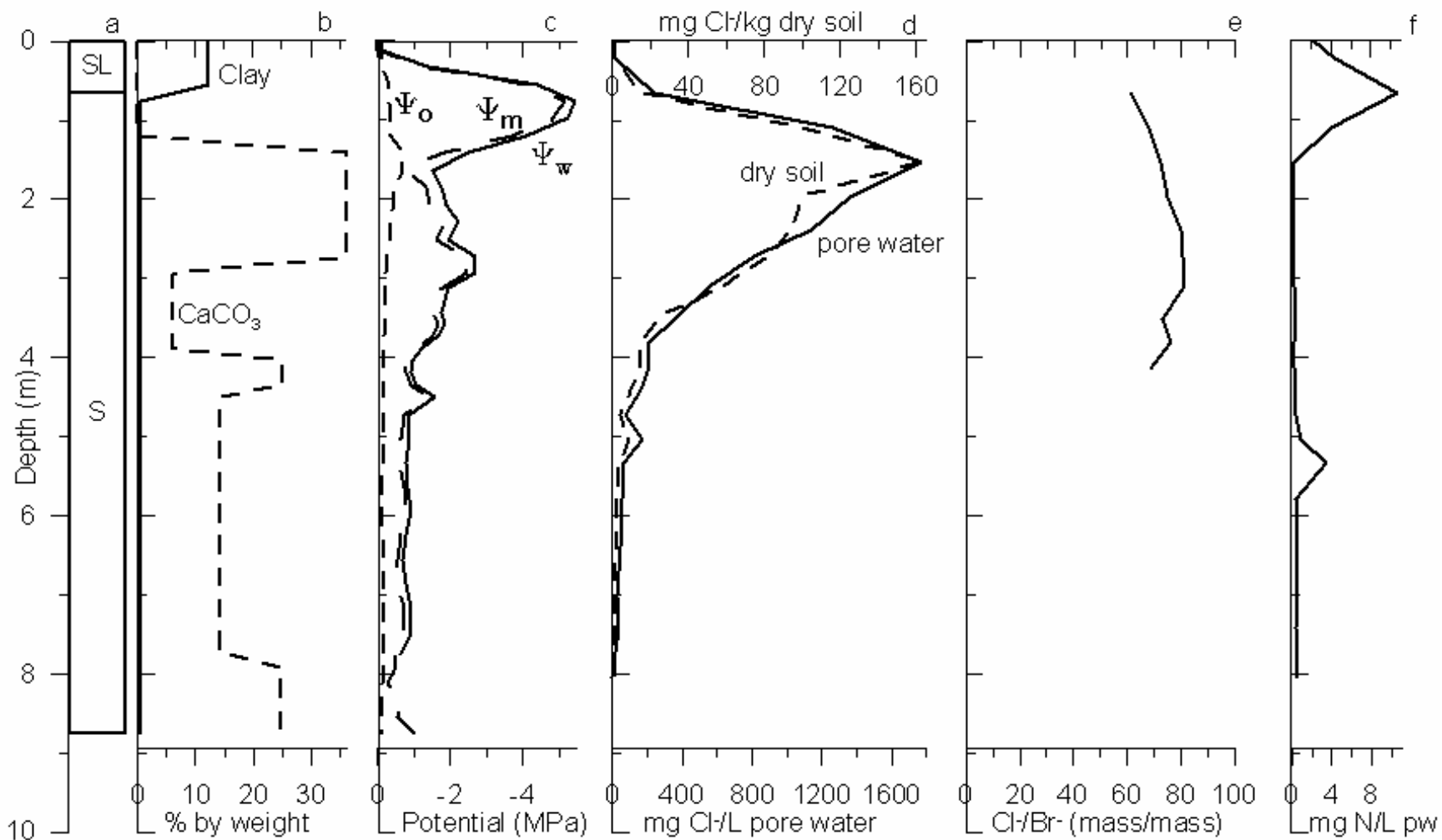
Figure 4.34. Profiles for Site 9 of a) soil texture, b) % CaCO3 and clay by weight, c) osmotic (Ψ_o), matric (Ψ_m), and water (Ψ_w) potential, d) mg Cl- per Liter of pore water (pw) or per kg dry soil, e) Cl-/Br- ratio, does not include ratios with non-detect bromide levels, f), and mg total Nitrogen/Liter pw. SL = Sandy Loam, S= Sand Soil. $\Psi_o + \Psi_m = \Psi_w$

147

4.11.7. Soil Pit Characterization

No soil pit was dug at this site.

4.11.8. Root Density Analysis

No soil pit was dug at this site. The soil pit for determining juniper root properties was dug at Site 9 and the root density analysis for that site is considered representative of this site as well.

4.11.9. Bulk Density Data from Soil Core

Bulk density values from the soil core are shown in Table 4.23.

Site 9 – Core Ped Source		
Bulk Density (g cm^{-3})	Depth (m)	Texture
1.58	0.33	SL
1.59	1.63	S

Table 4.23. Bulk Density values from Site 9 soil core. LS = loamy sand, S = sand, and SL = sandy loam soil.

4.11.10. Infiltrometer Data

No infiltrometer measurements were taken at this site. The surface soil of this site is sandy loam, and the infiltrometer measurements for Site 3 on sandy loam soil are considered to representative of this site as well.

4.12. Site 10 – Ponderosa Pine - Forest Service Site

Figure 4.35. Picture of Site 10, with drill rig, facing south.

4.12.1. Site Description

Site 10 (Figure 4.35) is located in Cibola National Forest, just north of Magdalena, NM. The latitude and longitude of the site are 34.187367 and 107.453500 decimal degrees, respectively. The elevation is 2,300 meters above sea level, and the slope and aspect of the Site are 6 and 20 degrees, respectively. The depth of the drill hole at this site was 4.8 meters. The depth of the groundwater table below the surface is estimated at around 113 meters. This site lies within the San Agustin alluvial groundwater basin (Myers et al. 1994). The soil at this site is classified as a Haplustoll Mollisol. This classification was obtained from a map of soil taxonomy that was based on data from the Natural Resources Conservation Service (Soil Map 2005, Soil Survey Staff 1999).

The average annual temperature for this site is 9.5 ° C, the average annual

precipitation for this site is 336 millimeters, and the average annual potential evaporation is 1,220 millimeters, yielding an aridity index of 3.64. These data were obtained from the GIS maps in Section 2.2. The predominant vegetation of this site is ponderosa pine. This site is the coldest site and most humid of the transect. The Forest Service attempted to control grazing on its lands through strict enforcement of the law and the issuance of grazing permits beginning in 1912 (Scurlock 1998). Cattle grazing presently continues in this area.

4.12.2. EM31 Data

EM31 subsurface conductivity values were taken at Site 10. The results of this survey are shown in Figures 4.36 and 4.37. The difference in the EC values, not the absolute values of the measurements, is the important indicator of soil heterogeneity. Figure 4.36 shows the first EC survey taken of the area; since this survey demonstrated some heterogeneity in this area's soil, another site was surveyed. This second survey was located 910 meters west northwest of the original survey, and is shown in Figure 4.37. While the second site still shows significant variance in the conductivity measurements, variation was much less than in the first site. Both figures have the same contour interval, 1 mS m^{-1}. At the second site, which was chosen for drilling, the electrical conductivity measurements differ by 6 mS m^{-1} near the site
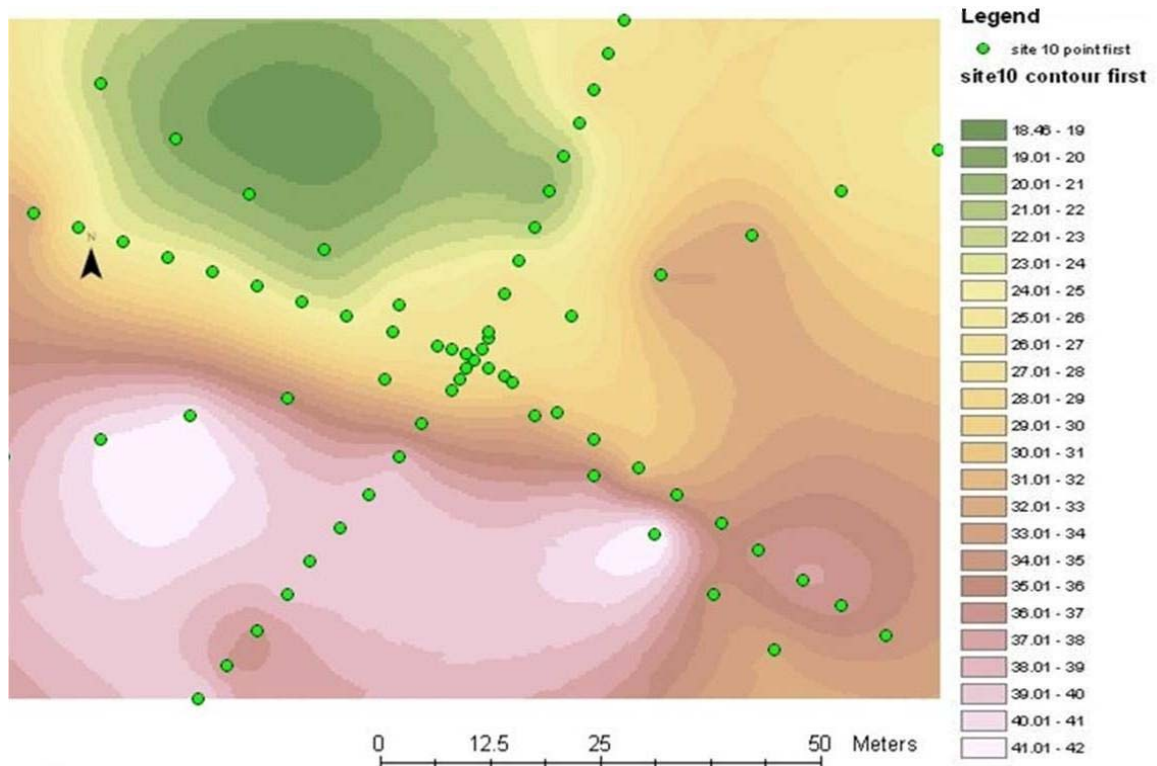
Figure 4.36. Contour of Site 10 conductivity values based on the measurements (green circles) along the transects. Conductivity values in legend in mS m^{-1} units. Site located at intersection of transects. This was the first survey of the Site 10 area. This site was not chosen for drilling as a result of the soil heterogeneities demonstrated in this survey. The latitude and longitude of the site are 34.184633 and 107.462800 decimal degrees, respectively. Contours were determined through kriging the EC measurements. The contour interval is 1 mS m^{-1}.
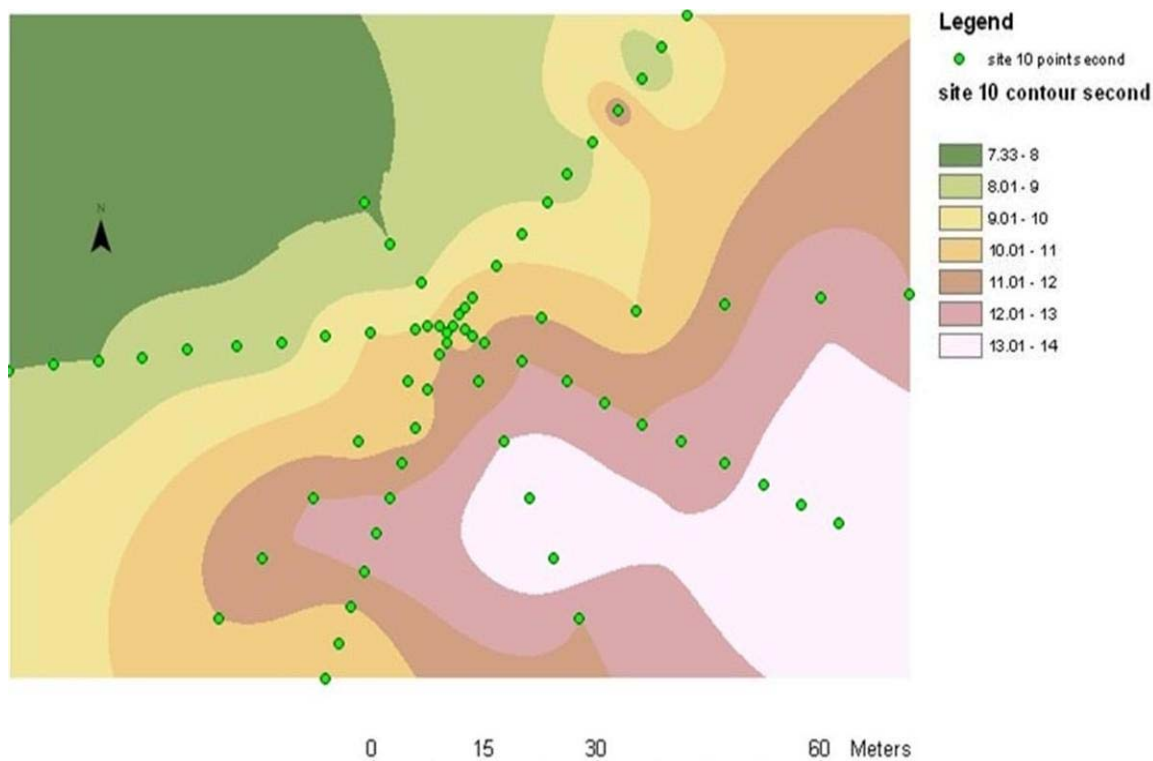
Figure 4.37. Contour of Site 10 conductivity values based on the measurements (green circles) along the transects. Conductivity values in legend in mS m^{-1} units. Site located at intersection of transects. This was the second survey done of the Site 10 area. Since it was less heterogeneous than the first survey, this site was chosen for drilling the soil core. Contours were determined through kriging the EC measurements. The contour interval is 1 mS m^{-1}.

4.12.3. Plant Identification and Density

Site 10 contains three mature ponderosa pines (*Pinus ponderosa*) within a ten meter radius of the drill site, each of which is over 30 meters tall. The site also contains one piñón pine (*Pinus edulis*) and one one-seed juniper (*Juniperus monosperma*) which are both around three meters tall. The predominant grass is black grama (*Bouteloua eriopoda*). Gyp threeawn (*Aristida gypsophila*) and hare barley (*Critesion murinum*) grasses are also present. Other plants at the site are netseed lambsquaters (*Chenopodium berlandieri*), red sorrel (*Rumex acetosella*), field pennycress (*Thlaspi arvense*), woolly plantain (*Plantago patagonica*), broom snakeweed (*Gutierre sarothrae*), and hairy

152

golden aster (*Heterotheca villosa*). Pine needles cover the site and are several centimeters deep near the trunks. The understory plants are about 30 to 60 centimeters apart and are connected.

4.12.4. Site Distance from Ecotone

This site is in an area of fairly continuous ecosystem dominated by ponderosa pine trees, with some juniper and piñón pine trees. The closest ecotone would be the ponderosa pine and piñón-juniper mix ecotone. The piñón-juniper mix ecosystem was not sampled, therefore this ecotone was not included in the study. Also, no juniper- and ponderosa-pine ecotone was present in the area of the transect.

4.12.5. Geology

All of the rocks that were in the soil core of Site 10 were igneous rocks. Continuous basalt rock was found between a depth of 2.74 meters and 4.8 meters (the end of the core). The basalt rocks were vesicular and contained large malachite veins as well as observable feldspar and olivine crystals. The boundary between the soil and the basalt rock at 2.74 meters was not distinct, with the soil becoming more compact with depth and transitioning gradually into the basalt rock. The basalt rock below a depth of 2.74 meters became increasingly dense with depth in the core. Tuff with biotite crystals was found in the soil section of this core.

4.12.6. Graphical Summary of Major Parameters

The major parameters that are associated with depth are shown in Figure 4.38.
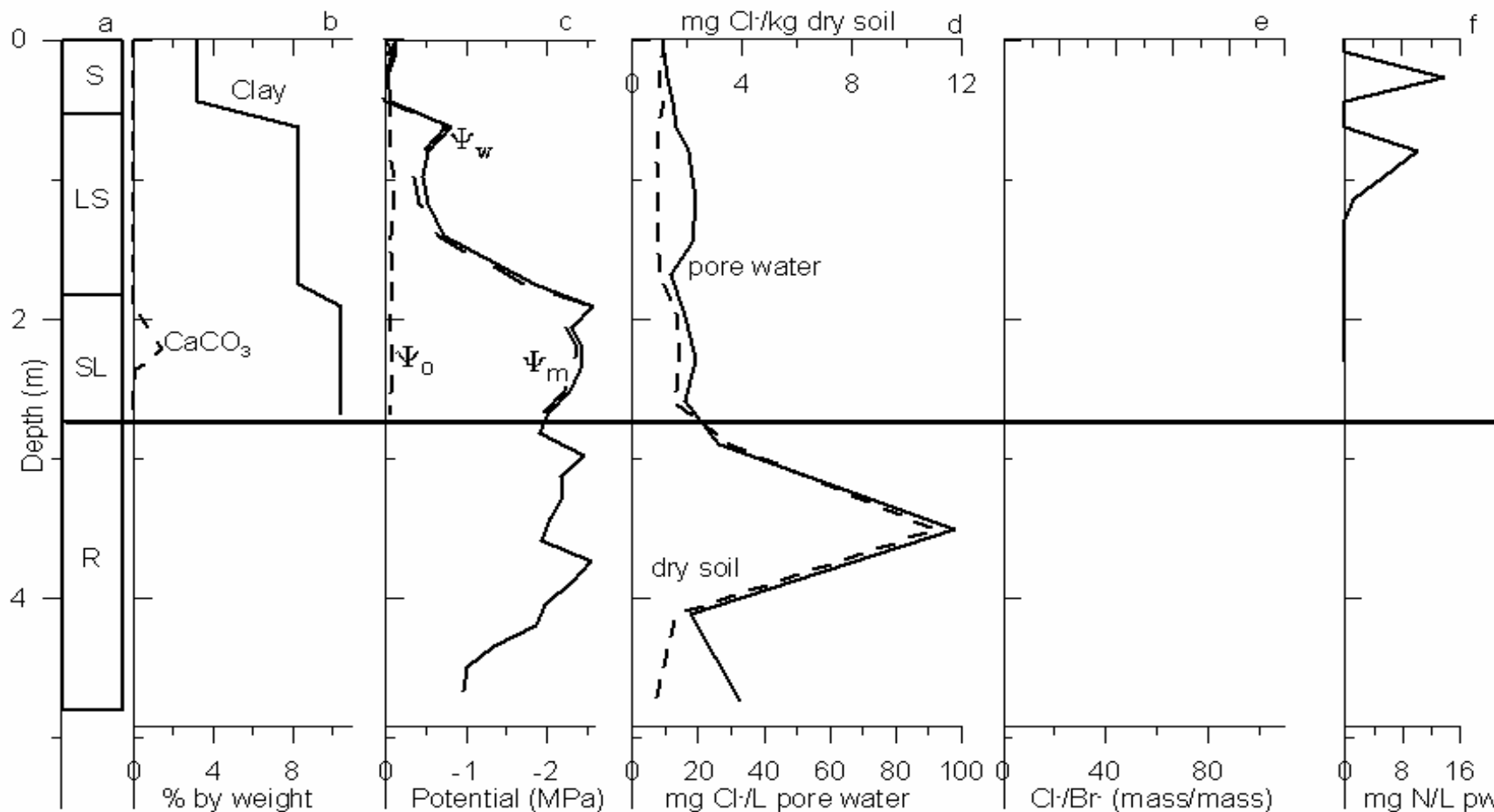
Figure 4.38. Profiles for Site 10 of a) soil texture, b) % CaCO3 and clay by weight, c) osmotic (Ψ_o), matric (Ψ_m), and water (Ψ_w) potential, d) mg Cl- per Liter of pore water (pw) or per kg dry soil, e) Cl-/Br- ratio, all bromide values were below detection levels, f), and mg total Nitrogen/Liter pw. LS = Loamy Sand, S= Sand, SL = Sandy Loam Soil, R = Rock (basalt, separated by line).
$\Psi_o + \Psi_m = \Psi_w$

154

4.12.7. Soil Pit Characterization

No soil pit was dug at this site.

4.12.8. Root Density Analysis

No soil pit was dug at this site. The soil pit for determining ponderosa pine root properties was dug at Site 11 and the root density analysis for that site is also considered representative of this site.

4.12.9. Bulk Density

The bulk density values from the soil core are shown in Figure 4.24.

Site 10 – Core Ped Source		
Bulk Density (g cm^{-3})	Depth (m)	Texture
1.81	0.09	S
1.55	1.41	LS
1.58	1.91	SL
2.02	4.04	R

Table 4.24. Bulk density values from the soil core at Site 10. S= sand, LS = loamy sand, SL = sandy loam, R= rock (vesicular basalt).

4.12.10. Infiltrometer Data

The infiltrometer data measured at Site 10 are summarized in Table 4.25. Four Ksat values were calculated from: three infiltrometer measurements for infiltrometer B and two measurements for infiltrometer A. The average Ksat value calculated from the data was only eleven percent of the default value for this soil type. The soil crust was not removed from the area; this could be one reason for the measured value being lower than the default value. The site also had a six degree slope, which could have contributed to this difference. The measurements were taken to represent actual field infiltration conditions of this site. This site is the only one with sandy soil, therefore this

measurement was not extrapolated to another site. Figure 4.38 shows a surface area where infiltrometer measurements were taken before and after surface preparation.

Site 10 – Sandy Soil					
Surface Soil Texture	Default Ksat (cm hr^{-1})	Average K sat (cm hr^{-1})	# of Measurements	Alpha	% Clay in Surface Soil
S	30	3.28 ± 0.38	4	0.17	3.18

Table 4.25. Infiltrometer data from Site 10. Default Ksat for sandy soil from Carsel and Parrish (1988). Ksat value an average of the four calculated Ksat values from the five measured infiltration values taken at two sites. Alpha is a Van Genuchten parameter. S = sandy soil.
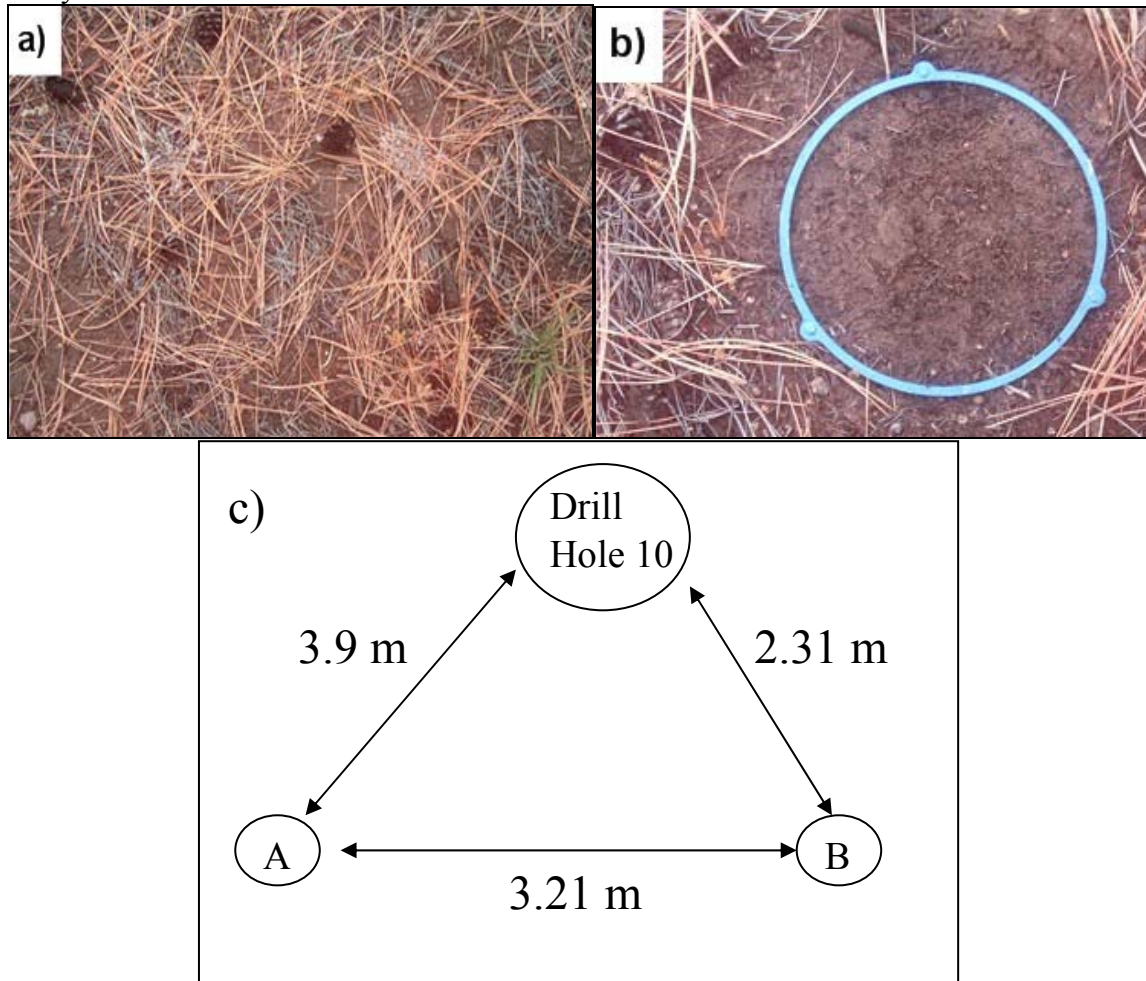
Figure 4.38. a) Surface area where infiltration measurements were taken, before litter was removed. The darker areas in the picture are pine cones. b) Surface area (area inside ring) where infiltrometer measurements were taken after surface preparation. The ring have a 20 cm diameter. A picture of the surface area for second infiltrometer used at this site not taken. c) A plan-view diagram of the infiltrometer setup with A = infiltrometer A and B = infiltrometer B and distances between infiltrometers and sites noted. Diagram is not to scale.

4.13. Site 11 – Ponderosa Pine - Forest Service Site
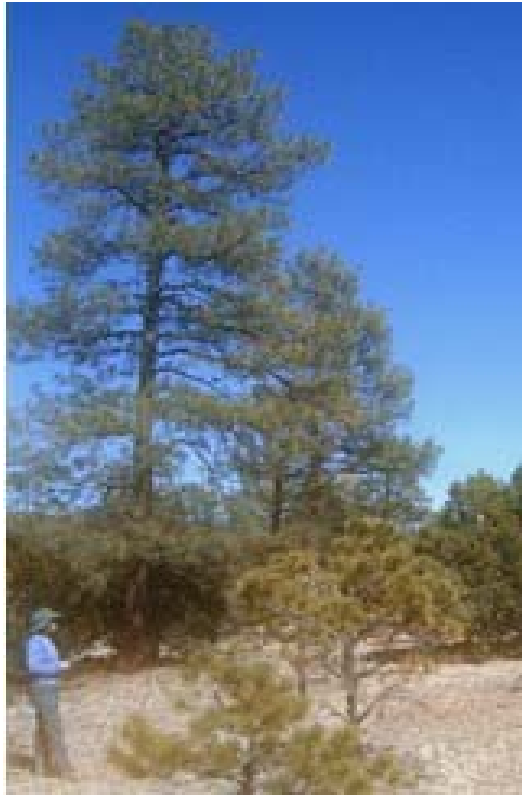
Figure 4.39. Picture of Site 11, facing south.

4.12.1. Site Description

Site 11 (Figure 4.39) is located in Cibola National Forest, just north of Magdalena, NM. The latitude and longitude of the site are 34.195067 and 107.479750 decimal degrees, respectively. The elevation is 2,380 meters above sea level, and the slope and aspect of the site are 2.5 and 10 degrees, respectively. The depth of the drill hole at this site was 4.8 meters. The depth of the groundwater table below the surface is estimated at around 122 meters. This site lies within the San Agustin alluvial groundwater basin (Myers et al. 1994). The soil at this site is classified as a Haplustoll Mollisol. This classification was obtained from a map of soil taxonomy that was based on data from the Natural Resources Conservation Service (Soil Map 2005, Soil Survey Staff 1999).

The average annual temperature for this site is 9.2 ° C, the average annual precipitation is 327 millimeters, and the average annual potential evaporation is 1,220 millimeters; yielding an aridity index of 3.72. These data were obtained from the GIS maps in Section 2.2. The predominant vegetation of this site is ponderosa pine. The Forest Service attempted to control grazing on its lands through strict enforcement of the law and the issuance of grazing permits beginning in 1912 (Scurlock 1998). Cattle grazing presently continues in this area.

4.13.2. EM31 Data

EM31 subsurface conductivity values were taken at Site 11. The results of this survey are shown in Figures 4.40 and 4.41. The difference in the EC values, not the absolute values of the measurements, is the important indicator of soil heterogeneity. Figure 4.40 was the first EC survey taken of the area. Since this survey demonstrated some heterogeneity in the area's soil, another site was surveyed. This second survey was located 74 meters west of the original survey and is shown in Figure 4.41. While the second site still shows significant variance in the conductivity measurements, variation was much less than in the first site chosen. Both figures have the same contour interval of 2 mS m^{-1}. At the second site, which was chosen for drilling, the electrical conductivity measurements differ by 12 mS m^{-1} near the site.
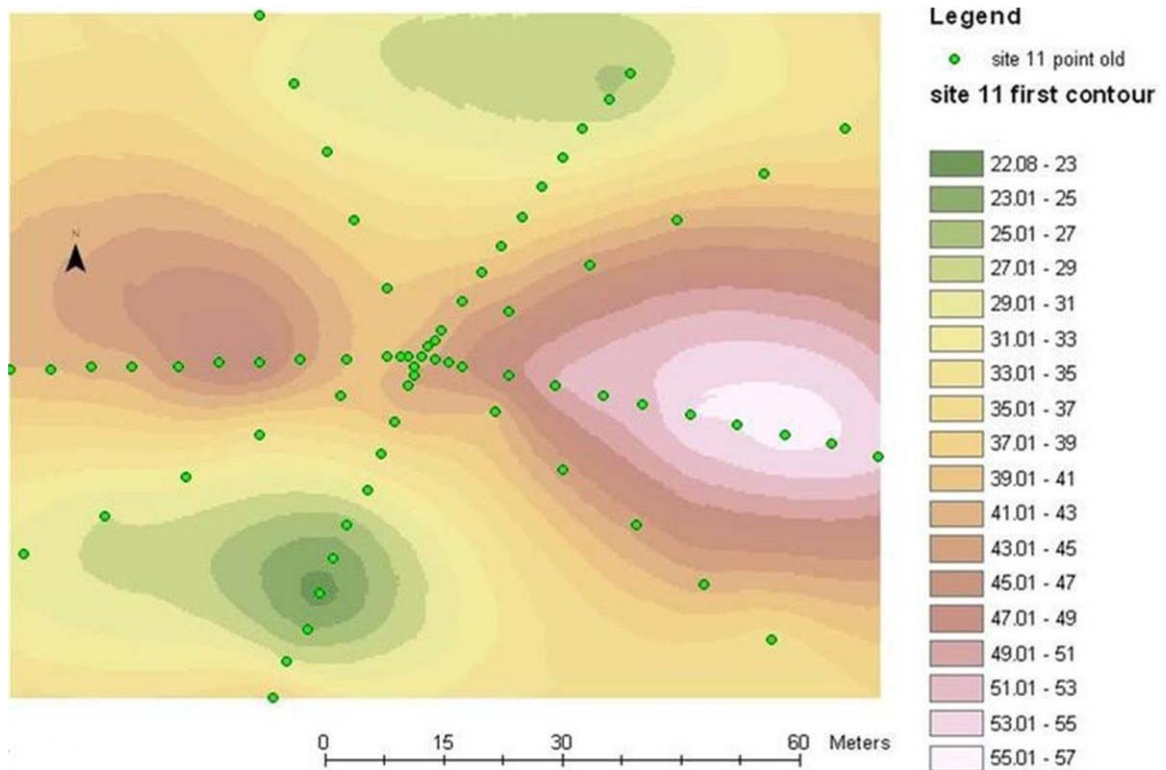
Figure 4.40. Contour of Site 11 conductivity values based on the measurements (green circles) along the transects. Conductivity values in legend in mS m^{-1} units. Site located at intersection of transects. The latitude and longitude of the site are 34.195000 and 107.47895 decimal degrees, respectively. This site was not chosen for drilling as a result of the soil heterogeneities demonstrated in this survey. Contours were determined through kriging the EC measurements. The contour interval is 2 mS m^{-1}.
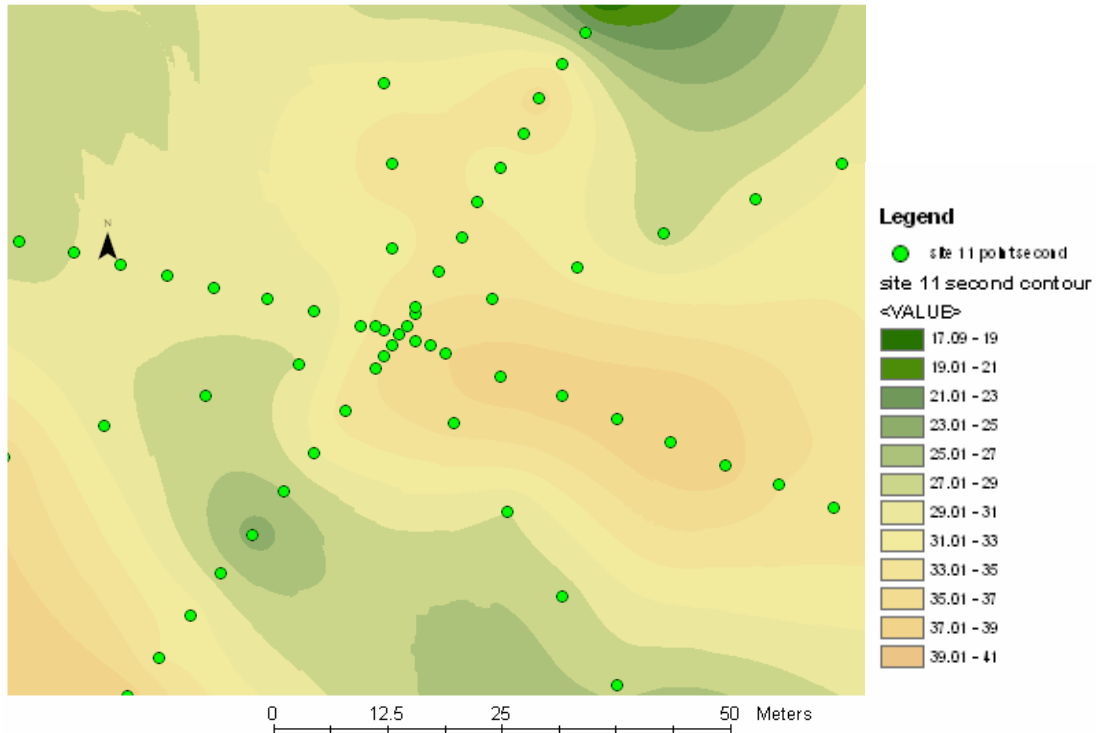
Figure 4.41. Contour of Site 11 conductivity values based on the measurements (green circles) along the transects. Conductivity values in legend in mS m^{-1} units. Site located at intersection of transects. Since it was less heterogeneous than the first survey, this site was chosen for drilling the soil core. Contours were determined through kriging the EC measurements. The contour interval is 2 mS m^{-1}.

4.13.2. Plant Identification and Density

Within a ten meter radius of the drill site, Site 11 contains thirteen ponderosa pine (*Pinus ponderosa*) trees that range from 1.5 to 9.1 meters tall and one large ponderosa pine over 30 meters tall. The site also contains two alligator junipers (*Juniperus deppeana*) and a single one-seed juniper (*Juniperus monosperma*). A third type of juniper, Utah juniper (*Juniperus osteosperma*), was found near the site. For examples of the three types of juniper found on or near this and other sites, see Figure 4.42. The predominant grasses are blue grama (*Bouteloua gracilis*) and black grama (*Bouteloua eriopoda*). Tobosa (*Hilaria mutica*) grass also grows at the site. Other plants at the site are broom snakeweed (*Gutierre sarothrae*), hairy golden aster (*Heterotheca villosa*), and

160

purple prickly pear (*Opuntia macrocentra*). A pine needle litter layer is present at the site, but only directly under the trees, and the interspaces are relatively free of pine needle cover. The understory plant interspaces are 15 to 30 centimeters across and are somewhat connected.
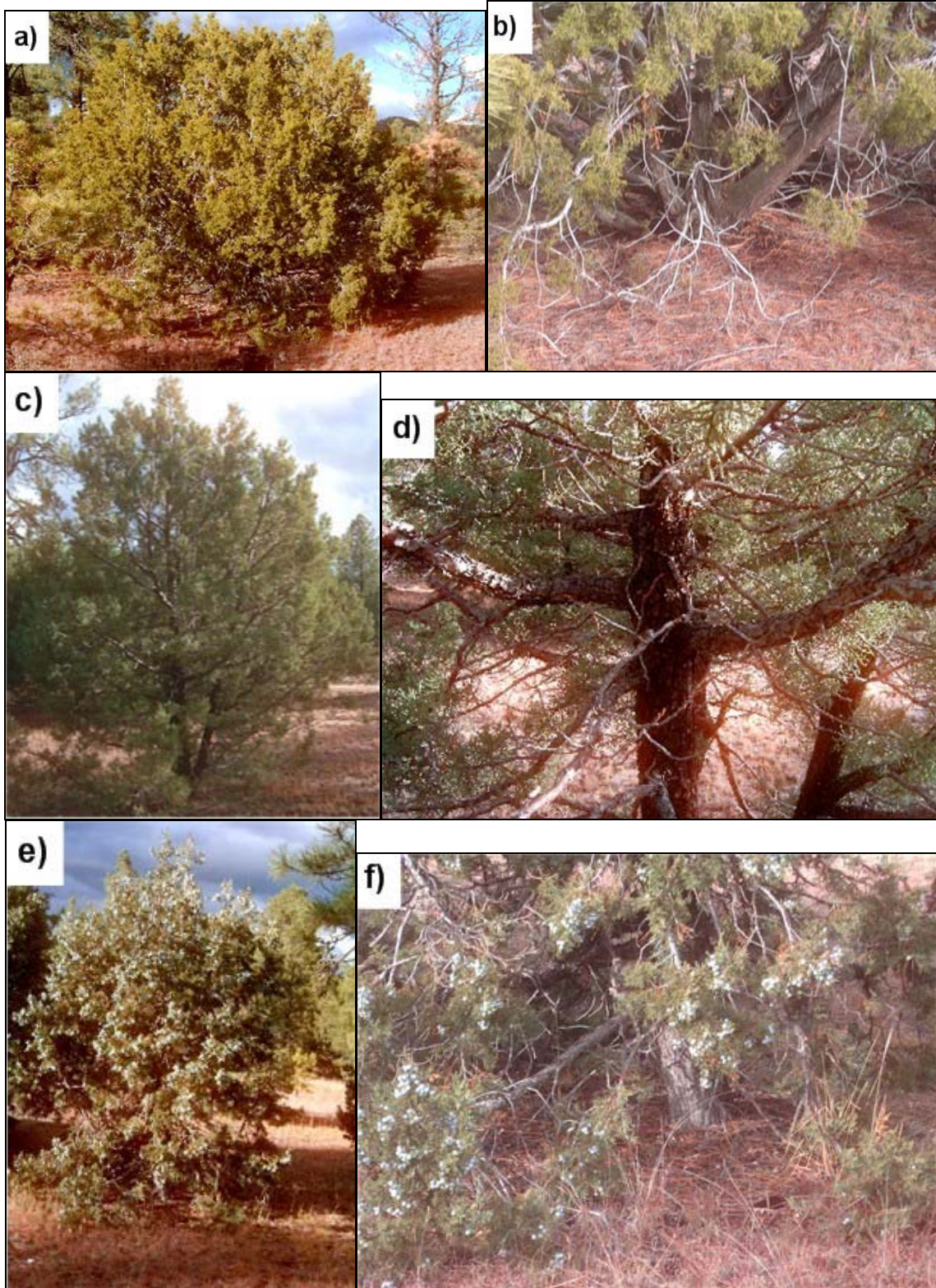
Figure 4.42. Examples of the three types of junipers found in study areas. a) one-seed juniper, b) the split trunk at soil surface identifies this as a one-seed juniper, c) alligator juniper, d) the single trunk and scaled bark identifies this as an alligator juniper, e) Utah juniper, f) the single trunk and non-scaled bark identifies this as a Utah juniper.

4.13.4. Site Distance from Ecotone

This site is in an area of fairly continuous ecosystem dominated by ponderosa pine trees, with some juniper and piñón pine trees. The closest ecotone would be the ponderosa pine and piñón-juniper mix ecotone. The piñón-juniper mix ecosystem was not sampled, therefore this ecotone was not included in the study. Also, there was no juniper- and ponderosa-pine ecotone in the area of the transect.

4.13.5. Geology

All of the rocks that were in the soil core of Site 11 were igneous. Continuous tuff rock was found between a depth of 2.85 meters and the end of the core at 4.8 meters. The boundary between the soil and the tuff rock was distinct. Between a depth of 2.85 to 3.8 meters, the tuff rock from depth was easily friable; below 3.8 meters depth, the tuff became gradually and significantly harder and dense. This tuff contained observable quartz veins and biotite and muscovite crystals. It was highly vesicular; with depth these vesicles became increasingly filled with weathering products. The weathering products were orange in color and were unreactive with carbonic acid, suggesting the parent material contained iron and was therefore likely to be biotite. Deeper in the core, some of the weathering products filling the vesicles were much lighter in color and reacted with carbonic acid, indicating the presence of calcium carbonate. Tuff with sanidine crystals was present in the soil section of this core.

4.13.6. Graphical Summary of Major Parameters

The major parameters that are associated with depth are shown in Figure 4.43.
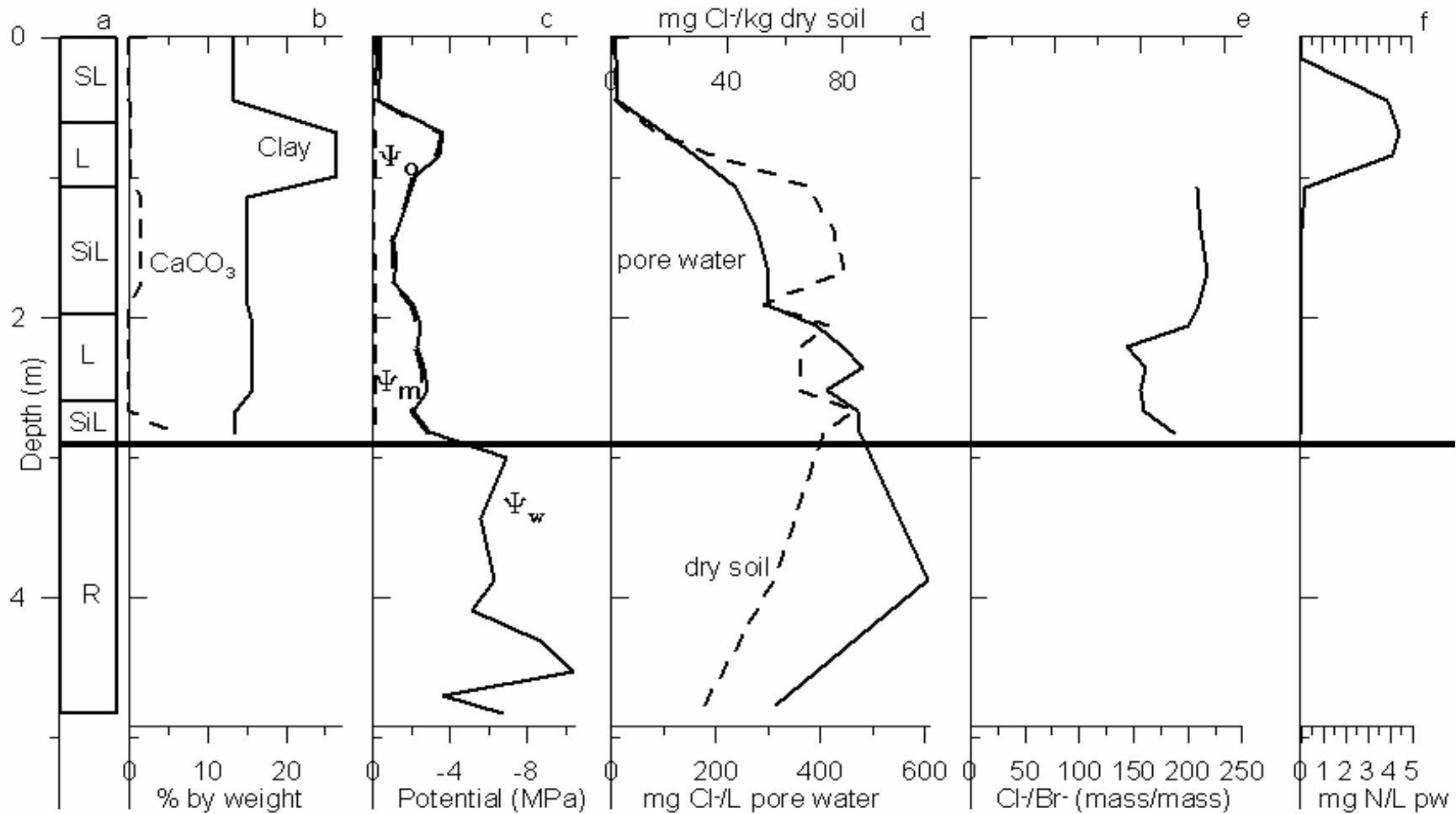
Figure 4.43. Profiles for Site 11 of a) soil texture, b) % CaCO3 and clay by weight, c) osmotic (Ψ_o), matric (Ψ_m), and water (Ψ_w) potential, d) mg Cl- per Liter of pore water (pw) or per kg dry soil, e) Cl-/Br- ratio, ratios not shown for bromide levels below detection, f), and mg total Nitrogen/Liter pw. L = Loam, SiL= Silty Loam, SL = Sandy Loam Soil, R = Rock (tuff, separated by line). $\Psi_o + \Psi_m = \Psi_w$

4.13.7. Soil Pit Characterization

A 95-centimeters soil pit was dug near drill Site 11. The soil profile is shown in Figure 4.44, and the soil description is shown in Tables 4.26, 4.27, and 4.28. Since rig access made drilling near the ponderosa trees impossible, the drill hole was not located close enough to a ponderosa pine tree in order to assess its roots. Therefore, the soil pit was located a short distance from the site in order to assess the roots of both smaller and larger ponderosa pine trees. The latitude and longitude of the clean face of the pit were 34.19495 and 107.47960 decimal degrees, respectively. This new location was approximately 19 meters southwest of the drill site. Pine needle and cone litter covered the soil reaching a maximum depth of 6 centimeters near the trees and thinning out with distance from the trees. The soil between the two large roots shown in Figure 4.44 different from the soil on either side of the root. This occurred between a depth of 15 to 40 centimeters.
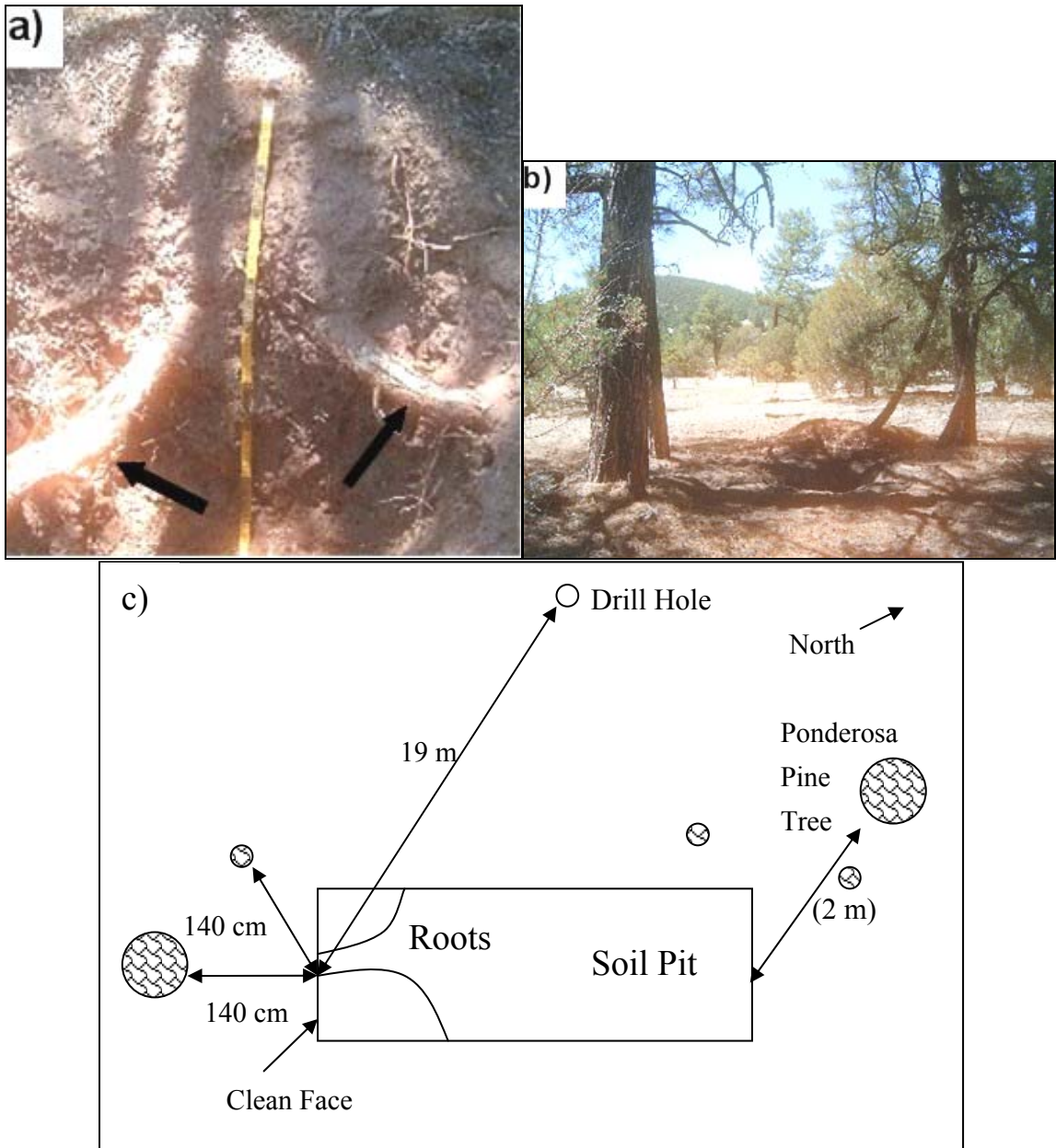
Figure 4.44. Soil pit at Site 11. This pit was dug to a depth of 95 cm. a) Clean face is shown and each black and yellow stripe on the measuring tape denotes 1 meter. The arrows indicate large roots in the pit at approximately 40 cm depth from the nearby ponderosa pine. b) Soil pit in relation to the surrounding ponderosa pine trees. The closest ponderosa pine trees (left side of picture) were both 1.4 meters from the soil pit; one was at a right angle to the clean face and the other was oriented at a 45° angle from the clean face. c) Plan-view diagram of the soil pit in relation to nearby ponderosa pine trees and drill site. Lengths in parentheses are estimated. Diagram is not to scale.

| | | | | Structure | | | | Consistence | | | |
| | | | | | | | | | Wet | | |
Horizon	Depth (cm)	Dry Color	Moist Color	Ped Grade	Ped Size	Ped Shape	% Gravel	Sticky	Plasticity	dry	Texture
A	0 to 15	2.5 YR 3/2	5 YR 4/2	2	c	sbk	<5	ss	po	sh	SL
A/B	15 to 40	2.5 YR 2.5/2	5 YR 3/3	2	m	sbk	0	ss	p	sh	SCL
B	25 to 40	2.5 YR 3/2	5 YR 4/2	3	c	sbk	0	s	p	h	SC
Bt	40 to 80	5 YR 4/4	7.5 YR 5/4	2	vc	sbk	0	vs	vp	vh	C
B/C	80 to 95	7.5 YR 5/3	7.5 YR 6/3	2	c	sbk	0	s	p	h	C

Location: Site 11, Forest Service
Aspect: North Northeast
Vegetation: Ponderosa Pine
Date/time: 6/18/2004 2:00 pm

Table 4.26. Soil pit characterization at Site 11. The soil description method used follows the procedure outlined by the Soil Survey Staff (1993). m = medium, c = course, vc = very course, sbk = subangular blocky, ss = slightly sticky, s = sticky, vs = very sticky, po = non-plastic, p = plastic, vp = very plastic, sh = slightly hard, h = hard, vh = very hard, SL = sandy loam, SC = sandy clay, C = clay, SCL = sandy clay loam.

| | Clay Films | | | Roots | | | Pores | |
Horizon	Amount	Distinctness	Location	Frequency Class	Size	Nature	Frequency Class	Size
A	none	none	none	3 (many)	vf - c	woody	none	none
A/B	none	none	none	3 (many)	f - c	woody	2 (common)	fine
B	none	none	none	2 (common)	f - c	woody	1 (few)	fine
Bt	2	distinct	pf	1 (few)	m	woody	1 (few)	fine
B/C	2	distinct	pf	1 (few)	m	woody	1 (few)	very fine

Table 4.27. Soil pit characterization at Site 11 (continued). The soil description method used follows the procedure outlined by the Soil Survey Staff (1993). pf = clay films on ped faces, vf = very fine, m = medium, c = course.

| | Boundary | | |
Horizon	Distinctness	Topography	Carbonate
A	diffuse	smooth	none
A/B	diffuse	irregular	none
B	diffuse	wavy	none
Bt	clear	smooth	none
B/C	buried	buried	none

Table 4.28. Soil pit characterization at Site 11 (continued). The soil description method used follows the procedure outlined by the Soil Survey Staff (1993).

4.13.8. Root Density Analysis

A root density analysis of the ponderosa pine trees growing near the soil pit at site 11 was performed using a ten by ten centimeter square. Some grass was present underneath the ponderosa pine and if they were located within the sampling square, the roots of this grass were also included in this analysis. Although juniper trees were present at the site, they were not near the clean face of the pit, which contained no juniper roots in the pit. The results of this analysis are shown in Table 4.29.

| Depth (cm) | Average # of Roots with noted Diameter | | | Total | % | |
	< 1 mm	1 - 10 mm	> 10 mm			
0 to 15	33	8.7	0	42	73	
25 to 40	0	4.3	3.3	7.7	13	3 large roots. (L to R) 2.86 cm, 6.36 cm, 7.0 cm diameters.
50 to 60	0	3.7	1.0	4.7	8	
70 to 80	0	2.3	0	2.3	4	
80 to 95	0	0.67	0	0.67	1	
			Total	57		Roots still in bottom of pit.

Table 4.29. Root density analysis of juniper at Site 11. Values shown are the average number of roots for that diameter of the three replicates taken at each depth interval. A 10 by 10 cm square was used to count the roots. The majority of the roots were located between 0 and 15 cm depth.

Figure 4.45. Root density analysis of ponderosa pine at Site 11. a) The arrows indicate large roots in the pit at approximately 40 centimeters depth from the nearby ponderosa pine. The large root on the left has a diameter of 3.18 cm, and the one on the right has a diameter of 3.5 cm. b) Some of the large roots found in the pit are shown in a close up laboratory picture. The ruler shown here is in centimeters. The diameters of these roots are 2 and 3.3 cm. c) Additional roots found in the pit. The ruler shown here is in centimeters. The diameters of the these roots ranged from 0.75 to 1.75 cm.

4.13.9. Bulk Density from Soil Pit and Soil Core.

The bulk density of peds found in the core and soil pit are shown in Table 4.30. Since peds from both the wall of the soil pit and the core were taken, any possible compaction of the peds in the soil core can be determined. When comparing the averages of the bulk densities of both the core and the pit peds, no significant difference between

them exists , demonstrating that there was slight-to-no compaction of the peds in this soil

core.

Site 11 – Pit Ped Source		
Bulk Density (g cm^{-3})	Depth (m)	Texture
1.49	0.19	SL
1.41	0.70	L
1.48	0.83	L
1.72	1.52	SiL
1.58	2.22	L
Average Bulk Density (g cm^{-3})		# Samples
1.54 ± 0.12		5
Site 11 – Core Ped Source		
Bulk Density (g cm^{-3})	Depth (m)	Texture
1.71	0.46	SL
1.32	0.69	L
1.43	1.45	SiL
1.89	2.06	L
1.89	2.67	SiL
Average Bulk Density (g cm^{-3})		# Samples
1.65 ± 0.26		5

Table 4.30. Bulk density values of peds from soil pit and soil core of Site 11. Peds from soil pit were taken from the wall of the clean face. SL = sandy loam, L = loam, and SiL = silty loam soil.

4.13.10. Infiltrometer Data

No infiltrometer measurements were taken at this site. The surface soil of this site

is sandy loam, and the infiltrometer measurements for Site 3 on sandy loam soil are

considered representative of this site as well.

CHAPTER 5

DISCUSSION

5.1. Ecohydrological Relations of Vadose Zone Moisture Fluxes to the Water Budget

The accurate determination of the water budget for the Río Grande Basin is crucial given that the area is arid and has an increasing population. This study has concentrated on the infiltration component of the water budget, which can, in part, be quantified by determining the partitioning of the water that has infiltrated the soil subsurface between evapotranspiration and deep percolation or recharge. Vadose-zone moisture fluxes are a key to quantifying the recharge to the groundwater that supplies much of the Southwest with drinking water.

Determination of these vadose-zone fluxes for an entire basin through point data is expensive and time consuming. If a surface feature could be found that would indicate the vadose-zone-water fluxes, this would substantially reduce the cost and effort. This surface indicator must have a strong linkage with deep vadose-zone moisture fluxes and be readily observable on the surface. In arid regions, the vegetation type has been previously determined as a possible surface indicator of deep vadose zone moisture fluxes (Scanlon et al. 2003, Walvoord and Phillips 2004, and Newman et al. 1997). Based on these previous findings, we hypothesize that arid vegetation communities play a significant role in controlling the soil-moisture fluxes in arid vadose zones.

171

5.2. Experimental Design

The experimental design consisted of the determination of a transect area along which the climate changed gradually and that also included all the ecosystems to be tested. After this transect area was established, sites within this area where chosen based on the following criteria, which were aimed at holding all non-climatic and non-ecological influences on soil-moisture fluxes as constant as possible: sandy soils, relatively flat topography and relatively homogenous subsurface soils. In order to have access to the land and the site, additional criteria included a site location close to an established road and land owners and managers amenable to drilling on their lands. The ecological and aridity trends of the chosen sites along the transect are shown in Figure 5.1. The aridity decreases along the transect, going from east to west, while the ecosystems change from creosote to grassland to juniper to ponderosa pine.
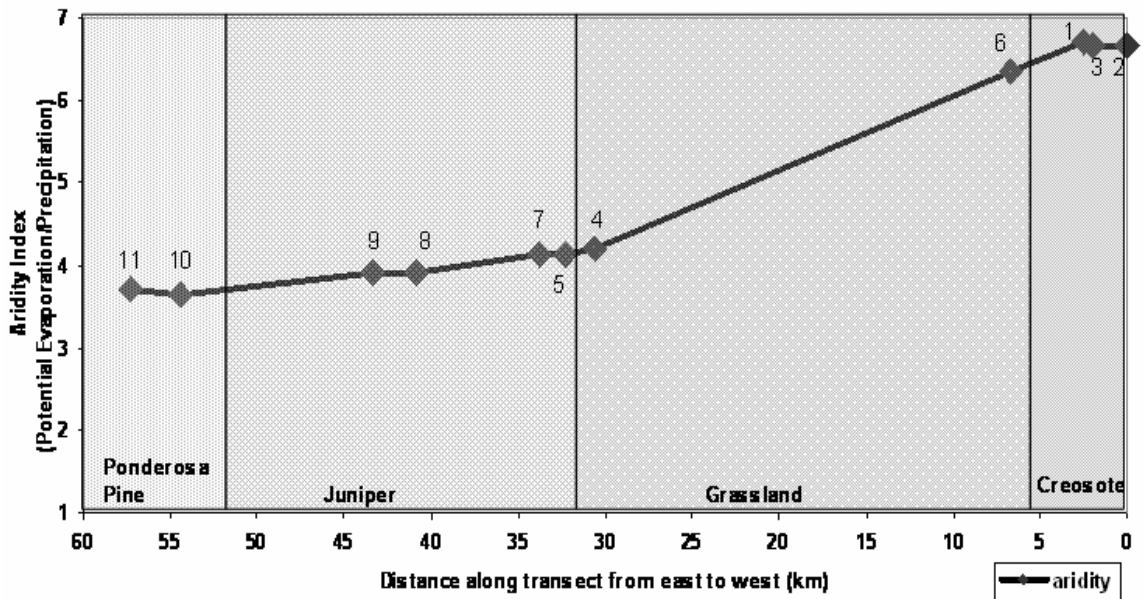
Figure 5.1. Aridity and ecological trend of the transect by distance along the transect. Site numbers noted by aridity values. Aridity line corresponds to y axis on left of graph, and general ecology noted with corresponding areas shaded.

5.3. Non-climatic and Non-ecological Influences on the Moisture Fluxes of the Transect

The experimental design was setup to hold all non-climatic and non-ecological influences on the vadose zone moisture fluxes of the transect as constant as possible. This section evaluates the extent to which the sites along the transect meet this criterion.

5.3.1. Infiltration of Water into the Subsurface

Sandy surface soils was one of the criteria of the experimental design. The soil textures of the study sites are plotted on a USDA textural triangle in Figure 5.2.
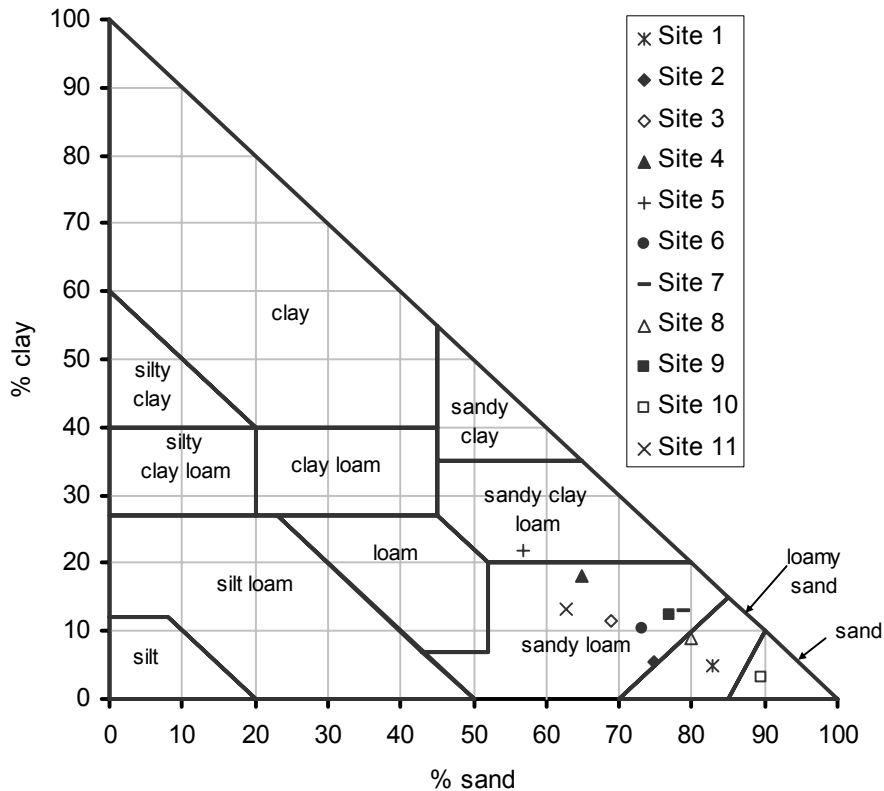
Figure 5.2. Soil texture of sites' surface soils plotted on a USDA soil textural triangle (Soil Survey Staff 1999). % silt = 100 - % sand - % clay. Plot made using program developed by Gerakis and Baer (1999).

Of four surface soil textures that were found along the transect, sandy and sandy

173

clay loam soils were each found at one site, loamy sand soil at two sites, and sandy loam

soil at the remaining seven sites. This soil textural analysis showed Site 5 to have high

levels of clay, between 5 and 31 percent by weight, in its soil profile, as shown

previously in Figure 4.17. These clay levels were of special concern since high levels

were located at or near the surface, with 22 percent clay at the surface to 60 centimeter

depth and 31 percent clay from 60 to 130 centimeters. High clay contents usually

decrease the infiltration capacity of soil. To determine if the high clay content of the

surface soil at Site 5 causes the surface soil to have an anomalously low infiltration rate

compared to the other sites, the saturated hydraulic conductivity of the surface soil at the

sites was measured with a disc infiltrometer. Examples of each type of surface soil found

at the sites were tested. These were assumed to be representative of the other study sites

with the same surface soil type. In each case, the area was cleared of rocks and

vegetation before measurements were taken, but the soil surface was otherwise

undisturbed. Results of the measurements are given in Table 5.1. All of the sites

investigated except for Site 5 had similar saturated hydraulic conductivities. Site 5

exhibited an anomalously low saturated hydraulic conductivity, which was less than one

seventh the next-highest value.

Site #	Surface Soil Texture	Default K sat (cm hr^{-1})	Average K sat (cm hr^{-1})	# Calculated Ksat Values	Alpha	% Clay in Surface Soil
3	SL	4.4	3.27 ± 2.69	6	0.24	11.6
5	SCL	1.3	0.58 ± 0.48	6	0.10	21.8
8	LS	15	4.59 ± 1.64	5	0.15	8.9
10	S	30	3.28 ± 0.38	4	0.17	3.2

Table 5.1. Comparison of infiltrometer results of each soil type. Default Ksat are cited from Carsel and Parrish (1988). The tabulated Ksat values represent the average of the calculated Ksat values from the individual infiltration tests. Alpha is a Van Genuchten parameter. SL = sandy loam, LS = loamy sand, and S = sandy soil

Since the saturated hydraulic conductivity value is considered the infiltration capacity of a soil (Hillel 1998), infiltration of precipitation is less at Site 5 than the other sites. A low infiltration rate combined with even a slight slope will result in an increase in runoff (Hillel 1998). The slope of Site 5 is 2°, therefore runoff processes at this site probably dominates any infiltration processes. The substantially decreased infiltration into the subsurface of this site would not only affect the subsurface moisture fluxes but would also reduce the chloride input, rendering it difficult to compare it with the chloride inventories at the other sites. Site 5 thus violates the experimental design criterion that all influences on vadose-zone moisture fluxes remain as constant as possible, with only the climate and vegetation changing. Site 5 was therefore considered anomalous and was not included in calculations of the average vadose-zone moisture fluxes by ecosystem.

5.3.2. Plant Roots

Data on the rooting depths of desert vegetation are sparse. A literature review of the rooting depth and lateral spread of the roots of plants in water-limited ecosystems was conducted by Schenk and Johnson (2002) and is summarized in Table 5.2.

Plant Type	Maximum Root Depth (m)	Arithmetic Average Depth (m)	Maximum Lateral Spread (m)	Arithmetic Average Lateral Spread (m)
Trees	58	5.8	50	11.5
Shrubs	20	3	50	4
Grasses and Weeds	6	1.1	8	1

Table 5.2. Summary of water limited plants root depths and lateral spread. Data from Schenk and Jackson (2002)

As these data pertain to this study, trees would be considered representative of ponderosa pine and junipers and shrubs representative of creosote. Data from Canadell et al. (1996) agree with these numbers, with non-mesquite shrubs possessing an average

rooting depth of 2.5 meters and mesquite possessing an average rooting depth of 15

meters. Ponderosa pine was cited as having an average rooting depth of 3.5 meters

(Canadell et al. 1996). Soil pits were dug to at each ecosystem to determine root

distribution, but the pits were only dug to depths between 77 and 130 centimeters.

Therefore, the maximum rooting depths of the plants could not be determined from this

study. The root distributions found in the soil pits are shown in Table 5.3.

Depth (cm)	% of Roots per Depth Interval			
	Creosote	Grass	Juniper	Ponderosa Pine
0 to 20	27	28	**38**	**73**
20 to 40	**29**	**47**	23	13
40 to 60	12	18	27	8
60 to 80	12	8	11	4
80 to 110	10		1	1
110 to 130	10			

Table 5.3. Distribution of roots found in soil pit. Bolded values are the highest found in
each pit.

Most of the roots were found in the upper 40 centimeters of the pits; they may

possibly be located there for plant stabilization. As Schenk and Jackson (2002) showed,

the average rooting depth for grasses is around one meter. No roots were seen at the

bottom of the grass soil pit, so a one-meter rooting depth for desert grasses is probably an

accurate assumption. Large roots were found spread laterally for creosote bush at

approximately 20 centimeters depth. The distribution of the remaining fine roots were

spread almost evenly throughout the soil pit. Roots were still present at the bottom of the

pits for the creosote, juniper, and ponderosa pine. Therefore, the literature data will be

used for these plants, assuming an average rooting depth of 3 meters for the creosote, 6

meters for the juniper (both from Schenk and Jackson (2002) study), and 3.5 meters for

the ponderosa pine (from Canadell et al. (1996) study).

5.3.3. Recharge from Preferential Pathways

There is evidence that preferential pathways could be present at some of the transect sites. Low chloride concentrations and corresponding high matric potentials in isolated areas of the soil core profiles can indicate the possibility of a preferential flow path, as discussed previously in Sections 1.3.3 and 1.3.4. Additional evidence of preferential flow, such as macropores or abrupt changes in soil texture or carbonate content, lend additional credence to the possibility of preferential flow in the area. Areas of the profiles from Sites 4, 7, 8, and 9 may contain evidence of preferential flow. Preferential flow could also be occurring at the ponderosa pine sites, but recent flushing events at these sites have essentially wiped out any possible evidence of this. Figure 5.3 shows the chloride concentration and matric potential profiles for these sites. The depths at which suspected preferential-flow indicators are found are designated by the horizontal lines and arrows.
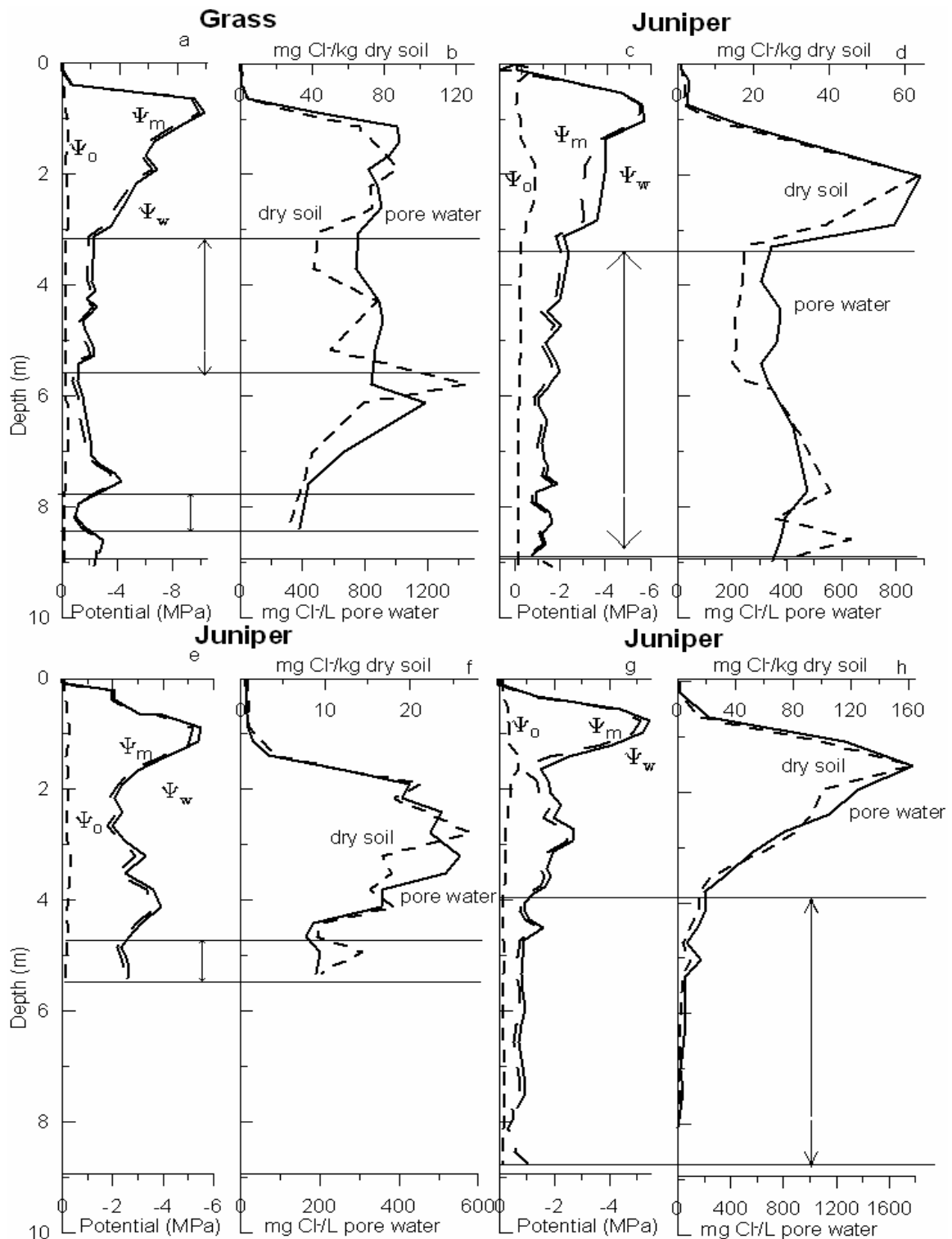
Figure 5.3. Indications of preferential flow paths in the chloride concentration and matric potential profiles. a, b) Site 4; c, d) Site 7; e, f) Site 8; g, h) Site 9; a, c, e, g) osmotic (Ψo), matric (Ψm), and water (Ψw) potential; b, d, f, h) mg Cl- per Liter of pore water (pw) or per kg dry soil. Lines and arrows note areas of possible preferential flow paths. Note changes in scale on x axes.

178

Site 4, a grass site, has two regions of possible preferential flow. These regions are separated by an area of increased chloride and decreased matric-potential levels. Sites 7, 8, and 9, which are all juniper sites, show areas in their profiles of possible preferential flow, starting at a depth of four meters and then continuing to the bottom of the profile. These suspected preferential flow areas have a substantial increase in matric potential and corresponding decrease in the chloride concentration values.

Preferential flow in the juniper ecosystems was suspected as a possibility in as much as the roots do not form a uniform pattern, which is shown in part c of Figure 5.3 below. As discussed in the previous section, junipers can have rooting depths of as much as six meters and the roots could extend into the areas of the profiles that indicate preferential flow. Tyler and Walker (1994) stated that root uptake may not be uniformly distributed, and the resulting flow field will therefore be strongly controlled by the root density and distribution, both horizontally and vertically. A one-dimensional, steady flow recharge model will therefore probably not be valid under these conditions. Contrasting with this, below the active rooting zone, the flow field is most likely to be steady and one-dimensional (Tyler and Walker 1994). The juniper roots can be large enough to allow water to run along them or through the macropores formed from decayed root holes. These decayed root holes were found in the soil pit dug at Site 8 near a juniper tree, as shown in Figure 5.4. Just on the clean face of the one meter deep soil pit were four decayed root holes, with some containing decaying root and some not. These same types of holes were also found on the other faces of the pit. With evidence of possible preferential flow in all of the juniper soil core-profiles and a significant number of macropores formed by decayed root holes in the juniper soil pit, preferential flow

appears likely to be common in the juniper ecosystem.
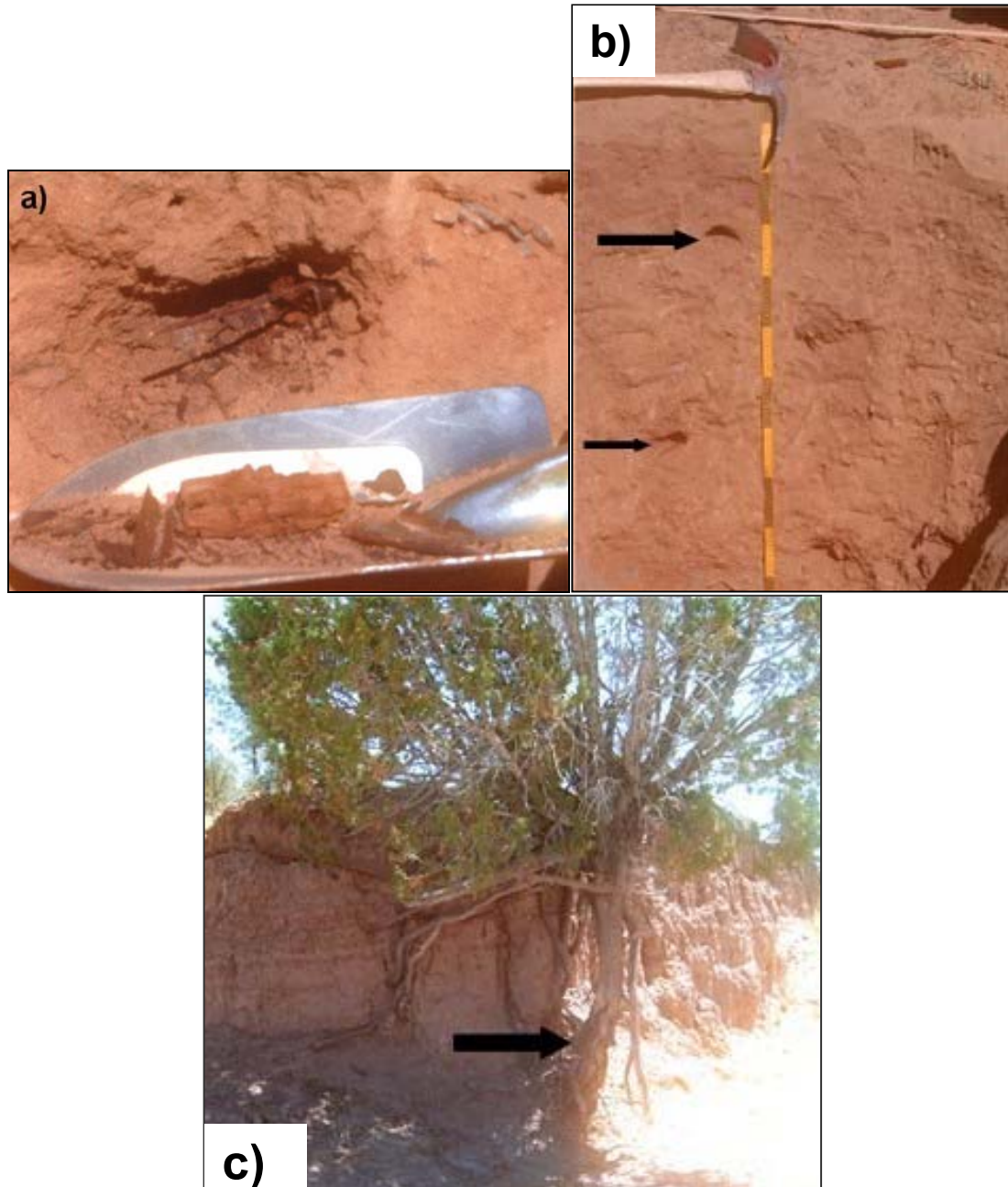
Figure 5.4. a) Decayed root holes found in soil pit dug at Site 8 near a juniper tree. b) Clean face of soil pit, with arrows noting two prominent macropores formed from decayed roots. c) Rooting structure of juniper tree shown in washed out arroyo. Arrow indicates tap root.

5.3.4. Subsurface Soil Texture

Sections of the soil cores were tested for soil texture. One sample was tested for

each section that contained similar soil textures. The results of this analysis are shown in Figure 5.5, plotted on a USDA textural triangle.
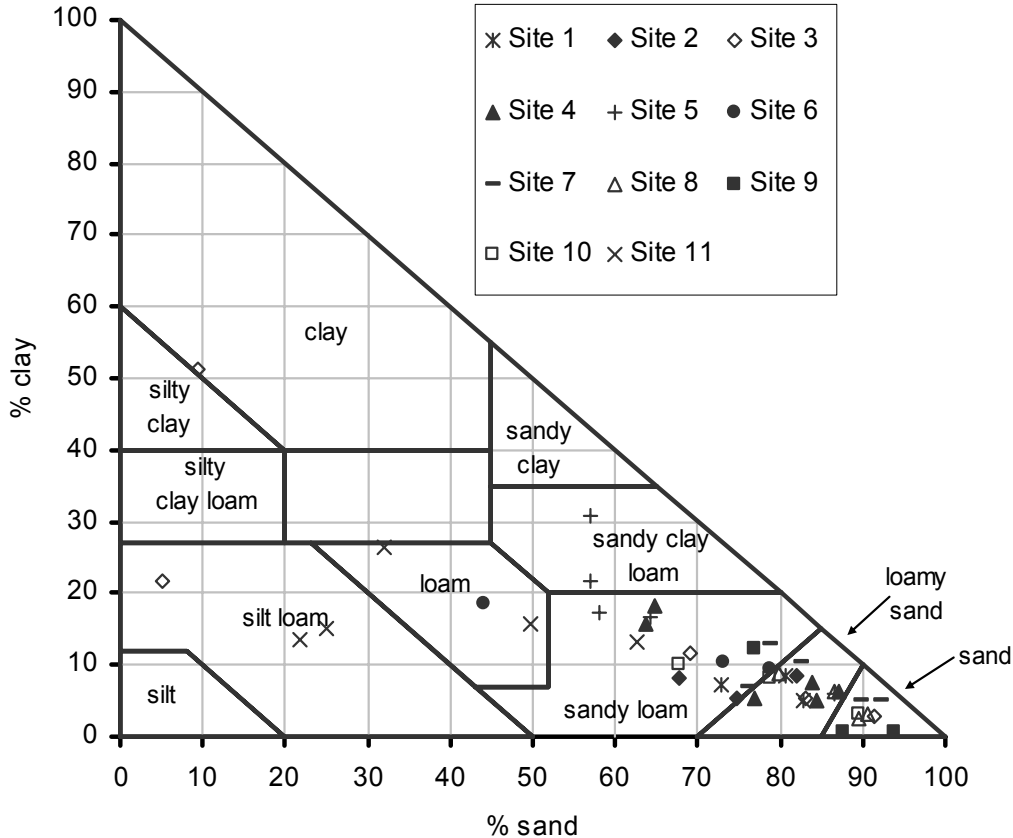
Figure 5.5. Soil texture results for all sites plotted on a USDA soil textural triangle (Soil Survey Staff 1999). % silt = 100 - % sand - % clay. Plot made using program developed by Gerakis and Baer (1999).

As can be seen from Figure 5.5, most of the soil samples are plotted in the sandy loam, loamy sand and sand areas of the triangle. As shown in Table 1.1, these soil textures do not have a significant amount of clay, and the hydraulic conductivities of these textures are not dramatically affected by the amount of clay. Therefore, most of the soil in the profiles conformed to the experimental design criterion of being sandy soils. Site 5, having sandy clay loam surface soils, deviated from this, as was discussed previously. In addition, loamy soils were found deep in the profiles of Sites 3 and 11.

The effect this clay- and silt-rich layer had on the moisture fluxes of Site 3 are discussed in the next section.

Clay-rich layers are common in areas where ponderosa pines are found. The sandy-loam soil that overlies the high-clay-content loam and silty-loam layers of this soil allowed water to infiltrate this profile, but it restricted the water's downward movement. An increase in chloride concentrations below clay-rich layers was also found by Newman et al. (1997). Their findings suggested that the clay-rich layer had a substantial inhibitory effect on the downward water movement at the ponderosa pine sites. Therefore, the profiles had not been flushed of chloride unlike the nearby areas. Site 11 is located only 3.2 kilometers from Site 10 and contains similar vegetation, yet the Site 10 profile shows substantial evidence of complete and recent flushing. Thus, the higher amount of chloride accumulation at Site 11 is then most likely the result of the restriction of downward flow by the clay-rich layer. Unlike Site 5, this site is not considered anomalous. This is because water can still enter the soil profile as a result of the surface soil being sandy loam, which is not clay rich and was seen at the surface of many of the other sites.

5.3.5. Lateral flow

Lateral flow can occur when soil stratigraphy changes abruptly, therefore changing hydraulic properties. The soil texture or clay content did not appear to affect the moisture fluxes of the profiles except in Site 5 and 11, as already discussed, and in Site 3. Site 3 has a sand layer (< 3 percent clay content) overlying a clay layer (51 percent clay content). This abrupt transition from sand to clay occurred at a depth of 6.2 meter and is correlated with an abrupt change in the matric potential and chloride

182

concentration profiles, as seen in Figure 5.6. As a result of the pore size of the soil

matrix, sand has a much lower unsaturated hydraulic conductivity than clay, as was

discussed in Section 1.3.5.2. The clay layer is deep in the profile, well below the average

root zone depth of creosote bushes of three meters (Canadell et al. 1996), as discussed in

Section 5.3.2, therefore this area is not subject to root zone, non-uniform, dynamic flow.

All creosote sites have high levels of chloride accumulation and very low matric

potentials throughout the profiles, therefore it is unlikely that flow could be occurring

laterally through this area that originated from another area. A more probable

explanation is this clay layer is behaving like a reservoir of water still present from a

complete flushing even that occurred before the last glacial maximum. While the

potential gradient is upward, out of the clay layer into the sand layer, the large difference

in unsaturated conductivities between the sand and the clay could create a partial air

resistive boundary condition slowing upward moisture flow. This slow movement of

water out of the clay layer would slow the drying process, resulting in this layer having

high matric potentials and high water content compared with the surrounding layers. The

sharp change in matric potential at the interface between the sand and clay layer

demonstrates that this area of the profile has not yet reached equilibrium since the last

flushing event.
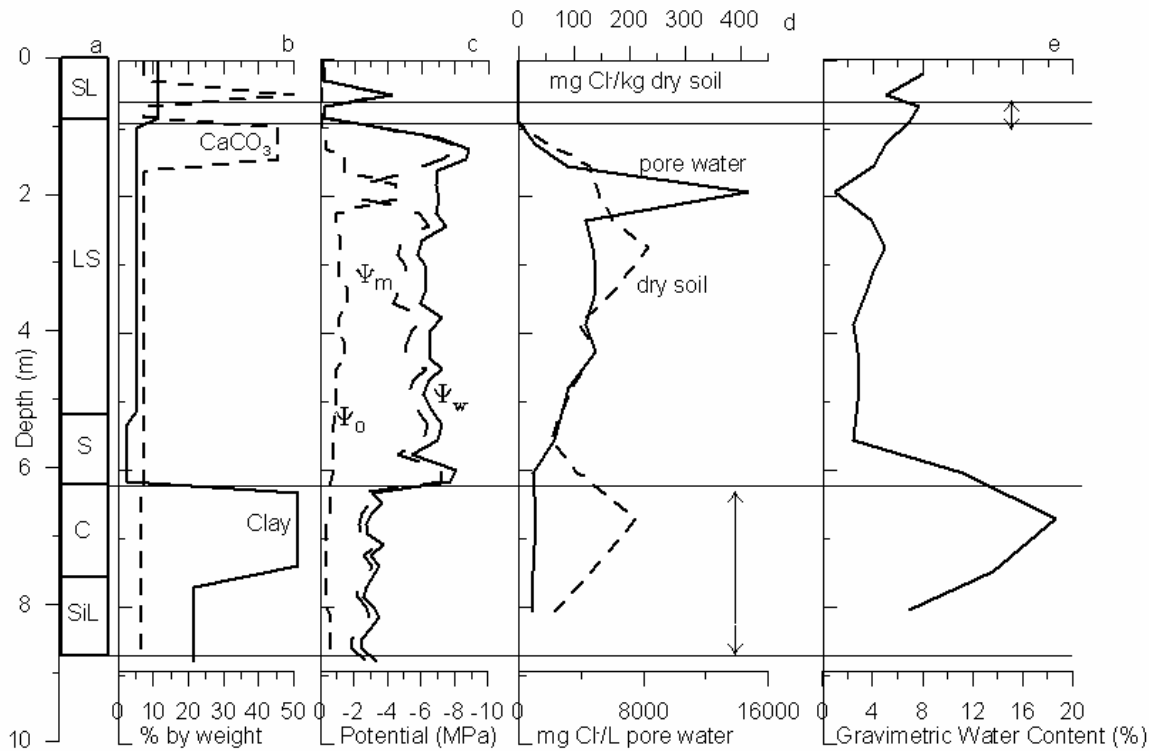
Figure 5.6. Indications of more conductive areas in the profiles for Site 3. a) soil texture, b) % CaCO₃ and clay by weight, c) osmotic (Ψ_o), matric (Ψ_m), and water (Ψ_w) potential, d) mg Cl⁻ per Liter of pore water (pw) or per kg dry soil, e) Cl⁻/Br⁻ ratio, and f) mg total Nitrogen L^{-1} pw. SL = Sandy Loam, LS = Loam Sand, C = Clay, SiL = Silty Loam, S = Sand Soil. Lines and arrow indicate area of higher conductivity.

Profile 3 also shows an abrupt decrease in calcium carbonate levels exactly correlated with an increase in matric potential values, at a depth of 60 to 90 centimeters; both parameters then returned to previous levels. Water content also increased in this area. This area is within the root zone of the creosote and therefore could be subject to the seasonal fluctuations in chloride concentrations and matric potentials that can occur there. The larger roots of the creosote bush that would cause preferential flow are too shallow (~ 20 centimeters depth) to cause of this sudden decrease in carbonate and increase in matric potential and water content, although it is close enough not to rule out root flow as a possible cause. This area is better correlated with a change in soil texture, going from sandy loam to loamy sand soil with depth, with a corresponding decrease in

184

clay content from 11.6 to 5.3 percent. As in the above example, the area of high matric

potentials and water contents, and low chloride concentrations and carbonate levels are

located in the slightly less conductive layer under saturated conditions, sandy loam. In a

lateral flow condition, the less conductive layer is underneath the more conductive layer,

causing ponding on top of the less conductivity layer and subsequent lateral flow.

Therefore, this possibility is also unlikely.

A third possible explanation is the levels of calcium carbonate seen in this area of

the profile. As described in the next section, a 45 percent carbonate content in the soil

could result in cementation and plugged pores (Gile et al. 1981 and Machette 1985). This

restriction in flow may have caused the area in between these two layers that contain high

levels of calcium carbonate to become an area of lateral flow, therefore increasing the

matric potential of only this area and not the surrounding areas. The shallowest

carbonate layer is very thin and possibly not laterally continuous, therefore water could

infiltrate elsewhere, away from the site. The second carbonate layer is thicker, possibly

having a greater lateral extent. Therefore, when water infiltrates through the less

continuous upper layer and encounters this second layer, it would flow laterally on top of

this cemented layer through this area of Site 3. However, not enough data exists to

determine conclusively the cause of this sudden change in matric potential corresponding

with an abrupt change in calcium carbonate.

5.3.6. Carbonate Deposition

Calcium-carbonate deposition is common in arid soils (Birkeland 1999).

Substantial amounts of calcium carbonate were found in all of the profiles except Sites 10

and 11. This was expected because Sites 10 and 11 were the only sites shown to have

significant and frequent downward liquid fluxes. Sites 3, 4, and 5 have carbonate levels

that may restrict downward water flow through plugged pores and cementation. Besides

the creation of a possible preferential flow area mentioned in the previous section for Site

3, the carbonate deposition does not appear to affect the matric potential or the chloride

levels of the soil profiles. The only possible connection is also at Site 3, where the soil is

extremely dry (less than one percent water gravimetric water content) just below the

calcium carbonate layer. This layer has 45 percent carbonate deposition, and the data

shown in Table 5.4 indicate that this level of carbonate could plug pores and restrict

downward moisture flow, thereby possibly causing this extremely dry layer.

Carbonate Stage	Level of Development	% Calcium Carbonate by Weight	Sites with These Carbonate Levels
I	discontinuous coatings	<10%	2, 3, 4, 6, 8, 9, 10, 11
II		10 to 15%	1, 2, 4, 7
III	continuity of fabric high in carbonate	20 to 25%	1, 2, 4, 5, 7, 9
III+	continuity of fabric high in carbonate, pores plugged, cementation mostly continuous	> 40%	3, 4, 5
IV	partly or entirely cemented	75 to 90% in upper part of layer 50-75% rest of layer	

Table 5.4. Carbonate stage relative to percent calcium carbonate. Modified from Gile et al. (1981) and Machette (1985).

At Site 3, there is a significant calcium-carbonate layer above the chloride bulge.

Calcium carbonate is much less soluble than chloride, so the partial leaching events that

transported chloride deeper into the profile did not wash most of the calcium carbonate to

the same depth. At all of the other sites, the significant calcium carbonate layers are

within or below the chloride bulge, which could be the result of a previous partial

leaching event. This event would have reprecipitated the calcium carbonate deeper into the profile, and then the chloride redeposited in the upper parts of the profile. Another possible explanation is that these deeper calcium-carbonate layers were deposited near the surface and another alluvial depositional event buried this area, then allowing the chloride levels to be establish above these carbonate layers. If this were the case, then these layers should be near an area with a change in strata that indicate a depositional event. Only Sites 5 and 8 have changes in soil texture that correlate with the position of the calcium carbonate layer.

5.3.7. Soil Compaction and Bulk Density

The results of the bulk-density measurements, grouped by soil texture, are shown in Table 5.5. These include both the bulk-density values of the peds taken from the core and those taken from the soil pits. The bulk density values averaged according to soil texture were used to extrapolate bulk-density values to areas of the soil core that did not have any useable peds. As seen in the table, loam soils are the least dense, while silty loams were the most dense. Both the least dense and most dense soils have the smallest amount of sample measurements, so these averages are more likely to be affected by outlier values or to not accurately represent the soil texture.

Soil Texture	Average $(g\ cm^{-3})$	Minimum $(g\ cm^{-3})$	Maximum $(g\ cm^{-3})$	Number of Samples
loam	1.51 ± 0.21	1.32	1.89	6
sandy clay loam	1.51 ± 0.09	1.44	1.62	3
loamy sand	1.60 ± 0.16	1.18	1.96	23
sandy loam	1.67 ± 0.22	1.45	2.30	18
sand	1.69 ± 0.08	1.59	1.81	4
silty loam	1.77 ± 0.26	1.43	2.04	4

Table 5.5. Soil dry bulk density grouped by soil texture. Ped source from both soil pits and soil cores.

To determine if the peds taken from the soil cores were compacted from the use

187

of hammer percussion to advance the split-spoon sampler, peds were taken from the clean face of the soil pits dug near drill Sites 1, 5, 8, and 11. Table 5.6 compares the peds from the soil pit with the peds from the cores taken at that site and approximate depth.

Site	Ped Source	Average Bulk Density ($g \, cm^{-3}$)	Number of Samples	% difference
1	pit	1.57 ± 0.17	6	5.47
	core	1.66 ± 0.07	3	
5	pit	1.50 ± 0.10	3	3.57
	core	1.56 ± 0.08	3	
8	pit	1.51 ± 0.21	5	6.58
	core	1.62 ± 0.04	2	
11	pit	1.54 ± 0.12	5	6.75
	core	1.65 ± 0.26	5	

Table 5.6. Comparison of peds from soil pits and soil cores to determine possible compaction of the peds in the soil cores.

The percent differences between the bulk density values obtained from the soil pits and the values obtained from the cores ranged from 3.6 to 6.8 percent. This demonstrates that while there was some compaction in the core samples, it was small.

5.3.8. Topography

Most of the sites had slopes ranging from 1.0° to 2.5°. Only Site 10 had a higher slope of 6.0°. This site had the highest amount of downward moisture flux, therefore the steep slope does not appear to have much of an effect on the vadose-zone moisture fluxes. This may be due to the surface soil consisting of sand, the most conductive of the soil textures, as shown in Table 1.1. The effect of the slope may be a possible explanation for the infiltrometer measurements at this site being 10-fold less than the default values for that soil type. This site is not considered anomalous since, from the chloride concentration and matric-potential profiles, liquid water is obviously infiltrating the profile. The slope may have affected the vadose zone fluxes of Site 5. The very low

conductivity of the surface soil at Site 5 combined with the 2° slope would likely cause runoff, not infiltration of the precipitation, as was discussed previously in Section 5.3.1.

5.3.9. Groundwater-Table Depths

The groundwater-table depths of the sites ranged from 40 to 122 meters, as estimated by Anderholm (1987a and 1987b) and Myers et al. (1994), with the depths increasing with distance from the Río Grande and increasing elevation. Walvoord et al. (2002a) determined that the upward vapor flux exceeded the upward liquid flux by a least one order of magnitude for thick vadose zones (greater than 25 meters depth). In contrast, they found that the upward liquid flux exceeded the upward vapor flux below 10 meters depth when the vadose zones were shallower than 25 meters depth. Capillarity draws enough water upward from the water table of shallow vadose zones to significantly increase the unsaturated permeability and consequently increases the net upward moisture flux. Vadose zones with thicknesses greater than 100 meters show little sensitivity to increases in water table depth (Walvoord et al. 2002a). All of the sites in this study have groundwater tables deep enough such that they should not significantly affect the moisture fluxes in the vadose zone.

5.3.10. Geology

All sites had mostly volcanic rocks within the soil profiles and seen in the area. The presence of large rocks halted drilling at Sites 5, 6, and 8. A large rhyolitic rock that was significantly larger than the sampler, which had an outer diameter of 7.6 centimeters, was also encountered at Site 7. The amount of rocks in the soil portion of the profiles was small, less than 10 percent. Therefore, the presence of rocks in the soil portion of the

189

profiles did not have a significant affect on the soil-moisture fluxes in this study.

Bedrock was encountered at Sites 10 and 11 at around 2.8 meters depth. At Site 11, the

vesicles became increasingly filled with weathering products with depth, indicating water

flow through the matrix.

5.4. Electrical Conductivity

The purpose of performing the electrical-conductivity surveys was to determine

any subsurface soil heterogeneity or presence of large rocks that would halt drilling

progress. Table 5.7 lists the sites where surveys were taken and the range of electrically

conductivity values found within 25 meters of the site. The number of soil textures found

at the site, any significant changes in subsurface soil texture, and the presence of rocks in

the subsurface that stopped drilling were also noted for each site to determine the

effectiveness of the surveys in detecting soil heterogeneity and large rocks.

Site #	EC Range ($mS\ m^{-1}$)	# of Different Soil Textures	Notes
2	5	1	
3	6	3	deep clay layer (6.2 m), shallow carbonate layer
4	2	2	
5	2	3	rocks in subsurface that stopped drilling
7	3	2	
8	3	2	rocks in subsurface that stopped drilling
9	6	2	
10	6	3	shallow bedrock
11	12	3	clay-rich layer in subsurface (0.5 m), shallow bedrock.

Table 5.7. Range of electrical conductivity values (EC) found within 25 meters of the
drill site. Number of different soil textures found in the top 6 meters. Notes of clay
layers or rock impeding drilling shown for comparison.

There does not appear to be any correlation between the large variations in

electrical conductivity readings indicating more heterogeneous soils and determined

subsurface heterogeneity. Both sites with significant changes in soil textures from sandy

to clay soils, Sites 3 and 11, have large variations in electrical conductivity readings. Although the clay layer at Site 3 is near the limit of penetration into the subsurface of the EM31 of 6 meters. However, Sites 2, 9, and 10 also have high variations in EC readings, there is no significant corresponding change in subsurface strata. Both sites where rock impeded the progress of drilling at 5 meters yielded low variations in electrical conductivity readings. According to the results of this study, the use of the EM31 meter to determine subsurface heterogeneity yielded mixed results; therefore it was not very effective in this study. Some of the problems with effectiveness in detecting subsurface heterogeneities may be the result of the six meter depth limit of penetration of the EM31.

5.5. Nitrogen

Overall, concentrations of soil nitrogen were low at the drill sites. The total soil nitrogen content for each site was calculated as the sum of nitrate and nitrite. There was no correlation between the chloride profiles and the nitrate profiles, as was found in some of the profile in Walvoord et al. (2003). Walvoord found 300 to 1000 kg ha^{-1} of total nitrogen below one meter in the Chihuahuan Desert, the same desert that contained the sites in this study. Table 5.8 lists the amount of total nitrogen found at the study sites, above and below one meter depth.

Site #	Total Nitrogen < 1 m (kg ha^{-1})	Total Nitrogen > 1 m (kg ha^{-1})
1	1.62	1.30
2	6.13	4.00
3	14.6	30.2
4	45.0	28.7
5	2.80	0.92
6	1.94	306
7	2.37	8.18
8	5.82	1.18
9	6.49	3.42
10	6.38	0.14
11	6.04	0.24

Table 5.8. Amount of total nitrogen found above and below one meter depth.

All sites have total nitrogen levels that are lower than the ones found by Walvoord et al (2003) except Site 6, the grass site in the Sevilleta, which had a value of 306 kg ha^{-1}. Jackson et al. (2004) reported total nitrogen values in the Chihuahuan Desert to be between 50 and 100 kg ha^{-1}. The nitrogen levels found in this study are closer to that range. The nitrogen levels measured under the Chihuahuan Desert in Walvoord et al. (2003) were the lowest of all of the deserts of the Western US, as seen in Figure 5.7, so this result is not unexpected. The vegetation in the Chihuahuan Desert may be more efficient users of nitrogen than that found at the other desert sites.
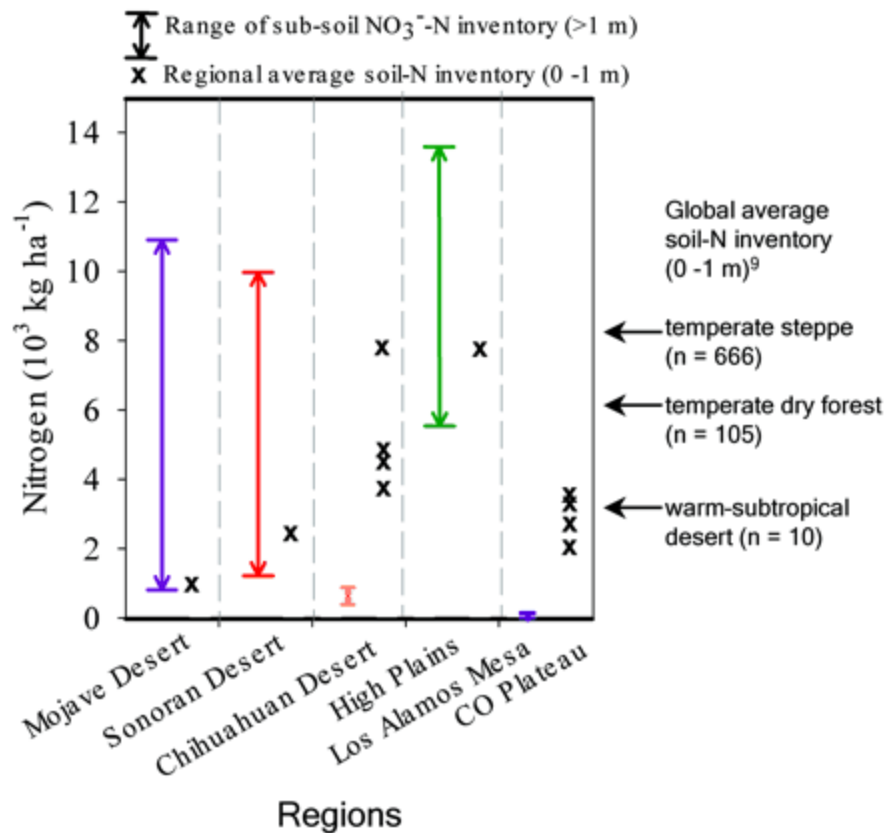
Figure 5.7. Comparison of subsoil nitrogen inventories. From Walvoord et al. (2003).

5.6. Determination of Vadose-Zone Moisture Fluxes

The above analysis of non-ecological and non-climatic influences on vadose-zone moisture fluxes demonstrated that one site, Site 5, did not conform to the criteria for selection of sample site and therefore cannot be considered representative in the same sense as the other site. As previously mentioned, the data for Site 5 will be included when displaying data from individual sites, but will not be included in the averages calculated per vegetation type. The vadose-zone moisture fluxes and their relation to the climate and ecology of the area were determined through the use of matric-potential and chloride-accumulation values.

5.6.1. Soil-water Potentials

5.6.1.1. Osmotic Potential

Osmotic potential does not strongly affect the movement of liquid water unless there is a semi-permeable barrier present (Hillel 1998). While there are no known semi-permeable barriers at the sites, when soil wetness decreases and the water films shrink to a thickness on the same order as the diffuse layer of adsorbed cations, an appreciable degree of solute restriction can be expected to take place. This restriction could result in the soil exhibiting membrane-like properties of selective permeability when a solution is driven through a soil by a hydraulic gradient (Hillel 1998). While some of the soils in this study are fairly dry, whether this phenomenon is occurring is unknown. Therefore, the osmotic potential was subtracted out of the measured water potential to determine only the matric potential. Osmotic potentials were calculated based on the eletrical conductivity of the soil leachate, as discussed previously in Section 3.3.7. These calculated osmotic potentials are shown in Figure 5.8. The only sites that had any significant osmotic potentials were Sites 1, 2, 3, and 6, which are located in the Sevilleta, and Site 7, which is located near Magdalena. These sites have fairly high levels of calcium carbonate and chloride salts, both of which could contribute to the osmotic potential.   Even at these sites, the osmotic potential is very low compared to the water potential. Site 3 had the greatest osmotic potential, particularly at a depth of 1.8 to 2 meters. Here, the water content of this level was very low, less than one gravimetric percent, which would concentrate the salt in the pore water in this area to into a smaller volume of water. The osmotic potential values were subtracted from all the water-potential values to determine the matric potential.
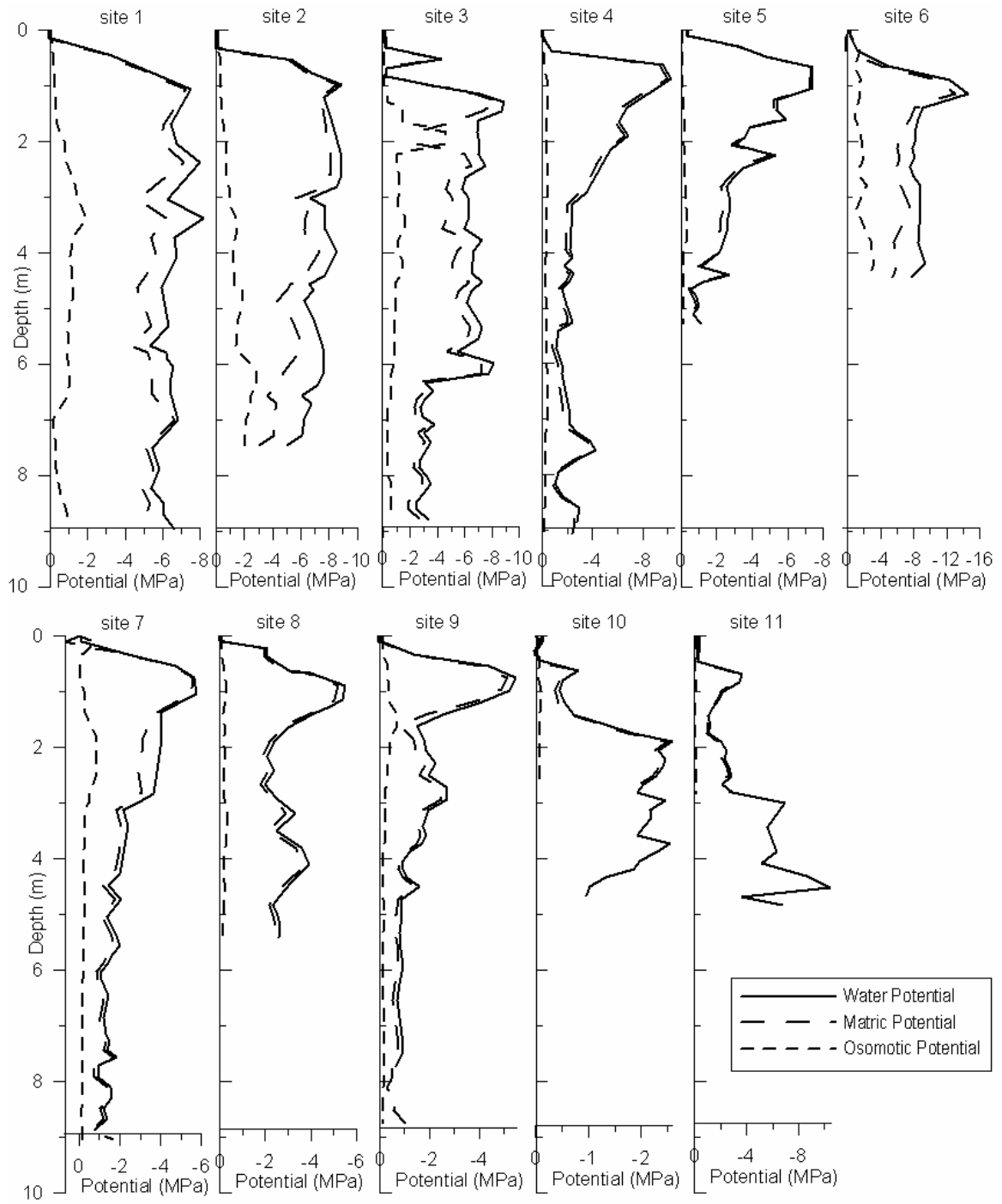
Figure 5.8. Osmotic, matric, and water potentials with depth for each site. Note changes in scale for x axes. $\Psi_m + \Psi_o = \Psi_w.$

5.6.1.2. Matric Potential

The matric potential, along with the gravitational potential, determines the

195

movement of liquid water in the subsurface. Since the depth profiles in this study are shallow, less than ten meters, the gravitational potential is relatively small compared to the matric potential. The matric potential profiles for all of the sites are shown in Figure 5.9. The profiles are grouped by ecosystem, and, for inter-ecosystem comparison, the axes are the same in all four graphs.
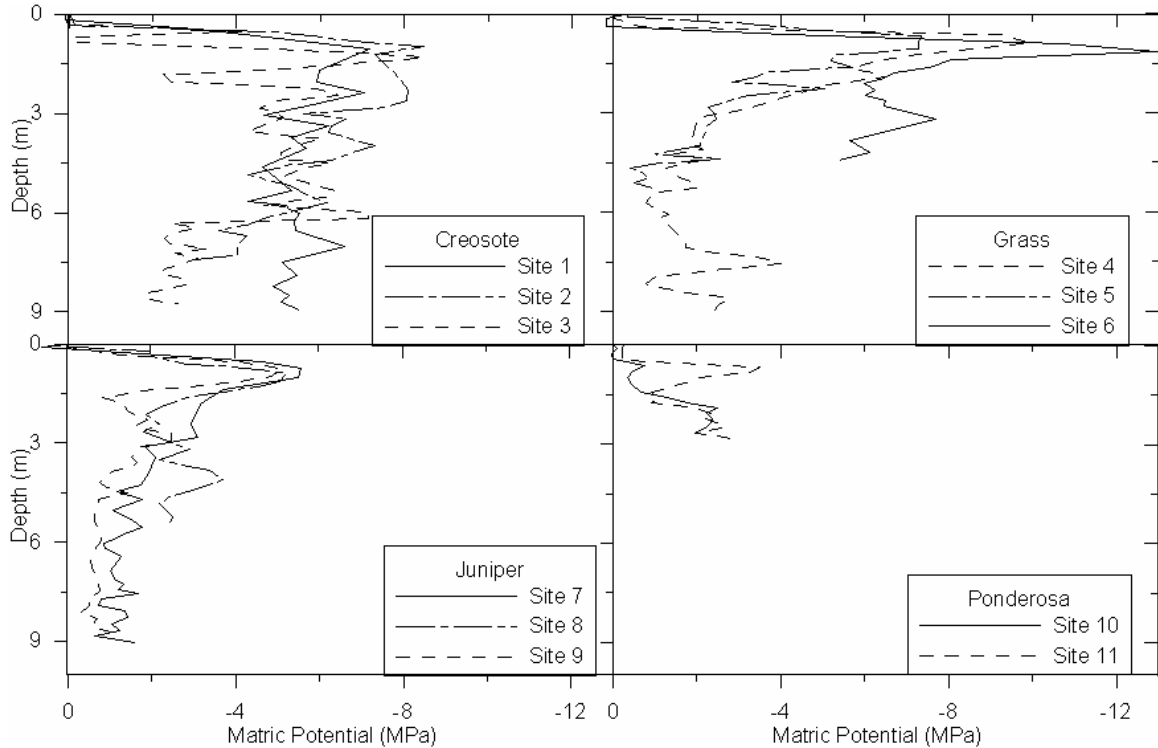
Figure 5.9. Matric potential with depth grouped by ecosystem. To facilitate intercomparison, x and y axes are the same on all graphs.

When the data are grouped by ecosystem, a good correlation between the sites within an ecosystem is observed. A systematic trend of increasing overall matric potentials going from grass to creosote to juniper to ponderosa ecosystems is also present. These profiles were then averaged and displayed on one graph, Figure 5.10, for ease of comparison between the ecosystems.
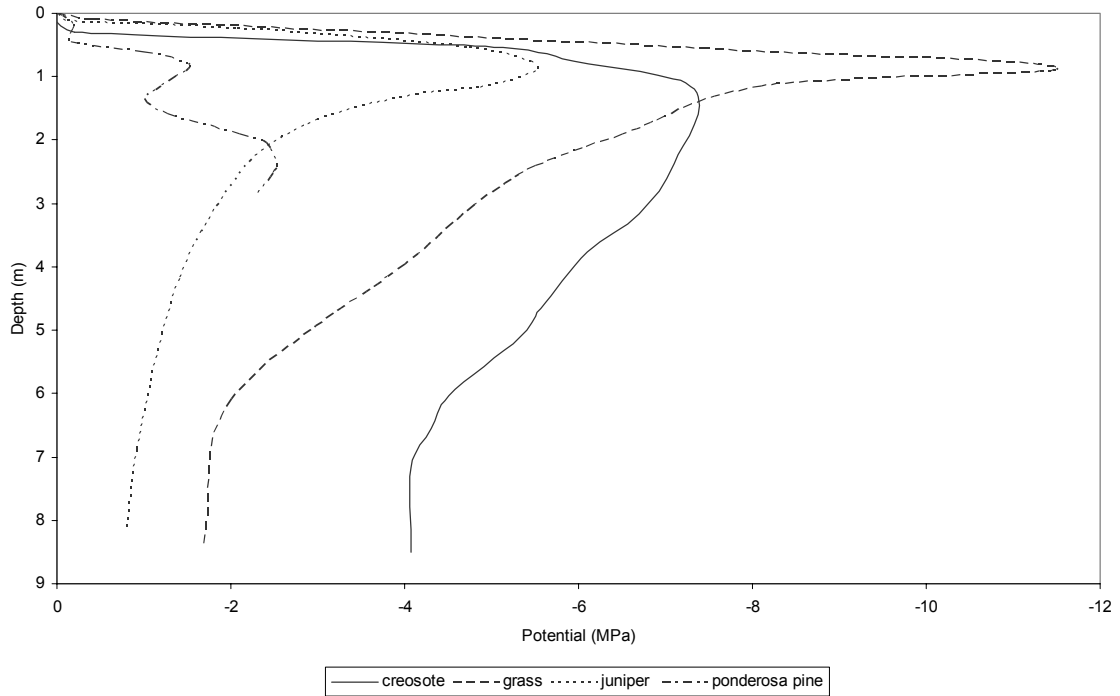
Figure 5.10. Matric potential averaged for each ecosystem. Site 5 is not included in the average for the grass ecosystem.

The systematic trend discussed above can be seen even more clearly in this graph. Additionally, the creosote profile is distinguished by very low matric potentials, -4 MPa or less, that persists to the bottom of the profile. Previous modeling by Walvoord and Phillips (2004) indicated that it would take over 16 kyr of drying from an initial, relatively wet condition throughout the profile, to establish matric potentials this low at this depth in the profile. Figure 1.6 shows the results of their simulation, noting that -4 MPa $\tilde{=} - 400$ meters of water. This demonstrates that the vadose zone under the creosote is in a long-term drying phase, and the effects of this drying have propagated beyond the depth of sampling. The high matric potentials under the juniper and grass ecosystems could be the result of preferential flow as discussed earlier in Section 5.3.3, or they could also be the result of flushing of the profile, with the subsequent re-establishment of low potentials near the surface by the vegetation. Preferential flow seems to be the most

197

probable explanation for the juniper ecosystem because of the presence of macropores in the juniper soil pit and the rooting structure of the juniper tree. However, the data available (matric potential and chloride concentration profiles) cannot definitively identify the responsible process. Some form of flushing, either through preferential flow path or more uniform flow, is certainly affecting the profiles in the grass, juniper and ponderosa pine ecosystems. This flushing seems most frequent in the ponderosa pine ecosystem, and decreases in frequency going from the juniper to the grass ecosystem.

5.6.1.3. Potential Gradients

Liquid water moves in response to potential gradients, with gravitational and matric potentials contributing to the total potential of liquid water movement in the vadose zone. Osmotic potential was not included in the total potential, as was discussed in Section 5.6.1.1. The potential gradients for each site are shown in Figure 5.11, with negative gradients indicating downward flow and positive gradients indicating upward flow. The profiles are grouped by ecosystem, and, for inter-ecosystem comparison, the axes are identical in all graphs.
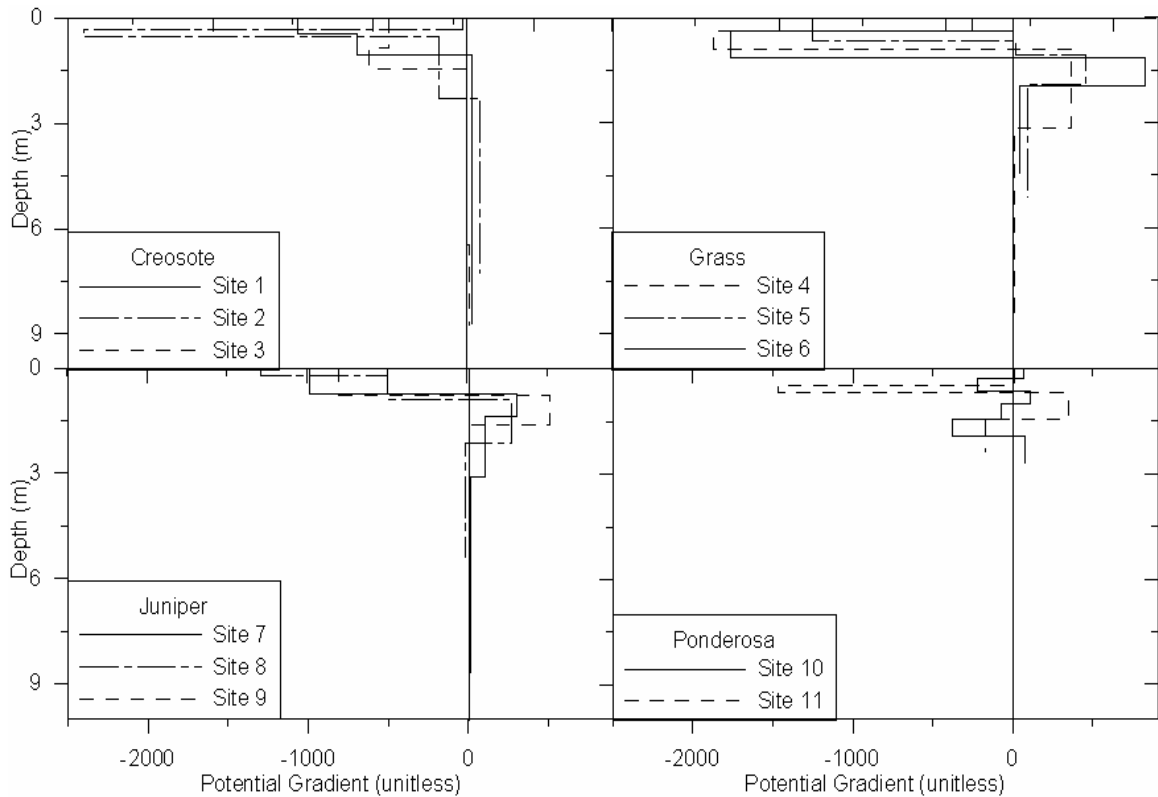
Figure 5.11. Liquid-water potential gradients grouped by ecosystem; includes matric and gravitational potential. Negative gradients represent downward fluxes and positive gradients represent upward fluxes. Zero gradient line placed on graph for clarification. To facilitate intercomparison, x and y axes are the same on all graphs.

The gradients are highest in the grass ecosystem, followed by the creosote, then juniper, then the ponderosa pine ecosystem. A strong correlation between sites within an ecosystem and a systematic difference between ecosystems exists. For comparison, Figure 5.12 shows the average gradients of each ecosystem on the same graph. Flow in the root zones of plants is not often one-dimensional, since the flow field is strongly controlled by root density and distribution, which is usually non-uniform (Tyler and Walker 1994). Therefore, flow directions within the root zones can change directions several times and do not necessarily reflect the flow in the deeper vadose zone below the root zone. In this study, the root zones of the juniper and ponderosa pine appear most likely to produce non-uniform flow, since, among the ecosystems tested, their roots are

199

the least uniform in size and distribution.
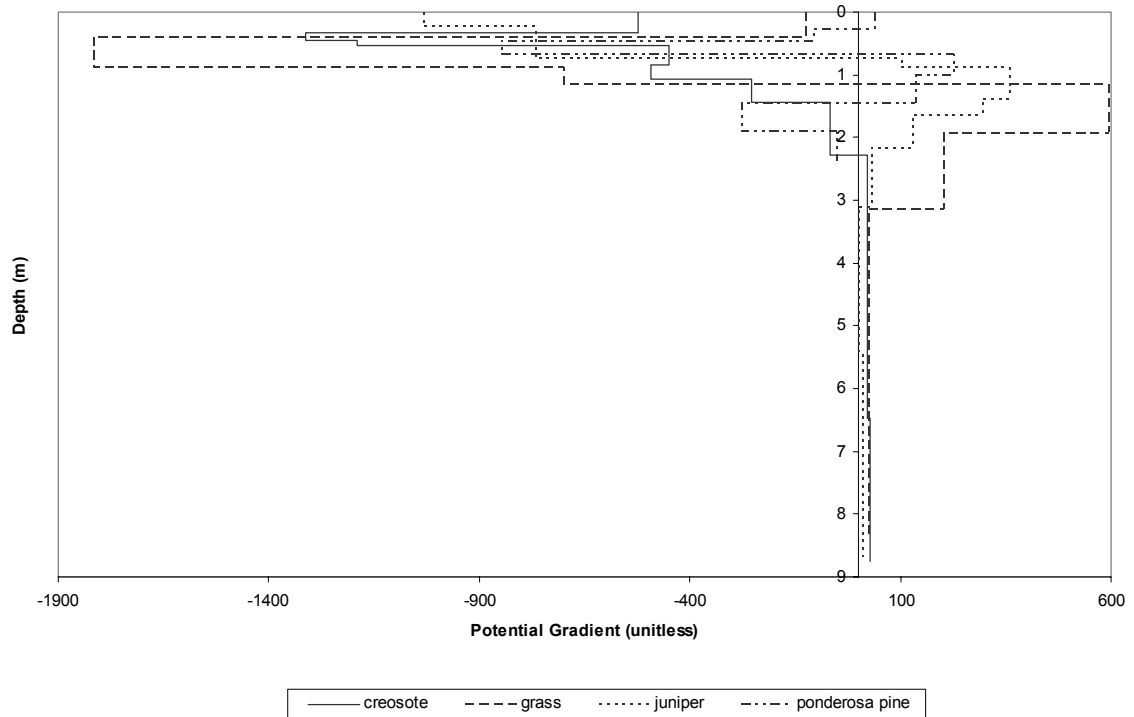
Figure 5.12. Liquid-water potential gradients averaged for each ecosystem. The liquid potential includes matric and gravitational potentials. Negative gradients represent downward fluxes and positive gradients represent upward fluxes. Zero gradient line placed on graph for clarification. x and y axes same on all graphs for to facilitate intercomparison. Site 5 is not included in the average for the grass ecosystem.

The gradients in the creosote and grass ecosystems switch from negative to positive gradients only once in the profile, as shown in Table 5.9. This switch is also well correlated with the root-zone average depth-estimates for that ecosystem, discussed in Section 5.3.2, with the root zone of creosote ending on average at three meters depth and the grass root zone ending at one meter. The root systems of these plants are also fairly uniform, so it expected that the gradients would switch flow directions in the profile only once. The gradients in the juniper and ponderosa pine ecosystems switch from negative to positive gradients several times in the profile. The deepest switch in gradient direction in the juniper trees correlates fairly well with the root-zone depth estimate for this ecosystem of six meters. The soil section of the ponderosa-pine profile

200

is less than the root-zone depth estimate of 3.5 meters, therefore much of the flow in these profiles can be considered root zone dynamics. Except for the ponderosa pine, the gradients in the bottom sections of all of the profiles are upward, which is common in arid vadose zones, as discussed in Section 1.2.2.2.

Ecosystem	Depth Interval (m)	Sign of Gradient	Direction of Flow
creosote	0 – 2.5	negative	down
	2.5 - 9	positive	up
grass	0 – 1.1	negative	down
	1.1 – 9	positive	up
juniper	0-0.5	negative	down
	0.5 – 3	positive	up
	3 – 5	negative	down
	5 – 9	positive	up
ponderosa	0 – 0.3	positive	up
	0.3 – 0.6	negative	down
	0.6 – 1	positive	up
	1 – 2.7	negative	down

Table 5.9. Flow directions for profile depth intervals of the average gradients by ecosystem.

5.6.2. Environmental Tracers

5.6.2.1. Chloride Deposition

The results of the chloride-deposition measurements taken in the Sevilleta are discussed in depth in Appendix A. The chloride-deposition rates used in this study that were calculated in Appendix A, are listed in Table 5.10 on a per-site basis.

Site #	Total Chloride Deposition $(mg\ m^{-2}\ yr^{-1})$
1	57.2
2	57.9
3	57.1
4	68.2
5	68.8
6	57.1
7	68.9
8	69.2
9	70.4
10	73.5
11	72.1

Table 5.10. Chloride-deposition values for each study site. Total chloride deposition is the sum of the wet and dry chloride depositions.

5.6.2.2. Water Content Effect on Chloride Concentrations

To determine the effect of water content on the concentration of chloride in the pore water, chloride concentrations were determined on a per-pore-water and per-dry-soil basis. Chloride concentrations are used to determine the movement of soil-moisture. Therefore, the expression the chloride concentration on a pore-water basis is more appropriate, since water moves in response to concentration gradients. Water content did not significantly affect the overall trends of most chloride profiles. Sites 3, 5, 6, and 11 had demonstrated some effect, as shown in Figure 5.13.
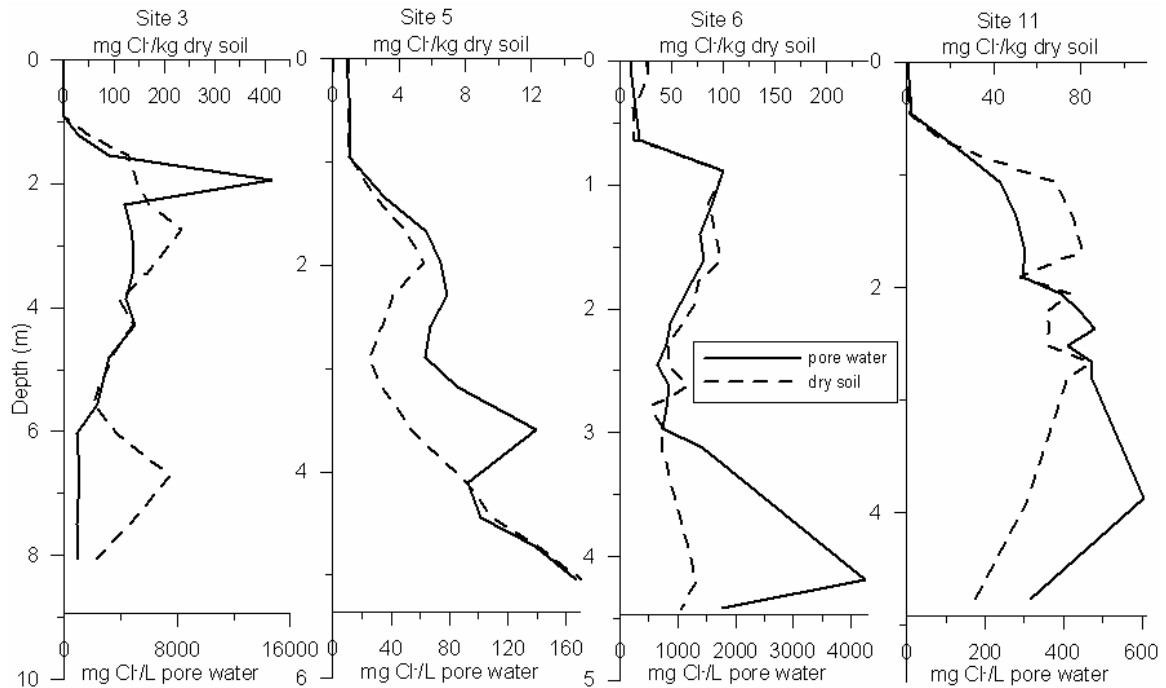
Figure 5.13. Chloride with depth, expressed in terms of pore-water concentration and per mass of dry soil. Note different scales on the x and y axes, and the two x axes on each graph.

If the chloride values on a per-liter-of-pore-water basis are greater than those on a per-dry-soil basis, then that area is unusually dry compared to other areas of the profile. If the opposite pattern occurs, than that area is unusually wet. The scale of the profiles were changed until both profiles matched as well as possible. In Site 3, the amount of pore-water chloride exceeds the amount of chloride per dry mass at 1.9 meter depth indicates an extremely dry area, and an opposite pattern from six to eight meters that corresponds with a clay-rich layer. This site is discussed in more detail in Section 5.3.5 above. Site 5 showed an area of low water content that affected the two types of chloride concentrations, and this also corresponds with an area of lower clay content than were present in other areas of the profile. Site 6 contains an area of extremely dry soil, from three to four meters depth, which corresponds with a change in soil texture from loam

above to sandy loam at this depth. The increase in sand content should result in lower water content in this interval. At Site 11, an area with unusually high water content for the profile is found from one to two meters. This interval corresponds with a change in soil texture from loam to silty loam. These results demonstrate that soil texture can affect chloride concentrations by affecting the water content of the soil.

5.6.2.3. Chloride Profiles

Chloride is non-volatile and does not react with the soil matrix (conservative), making it an excellent tracer of water movement in the subsurface. The chloride concentrations for each site, grouped by vegetation type and plotted on the same axes for comparison, are shown in Figure 5.14.
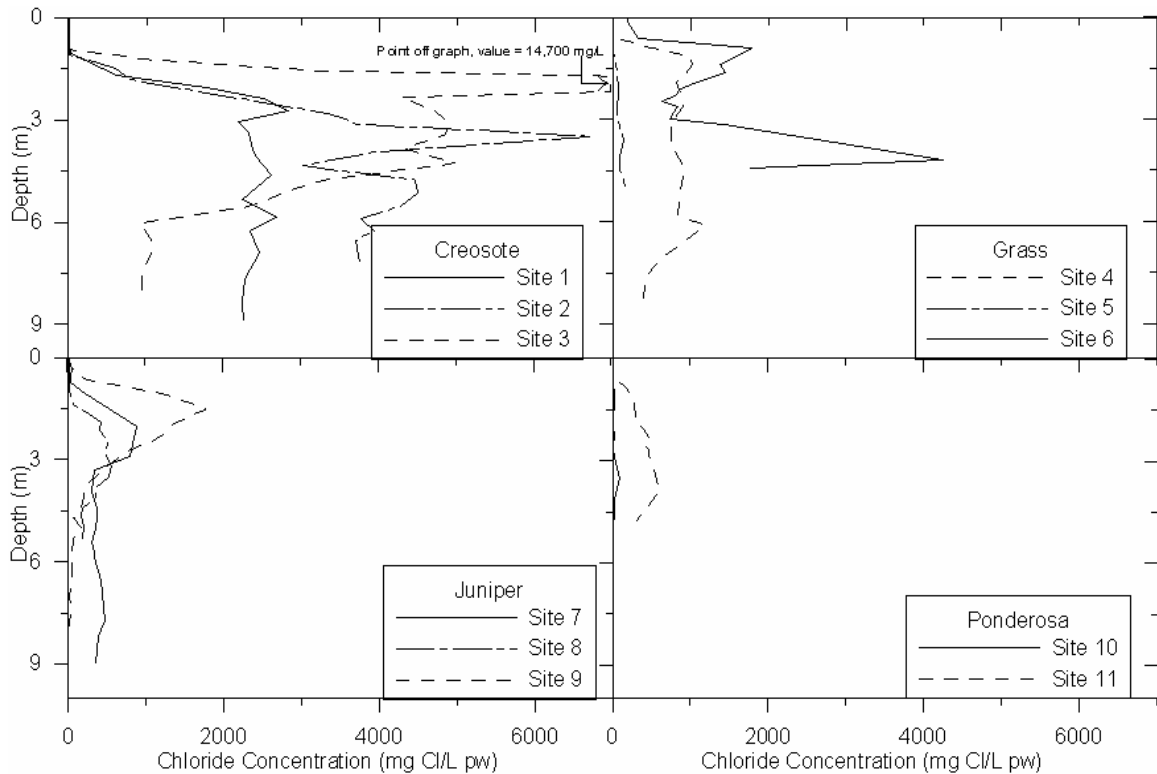
Figure 5.14. Chloride concentration data with depth grouped by ecosystem. x and y axes are the same on all graphs for to facilitate intercomparison. pw = pore water.

The chloride profiles have fairly strong correlations within each ecosystem, with the exception of Site 5 which is considered anomalous. There is a systematic trend between ecosystems, with creosote having the most chloride accumulation within the profile, followed by grass, juniper, then ponderosa pine. The averages of each ecosystem's chloride profiles are shown in Figure 5.15, plotted on the same graph for ease of comparison.
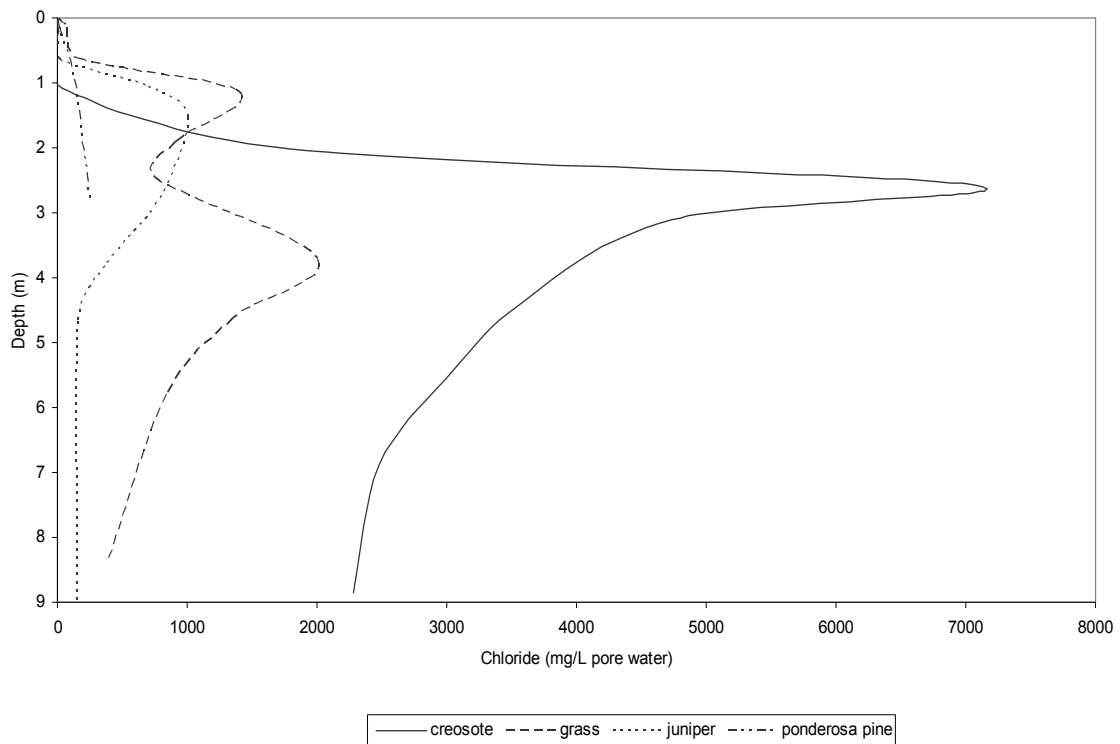
Figure 5.15. Chloride concentration with depth averaged for each ecosystem. Site 5 is not included in the average for the grass ecosystem.

The systematic trend discussed above can be seen even more clearly in the graph above. A particularly noteworthy feature is the very high chloride concentrations, over 2000 mg Cl$^-$ L^{-1} pw, that persist to the bottom of the profile in the creosote ecosystem. Previous modeling by Walvoord and Phillips (2004) indicated that it would take over 16 kyr of drying after flushing of the profile, to establish chloride concentrations this large at

205

this depth in the profile. Figure 1.6 shows the results of this simulation. This indicates

that the vadose zones under the creosote is in a long-term drying phase. The lower

chloride concentrations under the juniper and grass ecosystems could be the result of

preferential flow, as discussed earlier in Section 5.3.3, or could also be the result of

flushing of the profile, with the subsequent re-establishment of high chloride

concentrations near the surface. Preferential flow seem to be the most probable

explanation, but more uniform flushing cannot be ruled out. There is definitely some

form of leaching, whether it is uniform or focused, that is removing the chloride in the

grass, juniper, and ponderosa pine ecosystems. This leaching is most frequent in the

ponderosa pine ecosystem, and apparently decreases in frequency going from the juniper

to the grass ecosystem.

5.6.2.4. Chloride Mass Balance Method

The amount of groundwater recharge can be estimated through the chloride mass-

balance method. This method uses the deposition rate of chloride on the soil surface and

the concentration of chloride measured in the soil water in the vadose zone to determine

the rate of groundwater recharge (Phillips 1994), as was discussed in Section 1.2.3.3.

The value of C_{Cl} (chloride concentration) is best determined by plotting the cumulative

chloride content (mass per unit volume of soil) with depth against the cumulative water

content (volume of water per unit volume of soil) at the same depth. The data on this

graph usually plot in straight line segments whose slopes correspond to C_{Cl} for that depth

interval. These graphs are shown in Figure 5.16 and are grouped by ecosystem and

plotted on the same axes for ease of comparison. The higher the slope, the lower the

amount of groundwater recharge or residual flux.
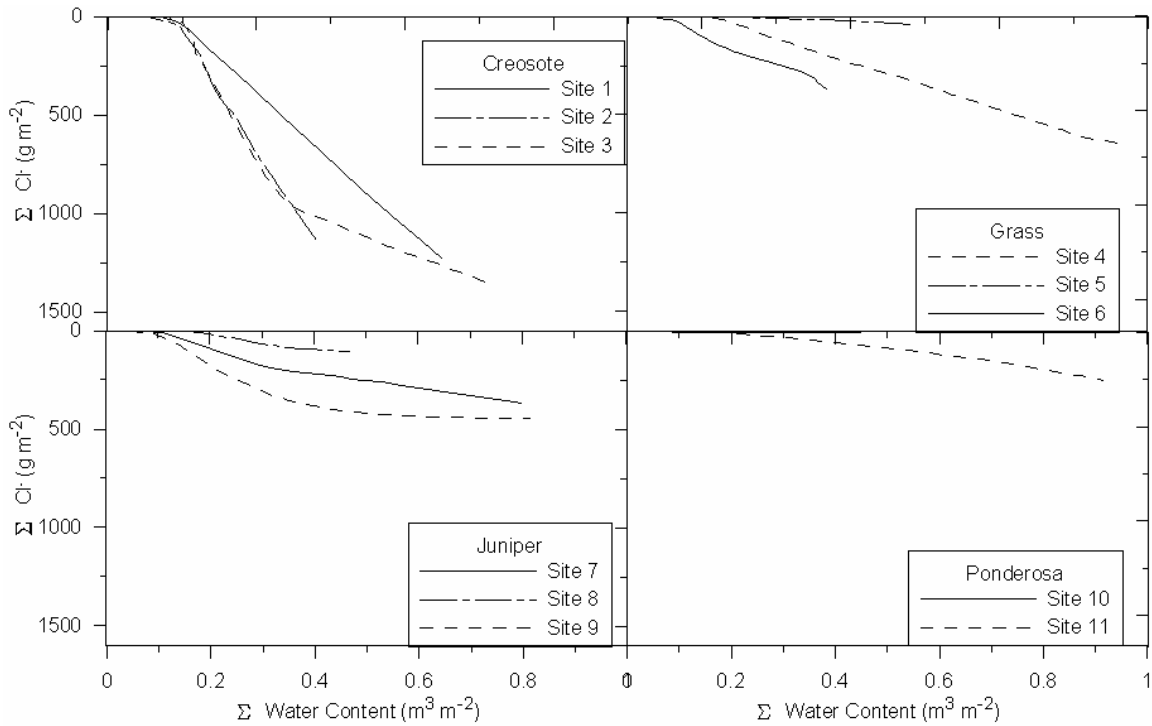
Figure 5.16. Plots of cumulative chloride versus cumulative water content for soil chloride profiles grouped by ecosystem. To facilitate intercomparison, x and y axes are the same on all graphs for.

The sites correlate well with each other within each ecosystem, and a systematic difference between sites is present. Creosote has the greatest slope, followed by grass then juniper then ponderosa. This follows the trends seen above in chloride concentrations and matric potentials. Figure 5.17 below shows the average plot for each ecosystem plotted on the same graph for ease of comparison. The accumulation time of chloride deposition for each ecosystem is shown next to the appropriate graph.
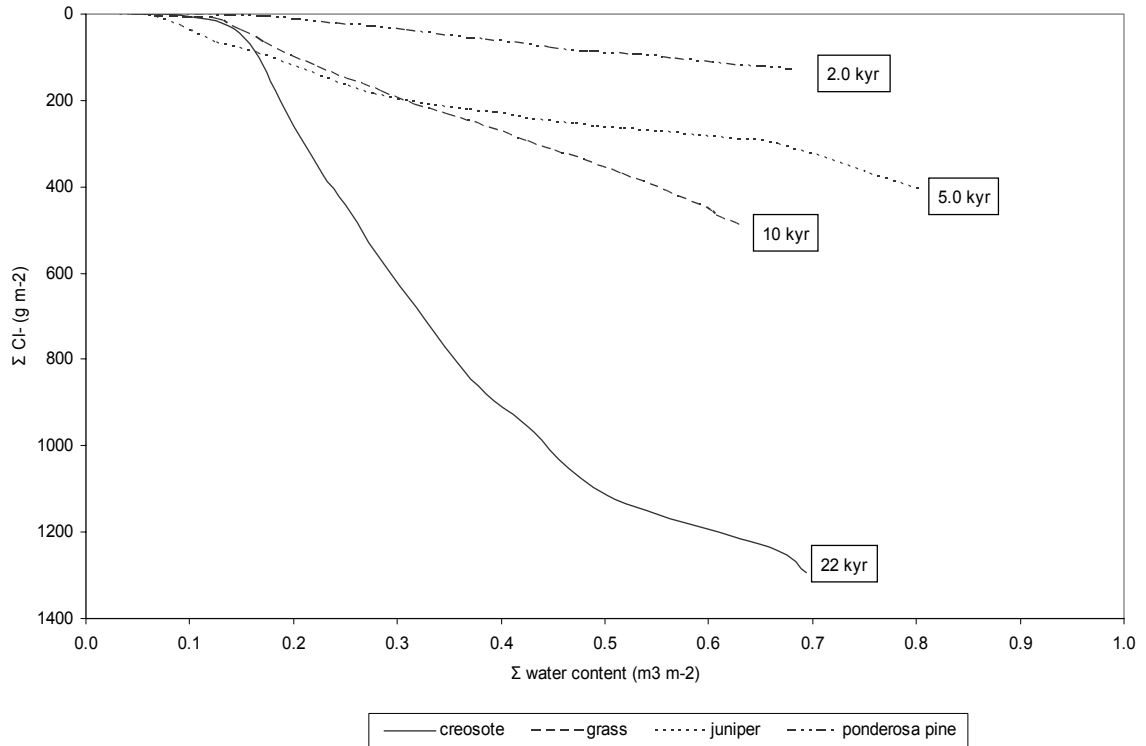
Figure 5.17. Plot of cumulative chloride versus cumulative water content for soil chloride profiles averaged for each ecosystem. Site 5 is not included in the average for the grass ecosystem. Accumulation time for chloride deposition within each ecosystem given to the right of each line.

The chloride mass-balance approach to determining residual flux can be used for Sites 10 and 11, because downward fluxes are evident from the profiles. The grass and juniper sites are possibly in a steady-state or near steady-state condition in which the chloride near the bottom of the profile is in equilibrium with the chloride input and thus represents the actual deep flux. The estimates of the residual flux through the soil matrix for the grass and juniper ecosystems are considered maximum estimates since preferential flow would reduce the amount of chloride accumulation in the profiles, thereby increasing the calculated residual flux. The residual flux for the creosote ecosystem was not calculated since the site in this ecosystem have evidence of sustained upward flow gradients and large chloride accumulation, therefore violating the downward

flow assumption critical to using this method. The accumulation time of chloride

deposition and the residual flux estimates are shown in Table 5.11.

Site #	Vegetation	Chloride Accumulation (yrs)	Residual Flux (mm yr^{-1})	Average Residual Flux (mm yr^{-1})
1	creosote	20,000		
2	creosote	21,000		
3	creosote	25,500		
4	grass	9,900	0.082	(0.067 ± 0.020)
5	grass	1,400	0.71	
6	grass	12,000	0.053	
7	juniper	5,100	0.19	(0.439 ± 0.43)
8	juniper	3,000	0.20	
9	juniper	6,900	0.94	
10	ponderosa	288	4.3	2.26 ± 2.89
11	ponderosa	3,60	0.22	

Table 5.11. Accumulation time of chloride deposition by site and residual flux for each
site and by ecosystem. Grass Site 5 was not included in the average residual flux
calculation for that ecosystem. Average residual flux calculations for the juniper and
grass ecosystems are in parentheses because of the uncertainty of the whether the sites are
in a steady-state condition. The values for these two ecosystems are considered the
maximum flux estimate for these ecosystems.

The residual fluxes calculated for the grass and juniper ecosystems are 0.067 and

0.439 mm yr^{-1}, respectively. These estimates are considered the maximum values

possible for these ecosystems and are somewhat uncertain, as previously discussed. The

residual flux calculated for the ponderosa pine is 2.26 mm yr^{-1}. The chloride

accumulations of the two ponderosa pine sites varies significantly, most likely the result

of clay-rich layers at Site 11, as was discussed in Section 5.3.4. These sites are still

considered representative of ponderosa pine areas, since clay-rich layers are common in

soils in ponderosa pine areas. In contrast, under the creosote sites, the accumulation time

predates the last major climate change 15 ka under the creosote sites. This demonstrates

that these profiles have not been flushed in approximately 22 kyr. Accumulation times of

less than 15 kyr under the other ecosystems indicates that there has been partial or full flushing of the soil profiles since the inception of an arid climate at the end of the last glaciation. Preferential flow that through isolated sections of the profile would cause the calculations of time since the last *complete* flushing of the profile to be underestimated. Therefore, in the juniper sites, it has been *at least* 5 kyr since complete flushing of the profile and 10 kyr for the grass profiles. Preferential flow could be flushing portions of the ponderosa pine profiles, but the downward liquid fluxes have wiped out any evidence of this. Since it has a root system as varied in distribution and root size as do the junipers, preferential flow is likely. Given this, it has been at least 290 years since the last flushing event at Site 10 and 3.6 kyr at Site 11.

The calculated residual flux for each ecosystem was used to estimate the groundwater recharge amount for the transect area. This was done to demonstrate how the determination of recharge rates for individual ecosystems could be utilized to estimate the recharge rate of an area, such as a groundwater or surface-water basin. This assessment has some uncertainties including: the low resolution of the vegetation map, the inaccuracy of all vegetations maps which show vegetation trends and not the actual discrete changes in vegetation, and the limited amount of data obtained in this study. Recharge and precipitation volumes were not calculated for the non-vegetated transect areas. The piñón-juniper ecosystem was not sampled in this study, so the recharge rate for the juniper ecosystem was used to approximate the recharge for this area. Table 5.12 and 5.13 show the results of this analysis. For the transect area, the recharge amount as a percentage of the precipitation is 0.1 percent. This groundwater recharge value only represents diffuse recharge through the soil surface and not focus, localized recharge.

Vegetation	Area (m^2)	Recharge Rate (mm/yr)	Recharge Volume (m^3/yr)
creosote	4.2E+08	0	0
grass	1.0E+09	0.067	7.0E+04
juniper	1.3E+09	0.44	5.9E+05
ponderosa	7.8E+07	2.3	1.8E+05
Recharge Over Transect Area (m^3/yr)			8.4E+05
Average Recharge Over Transect Area (m/yr)			2.9E-04

Table 5.12. Groundwater recharge estimate over the transect area. Calculated from residual flux estimates from Table 5.11. Area covered by each ecosystem was determined from Figure 2.7. Recharge volume = recharge rate * area.

Precipitation Rate (mm/yr)	Area (m^2)	Precipitation Volume (m^3/yr)
230	2.0E+08	4.7E+07
250	3.0E+08	7.5E+07
270	5.1E+08	1.4E+08
290	5.0E+08	1.5E+08
310	5.2E+08	1.6E+08
330	4.6E+08	1.5E+08
350	9.6E+07	3.4E+07
390	2.1E+07	8.3E+06
Precipitation Over Transect Area (m^3/yr)		7.6E+08
Average Precipitation Over Transect Area (m/yr)		2.9E-01

Table 5.13. Precipitation estimate over the transect area. Precipitation values were average of grid cell range as shown in Figure 2.4 and the area these grid cells represented was determined from this figure. Precipitation volume = precipitation rate * area.

5.6.2.5. Chloride/Bromide Ratios

Cl^-/Br^- ratios (mass/mass) are used to determine if the chloride in the profile originated from the atmosphere; the Cl^-/Br^- ratios from this source usually range from 80 and to 120 (Davis et al. 1998). Small standard deviations of the ratio within a profile also indicate that all of the water in the profile had the same origin. Several sample bromide levels were below the detection limit, therefore no Cl^-/Br^- was determined for that sample.

The average Cl⁻/Br⁻ ratios for the sites are shown in Table 5.14.

Site #	Range of Bromide Concentrations (mg L^{-1})	Average Cl⁻/Br⁻ ratios (mass/mass)	Maximum Cl⁻/Br⁻ ratios (mass/mass)	Minimum Cl⁻/Br⁻ ratios (mass/mass)
1	0.55 – 1.7	82 ± 5.4	94	75
2	0.27 – 3.0	91 ± 8.2	100	74
3	0.47 – 2.3	103 ± 8.0	110	85
4	0.23 – 1.1	110 ± 10.4	110	95
5	**0.11 – 0.19**	63 ± 18.5	84	35
6	0.51	98	one point with bromide levels above detection limit	
7	0.13 – 0.77	79 ± 7.6	100	70
8	**0.14 – 0.4**	72 ± 32	146	31
9	0.26 – 2.2	74 ± 6.2	81	62
10	-	all bromide concentrations non-detects		
11	**0.22 – 0.39**	185 ± 28	217	144

Table 5.14. Cl-/Br- ratios for the sites. Ratios were not calculated for samples in which the bromide level was below detection (0.1 mg L^{-1}). Ranges of bromide concentration do not include non-detects and bolded ranges represent unusually low bromide concentrations.

Most of the sites have Cl⁻/Br⁻ ratios between 80 and 120 and standard deviations less than 10. Sites 5, 8, and 11 did not meet these criteria. The bromide concentrations at these sites were very close to the detection limit of 0.1 mg L^{-1}, which may have introduced substantial error in the calculated Cl⁻/Br⁻ ratios, as shown in Table 5.14. The samples from Sites 6 and 10 had bromide levels that were all or almost all below the detection limit. While these low concentrations of bromide make the analysis of the Cl⁻/Br⁻ ratios somewhat uncertain, there was no evidence that the local geology affected the ratios. Of the minerals that have been shown to affect the ratios, the amount of ferrihydrite (Brooks et al. 1998) was not determined and halite (Davis et al. 1998) was not found in the geological analysis. The amount of organic matter, which was also found to affect the ratios (Gerritse and George 1988), in the areas around the sites and in the subsurface is very minimal. The accumulation of bromide found in plant matter ranges from 7 kg ha^{-1} (700 mg m^{-2}) in ryegrass (Schnabel et al. 1995) to 54 kg ha^{-1}

(5,400 mg m^{-2}) in orchardgrass (Owens et al.1985). The amount of bromide uptake and accumulation would vary with the amount and productivity of the vegetation (Owens et al. 1985). The vegetation types in this study are less productive then the agricultural vegetation in the studies that determined the bromide uptake values. The bromide accumulation values of the study sites are shown in Table 5.15.

Site #	Bromide in Profile (mg /m^2)	# Samples Above Detection
1	15,000	16
2	12,000	14
3	13,000	15
4	6,000	17
5	400	7
6	100	1
7	4,600	16
8	3,100	14
9	4,400	10
10	0	0
11	1,200	10

Table 5.15. Bromide accumulation at the study sites. Only the bromide levels that were above detection were included in the profile accumulation values.

The levels of accumulation of bromide in the profiles were low enough for root uptake to be of concern. As discussed by Owens et al (1985) and Kung (1990), bromide would cycle in and out of the soil with the growth and decay of the vegetation. This cycling may affect the bromide levels on a seasonal basis, but for the time periods of chloride accumulation seen in this study, hundreds to thousands of years, it may be assumed that this cycling is at a steady state. This, along with the low productivity of the ecosystems under study, demonstrates that the effect of uptake of bromide by the vegetation in this study is probably minimal. Therefore, there is no indication that the chloride found at the sites was from non-atmospheric origins, such as halite weathering and connate waters (Davis et al. 1998).

5.7. Calculation of Integrated Profiles

In order to easily compare the data among sites, the data for each profile was integrated into a single point.

5.7.1. Depth-Integrated Matric Potential

To determine the depth-integrated matric potential for a single profile, the matric potential values for each measurement in the profile were multiplied by the depth interval represented by that measurement. These values were then summed together to determine the total depth-integrated matric potential for each site.

5.7.2. Accumulation Time for Chloride Deposition

To determine the accumulation time for chloride deposition for each profile, the amount of chloride, in mg (kg of dry soil)$^{-1}$, for each measurement in the profile, was multiplied by the bulk density of that sample and by the depth interval represented by that sample. This results in a chloride inventory in units of mg Cl m^{-2} for the interval. These values are summed together for the whole profile to determine the total amount of accumulation for the site. This values is then divided by the estimated chloride deposition rate on the soil surface to obtain the accumulation time for chloride deposition in the subsurface for each site.

5.7.3. Data Extrapolation

Although the design depth for the boreholes was ten meters, actual depths in some cases were less because large rocks in the vadose-zone terminated drilling progress. This presents a problem when comparing data from different sites, because it is important that the data represent equivalent depth intervals. This is especially true when integrating the

214

profile data into a single value. This problem was addressed by extrapolating the data

from all cores shorter than nine meters to a length of nine meters. The parameters that

were extrapolated were chloride accumulation and matric potential. This was

accomplished by imparting the data from the deepest core for each vegetation type into

the missing sections for the cores of that same vegetation type that terminated at

shallower depths. This provided estimated or measured data for all profiles down to a

depth of 9 meters. However, for the grass and ponderosa ecosystems, the deepest

samples were less than nine meters. The deepest chloride measurement for a grass site

was 8.4 meters, so in order to make the grass sites comparable to the other sites, the

chloride concentration from the deepest grass sample was extended down to nine meters

and was also imported into the other two profiles for that vegetation type. For the

ponderosa pine site, bedrock was encounter at three meters depth for both cores, therefore

the profiles were six meters shallower than the other profiles. The method described for

the grass sites was used for the ponderosa sites. The data from Site 10 were used for

extrapolation to nine meters in both Site 10 and Site 11. While ponderosa pines are

adapted to growing in areas with shallow bedrock, they are also found in areas with deep

alluvial soils. Therefore, extending the ponderosa pine profiles to a depth of nine meters

is considered valid for the purpose of inter site comparison.

5.8. Ecological and Climatic Influences on Vadose-Zone Moisture Fluxes

If vadose-zone moisture fluxes were controlled solely by the climate of the area,

quantified by using the aridity index in this study, then the vadose-zone moisture fluxes

should also change gradually as the aridity index changes gradually along the transect.

This would result in with the integrated matric potentials becoming gradually less

negative as the aridity decreased. The accumulation time for chloride deposition should also exhibit a similar relationship, with chloride accumulation time decreasing as the aridity index decreased. The integrated matric potential and chloride accumulation time for each site was plotted against the aridity index and are shown in Figures 5.18 and 5.19, respectively. The straight line on these graphs represents the trend that would be expected if climate were the only influence on the moisture fluxes. The exact shape of this relationship between climate and vadose-zone moisture fluxes is unknown, but it is shown here as linear for simplicity. This line was fitted so as to most closely match the data.
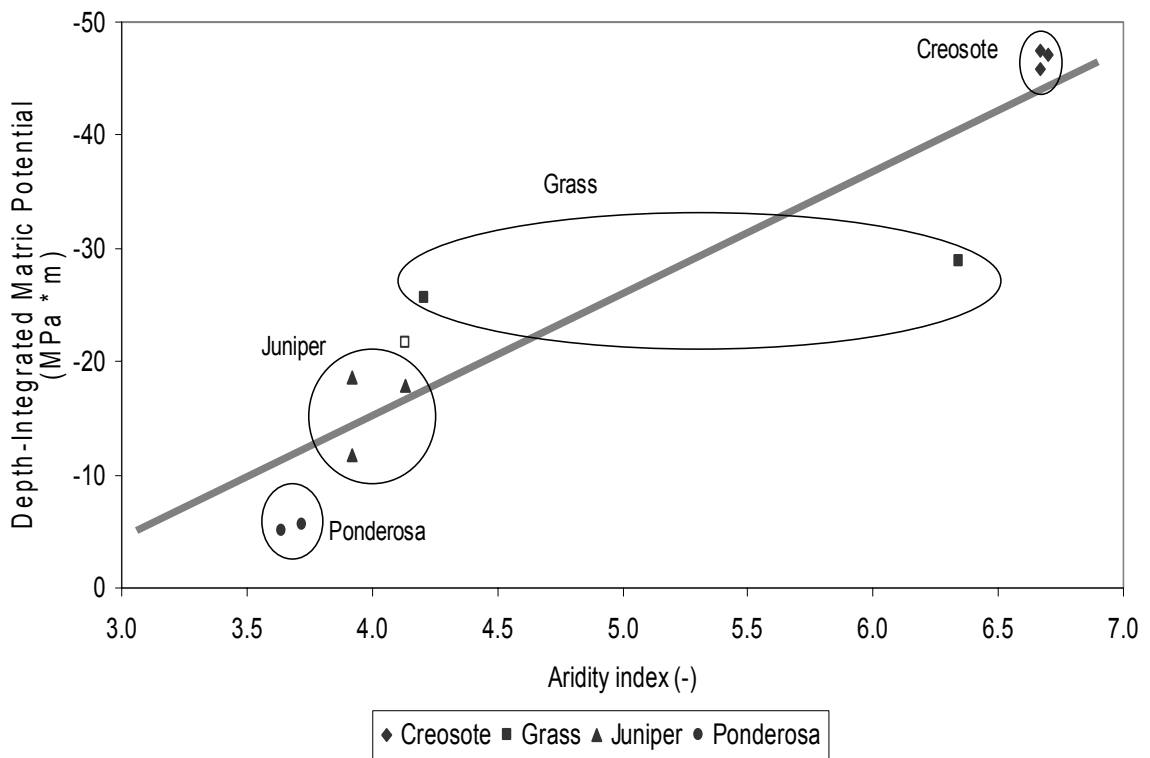
Figure 5.18. Depth-integrated matric potential values for each site. Ecosystems are circled to clarify trends. Site 5 marked by a hollow square and is not included in the ecosystem circle. Straight line notes the depth-integrated matric potential trend expected if climate were the sole influence on vadose-zone moisture fluxes.

The data within each ecosystem are characterized by similar depth-integrated matric potentials and differ systematically from each other. The data do not all plot near

216

the postulated line of predominant climatic influence, but the points do follow the overall trend. The aridity varies the most over the grass section of the transect. The two sites located within the grass circle on the graph vary in aridity index by more than two, but both points have similar depth-integrated matric potential values. The grass site with the highest aridity index value is similar to the aridity values of the creosote sites, but the depth-integrated matric potentials for the grass and creosote are significantly different. These results indicate that the vegetation strongly influences moisture fluxes in addition to the effect of climate.
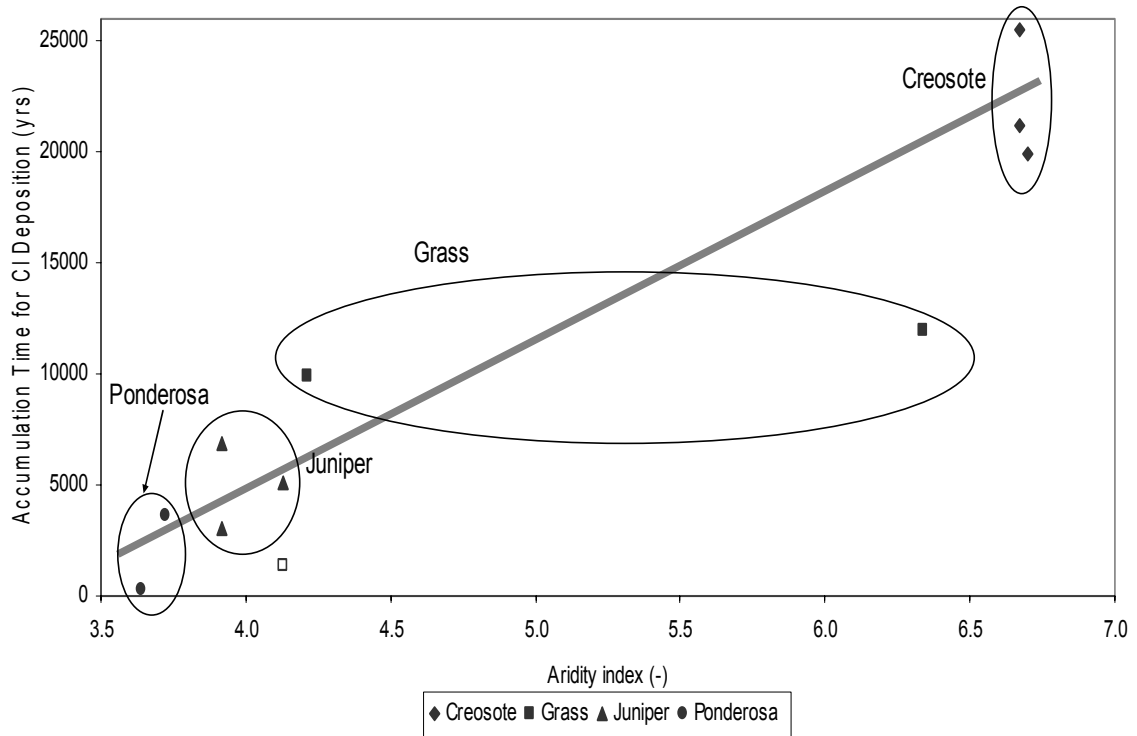
Figure 5.19. Accumulation time for chloride deposition values for each site. Ecosystems are circled to clarify trends. Site 5 marked by a hollow square and is not included in the ecosystem circle. The straight line notes the accumulation time for chloride deposition trend that would occur if climate were the sole influence on vadose-zone moisture fluxes.

The trends exhibited by the data for the accumulation time for chloride deposition are similar to the trends for the depth-integrated matric potential. Since the trends seen

on both plots are very similar, then the same inference, that the vegetation strongly influences moisture fluxes in addition to the effect of climate, can also be drawn for the accumulation time for chloride deposition.

To obtain a more comprehensive perspective on vadose zone conditions, the data, integrated matric potential and chloride accumulation, were plotted together without their associated aridity values, as shown in Figure 5.20. The area of the graph with very negative integrated matric potentials and high chloride accumulations indicates that the vadose zone is in a persistent and static condition. The profiles of sites plotted in this region have not been flushed in a very long time and have been drying out long enough to produce extremely negative matric potentials (Walvoord et al. 2002). Conversely, the area of the graph with high matric potentials and low chloride accumulations indicates that the fluxes are dynamic and presumably often downward. The profiles of the sites plotted in this region have apparently been flushed regularly, resulting in a clearing of the chloride accumulation and an increase in the matric potentials. Areas of the graph in between these two extremes represent conditions that are neither completely persistent nor dynamic, but that have characteristics that fall inbetween along a continuum.
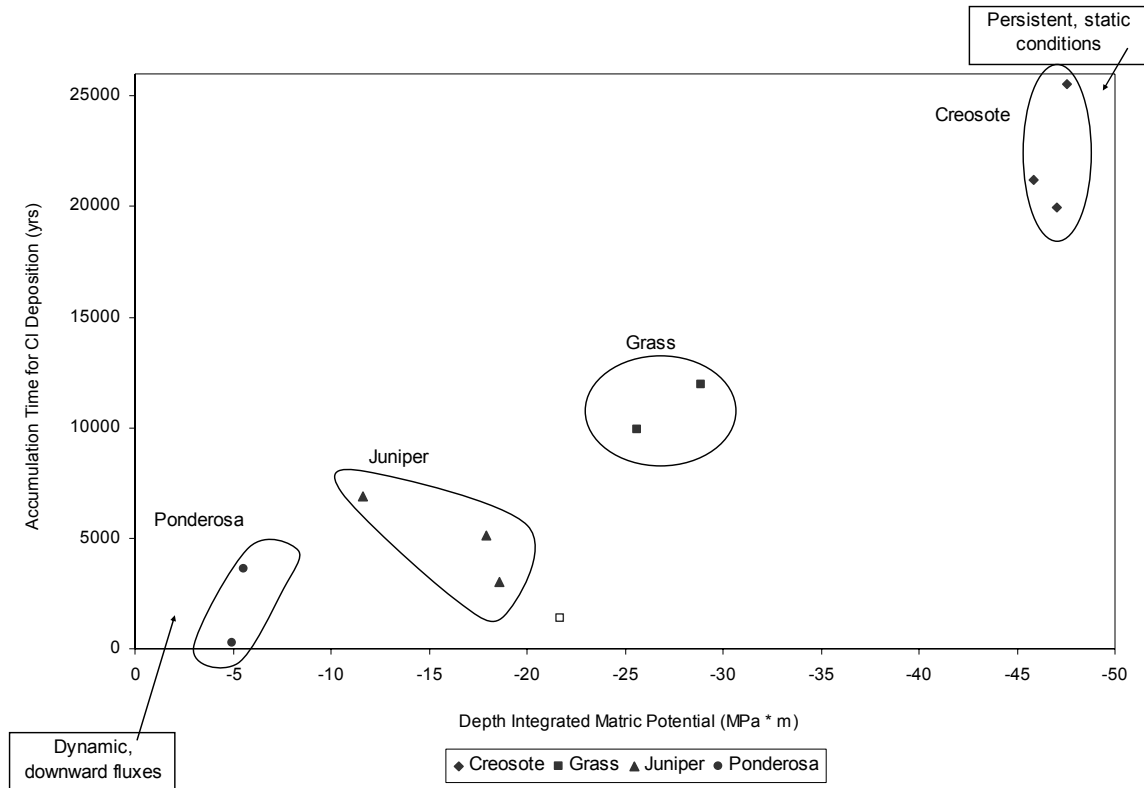
Figure 5.20. Accumulation time of chloride deposition versus depth-integrated matric potential for each site. Ecosystems are circled to clarify trends. Site 5 marked by a hollow square and is not included in the ecosystem circle.

The sites within each ecosystem plot on the above graph as distinct clusters, demonstrating systematic differences between these ecosystems. The sites from the creosote ecosystem plot in the persistent and static area of the graph, while the sites from the ponderosa ecosystem plots in the dynamic and downward flux area of the graph. The large difference in the position of these two ecosystems on the graph indicates a marked difference in the water dynamics of the vadose zones that underlie them. The grass and juniper ecosystems plot in between the creosote and ponderosa ecosystems, indicating that the vadose-zone behavior at these sites have properties in-between the extremes. As discussed above, these profiles may have been fully flushed in the past, but such events must have been highly episodic, on a thousands-of-years time scale. The shapes of the

profiles and matric potential and chloride concentrations deep in the profiles of the grass and juniper ecosystems seem to indicate that preferential flow is the most likely explanation of the observed properties of these ecosystems. The plotting of the sites from the same ecosystems in distinct clusters demonstrates that there are strong ecological influences on the vadose-zone moisture fluxes.

5.9. Sensitivity Analysis

A sensitivity analysis was performed on the integrated matric potential and the accumulation time of the chloride deposition data. The first meter of each profile was set to zero for both parameters in order to simulate a flushing caused by a large precipitation event. This would determine both the sensitivity of the data to a change in surface conditions and the impact of short-term disturbances. The results of this analysis are shown in Table 5.16, which also presents the percent difference between the measured data and the data from the profiles where the first meter was changed to zero. Figures 5.21, 5.22, and 5.23 below show the affects of this sensitivity analysis on the data trends shown in the previous three figures.

Site #	AI	Accumulation Time of Cl⁻ Deposition (yrs)			Integrated Matric Potential (MPa * m)		
		measured	sensitivity	% difference	measured	sensitivity	% difference
1	6.7	20,000	20,000	0	-47	-39	16
2	6.7	21,000	21,000	0	-46	-41	9.5
3	6.7	25,500	25,500	0	-48	-46	3.2
4	4.2	9,900	9,500	4	-26	-21	20
5	4.1	1,400	920	35	-22	-16	27
6	6.3	12,000	10,400	13	-29	-25	13
7	4.1	5,200	5,000	3	-18	-13	25
8	3.9	3,000	3,000	0	-19	-15	21
9	3.9	6,900	5,800	16	-12	-8.3	29
10	3.6	300	120	59	-5.0	-4.7	5.8
11	3.7	3,600	3,000	16	-5.6	-4.1	27

Table 5.16. Sensitivity analysis of accumulation time of chloride deposition and integrated matric potential**.**
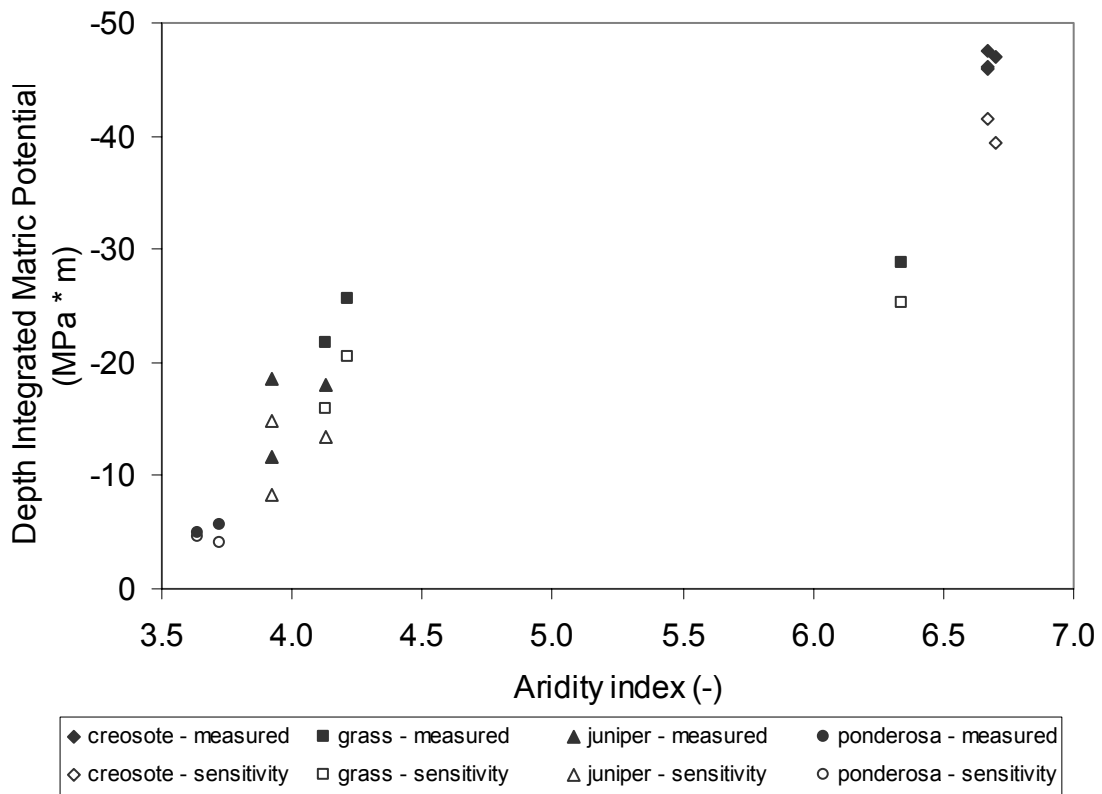
Figure 5.21. Sensitivity analysis performed on integrated matric potential.

221
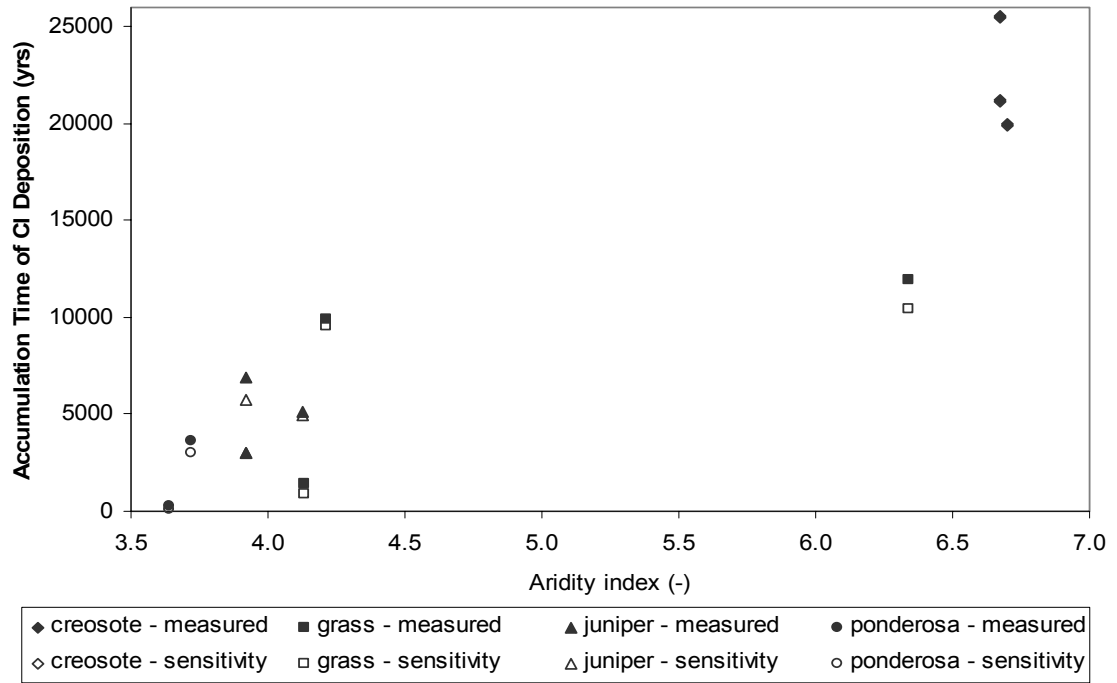
Figure 5.22. Sensitivity analysis performed on accumulation time of chloride deposition.
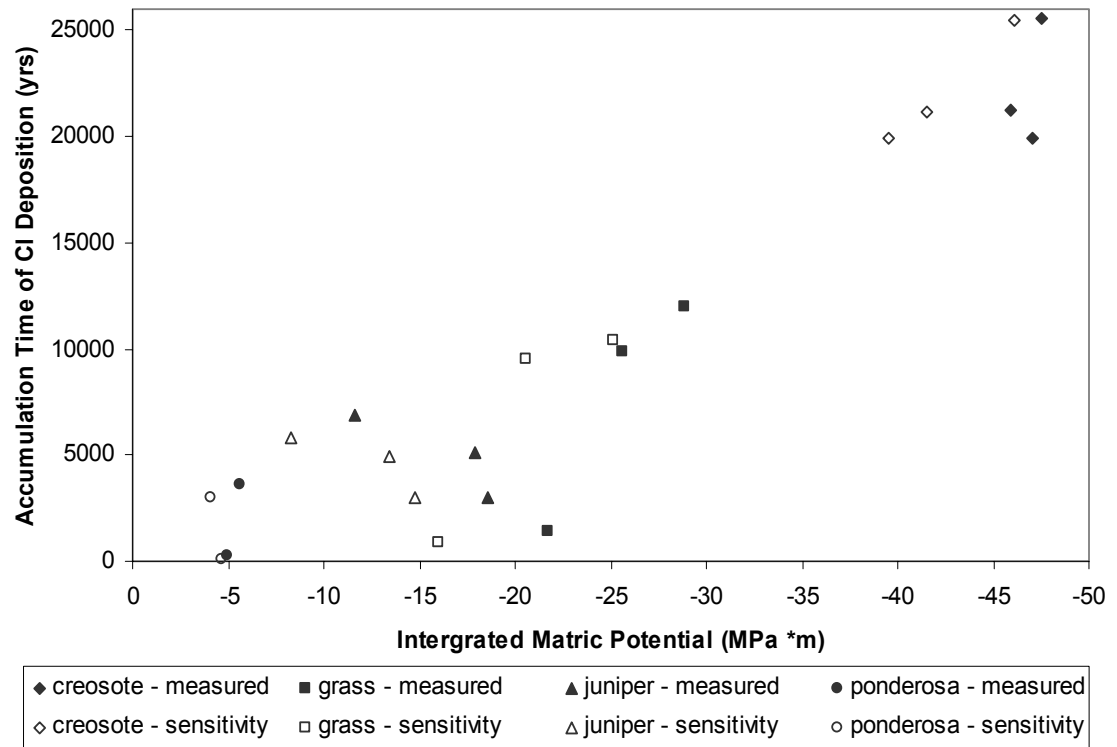
Figure 5.23. Sensitivity analysis performed on both integrated matric potential and accumulation time of chloride deposition.

As shown in the above table and figures, the sensitivity analysis had more of an effect on the integrated matric potential than the accumulation time for chloride deposition. This was a result of the dry conditions at the soil surface at the time of drilling. The overall trend on the figures is the same with the sensitivity analysis as it was without; therefore, these sites are not sensitive to surface conditions or fluctuations. If the surface conditions were as they are in the sensitivity analysis, after a large rainstorm for example, the conclusions would remain the same.

5.10. Statistical Analysis

5.10.1. ANOVA

To test whether that the ecosystems had significantly different vadose-zone properties, a statistical analysis was conducted. An analysis of variance test, ANOVA, was run using the depth-integrated matric potentials and the accumulation times for chloride deposition. These analyses excluded Site 5, since it was determined to be anomalous. The ANOVA test determines whether the means of three of more populations are equal (Davis 2002). These analyses were conducted with the acknowledgement that the small sample populations lead to enhanced uncertainty in the results. The null hypothesis for both ANOVA analyses was that the means of the populations are equal. The alternative hypothesis was that at least one mean is different. A 0.05 level of significance (alpha) was used. The ANOVA test is based on two different estimates of variance: variance between the populations using the population means and the variance within the populations (Davis 2002). A one-way ANOVA test was performed, meaning that the sample data were grouped according to one characteristic, in

this case the ecology. To reject the null hypothesis, the calculated test statistic, F, must

be larger than the critical F value, which is determined by the degrees of freedom of the

populations (Davis 2002). The result of the ANOVA analyses for the integrated matric

potential and the accumulation times of chloride deposition are shown in Tables 5.17 and

5.18, respectively.

SUMMARY

Groups	Count	Sum	Average	Variance
creosote	3	141	47	1
grass	2	55	27.5	4.5
juniper	3	49	16.3	14.3
pp	2	12	6	2

ANOVA

Source of Variation	SS	df	MS	F	P-value	F crit
Between Groups	2406.9	3	802.3	129.5	7.65E-06	4.76
Within Groups	37.2	6	6.2			
Total	2444.1	9				

Table 5.17. Results of ANOVA analysis for depth-integrated matric potential values.
SS= sum of squares, df = degrees of freedom, MS = mean square, F = test statistic, P-
values = probability the null hypothesis is true, F-crit = critical F value. Alpha value for
run was 0.05. Site 5 was not included in this analysis.

SUMMARY

Groups	Count	Sum	Average	Variance
creosote	3	67,000	22,000	8,500,000
grass	2	21,000	10,000	1,900,000
juniper	3	15,000	5,100	3,800,000
pp	2	5,200	2,600	12,000,000

ANOVA

Source of Variation	SS	df	MS	F	P-value	F crit
Between Groups	630,000,000	3	210,000,000	32.4	0.00042	4.76
Within Groups	39,000,000	6	6,500,000			
Total	670,000,000	9				

Table 5.18. Results of ANOVA analysis for accumulation time for chloride deposition
values. SS= sum of squares, df = degrees of freedom, MS = mean square, F = test
statistic, P-values = probability the null hypothesis is true, F-crit = critical F value. Alpha
value for run was 0.05. Site 5 was not included in this analysis.

For both analyses, the F statistic was much greater than the critical F value, therefore the null hypothesis that all the means are equal can be rejected. The p-values, the probability that the null hypothesis is true, for both of the analyses are extremely low, which also demonstrates that the null hypothesis should be rejected. To determine the robustness of this conclusion, the alpha value was changed to 0.01 and Site 5 was included in the analyses. While the F statistic was closer to the critical F value, it was still greater than the critical F value. This adds more certainty to the conclusion of this analysis, which is that the means of the populations (ecosystems) are distinct.

5.10.2. Standard Deviation

To further determine whether or not the means of the ecosystems were unique, a plot of the means and their standard deviations was developed, as shown in Figure 5.24. Standard deviation is defined as a measure of the amount of spread of data in a frequency distribution (Davis 2002). In a normal distribution, one standard deviation above and below the mean encompasses 68 percent of the observations. If the standard deviations of the population means overlap, then there is less than 68 percent probability that the means are distinct.
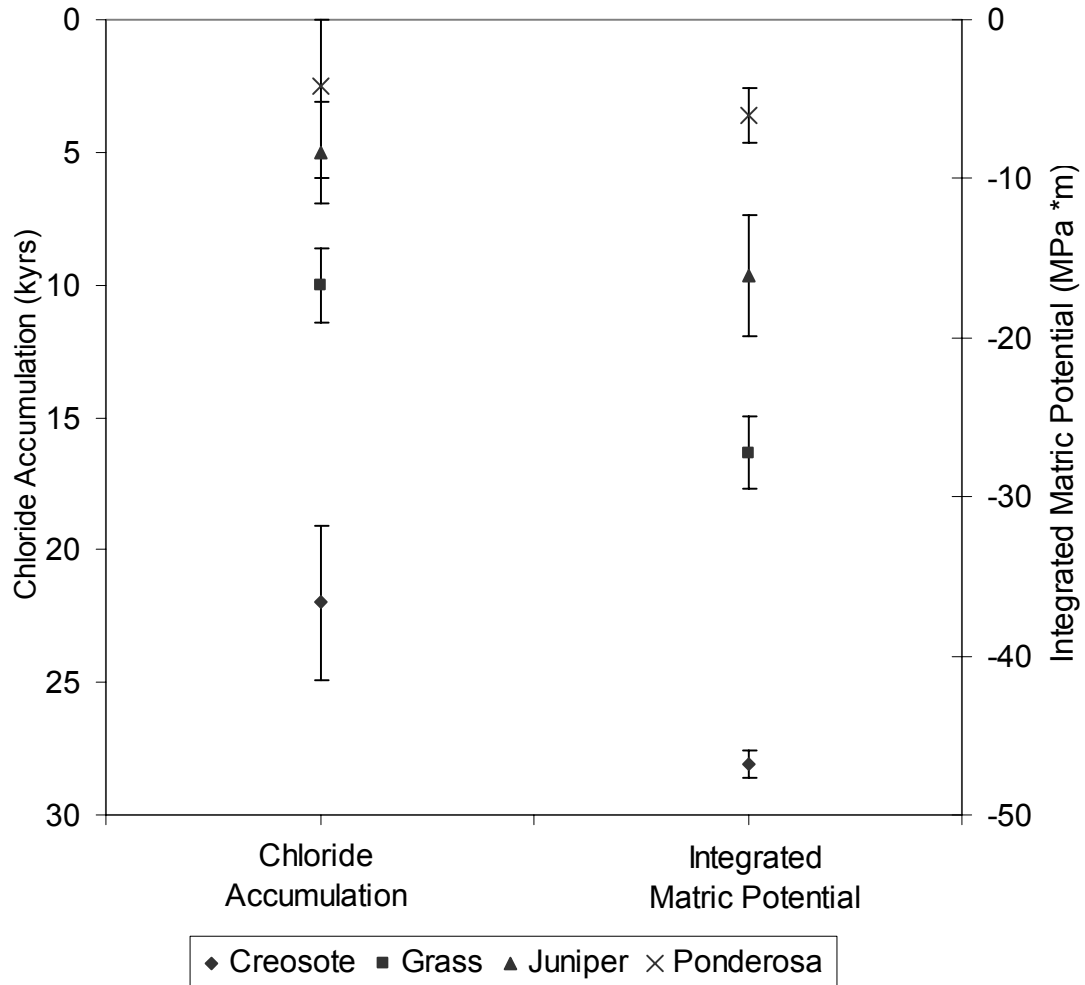
Figure 5.24. Standard deviation of each ecosystem for accumulation time for chloride deposition and depth-integrated matric potential. Data point is the average for each ecosystem and error bars represent one standard deviation from the mean. Site 5 was not included in the mean for the grass ecosystem. Note separate y axes for each parameter.

As seen in Figure 5.23, the standard deviations of the ecosystem means overlap only for the juniper and ponderosa pine ecosystems for the chloride accumulation parameter. The large standard deviation values for these ecosystems is probably the result of their non-uniform rooting structures causing non-uniform flow, as discussed previously. The standard deviation for chloride accumulation of the creosote and grass ecosystems and all of the ecosystems for the integrated matric potential parameter do not overlap. This indicates that the means of these ecosystems are distinct.

CHAPTER 6

CONCLUSIONS AND FUTURE RESEARCH

6.1. Introduction

It was initially hypothesized that arid vegetation has a significant influence on soil-moisture fluxes. The determination of whether the vegetation can be a surface indicator of underlying vadose-zone moisture fluxes was the main objective of this study. If this can be determined, then the vegetation can be used to estimate basin-wide soil-moisture fluxes.

6.2. Summary of Conclusions

6.2.1. Non-climatic and Non-ecological Influences

To determine the influences of climate and ecology on moisture fluxes, we attempted to hold all other parameters affecting vadose zone moisture fluxes as constant as possible at the sites. The only major violation of these criteria was identified at Site 5, where the surface soil was clay rich and the infiltration rate was found to be very low compared to the other sites. A low infiltration rate of the surface soil combined with a slope of 2° probably results in runoff dominating over infiltration at this site. Therefore, the site was considered anomalous and was not included in the ecosystem averages.

6.2.2. Preferential Flow

The matric-potential and chloride-concentration profiles indicate that preferential flow could be occurring deep in the profiles of the juniper sites and at Grass Site 4. The

227

preferential flow at the juniper sites was likely the result of non-uniform flow through juniper root cavities having varying root sizes and distributions. Preferential flow apparently affected the total matric potential and chloride accumulation in the juniper and grass profiles and the shape and magnitude of the bulges.

6.2.3. Calcium Carbonate and Soil Texture

Calcium carbonate was found in most of the profiles, but did not affect the overall trend of the moisture fluxes in those profiles. The only effect of calcium carbonate that was identified was a possible lateral flow path located between two levels of high carbonate content at Site 3. A clay-rich layer at Site 11 appeared to impede downward flow and increase chloride accumulation. There was also an indication of a reservoir of soil water in a clay layer deep in the profile of a Creosote Site 3 that is not currently in equilibrium with the rest of the profile. Besides the effects seen at these two sites, no other effects from subsurface soil texture were seen.

6.2.4. Ecohydrological Influences on Vadose-Zone Fluxes

While some variation existed within the ecosystems tested, there were marked systematic differences between the ecological communities. These systematic differences indicate that, in addition to the influences on the fluxes from climate alone, vegetation ecology influences vadose-zone moisture fluxes. The observed vadose-zone moisture regimes are the result of the complex interactions between soil moisture, vegetation and climate. The soil moisture determines the location of vegetation communities, while those communities also influence the soil moisture. The climate of an area also can influence the distribution of the vegetation and influence the soil

moisture through input of water into the soil profile via precipitation. This system is best described as a multiple feedback loop with each part affecting the other.

Consistent with previous work (Scanlon et al. 2003, Walvoord and Phillips 2004, Newman 1997), the data gathered in this study support the scenario that, under the creosote, there has been no downward liquid movement past the root zone sites, since the last glacial termination. There appears to have been periodic, downward fluxes past the root zone under the grass and juniper sites, as well as preferential flow. While under the grass and juniper ecosystems, preferential flow appears to be the dominant downward flow process into the deeper vadose zone rather than complete flushing of the profile, the extent to which either process dominates the moisture fluxes cannot be determined conclusively. The data from the ponderosa pine sites differ slightly, but indicate periodic, downward, liquid fluxes below the root zone of a greater magnitude and frequency than the grass and juniper sites. Any downward, residual moisture-flux is essentially zero under creosote, and is very small (less than 0.44 mm yr^{-1}) under the grass and juniper ecosystems, with appreciable (~2.9 mm yr^{-1}) downward residual flux under the ponderosa pine ecosystem.

Since we have shown that vegetation ecology significantly influences vadose-zone moisture fluxes, in addition to the influence from the climate of the area, the use of vegetation as an indicator of vadose-zone moisture fluxes may prove to be an efficient means of estimating basin-wide vadose-zone moisture fluxes, and hence groundwater recharge. A map of only climatic factors may not adequately estimate the soil-moisture fluxes, as the ecology also influences these moisture fluxes. The climate can influence the distribution of the vegetation and the climate and the vegetation then influences the

soil-moisture fluxes. Therefore, vegetation may be a better predictor of soil-moisture fluxes. More data from more ecosystems needs to be collected in order to adequately test this hypothesis.

6.3. Suggestions for Future Research

Not enough data has been collected within the ecosystems tested in this study to conclusively determine the effects of vegetation on the soil-moisture fluxes. Data are especially needed in the higher elevation ecosystems, as previous studies have focused on grass and creosote/mixed desert shrub ecosystems. More ecosystems would also need to be tested to encompass all of the ecosystems present in the Río Grande Watershed. Ecosystems that still need to be tested are piñón-juniper mix woodland, salt bush, and the higher elevation ecosystems, such as montane grasslands and those ecosystems containing trees such as aspen, spruce, fir and oak. However, the problems we encountered regarding access of the drill rig to the sites and drilling difficulties due to shallow rocky soils will only increase as the elevation of the ecosystems increases.

More extensive root analyses of the vegetation would also be very useful in determining the relationship between the soil-moisture fluxes and the vegetation. Drilling the soil cores in combination with long-term measurements of the vegetation and the surrounding environment would also be useful. Seasonal and yearly measurements of transpiration, possibly through sap-flow studies, would provide additional information about the relationship between the vegetation and the soil-moisture fluxes. To better understand the relationship between the climate and the soil-moisture fluxes, seasonal and yearly measurements of the actual and potential evaporation and rainfall at the drill sites would also increase the accuracy of the climatic parameters.

REFERENCES

Abrol, I., Yadav, J., and Massoud, F. (1988) *Salt-Affected Soils and Their Management. FAO Soils Bulletin 39.* Food and Agriculture Organization of the United Nations (FAO), Rome. 144 pp.

Allison, G., Gee, G., and Tyler, S. (1994) "Vadose-Zone Techniques for Estimating Groundwater Recharge in Arid and Semiarid Regions." *Soil Science Society of American Journal.* 58. p. 6 - 14.

Anderholm, S. (1987a) "Hydrogeology of the Socorro and La Jencia Basins, Socorro County, New Mexico." *Water Resources Investigation Report 84-4342*, US Geological Survey, Albuquerque, New Mexico. 62 pp.

Anderholm, S. (1987b) "Reconnaissance of Hydrology, Land Use, Groundwater Chemistry, and Effects of Land Use on Groundwater Chemistry in the Albuquerque -Belen Basin, New Mexico." *Water Resources Investigation Report 86-4174*, US Geological Survey, Albuquerque, New Mexico. 37 pp.

Andraski, B. (1997) "Soil-water Movement Under Natural-site and Waste-site Conditions: A Multiple-year Field Study in the Mojave Desert, Nevada." *Water Resources Research.* 33(8). p.1901 - 1916.

Ankeny, M., Ahmed, M., Kaspar, T., and Horton, R. (1991) "Simple Field Method for Determining Unsaturated Hydraulic Conductivity." *Soil Science Society of America Journal.* 55. p. 467 - 470.

Aronovici, V., Schneider,A., Asce, A., and Jones, O. (1972) "Basin Recharge of the Ogallala Aquifer." *Journal of the Irrigation and Drainage Division, Proceedings of the American Society of Civil Engineers.* 98. p. 65 - 76.

Arora, V. (2002) "The Use of the Aridity Index to Assess Climate Change Effect on Annual Runoff." *Journal of Hydrology*. 265. p. 164 - 177.

Baumhardt, R. and Lascano, R. (1993) "Physical and Hydraulic Properties of Calcic Horizons." *Soil Science Society of America.* 155 (6). p. 368 - 375.

Birkeland, P. (1999) *Soils and Geomorphology.* New York, NY, Oxford University Press. 430 pp.

Booker, J., Michelsen, A., and Ward, F. (2005) "Economic Impact of Alternative Policy Responses to Prolonged and Severe Drought in the Rio Grande Basin." *Water Resources Research*. 41. doi:10.1029/2004WR003486.

Bouwer, H. and Rice, R. (1983) "Effect of Stones on Hydraulic Properties of Vadose Zones." *Characterization and Monitoring of the Vadose Zone.* National Water Well Association Conference. December 8-10, 1983. Las Vegas, Nevada. p. 77 - 93.

Brooks, S., Taylor, D., and Jardine, P. (1998) "Thermodynamics of Bromide Exchange on Ferrihydrites: Implications for Bromide Transport." *Soil Science Society of America Journal.* 62. p. 1275 - 1279.

Budyko, M. (1974) *Climate and Life*. David H. Miller, translator. Academic Press, New York, New York. 508 pp.

Canadell, J., Jackson, R., Ehleringer, J., Mooney, H., Sala, O., and Schulze, E. (1996) "Maximum Rooting Depth of Vegetation Types at the Global Scale." *Oecologia.* 108. p. 583 - 595.

Carsel, R. and Parrish, R. (1988) "Developing Joint Probability Distributions of Soil Water Retention Characteristics." *Water Resources Research.* 24 (5). p. 755 - 769.

Climate Source. (2004) *Mean Monthly and Annual Maximum, Minimum, and Mean Temperature.* http://www.climatesource.com/us/fact_sheets/fact_tmean_us.html

Collectors. (2005) *Wet and Dry Chloride Deposition Collectors at Río Salado LTER Weather Station.* http://sevilleta.unm.edu/places/refuge/profile/riosalado

Cook, P., Edmunds, W., and Gaye, C. (1992) "Estimating Paleorecharge and Paleoclimate From Unsaturated Zone Profiles." *Water Resources Research.* 28 (10). p. 2721 - 2731.

Davis, J. (2002) *Statistics and Data Analysis in Geology*. Wiley, Third Edition. 638 pp.

Davis, S., Whittemore, D., Fabryka-Martin, J. (1998) "Uses of Chloride/Bromide Ratios in Studies of Portable Water." *Ground Water.* 36 (2). p. 338 - 349.

Davis, S., Fabryka-Martin, J., and Wolfsberg, L. (2004) "Variations of Bromide in Potable Ground Water in the United States." *Ground Water.* 42 (6-7). p. 902 - 909.

Dick-Peddie, W. (1993) *New Mexico Vegetation, Past, Present, and Future.* University of New Mexico Press. Albuquerque, New Mexico. 244 pp.

Eco. (2005) *Ecosystem Definition.* http://www.cfl.scf.rncan.gc.ca/ecosys/def_eco_e.htm

Estrella, R., Tyler, S., Chapman, J., and Miller, M.. (1993) *Area 5 Site Characterization Project Report of Hydraulic Property Analysis through August 1993.* Water Resource Center 45121, Desert Research Institute, Reno, NV. 51 pp.

Evaporation Map. (2004) *Average Annual Potential Evaporation Map from RGIS.* http://rgisedac.unm.edu/metadata/climate/cli0002.txt

Feth, J. (1981) *Chloride in Natural Continental Water - A Review. USGS Water Supply Paper 2176.* Washington, DC. 29 pp.

Fetter, C. (1994) *Applied Hydrogeology.* Prentice-Hall, Inc., Upper Saddle River, NJ. 691 pp.

Gee, G. and Hillel, D. (1988) "Groundwater Recharge in Arid Regions: Review and Critique of Estimation Methods." *Hydrological Processes.* 2. p. 255 - 266.

Gee, G., Campbell, M., Campbell, G., and Campbell, J. (1992) "Rapid Measurement of Low Soil Water Potential Using a Water Activity Meter." *Soil Science Society of America Journal.* 56. p. 1068 - 1070.

Gee, G., Wierenga, P., Andraski, B., Young, M., Fayer, M., and Rockhold, M. (1994) "Variations in Water Balance and Recharge Potential at Three Western Desert Sites." *Soil Science Society of America Journal.* 58. p. 63-72.

Gerakis, A. and Baer, B. (1999) "A Computer Program for Soil Textural Classification" *Soil Science Society of America Journal.* 63. p. 807 – 808. Program available at http://nowlin.css.msu.edu/software/triangle_form.html

Germann, P. (1990) "Macropores and Hydrologic Hillslope Processes – Chapter 10". *Process Studies in Hillslope Hydrology.* M. Anderson and T. Burt, editors. p. 327 - 363.

Gerritse, R. and George, R. (1988) "The Role of Soil Organic Matter in the Geochemical Cycling of Chloride and Bromide." *Journal of Hydrology.* 101. p. 83 - 95.

Gile, L. (1961) "A Classification of Ca Horizons in Soils of a Desert Region, Donna Ana County, New Mexico." *Soil Science Society Proceedings.* 25. p. 52 - 61.

Gile, L., Hawley, J., and Grossman, R. (1981) *Soils and Geomorphology in the Basin and Range area of Southern New Mexico - Guidebook to the Desert Project.* New Mexico Bureau of Mines and Mineral Resources Memoir 39. 222 pp.

Hendrickx, J., Khan, A., Bannink, M, Birch, D. and Kidd, C. (1991) "Numerical Analysis of Groundwater Recharge Through Stony Soils Using Limited Data." *Journal of Hydrology.* 127. p. 173 – 192.

Hendrickx, J. and Walker, G. (1997) "Chapter 2 - Recharge From Precipitation." *Recharge of Phreatic Aquifers in (Semi-) Arid Areas.* I. Simmers (ed). AA Balkema Publishers, Brookfield, VT. p. 19 - 111.

Hernandez, J., Dick-Peddie, W., and Boswell, T. (1971) *A Socio-economic Evaluation of the Sevilleta Land Grant.* The New Mexico Environmental Institute, Las Cruces, New Mexico. 86 pp.

Hillel, D. (1998) *Environmental Soil Physics.* Academic Press, San Diego, CA. 771 pp.

Jackson, R., Berthong, S., Cook, C., Jobbagy, E, and McCulley, R. (2004). "Comment of "A Reservoir of Nitrate Beneath Desert Soils." *Science.* 304. p. 51.

Janitzky, P. (1986) "Particle-Size Analysis." *Field and Laboratory Procedures Used in a Soil Chronosquence Study*, M. Singer and P. Janitzky, eds., United States Government Printing Office, Dept. Interior, USGS, Washington, DC. p. 11 - 16.

Johnson, R. (1997) *Introduction to Macrobiotic Crusts.* Soil Quality and Grazing Land Technology Institutes. Natural Resource Conservation Service. United States Department of Agriculture. Washington, DC.

Johnston, C. (1987) "Distribution of Environmental Chloride in Relation to Subsurface Hydrology." *Journal of Hydrology.* 94. p. 67 - 88.

Kung, K. (1990) "Influence of Plant Uptake on Performance of Bromide Tracer." *Soil Science Society of America Journal.* 54. p. 975 – 979.

Land. (2004) *Land Ownership Map.* Map obtained from RGIS. http://www.nm.blm.gov/nmso/nm952/geo_sci/metadata/nm_own.htm

Loope, W., and Gifford, G. (1972) "Influence of a Soil Microfloral Crust on Select Properties of Soils under Pinyon-Juniper in Southeastern Utah." *Journal of Soil and Water Conservation.* 27. p. 164 - 167.

LTER. (2004) *Long Term Ecological Research Station, Sevilleta National Wildlife Refuge, Meteorology*. http://sevilleta.unm.edu/research/local/climate/meteorology/summaries/monthly/a llyears/

Machette, M. (1985) "Calcic Soils of Southwestern United States." *Soils and Quaternary Geology of Southwestern United States: Geological Society of America Special Paper.* 203. p. 1 – 21.

Machette, M. (1986) "Calcium and Magnesium Carbonates." *Field and Laboratory Procedures Used in a Soil Chronosquence Study,* Singer, M. and Janitzky, P. (eds.), United States Government Printing Office, Dept. Interior, USGS, Washington, DC. p. 30 - 33.

Markgraf, V., Bradbury, J., Forester, R., and Sternberg, R. (1984) "San Agustin Plains, New Mexico: Age and Paleoenvironmental Potential Reassessed." *Quaternary Research.* 22. p. 336 - 343.

McGurk, B., and Stone, W. (1985) *Evaluation of Laboratory Procedures for Determining Soil-water Chloride. Open File Report 215.* New Mexico Bureau of Mines and Mineral Resources, Socorro, NM. 34 pp.

McNeil, J. (1980) *Electrical Conductivity of Soil and Rocks. Geonics Limited Technical Note TN-5.* Mississauga, Ontario, Canada. p. 5 - 22.

Moore, J. (1997) *Monitoring Infiltration of Atmospheric Chloride Across the Land Surface in Central New Mexico.* MS Independent Study, New Mexico Institute of Mining and Technology, Socorro, NM. 166 pp.

Myers, R., Everheart, J., and Wilson, C. (1994) "Geohydrology of the San Agustin Basin, Alamosa Creek Basin Upstream From Monticello Box, and Upper Gila Basin in Parts of Catron, Socorro and Sierra Counties, New Mexico." *Water Resources Investigation Report 94-4125*, US Geological Survey, Albuquerque, New Mexico. 70 pp.

NCDC. (2004) *National Climatic Data Center Station's Historical Listing for the National Weather Service's Cooperative Network.* The station's number in the network was 295353. http://www.wrcc.dri.edu/cgi-bin/cliMAIN.pl?nmmagd

Newman, B., Campbell, A., and Wilcox, B. (1997) "Tracer-based Studies of Soil Water Movement in Semi-arid Forests of New Mexico." *Journal of Hydrology.* 196. p. 251 - 270.

Nuttle, W. (2002) "Is Ecohydrology One Idea or Many?" *Hydrological Sciences Journal.* 47(5). p. 805 - 807.

Owens, L., Van Keuren, R., and Edwards, W. (1985) "Groundwater Quality Changes Resulting from a Surface Bromide Application." *Journal of Environmental Quality.* 14 (4). p. 543 – 548.

Peck, A., Johnston, C., and Williamson, D. (1981) "Analysis of Solute Distribution in Deeply Weathered Soils." *Agricultural Water Management.* 4. p. 83 - 102.

Phillips, F., Campbell, A., Kruger, C., Johnston, P., Roberts, R., and Keyes, E. (1992) "A Reconstruction of the Response of the Water Balance in Western United States Lake Basins to Climatic Conditions." *WRRI Report Number 269*, Volume 1, New Mexico Water Resources Research Institute, Las Cruces, New Mexico. 167 pp.

Phillips, F. (1994) "Environmental Tracers for Water Movement in Desert Soils of the American Southwest." *Soil Science Society of America Journal.* 58. p. 15 - 24.

Plummer, M. (2002) *Paleoclimatic Conditions During the Last Deglaciation Inferred from Combined Analysis of Pluvial and Glacial Records.* Ph.D. Dissertation, New Mexico Institute of Mining and Technology, Socorro, New Mexico. 345 pp.

Pokeman, W. and Sperry, J. (2000) "Vulnerability to Xylem Cavitation and the Distribution of Sonoran Desert Vegetation." *American Journal of Botany.* 87 (9). p. 1287 - 1299.

Ponce, V., Pandey, R., and Ercan, S. (2000) "Characterization of Drought Across Climate Spectrum." *Journal of Hydrologic Engineering.* 5 (2). p. 222 - 224.

Precipitation Map. (2004) *Average Annual Precipitation Map from RGIS.* http://rgisedac.unm.edu/metadata/climate/nmanprecip.htm

PRISM. (2004) *PRISM Spatial Climate Layers Introduction.* http://www.climatesource.com/docs/csguid.pdf

Purdue. (2005) *Purdue University Center for New Crops and Plant Procedures. New Mexico CropMAP, Socorro County.* http://www.hort.purdue.edu/newcrop/cropmap/newmexico/counties/socorro.html

RAWS. (2004) *Remote Automated Weather Station Listing for the National Weather Service's Cooperative Network.* http://weather.nmsu.edu/cgi-shl/cns/stninfo.pl?stn=77

Reheis, M. and Kihl, R. (1995) "Dust Deposition in Southern Nevada and California, 1984 – 1989: Relations to Climate, Source Area, and Source Lithology." *Journal of Geophysical Research.* 100 (D5). p. 8893 - 8918.

RGIS. (2004) *Resource Geographic Information System (RGIS) Clearinghouse,* a cooperative program between the University of New Mexico (UNM) and the State of New Mexico Information Technology Commission (ITC). http://rgis.unm.edu/intro.cfm

Roads. (2004) *Roads of Socorro County from RGIS.* http://rgisedac.unm.edu/metadata/tigerrds94/TLF253.TXT

Rodriguez-Iturbe, I. (2000) "Ecohydrology: A Hydrologic Perspective of Climate-Soil-Vegetation Dynamics." *Water Resources Research.* 36 (1). p. 3 - 9.

Salado Station. (2005) *Annual Precipitation Values for all Sites. Río Salado Weather Station #44.*
http://sevilleta.unm.edu/research/local/climate/meteorology/summaries/annual/

Scanlon, B. (1991) "Evaluation of Moisture Flux From Chloride Data in Desert Soils." *Journal of Hydrology.* 128. p. 137 - 156.

Scanlon, B., Tyler, S., and Wierenga, P. (1997) "Hydrologic Issues in Arid, Unsaturated Systems and Implications for Contaminant Transport." *Reviews of Geophysics.* 35 (4). p. 461 - 490.

Scanlon, B., Langford, R., and Goldsmith, R. (1999). "Relationships Between Geomorphic Settings and Unsaturated Flow in an Arid Setting." *Water Resources Research.* 35 (4). p. 983 - 999.

Scanlon, B., Kesse, K., Reedy, R., Simunek, J., and Andraski, B. (2003) "Variations in Flow and Transport in Thick Desert Vadose Zones in Response to Paleoclimate Forcing (0-90 kyr): Field Measurements, Modeling and Uncertainty." *Water Resources Research.* 39 (7). doi:10.1029/2002WR001604

Schenk, H. J., and Jackson, R. (2002) "Rooting Depths, Lateral Root Spreads, and Below-ground/above-ground Allometries of Plants in Water Limited Ecosystems." *Journal of Ecology.* 90. p. 480 - 494.

Schnabel, R., Stout, W. and Shaffer, J. (1995) "Uptake of Hydrologic Tracer (Bromide) by Ryegrass from Well and Poorly-Drained Soils." *Journal of Environmental Quality.* 24. p. 888 - 892.

Scurlock, D. (1998) "From the Río to the Sierra: An Environmental History of the Middle Río Grande Basin." *General Technical Report RMRS-GTR-5*, U.S. Department of Agriculture, Forest Service, Rocky Mountain Research Station., Fort Collins, CO. 440 pp.

Seyfried, M., Schwinning, S., Walvoord, M., Pockman, W., Newman, B., Jackson, R., and Phillips, F. (2005) "Ecohydrological Controls of Deep Drainage in Arid and Semiarid Regions." *Ecology.* 86 (2). p. 277 – 287.

Singer, M. (1986) "Bulk Density - Paraffin Clod Method." *Field and Laboratory Procedures Used in a Soil Chronosquence Study.* Singer, M. and Janitzky, P., eds., United States Government Printing Office, Dept. Interior, USGS, Washington, DC. p. 18 - 19.

Smith, S., Monson, R. & Anderson, J. (1997) *Physiological Ecology of North American Desert Plants.* Springer, Berlin.

SNWR. (2005) *Sevilleta National Wildlife Refuge Website: History of the Refuge.* http://southwest.fws.gov/refuges/newmex/sevilleta/history.html

Soil Map. (2005) *General Soil Map of New Mexico.* http://rgisedac.unm.edu/soils/soi1shp.zip

Soil Survey Staff. (1993) "Soil Survey Manual." *USDA - Soil Conservation Service, Agricultural Handbook No. 18,* U.S. Government Printing Office, Washington, DC. 437 pp.

Soil Survey Staff. (1999) "Soil Taxonomy, 2nd Ed. A Basic System of Soil Classification for Making and Interpreting Soil Surveys." *USDA - Soil Conservation Service, Agricultural Handbook #436*, U.S. Government Printing Office, Washington, DC. 869 pp.

State. (2005) *Family Education Website.* http://www.familyeducation.com/printables/package/0,2358,1-31486,00.html

Stephens, D. (1994) "A Perspective on Diffuse Natural Recharge Mechanisms in Areas of Low Precipitation." *Soil Science Society of America Journal.* 58. p. 40 - 80.

Stephens, D. (1996) *Vadose Zone Hydrology.* Lewis Publishers. New York, NY. 339 pp.

Sterling, J. (2000) *Spatial Distribution of Chloride and ^{36}Cl in the Conterminous United States.* MS Independent Study. New Mexico Institute of Mining and Technology, Socorro, NM. 155 pp.

Steudle, E. (2000) "Water Uptake by Plant Roots: an Integration of Views." *Plant and Soil*. 226. p. 45 - 56.

Thornthwaite, C. (1948) "An Approach Toward a Rational Classification of Climate." *Geographical Review*. 38. p. 55 - 94.

Tyler, S., and Walker, G. (1994) "Root Zone Effects on Tracer Migration in Arid Zones." *Soil Science Society of America Journal*. 58. p. 25 - 31.

USGS. (2005) *Water Budget Definition.* http://answers.usgs.gov/cgi-bin/gsbrowse?tcode=108

Van Devender, T. (1990) "Late Quaternary Vegetation and Climate of the Chihuahuan Desert, United States and Mexico." in *Packrat Middens, The Last 40,000 years of Biotic Change*. Betancourt, J., Van Devender, T., and Martin, P., (eds.). The

University of Arizona Press, Tucson, Arizona. p. 104 - 133.

Vegetation Map. (2004) *General Vegetation Map from RGIS.*
http://rgisedac.unm.edu/metadata/vegetation/veg0001.txt

Walvoord, M., Plummer, M., Phillips, F., and Wolfsberg, A. (2002a) "Deep Arid
System Hydrodynamics: 1. Equilibrium States and Response Times in Thick
Desert Vadose Zones." *Water Resources Research.* 38 (12).
doi:10.1029/2001WR000824.

Walvoord, M., Phillips, F., Tyler, S., and Hartsough, P. (2002b) "Deep Arid System
Hydrodynamics: 2. Application to Paleohydrologic Reconstruction Using Vadose
Zone Profiles From the Northern Mojave Desert." *Water Resources Research.*
38(12). doi:10.1029/2001WR000825.

Walvoord, M. (2002c) *A Unifying Conceptual Model to Describe Water, Vapor, and
Solute Transport in Deep Arid Vadose Zones.* Ph.D. Thesis. Earth and
Environmental Science. New Mexico Institute of Mining and Technology.
Socorro, NM. 297 pp.

Walvoord, M., Phillips, F., Stonestrom, D., Evans, D., Hartsough, P., Newman, B., and
Striegl, R. (2003) "A Reservoir of Nitrate Beneath Desert Soils." *Science.* 302.
p. 1021 - 1024.

Walvoord, M. and Phillips, F. (2004) "Identifying Areas of Basin-Floor Recharge in the
Trans-Pecos Region and the Link to Vegetation." *Journal of Hydrology.* 292. p.
59 - 74.

Weather Station. (2005) *Sevilleta National Wildlife Refuge Weather Station Map.*
http://sevilleta.unm.edu/places/refuge/metstations/

Whitmer, S., Baker, L, and Wass, R. (2000) "Loss of Bromide in a Wetland Tracer
Experiment." *Journal of Environmental Quality.* 29. p. 2043 - 2045.

Whitson, T. (2001) *Weeds of the West.* Grand Teton Lithography, Jackson, Wyoming.
628 pp.

Williams, J. (1986) *New Mexico In Maps*. University of New Mexico Press,
Albuquerque, New Mexico. 409 pp. Map made by Ivan Bennett.

Williams, J., Dobrowolski, J., and West, N. (1995) "Microphytic Crust Influence on
Interrill Erosion and Infiltration Capacity." *Transactions of the American Society
of Agricultural Engineers.* 38. p. 139 - 146.

WP4. (1998) *Dewpoint Potential Meter for Models WP3 and WP4-T Operator's Manual*.
Version 2.2. Decagon Devices, Inc. 83 pp.

APPENDIX A

CHLORIDE DEPOSITION

A.1. Use and Determination of Chloride Deposition Rate

The processes of chloride deposition and transport is discussed in depth in Section 1.2.3. In order to accurately determine the rate of groundwater recharge using the chloride mass balance method, the amount of chloride deposited on the soil surface of the study area must be known.

Efforts to determine chloride deposition rates have been ongoing at the New Mexico Institute of Mining and Technology for over a decade. In November 1996, hydrology graduate student, Jim Moore, emplaced a field of 38 column collectors into the subsurface at the Sevilleta National Wildlife Refuge to determine if the various artificial chloride collectors properly mimicked the natural processes of wet and dry chloride deposition infiltration into the subsurface and subsurface evapotranspiration. Additionally, a Reheis-type collector (Reheis and Kihl 1995) was installed at the column field for comparison dust measurements. Jim Moore sampled the Reheis-type collector and unearthed a column for analysis once a month for six months. The columns and Reheis-type collector were not sampled again for five years, at which time they were sampled once a year for three years.

A network of weather stations is maintained in the Sevilleta National Wildlife refuge by the University of New Mexico's Long Term Ecological Research Center

(LTER). Chloride deposition measurements are taken at most of these stations, since

mid-1989, by Doug Moore. Chloride deposition measurements from the Río Salado and

Deep Well Weather Stations maintained by the LTER have been used in this study.

These stations maintain both bulk deposition collectors and wet and dry collectors. These

data have been used in this study with the permission of Doug Moore.

A.2. Chloride Deposition Collectors

Four types of chloride deposition collectors located in the Sevilleta National

Wildlife Refuge near the drilling transect were used to determine the chloride deposition

rate of the area.

A.2.1. Bulk Deposition Collector

The most common method of chloride deposition is the bulk collector. The bulk

collector traps dry chloride deposition in a funnel with a surface area of 560 square

centimeters. This dry deposition is washed down into the collection jug below by

subsequent precipitation. Therefore, both wet and dry chloride depositions are collected

in the jug. During sample collection, a known amount of de-ionized water is used to

wash the chloride deposition from the funnel and connection tube, into the jug. The jug

is also washed with de-ionized water into a sampling jar. See Figure A.1 for a picture of

the bulk collector at the Río Salado Weather Station.

A benefit of this design is that once the dry and wet deposition are in the

collection jug, it is unlikely that the deposition will be lost to the atmosphere through the

wind. If a long period of time passes between the dry deposition of the chloride and a

precipitation event that washes it into the jug below, the possibility exists that this

deposition could be blown out of the funnel again. On the soil surface, this redistribution

of the dry deposition between precipitation events also occurs, but the similarity of the

redistribution of the dry deposition that occurs in the funnel and on the soil surface is

unknown. Besides possible redistribution of the dry chloride deposition, another

downside of this collection method is that determining what amount of the total

deposition came from wet or dry deposition individually is impossible. The bulk

collectors used in this study were at the Río Salado Weather Station and the Deep Well

Weather Station and are maintained by Doug Moore of LTER.
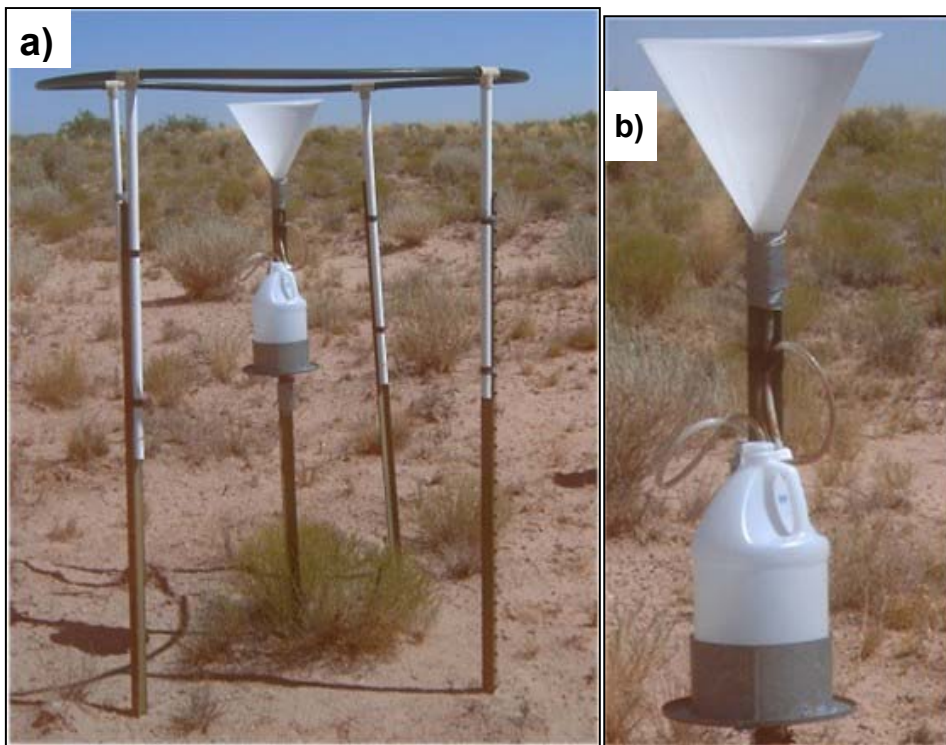
Figure A.1. a) Bulk collector with protective ring to discourage birds from landing on
the collector. b) Close-up of bulk collector. The funnel collects dry and wet depositions,
that are then washed down into the jug below by precipitation.

A.2.2. Wet/Dry Deposition Collector

Another method of determining chloride deposition is "wet and dry" collectors.

These collectors are designed to determine the individual contribution of the wet and dry

chloride deposition to the total chloride deposition. This is achieved through the use of

two bucket collectors with a surface area of 640 square centimeters, one for wet deposition and one for dry deposition. Normally, the wet deposition collector is covered and the dry deposition collector is left exposed to the atmosphere. When a sensor detects precipitation, the cover on the wet deposition collector moves to cover the dry collector and expose the wet collector. See Figure A.2. for a picture of the wet and dry deposition collector that was located at the Río Salado Weather Station. During the sampling, both collectors are rinsed with a known amount of de-ionized water into separate sampling containers.

The downside of this collection method is that since precipitation never enters the dry collector, the dry deposition is not washed into the bottom of the collector. This allows for easy mobilization of the dry deposition out of the collector by the wind, possibly causing the dry deposition to be blown out of the collector. Another problem is that precipitation must have already started to fall in order for the sensor to detect it and signal the cover to move from the wet to the dry collector. During this time, the initial precipitation falls into the dry collector, not the wet collector. This initial precipitation has a higher chloride concentration than later precipitation during the storm event, since the initial precipitation is the first to wash out the atmosphere. This phenomenon may cause the amounts of dry and wet deposition not to be completely accurate, with the dry deposition values possibly being artificially high as a result. However, the potential loss of the chloride deposition in the dry collector also may cause the underestimation of dry deposition. The degree to which these two processes balance each other out and the degree to which this method accurately determines the amount of chloride deposition that is from dry and wet fallout are unknown. The wet/dry collectors used in this study were

located at the Río Salado Weather Station and the Deep Well Weather Station and are

maintained by Doug Moore of LTER.

Figure A.2. Wet and dry chloride deposition collectors at the Río Salado Weather
Station, number 44. Located above the left bucket, the wet deposition collector, is a
cover that is switched to the other bucket, the dry deposition collector, during
precipitation events. Picture from LTER website (Collectors 2005).

A.2.3. Reheis-type Deposition Collector

A dust collector based on that described in Reheis and Kihl (1995) was set up in

November 1996 by Jim Moore near the column experiment described in the next section.

This collector is referred to as a Reheis-type collector and is shown in Figure A.3. The

collector consists of an angel-food cake pan, with a surface area of 480 square

centimeters, mounted on a fence post two meters off the ground. The two meter height

prevents any particles moving along the surface by wind from getting into the collector.

A circular piece of 1.4 inch mesh cloth is fitted into the pan so that it rests 3 to 4

centimeters below the rim and glass marbles fill the upper part of the pan resting on the cloth. After rinsing the marbles with de-ionized water, this screen is used to life them out of the pan so that the rest of the pan can be rinsed. The pan is coated with Teflon, which should not be reactive or cause any chloride contamination. The empty space between the screen and the bottom of the pan provides a reservoir that prevents water from overflowing from the pan during large storm events. The marbles prevent most of the dust that has been deposited in the pan from being blown away. The pan is also fitted with two metal straps looped in an inverted basket shape, and the surface of the straps are coated with Tanglefoot to deter birds from perching on the collector and contaminating the sample (Reheis and Kihl 1995). While this setup prevents most of the chloride deposition from being redistributed by the wind, this may overestimate actual dust deposition on the soil surface, since some natural redistribution does occur on the soil surface.
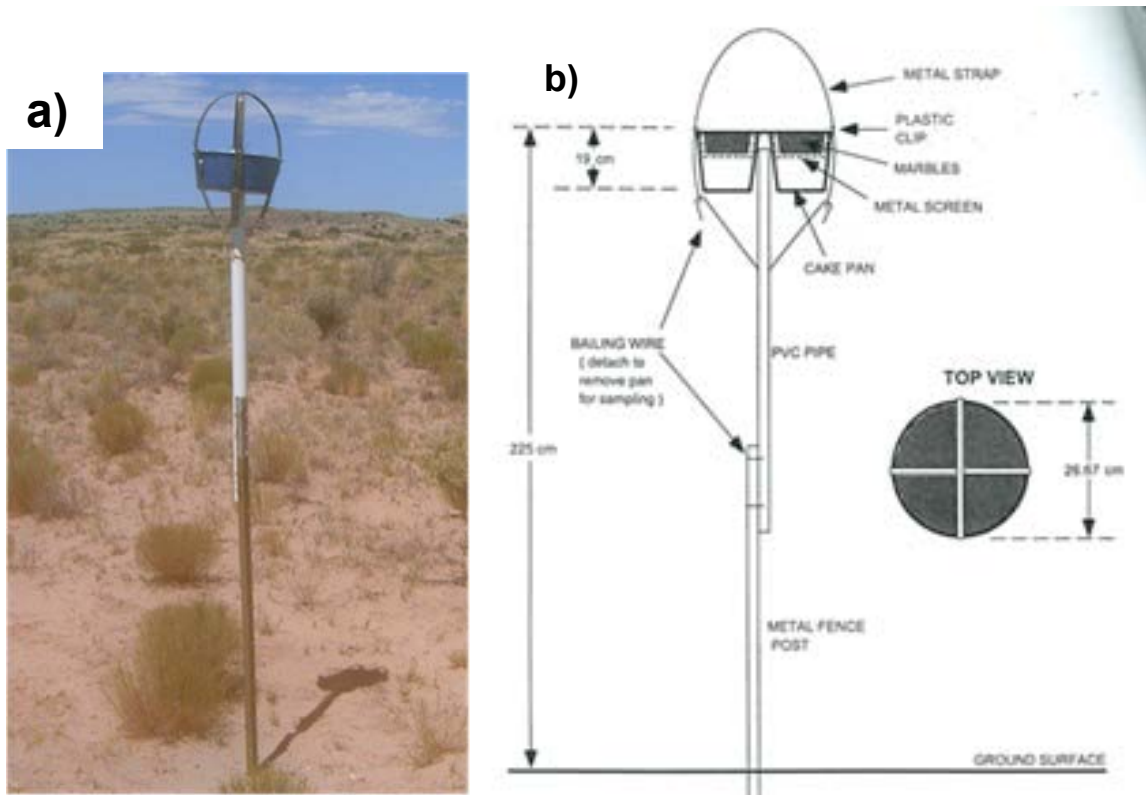
Figure A.3. a) Reheis-type chloride deposition collector at the column site. b) Diagram of the Reheis type collector at the site. Diagram from Moore (1997).

A.2.4. Column Deposition Collectors

Although numerous devices have been used to sample the atmospheric deposition of chloride (such as buckets in the dry/wet collector, a funnel in the bulk collector, and a pan in the Reheis-type collector) there still remains considerable uncertainty as to whether or not these collection devices mimic the deposition of atmospheric chloride onto the natural soil surface. These collectors are referred to as a group in this document as artificial collectors. The redistribution of the dry chloride deposition on the soil surface is likely to be the greatest difference between the artificial collectors and the column collectors, as the soil surface roughness and wind flux across the surface will affect this redistribution in a much different manner than the artificial collectors would. The artificial collector method also assumes that all of the wet deposition infiltrates the

soil subsurface, taking all of the dry deposition that is present along with it. If the chloride deposition rate determined for the column collectors was higher than those of the other artificial collectors, this would indicate that the chloride deposition in the artificial collectors is being blown out by the wind, thus trapping dry deposition less effectively than the soil surface could. If the chloride deposition rate determined for the chloride column collectors was lower than that of the artificial collectors, this would indicate either that not all of the chloride that has been deposited on the soil surface infiltrates the soil subsurface or that the artificial collector traps chloride deposition more efficiently than the soil surface.

It is unfeasible to have a large-scale monitoring network of chloride deposition collectors below the soil surface to properly mimic the deposition, evaporation, and infiltration processes as they occur naturally. It is unfeasible because of the time period of column emplacement necessary, the disturbance of the soil surface in the monitoring area, monitoring the area so it is protected and undisturbed after column emplacement, and the planning and long term-commitment of the monitoring. Therefore, the most feasible option would be to determine how effectively the artificial collectors function, by comparing them to buried column collectors in close proximity to these artificial collectors. To achieve this, 38 columns were emplaced into the ground by Jim Moore, flush with the soil surface, on November 2, 1996. These columns were made of plastic piping, with a surface area of 81 square centimeters and packed with pre-leached sand. The columns were sealed at the bottom but left open at the top to allow for water to naturally infiltrate the columns and evaporate out of them. The design specifications of these columns are shown in Figure A.4. The sand inside the columns was pre-leached of

chloride ions by washing the sand with de-ionized water and then drying the sand before

emplacement. Thus, all of the chloride found in the column after emplacement should be

the result of deposition since emplacement. This experiment was designed by and the

columns were emplaced by James Moore, as described in Moore (1997). After

placement, the columns were sampled once a month for six months. After this, they were

not sampled for five years; they were then sampled every year afterward for three years.
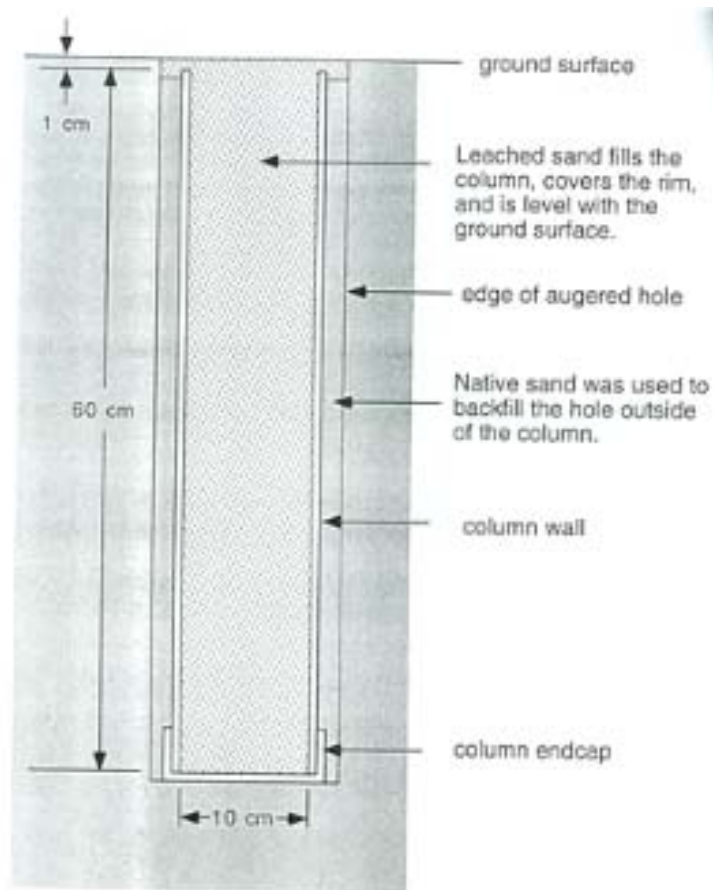
Figure A.4. Diagram of chloride deposition column and dimensional specifications.
Diagram from Moore (1997).

A.3. Additional Possible Source of Chloride

The Río Salado is a major tributary of the Río Grande. It flows from northwest to

the southeast. The Río Salado is located around 3.2 kilometers north of the column sites; the name of the river is Spanish for "Salt River". This river has emphemeral flow, being dry most of the year, and was suspected of being a possible source of salt to the nearby column site. To test this possibility, a soil sample of the Río Salado was taken when there was no water present. Figure A.5. shows what the sampled area of the Río Salado was like on the day of sampling, October 28, 2004. The latitude and longitude of the sample location in the Río Salado was 34.30293 and 106.9137 decimal degrees, respectively.

Figure A.5. Picture of the bed of the emphemeral Río Salado at the sampling location, facing west. The vegetation shown in the picture is mostly salt cedar, an invasive shrub.

The soil sample was analyzed using the method outlined in Section 3.3.1. This sample had a bromide concentration below the detection limit of 0.01 mg L^{-1}. The

sample had a chloride concentration of 42.8 mg Cl⁻ L⁻¹ pore water or 4.05 mg Cl⁻ kg⁻¹ dry

soil. Drill Sites 2 and 3 are near the column site and the Río Salado. The chloride

concentration of the surface soil of these two sites was compared to the Río Salado soil

sample to determine if the Río Salado is a source of salt for these nearby sites. The Río

Salado soil sample was also compared to the surface soil of the other sites to determine if

the sample had an unusually high chloride concentration. Table A.1 lists the chloride

concentration of the first three soil samples in the profile of all of the drill sites, down to a

depth of approximately 70 centimeters.

Site #	First (mg Cl⁻ kg⁻¹ dry soil)	Second (mg Cl⁻ kg⁻¹ dry soil)	Third (mg Cl⁻ kg⁻¹ dry soil)
1	1.02	1.00	1.75
2	0.92	0.88	0.86
3	0.98	0.89	1.04
4	1.14	1.86	3.89
5	1.00	0.97	1.02
6	27.6	12.5	14.2
7	1.00	2.13	2.05
8	0.92	1.02	0.96
9	1.00	14.9	98.0
10	1.13	1.01	1.13
11	1.21	1.61	16.0
Average	3.45	3.52	12.8

Table A.1. Chloride concentrations of the first three soil samples of all the drill sites.
These samples cover about the first 70 centimeters of depth of the soil core.

The Río Salado sample's chloride concentration of 4.05 mg Cl⁻ kg⁻¹ dry soil is

higher in concentration than both Site 2 and 3. Additionally, Sites 2 and 3 have chloride

concentrations that are also very similar to the other sites' surface soil concentrations.

This demonstrates that the Río Salado does not contribute a significant amount of

chloride to these nearby sites. The Río Salado soil sample's chloride concentration is

also within the range of the surface samples of all the drill sites, demonstrating that it

does not have an unusually high level of surface chloride concentration. Even though the

surface soil of the Río Salado is saturated for part of the year and therefore has a different environment for water chemistry, the chloride concentration of the surface soil while the river was dry demonstrates that the Río Salado is not a significant source of chloride to the surrounding area, including the column collector site and Sites 2 and 3.

A.5. Locations of Weather Stations and Columns

The chloride column collector site and the weather stations used to determine the chloride deposition are located in the Sevilleta National Wildlife Refuge. Drill Sites 1, 2, 3, and 6 are also located in the Sevilleta and near these weather stations. The Río Salado Weather Station number 44 is 450 meters west of the chloride column collector site. Therefore, this weather station was used to determine the chloride deposition values at the column site. Site 3 is also 0.76 kilometers away from the Río Salado Weather Station. The chloride deposition values from this weather station are considered the be represent the chloride deposition at Site 3. See Figure A.6 for a map of the Sevilleta Weather Stations. The Río Salado Weather Station number 44 is located at 34.296 N and 106.927 W, the Deep Well Weather Station is located at 34.35197 N and 106.6889 W, and the Reheis-type and column collectors are both located at 34.29648 N and 106.9222 W decimal degrees.
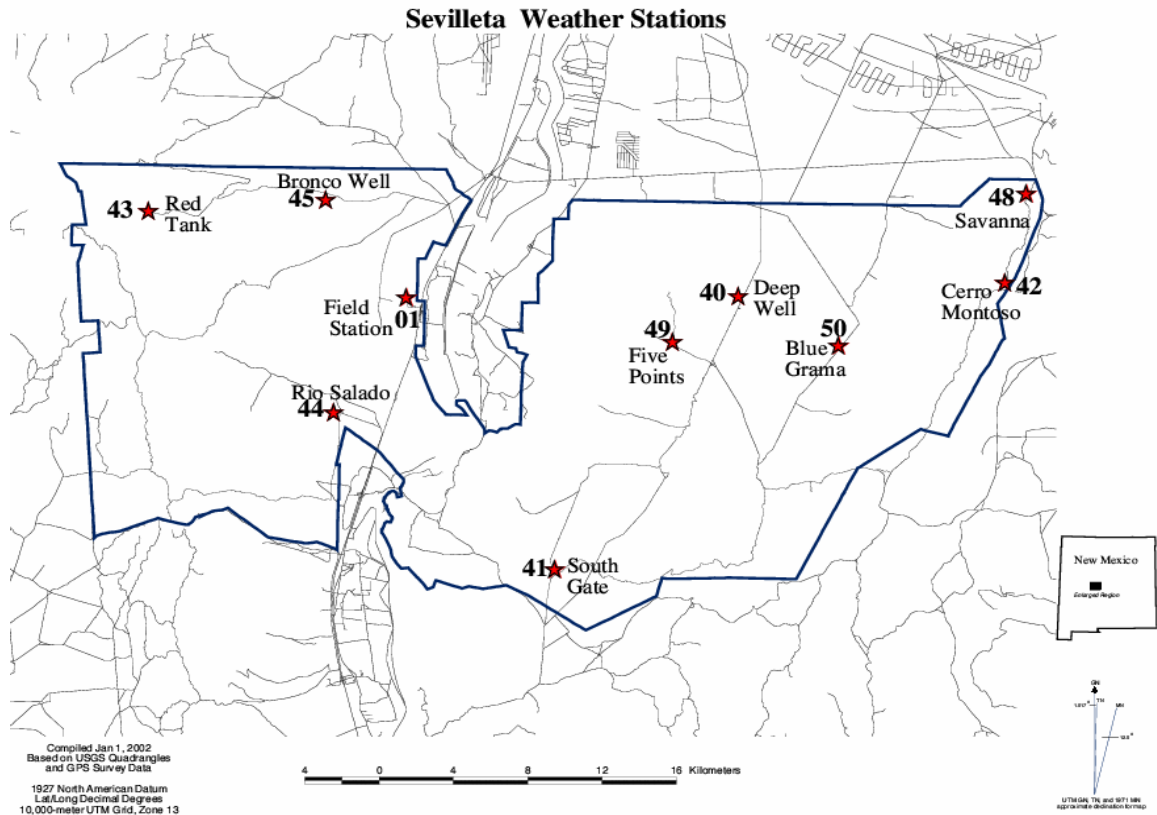
Figure A.6. Locations of the weather stations within the Sevilleta National Wildlife Refuge. Chloride deposition data from both the Deep Well site number 40 and Río Salado site number 44 were used. Weather data from the Río Salado site number 44 and Bronco Well Station number 45 were used in Chapter 2, Study Area. Sevilleta Refuge is located approximately halfway between the City of Albuquerque and Socorro, New Mexico. Map obtained from the LTER website (Weather Stations 2005).

A.6. Source of Data from Collectors

The data for the bulk and wet/dry collectors from both the Río Salado and the Deep Well sites were obtained from the LTER website (Weather Station 2005). For the past 15 years, these data have been collected by this organization. New Mexico Tech collected and analysized the data from the Reheis-type collector and the column collector. See Figure A.7 for the monthly chloride deposition data and Figure A.8 for the cumulative chloride deposition data from all of the collectors.
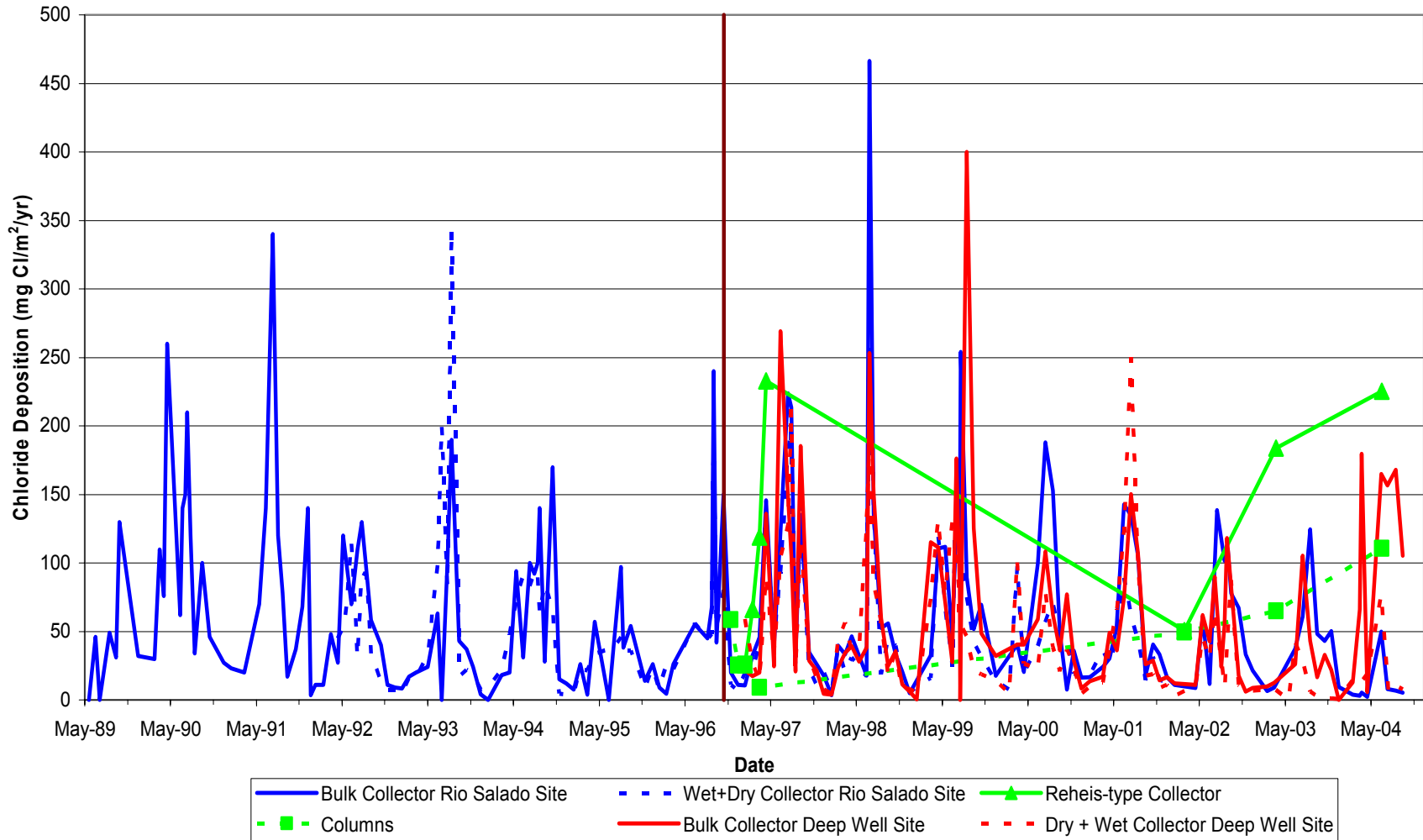
Figure A.7. Monthly chloride deposition graph. This graph is a comparison of the different types of chloride deposition collectors. The vertical line denotes the emplacement of the chloride columns and Reheis-type collector. Note the seasonal fluctuation of chloride deposition, corresponding to the summer monsoon rains.

253
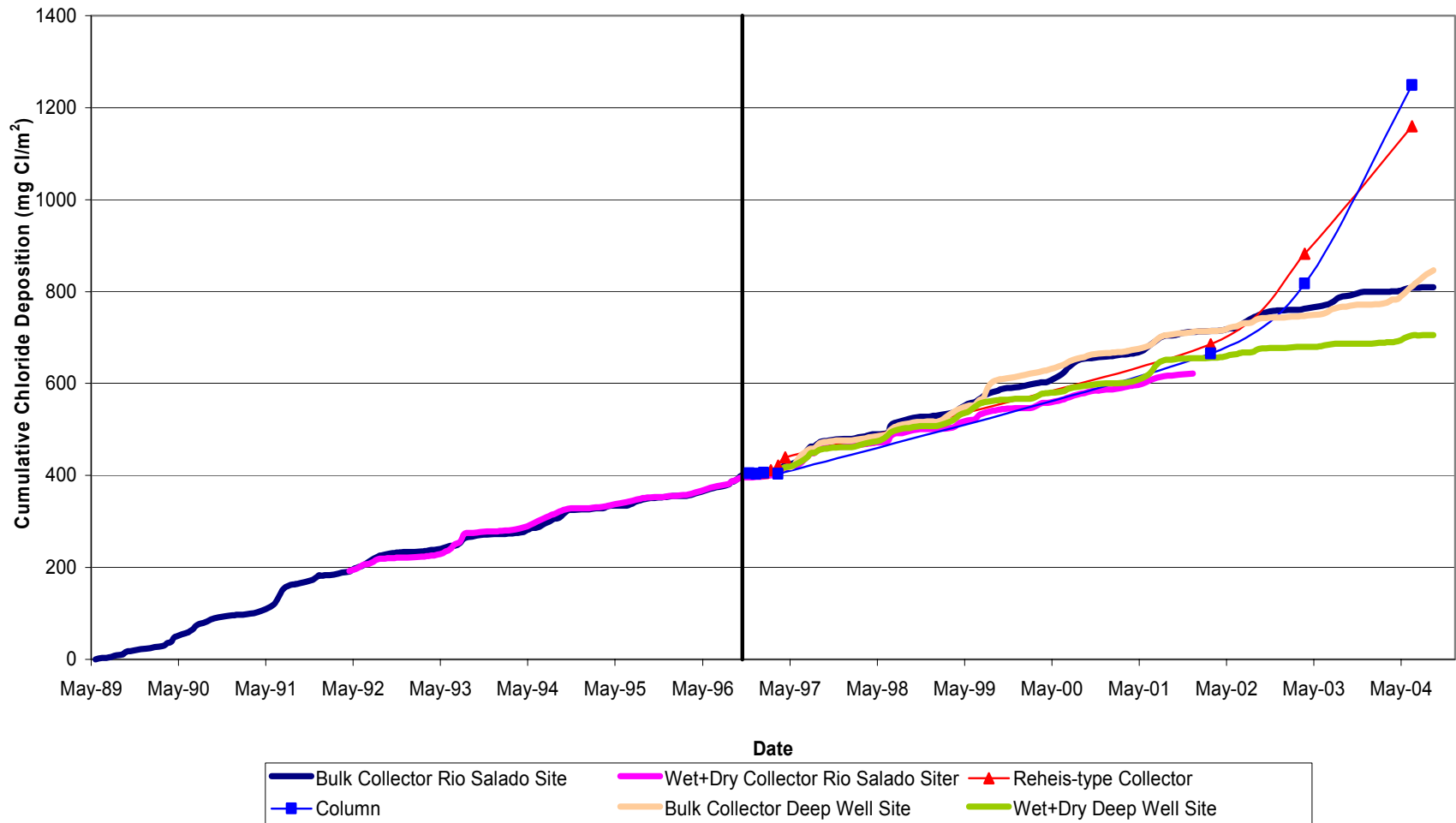
Figure A.8. Cumulative chloride deposition graph. This graph is a comparison of the different types of chloride deposition collectors. Data are plotted starting at the cumulative chloride deposition value of the general trend of the data on that date, not at zero. This was done to compare the overall data trend with time. The vertical line denotes the emplacement of the chloride columns and Reheis-type collector.

A.7. Average Chloride Deposition

The bulk and wet/dry collectors are sampled every month. During this sampling, the collectors are rinsed; therefore, each chloride value represents one month of time. The Reheis-type and column collectors have been sampled irregularly, with sampling occurring once a month for the first six months. After this, they were not sampled for five years, and they were then sampled every year afterward for three years. While the Reheis-type collector was rinsed during sampling and therefore only represents the chloride deposition since the last date of sampling, the columns represent the entire time period of chloride deposition since emplacement on November 2, 1996. To account for these irregularities in sampling time, rather than using a standard average as for the bulk and wet/dry collectors, a time weighted average (TWA) was used instead. The time weighted average for the Reheis-type collector was calculated using equation 16.

$$TWA = \frac{\sum (time\ between\ sampling * chloride\ concentration)}{\sum (time\ between\ sampling)} \tag{16}$$

The time weighted average for the column collector was calculated using equation 17.

$$TWA = \frac{\sum (time\ since\ column\ emplacement * chloride\ concentration)}{\sum (time\ since\ column\ emplacement)} \tag{17}$$

The averages of all types of collectors in the Sevilleta are shown in Table A.2. The wet/dry collector at the Río Salado Weather Station was moved to a new location in December 2001.

	Average Deposition (mg m^{-2} yr^{-1})	Duration of Data Collection		
		Beginning	Ending	Duration (years)
Bulk Collector (Río Salado Site)	64	8-Jun-89	1-Oct-04	15.3
Bulk Collector (Deep Well Site)	64	31-Jan-97	1-Oct-04	7.7
Wet Collector (Deep Well Site)	*28*	31-Jan-97	1-Oct-04	7.7
Dry Collector (Deep Well Site)	*17*	31-Jan-97	1-Oct-04	7.7
Wet + Dry Collector (Deep Well Site)	45	31-Jan-97	1-Oct-04	7.7
Wet Collector (Río Salado Site)	*34*	4-May-92	31-Dec-01	9.7
Dry Collector (Río Salado Site)	*19*	4-May-92	31-Dec-01	9.7
Wet + Dry Collector (Río Salado Site)	53	4-May-92	31-Dec-01	9.7
Reheis-type Collector (TWA)	99	2-Nov-96	2-Jul-04	7.7
Columns (TWA)	76	2-Nov-96	2-Jul-04	7.7
Average	67			

Table A.2. Monthly average chloride deposition values for each collection method. TWA stands for time weighted averaged, which was used for the Reheis-type collector and the columns. This was due to the irregular sampling of these collectors and the long time periods between some of the sampling events.

A.8. Comparison of Wet/Dry, Bulk, and Reheis-type Collector Data

The cumulative chloride-deposition graph in Figure A.8 shows that the different types of collectors follow a similar overall trend. Both of the bulk collectors and both of the wet/dry collectors located at different sites followed very similar trends, demonstrating a reproducibility within the collection method. The wet/dry collectors cumulatively trended below the bulk collectors. This indicates that the wind possibly blew some of the dry deposition out of the collector. The redistribution of the dry deposition out of the collector appears to greatly outweigh any additional chloride that may have been added to the dry collector from the initial precipitation (before the cover was moved over the dry collector), as mentioned earlier in Section A.2.2.

The Reheis-type collector had chloride-depositional rates greater than all the other collectors both with the monthly trend and the cumulative trend. This was most likely the result of the marbles in this collector trapping the dry deposition very effectively. These

marbles probably trap more of the dry deposition than the actual surface soil, since the marbles are much larger than sand and the pan has a collection area below the marbles that would effectively lock in the chloride deposition. The five years between the 1997 and 2002 sampling events could also cause some uncertainty in the 2002 measurement, since the average the chloride measurement was over the five year period. However, the efficient trapping of the dry deposition by this collector tends to minimize this uncertainty.

A.9. Uncertainties in the Column Collector Data and Comparison to Other Collectors.

During the construction of the columns, there were some problems with leaching the column sand of chloride, which were documented by Moore (1997). Moore subtracted out the background chloride levels (that he determined for the columns) from the measured chloride levels for that column. This background level was determined from the chloride level of the dry sand at the bottom of the sampled columns, assuming that the infiltrating water had not yet reached this area. When we dug columns up five years later, this method of determining background chloride levels was no longer possible, as the infiltrating water had penetrated the entire column, ponding at the bottom. Therefore, we leached similar quartz sand three times, rotating the samples for 24 hours each time, to determine the background chloride level of 0.000205 mg g^{-1} dry sand.

Even accounting for background chloride levels in this fashion, the chloride levels that were measured in the columns dug up at least five years after emplacement were higher than those of bulk and wet/dry collectors when the chloride levels were compared cumulatively. This could indicate that the original sand packed into the columns was not

fully leached of chloride. To determine this, the control column that was emplaced at the same time as the other columns but was sealed at both ends was unearthed and tested for chloride. This control column had chloride levels equivalent to a depositional rate of 113 mg Cl$^-$ m^{-2} yr^{-1}, which was very similar to the depositional rate of 110 mg Cl$^-$ m^{-2} yr^{-1} found for the non-control column unearthed at the same time. This obviously indicates that the sand pre-treatment failed to completely leach the chloride from the sand used to pack the columns. Since such a large amount of sand was needed to pack 38 columns, the sand was originally leached in several batches. We now suspect that some of these batches were not fully leached, while others were, since some of the chloride deposition values were similar to the other collectors and some were much higher. It is impossible to know at this time which columns contain sand batches that were not fully leached, as records of which leached batches were packed into which columns were never recorded. This obviously leads to much uncertainty in the chloride deposition values obtained from the columns. Based on the interpretation of the cumulative chloride deposition trend in Figure A.8, it is likely that the last column tested in 2004, and possibly the column tested in 2003, were not fully leached of original chloride. Unfortunately, the uncertainty introduced by the variable initial leaching precludes the use of the columns as a definitive measure of chloride infiltration into the subsurface in this study area.

Even with these uncertainties, some general observations between the columns and the artificial collectors can still be made. The monthly chloride trends in Figure A.7 show the columns having a similar, if slightly higher levels of chloride. The cumulative chloride trend in Figure A.8 shows the columns tracking well with the other collectors, until the last two column collectors were sampled. These last two collectors caused the

cumulative chloride trend to be significantly above that of the bulk and wet/dry collectors. As already mentioned, this is likely the result of background chloride levels present in the column sand before the columns were emplaced. Even with this uncertainty, the column chloride levels still trend fairly close to the other collectors, and this probably indicates that the artificial collectors are reasonably representative of the chloride deposition that enters into the subsurface.

A.10. Chloride Deposition Value

For the Río Salado Site, the best estimate of 60 mg m^{-2} yr^{-1} for a yearly chloride deposition of was decided upon, based on the averages shown in Table A.2. Given the uncertainties in the collection methods and the short time span of the data, only one significant figure was determined to be the level of accuracy for this value. The wet and dry chloride-deposition values for the Río Salado weather station were then scaled to a total value of 60 mg m^{-2} yr^{-1} using their percentages of the original total, as shown in Table A.3.

Chloride Deposition Collector Type	Chloride Deposition (mg m^{-2} yr^{-1})	%	Deposition Values Scaled to 60
wet	34	64	38
dry	19	35	22
wet + dry	53		
bulk	64		

Table A.3. Scaling of wet and dry deposition collectors at the Río Salado Weather Station.

A.11. Relationship of Chloride Deposition to Precipitation

The relationship between the chloride deposition at the Río Salado Weather Station and the associated precipitation amount was determined for wet, dry, and bulk chloride deposition. This study was only concerned with long-term average chloride deposition, rather than the deposition associated with an individual precipitation event.

Therefore, the data within specified precipitation intervals were averaged in order to assess the long-term correlation of chloride deposition and precipitation. These intervals consisted of ten millimeters of precipitation up to 80 millimeters, and each class had to contain at least three data points to be included in the regression analysis. To determine the relationship, this average chloride deposition was plotted against the sum of the precipitation that had fallen during the time period represented by the depositional values. The standard deviations of each interval were also determined and plotted on the graph. A regression analysis of the data was performed on the average chloride deposition values. The results are shown below in Figures A.9, A.10, and A.11.
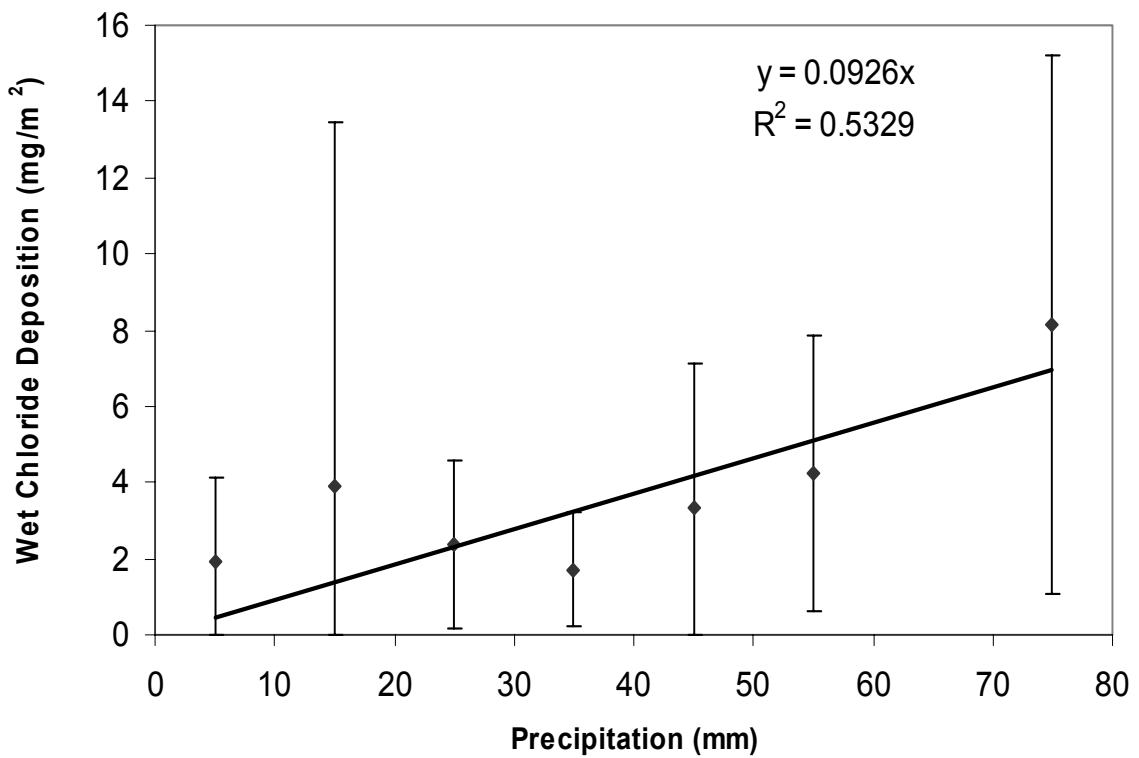
Figure A.9. Average wet chloride deposition versus precipitation for 10 millimeter precipitation intervals for the Río Salado Weather Station. All groups of data with less than 3 data points were not used in the regression analysis. Trendline equation and R^2 value shown on graph. Error bars represent ± one standard deviation to a limit of zero deposition.
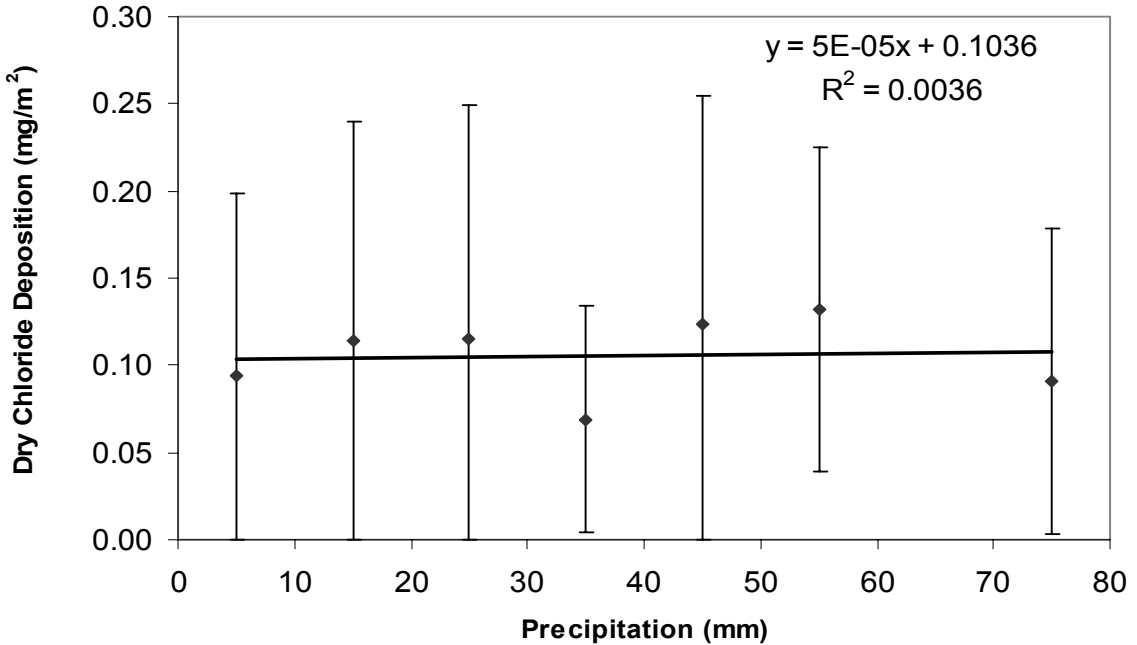
Figure A.10. Average dry chloride deposition versus precipitation for 10 millimeter precipitation intervals for the Río Salado Weather Station. All groups of data with less than 3 data points were not used in the regression analysis. Trendline equation and R^2 value shown on graph. Error bars represent ± one standard deviation to a limit of zero deposition.
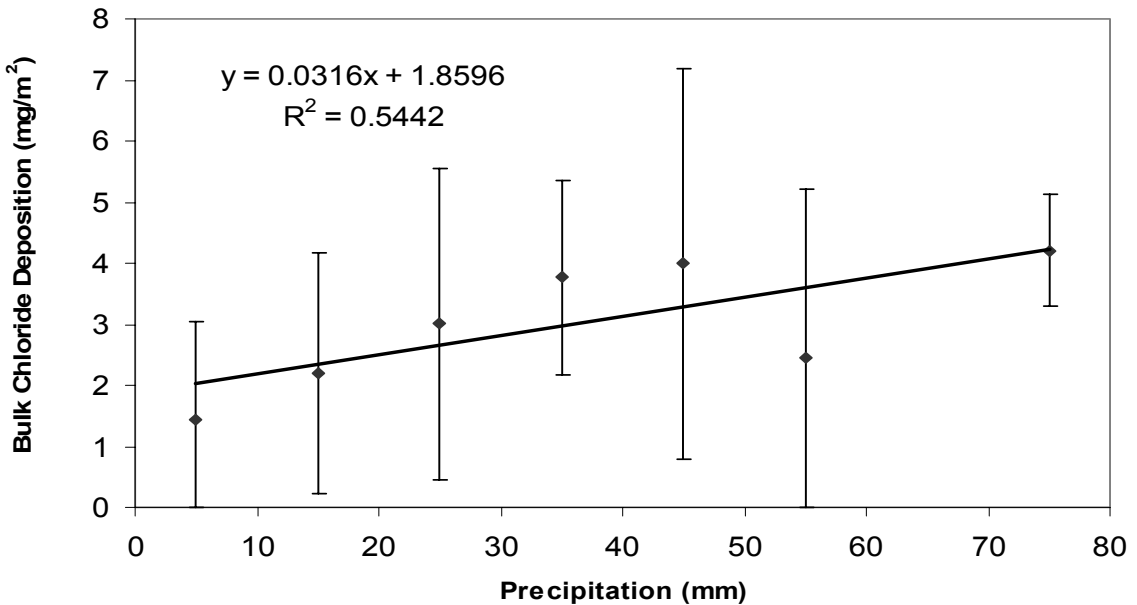
Figure A.11. Average bulk chloride deposition versus precipitation for 10 millimeter precipitation intervals for the Río Salado Weather Station. All groups of data with less than 3 data points were not used in the regression analysis. Trendline equation and R^2 value shown on graph.. Error bars represent ± one standard deviation to a limit of zero deposition.

261

The average wet chloride deposition from the Río Salado Weather Station is correlated with precipitation, while the average dry chloride deposition is not at all correlated with precipitation. Bulk deposition is all correlated with precipitation, which is expected since it is a measure of wet and dry depositions. All average chloride deposition values exhibit a large standard deviation, ranging from 70 to 240 percent. This demonstrates the large variability of chloride deposition values between storms of similar precipitation levels.

A.12. Chloride Deposition Determination for Each Site

The dry deposition amount varies according to distance from the ocean (Feth 1981), and it is affected very little by precipitation. This relationship was also seen at the Río Salado Weather Station, as was shown in the previous section. As a result, the dry chloride deposition rate is not thought to vary significantly over the length of the transect, since the transect length is only 58 kilometers. The dry chloride deposition amount from the Río Salado Weather Station will therefore be used for all the drill sites.

The wet chloride-deposition amount is determined by the amount of precipitation (Feth 1981, Sterling 2000). This relationship was also seen at the Río Salado Weather Station, as was shown in the previous section. Precipitation amount varies significantly over the transect length, as a result of the change in topography. The known amount of wet chloride deposition at the Río Salado Weather Station and the precipitation amount at that site was used to determine a slope value of milligrams of chloride deposition per centimeter of precipitation. This slope value was then used to extrapolate the wet deposition rate at the drill sites using those sites' average annual precipitation values. This extrapolation procedure follows the method outlined in Sterling (2000). The wet

deposition was determined by equation 18.

$$WD = \frac{P * S}{A}$$ (18)

where:

WD = wet chloride deposition (mg cm^{-2} yr^{-1})

P = precipitation (cm yr^{-1})

S = slope (mg cm^{-1})

A = Area (640 cm^2).

In order to determine the slope value that will be used to extrapolate the wet

deposition for all of the sites, a wet deposition value and corresponding precipitation

value must be known. The wet deposition data for the Río Salado Weather Station was

for the years 1992 to 2001; therefore, precipitation data for this time period only was

employed. As shown in Table A.4 the precipitation amount for these years was

somewhat higher than the average for the entire time period that the station has operated

and the time period represented by the GIS map, already discussed above in Section 2.3.2.

	Yearly Precipitation (mm)	Years
Entire period of weather station operation	229[a]	1989-2004
GIS Precipitation Map value for Site 3	230[b]	1961-1990
Time period of Cl$^-$ deposition data	248[a]	1992-2001

Table A.4. Comparison of precipitation values for Río Salado Weather Station # 44 and Site 3 for various time periods. "Precipitation" column footnotes refer to the source for that data, as listed below.
a. Salado Station 2005
b. Precipitation Map 2004

The scaled wet deposition value of 38.5 mg m^{-2} yr^{-1}, as shown in Table A.3, was

also used to determine the slope for the transect. Using the precipitation value for the

length of the chloride data of 248 mm and the scaled wet deposition value in equation 16

results in a slope of 0.099 mg cm^{-1}. This slope value is similar to the one obtained above

in Figure A.7 for wet deposition of 0.0926 mg m^{-2} mm^{-1} which converts to 0.0592 mg cm^{-1}. The slope from the graph is approximately two fold lower than the slope calculated above. This is possibly the result of there being a different trend of chloride deposition with precipitation for low rainfall amounts then there is for high rainfall amounts. The determination of this exact relationship is outside the scope of this study. The use of the average annual precipitation and long-term average chloride deposition in the equation 16 is considered to be the best estimate for the determination of the slope value. This slope value and the equation 16 was then used, along with the precipitation value for each site, to determine the wet deposition value for each site. The dry deposition value from the Río Salado Weather Station was used for all of the sites, as previously mentioned. These values were then summed to determine the total chloride deposition for each site, as shown in Table A.5. As expected, this method results in low chloride-deposition values for the sites at lower elevations and higher chloride deposition values for the sites at higher elevations.

Site #	Elevation (m)	Average Annual Precipitation (mm)	Wet Chloride Deposition (mg m^{-2} yr^{-1})	Dry Chloride Deposition (mg m^{-2} yr^{-1})	Total Chloride Deposition (mg m^{-2} yr^{-1})
1	1,590	231	35.7	21.5	57.2
2	1,470	235	36.4	21.5	57.9
3	1,500	230	35.6	21.5	57.1
4	1,900	302	46.7	21.5	68.2
5	1,900	306	47.3	21.5	68.8
6	1,560	230	35.6	21.5	57.1
7	1,930	306	47.3	21.5	68.9
8	2,040	308	47.6	21.5	69.2
9	2,050	316	48.9	21.5	70.4
10	2,300	336	52.0	21.5	73.5
11	2,380	327	50.6	21.5	72.1

Table A.5. Chloride deposition values for each study site. Wet deposition values calculated using the precipitation value of the site and a slope of 0.099 mg cm^{-1}, as described above. Dry deposition value from dry collector at Río Salado site, scaled to a total chloride deposition of 60 mg m^{-2} yr^{-1}. Total chloride deposition is the sum of the

wet and dry chloride deposition.

A.13. Conclusion

The bulk chloride collector is most likely the best overall choice for determining total chloride deposition. This collector does not underestimate the dry deposition, unlike the wet/dry collector. It also does not overestimate the total deposition as the Reheis-type collector does. The downside to this collector is that dry and wet deposition cannot be separately determined. If the ratio of dry to wet deposition is known for the area, than this can be determined from the bulk collector.

Both bulk collectors at the Río Salado and Deep Well Weather Stations have similar trends both monthly and cumulatively. This is also true for both sets of wet/dry collectors. This demonstrates a good reproducibility within collection methods. There are clearly large background chloride concentration uncertainties associated with the column chloride-deposition data. Even given the imperfections of the data, we conclude that the bulk collector generally represents the rate of chloride deposition that infiltrates into the subsurface.

DATA FROM DRILL SITES

Site 1

Depth (m)	Water Potential (MPa)	Osmotic Potential (MPa)
0.15	-0.05	-0.09
0.46	-3.3	-0.17
1.07	-7.5	-0.27
1.69	-6.4	-0.38
2.03	-6.8	-0.79
2.37	-8.0	-0.87
2.71	-7.1	-1.3
3.05	-6.2	-1.5
3.39	-8.2	-1.9
3.73	-6.6	-1.2
4.06	-6.7	-1.0
4.63	-5.9	-1.3
5.32	-6.3	-0.91
5.67	-5.3	-1.0
5.79	-6.2	-0.96
5.91	-6.2	-0.91
6.04	-6.6	-1.0
6.25	-6.5	-1.0
6.55	-6.4	-0.94
7.01	-6.8	-0.15
7.51	-5.4	-0.29
7.89	-5.8	-0.32
8.23	-5.4	-0.48
8.51	-6.1	-0.76
8.71	-6.1	-0.93
8.94	-6.5	-1.0

Table B.1. Water and osmotic potential measurements for Site 1. Depth value is the midpoint of depth interval the measurement represents. Osmotic potential was calculated from the electrical conductivity of the soil leachate

Depth (m)	Gravimetric Water Content (%)	Chloride (mg/kg ds)	Chloride (mg/L pw)	Bromide (mg/L pw)	Nitrate (mg/L pw)	Nitrite (mg/L pw)
0.15	6.6	1.0	15.5	ND	3.7	12.2
0.46	4.2	1.0	23.9	ND	ND	ND
1.07	3.4	1.8	51.4	ND	8.0	2.6
1.69	5.4	34.4	640.0	8.0	ND	ND
2.03	4.0	72.1	1801.6	20.9	ND	ND
2.37	3.5	89.0	2523.9	33.7	ND	ND
2.71	3.2	92.2	2857.8	31.4	ND	ND
3.05	4.3	95.0	2207.4	27.9	ND	ND
3.39	2.8	66.1	2350.6	25.1	ND	ND
3.73	3.8	90.3	2380.5	27.3	ND	ND
4.06	4.7	114.3	2420.5	30.8	ND	ND
4.61	4.4	115.1	2635.9	31.7	ND	ND
5.35	4.1	92.9	2259.6	28.5	ND	ND
5.85	4.7	126.3	2704.4	34.1	ND	ND
6.26	4.1	97.3	2363.3	30.9	ND	ND
6.90	3.2	79.3	2479.7	29.0	ND	ND
7.66	4.8	109.1	2291.7	28.2	ND	ND
8.36	4.3	97.1	2264.2	29.4	ND	ND
8.86	4.6	104.6	2279.0	29.2	ND	ND

Table B.2. Soil anions and gravimetric water content measurements for Site 1. Depth value is the midpoint of depth interval the measurement represents. ds = dry soil, pw = pore water, ND = non-detect (concentration level below the detection limit of 0.1 mg/L)

Depth (m)	Source	Bulk Density (g/g)	Average Bulk Density (g/g)
0.23	Core	1.63	1.67
		1.71	
1.95		1.48	1.58
		1.68	
3.34		1.68	1.72
		1.75	
5.15		1.68	1.67
		1.66	
5.70		1.77	1.78
		1.80	
6.17		1.92	1.79
		1.66	
8.71		1.80	1.79
		1.79	
0.09	Pit	1.77	1.77
		1.76	
0.34		1.35	1.38
		1.41	
1.02		1.67	1.61
		1.55	
1.71		1.76	1.69
		1.63	
2.22		1.38	1.34
		1.29	
2.98		1.66	1.61
		1.56	

Table B.3. Bulk density measurements from soil core and pit for Site 1. Two measurements were taken for each depth and then averaged. Depth value is the midpoint of depth interval the measurement represents.

Depth (m)	Sand (% weight)	Silt (% weight)	Clay (% weight)	Texture
0.23	82.8	12.2	5.0	loamy sand
1.95	72.8	19.8	7.4	sandy loam
7.38	80.5	11.1	8.4	loamy sand

Table B.4. Particle size analysis for Site 1. The textural classes were determined based on the USDA textural triangle (Soil Survey Staff 1999). Depth value is the midpoint of depth interval the measurement represents.

Depth (m)	Calcium Carbonate (% weight)
0.22	15.2
2.12	8.70
5.85	36.5
6.48	18.2
7.97	33.5
9.00	16.3

Table B.5. Calcium carbonate content measurements for Site 1. Depth value is the midpoint of depth interval the measurement represents.

Site 2

Depth (m)	Water Potential (MPa)	Osmotic Potential (MPa)
0.11	-0.13	-0.15
0.33	-0.18	-0.15
0.54	-5.4	-0.29
0.76	-6.8	-0.29
0.98	-8.8	-0.32
1.20	-7.7	-0.32
1.67	-8.2	-0.48
2.27	-8.9	-0.76
2.59	-8.9	-0.76
2.82	-8.6	-0.93
3.01	-6.7	-1.0
3.16	-7.7	-1.0
3.37	-7.8	-1.5
3.59	-7.7	-1.5
3.97	-8.5	-1.2
4.41	-7.6	-1.3
4.57	-6.5	-1.3
4.67	-6.9	-1.9
4.86	-6.2	-1.9
5.19	-6.9	-1.6
5.72	-7.6	-1.4
6.14	-7.7	-2.9
6.38	-7.2	-2.9
6.55	-6.1	-2.4
6.71	-6.7	-2.4
6.97	-6.2	-2.1
7.28	-6.1	-2.0
7.43	-5.1	-2.0

Table B.6. Water and osmotic potential measurements of Site 2. Depth value is the midpoint of depth interval the measurement represents. Osmotic potential was calculated from the electrical conductivity of the soil leachate

Depth (m)	Gravimetric Water Content (%)	Chloride (mg/kg ds)	Chloride (mg/L pw)	Bromide (mg/L pw)	Nitrate (mg/L pw)	Nitrite (mg/L pw)
0.22	5.5	0.9	16.8	ND	31.9	ND
0.65	2.7	0.9	32.5	ND	68.2	ND
1.09	2.4	0.9	36.0	ND	28.8	ND
1.49	2.8	17.5	624.1	8.4	ND	ND
1.83	2.2	18.1	835.2	24.2	ND	ND
2.82	3.2	106.3	3356.9	40.3	ND	ND
3.12	5.9	219.4	3737.3	39.3	ND	ND
3.48	3.7	250.0	6748.8	42.6	ND	ND
3.92	2.3	93.9	4030.5	44.0	ND	ND
4.35	3.4	102.8	3037.3	41.4	ND	ND
4.76	3.3	149.1	4488.2	44.9	ND	ND
5.14	3.4	152.8	4516.5	46.8	ND	ND
5.52	3.3	143.1	4296.1	47.4	ND	ND
5.91	3.1	119.5	3793.0	39.0	ND	ND
6.25	2.7	108.2	3949.8	42.8	17.4	ND
6.55	3.7	139.7	3724.9	39.6	ND	ND
7.16	3.4	127.9	3761.4	42.4	20.4	ND

Table B.7. Soil anions and gravimetric water content measurements for Site 2. Depth value is the midpoint of depth interval the measurement represents. ds = dry soil, pw = pore water, ND = non-detect (concentration level below the detection limit of 0.1 mg/L)

Depth (m)	Bulk Density (g/g)	Average Bulk Density (g/g)
1.85	1.8	1.7
	1.7	
3.16	1.5	1.5
	1.4	
4.86	1.5	1.6
	1.6	

Table B.8. Bulk density measurements from soil core for Site 2. Two measurements were taken for each depth and then averaged. Depth value is the midpoint of depth interval the measurement represents.

Depth (m)	Organic (% weight)	Sand (% weight)	Silt (% weight)	Clay (% weight)	Texture
0.326	1.5	73.5	20.8	5.6	sandy loam
0.326	1.5	75.9	18.9	5.2	loamy sand
3.59	1.7	67.6	24.1	8.3	sandy loam
6.71	1.4	82.1	9.5	8.3	loamy sand

Table B.9. Particle size analysis for Site 2. The textural classes were determined based on the USDA textural triangle (Soil Survey Staff 1999). Depth value is the midpoint of depth interval the measurement represents.

Depth (m)	Calcium Carbonate (% weight)
0.33	4.4
1.20	7.6
3.00	7.9
6.55	7.5
7.43	24.2

Table B.10. Calcium carbonate content measurements for Site 2. Depth value is the midpoint of depth interval the measurement represents.

Site 3

Depth (m)	Water Potential (MPa)	Osmotic Potential (MPa)
0.10	-0.21	-0.11
0.30	-0.31	-0.11
0.51	-4.3	-0.12
0.69	-0.28	-0.12
0.84	-0.25	-0.10
0.99	-3.7	-0.10
1.14	-7.1	-0.35
1.30	-8.9	-0.35
1.45	-8.7	-1.5
1.63	-7.0	-1.5
1.83	-6.9	-4.6
2.03	-7.1	-4.6
2.24	-7.0	-1.0
2.44	-7.5	-1.0
2.64	-6.1	-1.2
2.84	-5.8	-1.2
3.00	-6.2	-1.2
3.15	-6.3	-1.2
3.35	-6.3	-1.7
3.56	-6.0	-1.7
3.76	-7.2	-1.1
3.96	-6.6	-1.1
4.17	-6.6	-1.5
4.37	-6.5	-1.5
4.52	-7.2	-0.93
4.68	-6.5	-0.93
4.90	-6.1	-0.93
5.12	-6.7	-0.93
5.33	-7.2	-0.83
5.55	-7.0	-0.83
5.77	-5.5	-0.83
5.99	-8.1	-0.83
6.17	-7.8	-0.59
6.32	-3.1	-0.59
6.48	-3.7	-0.59

6.63	-3.1	-0.59
6.78	-2.7	-0.40
6.93	-2.9	-0.40
7.09	-3.8	-0.40
7.24	-3.0	-0.40
7.39	-3.5	-0.39
7.71	-2.7	-0.39
7.85	-2.6	-0.39
8.00	-3.2	-0.39
8.15	-3.5	-0.59
8.31	-3.0	-0.59
8.46	-2.5	-0.59
8.61	-2.5	-0.59
8.76	-3.2	-0.59

Table B.11. Water and osmotic potential measurements for Site 3. Depth value is the midpoint of depth interval the measurement represents. Osmotic potential was calculated from the electrical conductivity of the soil leachate

Depth (m)	Gravimetric Water Content (%)	Chloride (mg/kg ds)	Chloride (mg/L pw)	Bromide (mg/L pw)	Nitrate (mg/L pw)	Nitrite (mg/L pw)
0.20	8.1	1.0	12.2	ND	43.8	6.3
0.51	5.1	0.9	17.5	ND	71.8	ND
0.69	7.7	1.0	13.5	ND	17.6	1.5
0.91	6.9	1.0	14.8	ND	64.4	ND
1.22	5.1	51.1	1006.9	11.8	15.5	ND
1.55	4.0	128.2	3166.2	35.2	ND	ND
1.93	1.0	143.9	14686.8	137.7	ND	ND
2.34	4.0	169.9	4301.2	42.2	ND	ND
2.74	4.9	234.5	4741.1	43.6	ND	ND
3.10	4.0	199.3	4936.4	45.9	ND	ND
3.45	3.4	163.4	4850.3	44.6	ND	ND
3.86	2.5	109.8	4345.2	42.7	ND	ND
4.27	2.8	138.2	4990.2	48.0	ND	ND
4.80	3.0	95.5	3223.8	36.2	ND	ND
5.55	2.5	57.7	2329.2	22.5	82.6	4.5
6.03	11.3	106.6	945.1	8.6	27.5	0.0
6.71	18.7	211.3	1130.5	10.3	38.8	ND
7.49	13.7	131.7	963.9	9.0	22.9	ND
8.04	7.0	67.9	969.3	9.1	15.3	ND

Table B.12. Soil anions and gravimetric water content measurements for Site 3. Depth value is the midpoint of depth interval the measurement represents. ds = dry soil, pw = pore water, ND = non-detect (concentration level below the detection limit of 0.1 mg/L)

Depth (m)	Bulk Density (g/g)	Average Bulk Density (g/g)
0.30	1.66	1.66
	1.67	
0.51	1.34	1.53
	1.73	
3.35	1.57	1.58
	1.60	
5.55	1.62	1.68
	1.74	
7.71	1.94	2.04
	2.15	

Table B.13. Bulk density measurements from soil core for Site 3. Two measurements were taken for each depth and then averaged. Depth value is the midpoint of depth interval the measurement represents.

Depth (m)	Organic (% weight)	Sand (% weight)	Silt (% weight)	Clay (% weight)	Texture
0.10	2.5	69.0	19.4	11.6	sandy loam
4.37	1.3	83.1	11.7	5.3	loamy sand
5.55	1.0	91.4	5.9	2.7	sand
6.93	6.3	9.5	39.1	51.4	clay
8.30	3.9	5.1	73.1	21.8	silty loam

Table B.14. Particle size analysis for Site 3. The textural classes were determined based on the USDA textural triangle (Soil Survey Staff 1999). Depth value is the midpoint of depth interval the measurement represents.

Depth (m)	Calcium Carbonate (% weight)
0.51	49.9
1.14	45.7
4.17	7.5
7.71	6.5

Table B.15. Calcium carbonate content measurements for Site 3. Depth value is the midpoint of depth interval the measurement represents.

Infiltrometer	Run	Calculated Ksat (cm/hr)	Alpha
b	1,2	1.02	0.16
	2,3	7.54	0.33
	3,1	4.80	0.26
a	1,2	0.27	0.11
	2,3	3.85	0.33
	3,1	2.16	0.24

Table B.16. Calculated saturated hydraulic conductivity values from infiltrometer measurements for Site 3. Two infiltrometer measurements are necessary to calculate one saturated hydraulic conductivity (Ksat) value. Surface soil was sandy loam. Alpha is a Van Genuchten parameter.

Site 4

Depth (m)	Water Potential (MPa)	Osmotic Potential (MPa)
0.13	-0.09	-0.06
0.38	-0.76	-0.11
0.64	-9.6	-0.23
0.89	-10.3	-0.35
1.14	-8.4	-0.49
1.40	-6.7	-0.45
1.65	-6.1	-0.35
1.91	-6.9	-0.33
2.16	-5.4	-0.37
2.41	-4.8	-0.46
2.92	-3.5	-0.45
3.12	-2.4	-0.34
3.94	-2.2	-0.34
4.09	-2.4	-0.30
4.24	-1.8	-0.30
4.39	-2.5	-0.29
4.52	-2.1	-0.29
4.65	-1.6	-0.29
4.80	-1.7	-0.29
4.95	-1.9	-0.34
5.11	-2.2	-0.34
5.26	-2.4	-0.34
5.41	-1.3	-0.34
5.56	-1.2	-0.32
5.72	-1.1	-0.32
6.07	-1.7	-0.32
6.17	-1.6	-0.45
6.93	-2.2	-0.45
7.09	-2.2	-0.45
7.24	-2.8	-0.28
7.39	-3.8	-0.28
7.54	-4.3	-0.28
7.73	-2.8	-0.22
7.95	-1.2	-0.22
8.16	-1.0	-0.22
8.38	-1.7	-0.22
8.60	-3.0	-0.21
8.82	-2.7	-0.21
9.04	-2.6	-0.21

Table B.17. Water and osmotic potential measurements for Site 4. Depth value is the midpoint of depth interval the measurement represents. Osmotic potential was calculated from the electrical conductivity of the soil leachate.

Depth (m)	Gravimetric Water Content (%)	Chloride (mg/kg ds)	Chloride (mg/L pw)	Bromide (mg/L pw)	Nitrate (mg/L pw)	Nitrite (mg/L pw)
0.13	18.4	1.1	1.0	ND	3.4	ND
0.38	14.3	1.9	13.0	ND	229.5	ND
0.64	6.9	3.9	56.2	ND	133.0	ND
0.89	6.5	31.8	492.9	5.1	100.0	ND
1.14	6.6	66.1	1003.5	10.6	60.8	ND
1.40	7.2	73.3	1021.3	10.6	86.2	ND
1.65	8.5	81.2	955.7	9.3	17.1	ND
1.91	10.6	87.4	820.7	7.5	7.1	ND
2.22	8.2	72.0	880.5	7.5	17.6	ND
2.60	8.2	73.7	904.1	7.9	21.4	ND
3.06	5.7	43.2	761.8	6.0	28.3	ND
3.71	5.5	41.0	746.0	6.1	17.0	ND
4.28	8.6	76.1	888.3	7.2	6.3	ND
4.64	7.2	65.6	912.1	7.4	15.9	ND
5.17	5.8	50.0	862.1	7.6	1.7	ND
5.79	15.0	125.9	837.9	8.2	10.4	ND
6.12	5.8	68.6	1185.8	10.9	11.4	ND
7.01	6.1	40.1	658.2	6.1	15.4	ND
7.58	8.1	35.0	434.4	4.3	7.3	ND
8.38	6.9	26.4	381.8	3.3	1.4	ND

Table B.18. Soil anions and gravimetric water content measurements for Site 4. Depth value is the midpoint of depth interval the measurement represents. ds = dry soil, pw = pore water, ND = non-detect (concentration level below the detection limit of 0.1 mg/L)

Depth (m)	Bulk Density (g/g)	Average Bulk Density (g/g)
1.14	1.77	1.60
	1.43	
2.41	1.54	1.57
	1.60	
4.80	1.76	1.74
	1.73	
7.95	2.00	1.96
	1.91	

Table B.19. Bulk density measurements from the soil core for Site 4. Two measurements were taken for each depth and then averaged. Depth value is the midpoint of depth interval the measurement represents.

Depth (m)	Organic (% weight)	Sand (% weight)	Silt (% weight)	Clay (% weight)	Texture
0.13	4.3	64.8	17.1	18.1	sandy loam
0.89	2.2	63.7	20.9	15.4	sandy loam
0.89	2.5	63.9	20.2	15.9	sandy loam
1.91	2.9	76.9	17.8	5.4	loamy sand
3.50	2.0	83.7	8.6	7.6	loamy sand
5.26	1.4	87.2	6.6	6.3	loamy sand
7.24	2.1	84.3	10.6	5.1	loamy sand

Table B.20. Particle size analysis for Site 4. The textural classes were determined based on the USDA textural triangle (Soil Survey Staff 1999). Depth value is the midpoint of depth interval the measurement represents.

Depth (m)	Calcium Carbonate (% weight)
0.89	14.7
3.12	2.6
4.8	9.4
5.41	42.4
7.39	3.5
8.38	28.1

Table B.21. Calcium carbonate content measurements for Site 4. Depth value is the midpoint of depth interval the measurement represents.

Site 5

Depth (m)	Water Potential (MPa)	Osmotic Potential (MPa)
0.10	-0.39	-0.06
0.29	-3.2	-0.06
0.48	-4.8	-0.08
0.67	-7.4	-0.08
0.86	-7.4	-0.12
1.05	-7.4	-0.12
1.24	-5.5	-0.18
1.43	-5.4	-0.18
1.60	-5.9	-0.21
1.75	-3.9	-0.21
1.91	-3.6	-0.16
2.06	-3.0	-0.16
2.25	-5.3	-0.25
2.48	-3.5	-0.23
2.67	-2.9	-0.23
2.82	-2.6	-0.31
2.97	-2.7	-0.31
3.18	-2.8	-0.31
3.38	-2.6	-0.38
3.63	-2.6	-0.38
3.99	-2.2	-0.14
4.24	-1.1	-0.14
4.39	-2.7	-0.14
4.52	-1.2	-0.14
4.65	-0.56	-0.15
4.80	-0.85	-0.15
4.95	-1.0	-0.16
5.11	-0.68	-0.16
5.26	-1.1	-0.16

Table B.22. Water and osmotic potential measurements for Site 5. Depth value is the midpoint of depth interval the measurement represents. Osmotic potential was calculated from the electrical conductivity of the soil leachate

Depth (m)	Gravimetric Water Content (%)	Chloride (mg/kg ds)	Chloride (mg/L pw)	Bromide (mg/L pw)	Nitrate (mg/L pw)	Nitrite (mg/L pw)
0.19	9.9	1.0	10.0	ND	ND	ND
0.57	7.9	1.0	12.4	ND	ND	ND
0.95	8.9	1.0	11.5	ND	24.1	ND
1.33	7.2	2.5	34.7	ND	5.6	ND
1.68	6.8	4.4	64.8	1.5	ND	ND
1.98	7.4	5.5	74.4	1.2	ND	ND
2.29	4.7	3.7	78.3	2.2	ND	ND
2.59	4.5	3.0	66.8	ND	ND	ND
2.90	3.5	2.2	63.1	ND	ND	ND
3.18	3.4	2.9	85.4	ND	ND	ND
3.59	3.4	4.7	139.4	ND	ND	ND
4.10	8.7	8.0	92.3	1.5	ND	ND
4.45	9.5	9.7	101.7	1.4	ND	ND
4.72	8.9	12.4	138.9	1.7	1.8	ND
5.03	9.0	15.0	166.4	2.0	2.0	ND

Table B.23. Soil anions and gravimetric water content measurements for Site 5. Depth value is the midpoint of depth interval the measurement represents. ds = dry soil, pw = pore water, ND = non-detect (concentration level below the detection limit of 0.1 mg/L)

Depth (m)	Source	Bulk Density (g/g)	Average Bulk Density (g/g)
0.19	Pit	1.35	1.44
		1.53	
1.64		1.77	1.62
		1.46	
0.85		1.46	1.45
		1.43	
0.046	Core	1.47	1.48
		1.49	
1.60		1.50	1.55
		1.61	
4.65		1.66	1.63
		1.60	

Table B.24. Bulk density measurements from soil core and pit for Site 5. Two measurements were taken for each depth and then averaged. Depth value is the midpoint of depth interval the measurement represents.

Depth (m)	Organic (% weight)	Sand (% weight)	Silt (% weight)	Clay (% weight)	Texture
0.29	4.1	56.9	21.3	21.8	sandy clay loam
0.86	3.9	57.0	12.2	30.8	sandy clay loam
1.76	1.8	64.4	19.1	16.6	sandy loam
2.82	0.9	86.6	7.5	5.9	loamy sand
4.52	1.5	56.6	25.6	17.7	sandy loam
4.52	1.8	59.3	23.8	17.0	sandy loam

Table B.25. Particle size analysis for Site 5. The textural classes were determined based on the USDA textural triangle (Soil Survey Staff 1999). Depth value is the midpoint of depth interval the measurement represents.

Depth (m)	Calcium Carbonate (% weight)
0.86	19.8
2.67	49.6
4.95	25.9

Table B.26. Calcium carbonate content measurements for Site 5. Depth value is the midpoint of depth interval the measurement represents.

Infiltrometer	Run	Calculated Ksat (cm/hr)	Alpha
b	1,2	0.16	0.07
	2,3	0.28	0.10
	3,1	0.23	0.08
a	1,2	0.52	0.07
	2,3	1.35	0.18
	3,1	0.98	0.12

Table B.27. Calculated saturated hydraulic conductivity values from infiltrometer measurements for Site 5. Two infiltrometer measurements are necessary to calculate one saturated hydraulic conductivity (Ksat) value. Surface soil was sandy clay loam. Alpha is a Van Genuchten parameter.

Site 6

Depth (m)	Water Potential (MPa)	Osmotic Potential (MPa)
0.13	-0.43	-0.59
0.38	-1.3	-1.5
0.64	-5.0	-0.85
0.89	-12.3	-1.6
1.14	-14.6	-1.6
1.40	-9.2	-1.1
1.61	-8.5	-0.96
1.78	-8.3	-1.6
1.95	-8.2	-1.8
2.12	-7.8	-1.8
2.29	-8.2	-1.9
2.46	-7.5	-1.5
2.63	-8.0	-1.5
2.79	-8.8	-2.3
3.19	-8.8	-1.1
3.81	-8.6	-2.9
4.19	-9.4	-3.3
4.42	-7.9	-2.5

Table B.28. Water and osmotic potential measurements for Site 6. Depth value is the midpoint of depth interval the measurement represents. Osmotic potential was calculated from the electrical conductivity of the soil leachate

Depth (m)	Gravimetric Water Content (%)	Chloride (mg/kg ds)	Chloride (mg/L pw)	Bromide (mg/L pw)	Nitrate (mg/L pw)	Nitrite (mg/L pw)
0.13	13.9	27.5	198.1	ND	ND	ND
0.38	4.8	12.5	260.2	ND	10.6	ND
0.64	4.2	14.2	335.8	ND	ND	ND
0.89	5.5	99.6	1798.0	ND	33.3	ND
1.14	5.4	86.6	1610.0	ND	164.4	9.9
1.40	6.8	93.1	1377.7	ND	440.9	ND
1.61	6.7	96.7	1447.6	ND	605.6	4.4
1.78	6.0	75.6	1253.8	ND	675.1	5.9
1.95	7.0	72.6	1040.8	ND	638.3	2.6
2.12	7.0	61.0	874.0	ND	573.6	4.1
2.29	5.8	46.5	808.3	8.2	517.3	3.9
2.46	7.4	47.2	634.8	ND	385.9	ND
2.63	7.8	65.0	837.0	ND	538.1	3.2
2.79	3.7	29.5	794.9	ND	550.3	ND
2.96	5.5	40.5	739.6	ND	504.3	ND
3.12	2.8	40.9	1438.9	ND	535.4	ND
4.19	1.7	74.2	4257.7	ND	474.3	ND
4.42	3.4	60.1	1781.4	ND	445.3	ND

Table B.29. Soil anions and gravimetric water content measurements for Site 6. Depth value is the midpoint of depth interval the measurement represents. ds = dry soil, pw = pore water, ND = non-detect (concentration level below the detection limit of 0.1 mg/L)

Depth (m)	Bulk Density (g/g)	Average Bulk Density (g/g)
0.89	1.37	1.37
	1.38	

Table B.30. Bulk density measurements from the soil core for Site 6. Two measurements were taken for each depth and then averaged. Depth value is the midpoint of depth interval the measurement represents.

Depth (m)	Organic (% weight)	Sand (% weight)	Silt (% weight)	Clay (% weight)	Texture
0.38	1.4	73.1	16.5	10.4	sandy loam
1.95	1.5	44.1	37.5	18.4	loam
3.81	1.3	78.6	11.8	9.5	sandy loam

Table B.31. Particle size analysis for Site 6. The textural classes were determined based on the USDA textural triangle (Soil Survey Staff 1999). Depth value is the midpoint of depth interval the measurement represents.

Depth (m)	Calcium Carbonate (% weight)
1.14	7.9
2.79	9.7

Table B.32. Calcium carbonate content measurements for Site 6. Depth value is the midpoint of depth interval the measurement represents.

Site 7

Depth (m)	Water Potential (MPa)	Osmotic Potential (MPa)
0.11	-0.12	-0.75
0.32	-2.4	-0.18
0.53	-4.7	-0.09
0.75	-5.6	-0.08
1.04	-5.8	-0.28
1.37	-4.0	-0.28
1.83	-4.0	-0.89
2.44	-3.8	-0.89
2.82	-3.6	-0.53
2.97	-3.0	-0.53
3.11	-2.2	-0.31
3.42	-2.4	-0.31
3.92	-2.2	-0.23
4.27	-2.0	-0.23
4.47	-1.5	-0.30
4.72	-2.1	-0.30
5.03	-1.4	-0.29
5.33	-1.8	-0.24
5.56	-2.0	-0.24
5.72	-1.7	-0.23
5.87	-1.4	-0.23
6.02	-1.1	-0.23
6.17	-1.1	-0.18
6.45	-1.4	-0.18
6.86	-1.2	-0.18
7.14	-1.3	-0.17
7.29	-1.5	-0.17
7.44	-1.4	-0.17
7.57	-1.9	-0.18
7.72	-0.97	-0.18
7.91	-0.92	-0.18
8.10	-1.6	-0.20
8.29	-1.6	-0.20
8.48	-1.2	-0.14
8.67	-1.4	-0.14
8.86	-0.80	-0.16
9.05	-1.8	-0.16

Table B.33. Water and osmotic potential measurements for Site 7. Depth value is the midpoint of depth interval the measurement represents. Osmotic potential was calculated from the electrical conductivity of the soil leachate

Depth (m)	Gravimetric Water Content (%)	Chloride (mg/kg ds)	Chloride (mg/L pw)	Bromide (mg/L pw)	Nitrate (mg/L pw)	Nitrite (mg/L pw)
0.11	6.4	1.0	15.6	ND	5.1	ND
0.32	4.6	2.1	45.9	ND	18.6	ND
0.53	4.9	2.1	41.8	ND	32.7	ND
0.75	4.6	1.6	35.5	ND	9.2	ND
1.07	5.8	12.5	213.3	2.1	60.7	ND
2.02	7.2	63.6	889.3	10.2	3.6	ND
2.90	5.0	39.4	793.3	10.1	5.0	ND
3.30	5.2	17.8	342.2	4.9	ND	ND
3.93	5.7	17.3	305.3	4.1	ND	ND
4.44	4.2	15.8	377.0	4.4	ND	ND
4.72	4.1	15.2	370.2	5.0	ND	ND
5.03	4.4	15.8	363.1	4.7	ND	ND
5.41	4.7	14.5	307.7	4.4	ND	ND
5.72	5.4	18.0	332.4	4.2	ND	ND
5.87	7.2	25.0	346.2	4.0	ND	ND
6.55	7.3	31.1	425.3	5.2	3.3	ND
7.71	8.5	40.3	472.9	5.9	ND	ND
8.19	6.4	25.6	397.5	5.4	ND	ND
8.57	12.1	45.8	377.5	4.9	5.2	ND
8.95	8.2	28.7	350.3	4.6	ND	ND

Table B.34. Soil anions and gravimetric water content measurements for Site 7. Depth value is the midpoint of depth interval the measurement represents. ds = dry soil, pw = pore water, ND = non-detect (concentration level below the detection limit of 0.1 mg/L)

Depth (m)	Bulk Density (g/g)	Average Bulk Density (g/g)
0.11	1.49	1.52
	1.56	
1.83	1.73	1.73
5.33	1.62	1.65
	1.68	
6.45	2.25	2.30
	2.34	
7.72	1.54	1.47
	1.39	

Table B.35. Bulk density measurements from the soil core Site 7. Two measurements were taken for each depth and then averaged. Only one useable ped was available for the 1.83 depth. Depth value is the midpoint of depth interval the measurement represents.

Depth (m)	Organic (% weight)	Sand (% weight)	Silt (% weight)	Clay (% weight)	Texture
0.32	1.7	78.8	13.0	8.3	loamy sand
1.04	1.5	82.4	7.3	10.3	loamy sand
3.42	0.93	92.3	2.8	4.9	sand
5.56	0.93	89.8	5.0	5.1	sand
8.10	1.1	76.0	17.1	6.9	sandy loam

Table B.36. Particle size analysis for Site 7. The textural classes were determined based on the USDA textural triangle (Soil Survey Staff 1999). Depth value is the midpoint of depth interval the measurement represents.

Depth (m)	Calcium Carbonate (% weight)
2.82	30.4
5.32	30.0
7.14	6.7
8.48	12.0

Table B.37. Calcium carbonate content measurements for Site 7. Depth value is the midpoint of depth interval the measurement represents.

Site 8

Depth (m)	Water Potential (MPa)	Osmotic Potential (MPa)
0.08	-0.10	-0.09
0.10	-0.20	-0.09
0.23	-2.1	-0.12
0.38	-2.1	-0.12
0.64	-3.1	-0.21
0.66	-4.0	-0.21
0.89	-5.5	-0.31
1.14	-5.4	-0.31
1.27	-4.9	-0.18
1.40	-4.2	-0.17
1.65	-3.0	-0.24
1.91	-2.4	-0.20
2.16	-2.1	-0.25
2.41	-2.4	-0.21
2.67	-2.0	-0.21
2.92	-2.5	-0.21
3.20	-3.3	-0.38
3.51	-2.5	-0.32
3.81	-3.6	-0.24
4.11	-3.9	-0.22
4.42	-3.2	-0.19
4.66	-2.7	-0.28
4.85	-2.4	-0.19
5.03	-2.5	-0.19
5.21	-2.7	-0.17
5.39	-2.6	-0.17

Table B.38. Water and osmotic potential measurements for Site 8. Depth value is the midpoint of depth interval the measurement represents. Osmotic potential was calculated from the electrical conductivity of the soil leachate

Depth (m)	Gravimetric Water Content (%)	Chloride (mg/kg ds)	Chloride (mg/L pw)	Bromide (mg/L pw)	Nitrate (mg/L pw)	Nitrite (mg/L pw)
0.13	7.4	0.9	12.5	ND	28.6	ND
0.38	6.0	1.0	16.9	ND	44.5	ND
0.64	6.4	1.0	15.0	ND	9.8	ND
0.89	5.2	1.1	20.3	ND	14.6	ND
1.14	7.5	2.5	33.6	ND	2.5	ND
1.40	5.7	4.2	72.7	2.4	ND	ND
1.65	4.6	12.1	266.3	6.8	ND	ND
1.91	5.0	21.3	427.3	7.4	ND	ND
2.16	4.5	18.2	407.4	6.7	ND	ND
2.41	4.3	21.9	509.2	8.4	ND	ND
2.79	5.6	27.1	480.0	5.7	ND	ND
3.20	3.0	16.7	555.2	4.9	ND	ND
3.51	3.4	17.8	518.3	3.5	ND	ND
3.81	4.3	15.3	359.5	3.3	ND	ND
4.11	5.1	18.1	357.5	3.8	2.9	ND
4.42	5.2	9.6	184.6	3.1	10.0	ND
4.66	5.5	9.0	164.5	2.8	6.1	ND
4.94	7.2	14.3	199.4	4.0	ND	ND
5.30	5.1	9.7	191.0	3.9	ND	ND

Table B.39. Soil anions and gravimetric water content measurements for Site 8. Depth value is the midpoint of depth interval the measurement represents. ds = dry soil, pw = pore water, ND = non-detect (concentration level below the detection limit of 0.1 mg/L)

Depth (m)	Source	Bulk Density (g/g)	Average Bulk Density (g/g)
0.064		1.68	1.70
		1.72	
1.78		1.37	1.42
		1.46	
1.99	Pit	1.67	1.63
		1.59	
2.08		1.67	1.63
		1.59	
2.76		1.24	1.18
		1.13	
0.076		1.58	1.65
	Core	1.71	
1.27		1.48	1.59
		1.70	

Table B.40. Bulk density measurements from soil core and pit for Site 8. Two measurements were taken for each depth and then averaged. Depth value is the midpoint of depth interval the measurement represents.

Depth (m)	Organic (% weight)	Sand (% weight)	Silt (% weight)	Clay (% weight)	Texture
0.075	1.7	79.2	11.5	9.3	sandy loam
0.075	1.7	80.6	11.0	8.4	loamy sand
2.41	0.9	86.7	6.9	6.4	loamy sand
4.66	1.3	89.5	8.0	2.6	sand
5.21	1.0	90.6	6.1	3.3	sand

Table B.41. Particle size analysis for Site 8. The textural classes were determined based on the USDA textural triangle (Soil Survey Staff 1999). Depth value is the midpoint of depth interval the measurement represents.

Depth (m)	Calcium Carbonate (% weight)
3.5	8.97
4.85	6.37

Table B.42. Calcium carbonate content measurements for Site 8. Depth value is the midpoint of depth interval the measurement represents.

Infiltrometer	Run	Calculated Ksat (cm/hr)	Alpha
b	1,2	3.86	0.12
	2,3	5.94	0.15
	3,1	4.48	0.13
a	1,2	52.8 (outlier)	0.33
	2,3	2.33	0.12
	3,1	6.35	0.22

Table B.43. Calculated saturated hydraulic conductivity values from infiltrometer measurements for Site 8. Two infiltrometer measurements are necessary to calculate one saturated hydraulic conductivity (Ksat) value. Surface soil was loamy sand. Alpha is a Van Genuchten parameter.

Site 9

Depth (m)	Water Potential (MPa)	Osmotic Potential (MPa)
0.11	-0.09	-0.12
0.33	-1.4	-0.12
0.54	-4.4	-0.31
0.76	-5.5	-0.31
0.98	-5.2	-0.38
1.20	-4.1	-0.38
1.42	-2.5	-0.69
1.63	-1.5	-0.69
1.85	-1.8	-0.43
2.07	-1.9	-0.43
2.29	-2.2	-0.35
2.50	-2.0	-0.35
2.72	-2.7	-0.25
2.94	-2.7	-0.22
3.12	-1.9	-0.22
3.43	-1.7	-0.22
3.58	-1.9	-0.22
3.73	-1.7	-0.16
3.89	-1.2	-0.16
4.04	-0.95	-0.16
4.19	-0.92	-0.16
4.34	-1.1	-0.15
4.50	-1.6	-0.15
4.72	-0.89	-0.16
5.03	-0.86	-0.21
5.33	-0.77	-0.15
5.64	-0.85	-0.12
5.94	-0.92	-0.12
6.25	-0.78	-0.16
6.55	-0.69	-0.16
6.86	-0.79	-0.19
7.16	-0.90	-0.19
7.47	-0.93	-0.17
7.72	-0.65	-0.17
7.92	-0.69	-0.17
8.13	-0.43	-0.14
8.33	-0.84	-0.14
8.53	-0.71	-0.14
8.74	-1.1	-0.14

Table B.44. Water and osmotic potential measurements for Site 9. Depth value is the midpoint of depth interval the measurement represents. Osmotic potential was calculated from the electrical conductivity of the soil leachate

Depth (m)	Gravimetric Water Content (%)	Chloride (mg/kg ds)	Chloride (mg/L pw)	Bromide (mg/L pw)	Nitrate (mg/L pw)	Nitrite (mg/L pw)
0.22	6.5	1.0	15.5	ND	18.6	ND
0.65	6.4	14.9	233.4	3.8	46.7	ND
1.09	7.8	98.4	1262.1	18.6	17.3	ND
1.52	9.2	163.0	1773.0	24.4	1.1	ND
1.96	7.4	100.2	1359.0	18.1	1.3	ND
2.39	8.1	93.2	1143.5	14.3	1.2	ND
2.72	10.2	82.2	807.2	10.0	1.0	ND
3.09	10.2	57.6	562.0	6.9	1.1	ND
3.51	6.7	24.0	355.8	4.8	1.4	ND
3.81	7.3	15.2	206.8	2.7	1.3	ND
4.11	7.1	15.1	212.4	3.1	1.3	ND
4.42	5.8	9.2	159.0	ND	1.6	ND
4.72	5.2	3.7	71.5	ND	1.8	ND
5.03	5.2	9.0	174.1	ND	3.8	ND
5.33	5.6	3.5	62.9	ND	14.9	ND
5.79	5.1	2.8	54.7	ND	1.8	ND
6.40	4.3	2.0	45.7	ND	2.1	ND
7.01	4.0	0.9	23.2	ND	2.3	ND
7.42	4.4	1.6	36.7	ND	2.0	ND
8.03	4.8	1.1	0.0	ND	2.3	ND

Table B.45. Soil anions and gravimetric water content measurements for Site 9. Depth value is the midpoint of depth interval the measurement represents. ds = dry soil, pw = pore water, ND = non-detect (concentration level below the detection limit of 0.1 mg/L)

Depth (m)	Bulk Density (g/g)	Average Bulk Density (g/g)
0.33	1.71	1.58
	1.45	
1.63	1.58	1.59
	1.59	

Table B.46. Bulk density measurements from the soil core for Site 9. Two measurements were taken for each depth and then averaged. Depth value is the midpoint of depth interval the measurement represents.

Depth (m)	Organic (% weight)	Sand (% weight)	Silt (% weight)	Clay (% weight)	Texture
0.330	1.9	77.0	10.8	12.2	sandy loam
3.430	1.3	87.6	11.8	0.54	sand
7.920	1.1	93.9	5.5	0.54	sand

Table B.47. Particle size analysis for Site 9. The textural classes were determined based on the USDA textural triangle (Soil Survey Staff 1999). Depth value is the midpoint of depth interval the measurement represents.

Depth (m)	Calcium Carbonate (% weight)
1.85	36.0
3.58	6.0
4.19	25.0
5.33	14.2
8.33	24.9

Table B.48. Calcium carbonate content for Site 9. Depth value is the midpoint of depth interval the measurement represents.

Site 10

Depth (m)	Water Potential (MPa)	Osmotic Potential (MPa)
0.09	-0.14	-0.047
0.27	-0.01	-0.035
0.44	-0.06	-0.070
0.62	-0.81	-0.058
0.80	-0.52	-0.056
0.98	-0.46	-0.102
1.18	-0.53	-0.106
1.41	-0.72	-0.063
1.60	-1.4	-0.083
1.75	-1.8	-0.083
1.91	-2.6	-0.076
2.06	-2.3	-0.076
2.21	-2.5	-0.080
2.36	-2.4	-0.080
2.51	-2.3	-0.071
2.67	-2.0	-0.071
2.82	-1.9	bedrock
2.97	-2.5	
3.12	-2.2	
3.28	-2.2	
3.43	-2.1	
3.58	-1.9	
3.73	-2.6	
3.89	-2.3	
4.04	-2.0	
4.19	-1.9	
4.34	-1.3	
4.50	-1.0	
4.65	-0.96	
4.80	-1.4	

Table B.49. Water and osmotic potential for Site 10. Depth value is the midpoint of depth interval the measurement represents. Osmotic potential was calculated from the electrical conductivity of the soil leachate

Depth (m)	Gravimetric Water Content (%)	Chloride (mg/kg ds)	Chloride (mg/L pw)	Bromide (mg/L pw)	Nitrate (mg/L pw)	Nitrite (mg/L pw)
0.09	12.0	1.1	9.4	ND	ND	ND
0.27	9.4	1.0	10.8	ND	60.7	ND
0.44	9.4	1.1	12.1	ND	ND	ND
0.62	7.1	1.0	13.5	ND	ND	ND
0.80	5.4	0.9	17.0	ND	40.8	2.9
0.98	5.1	0.9	18.2	ND	23.6	ND
1.14	4.9	0.9	19.0	ND	5.3	ND
1.30	5.1	0.9	18.6	ND	ND	ND
1.45	5.4	1.0	18.2	ND	ND	ND
1.68	8.6	1.0	11.8	ND	ND	ND
1.98	10.3	1.7	16.2	ND	ND	ND
2.29	9.2	1.8	19.2	ND	ND	ND
2.59	9.8	1.6	15.9	ND	ND	ND
2.90	13.6	3.6	26.3	ND	ND	ND
3.20	12.3	NT	NT	NT	NT	NT
3.51	11.3	11.1	97.8	ND	ND	ND
3.81	9.9	NT	NT	NT	NT	NT
4.11	8.9	1.6	17.9	ND	ND	ND
4.42	8.1	NT	NT	NT	NT	NT
4.72	2.8	0.9	32.0	ND	ND	ND

Table B.50. Soil anions and gravimetric water content measurements for Site 10. Depth value is the midpoint of depth interval the measurement represents. ds = dry soil, pw = pore water, ND = non-detect (concentration level below the detection limit of 0.1 mg/L), NT = sample not taken since it consisted of bedrock.

Depth (m)	Bulk Density (g/g)	Average Bulk Density (g/g)
0.09	1.75	1.81
	1.87	
1.41	1.56	1.55
	1.53	
1.91	1.53	1.58
	1.64	
4.04	1.94	2.02
	2.09	

Table B.51. Bulk density measurements from the soil core for Site 10. Two measurements were taken for each depth and then averaged. Depth value is the midpoint of depth interval the measurement represents.

Depth (m)	Organic (% weight)	Sand (% weight)	Silt (% weight)	Clay (% weight)	Texture
0.27	1.4	89.6	7.2	3.2	sand
1.6	1.4	78.7	13.0	8.3	loamy sand
2.36	1.8	67.1	22.4	10.5	sandy loam
2.36	1.9	68.2	22.0	9.8	sandy loam

Table B.52. Particle size analysis for Site 10. The textural classes were determined based on the USDA textural triangle (Soil Survey Staff 1999). Depth value is the midpoint of depth interval the measurement represents.

Depth (m)	Calcium Carbonate (% weight)
2.06	0.73
2.21	1.41
2.36	0.13

Table B.53. Calcium carbonate content measurements for Site 10. Depth value is the midpoint of depth interval the measurement represents.

Infiltrometer	Run	Calculated Ksat (cm/hr)	Alpha
b	1,2	2.94	0.15
	2,3	3.26	0.16
	3,1	3.10	0.16
a	1,2	3.82	0.20

Table B.54. Calculated saturated hydraulic conductivity values from infiltrometer measurements for Site 10. Two infiltrometer measurements are necessary to calculate one saturated hydraulic conductivity (Ksat) value. Surface soil was sand. Alpha is a Van Genuchten parameter.

Site 11

Depth (m)	Water Potential (MPa)	Osmotic Potential (MPa)
0.15	-0.41	-0.18
0.46	-0.27	-0.067
0.69	-3.6	-0.12
0.84	-3.4	-0.13
0.99	-2.2	-0.10
1.14	-1.9	-0.10
1.30	-1.5	-0.11
1.45	-1.0	-0.11
1.60	-1.2	-0.12
1.75	-1.0	-0.12
1.91	-2.1	-0.11
2.06	-2.5	-0.15
2.21	-2.3	-0.16
2.36	-2.6	-0.17
2.51	-2.8	-0.16
2.67	-2.1	-0.18
2.82	-2.9	-0.16
3.00	-6.9	bedrock
3.44	-5.6	
3.88	-6.3	
4.09	-5.2	
4.31	-8.7	
4.52	-10.4	
4.70	-3.6	
4.83	-6.7	

Table B.55. Water and osmotic potential measurements for Site 11. Depth value is the midpoint of depth interval the measurement represents. Osmotic potential was calculated from the electrical conductivity of the soil leachate

Depth (m)	Gravimetric Water Content (%)	Chloride (mg/kg ds)	Chloride (mg/L pw)	Bromide (mg/L pw)	Nitrate (mg/L pw)	Nitrite (mg/L pw)
0.15	15.8	1.2	7.7	ND	ND	ND
0.46	13.3	1.6	12.2	ND	17.0	ND
0.69	15.8	16.0	101.3	ND	19.5	ND
0.84	21.6	34.1	157.9	ND	18.0	ND
1.07	28.7	68.4	238.5	1.1	ND	0.6
1.37	27.4	76.6	279.3	1.3	ND	ND
1.68	26.8	80.8	301.8	1.4	ND	ND
1.91	17.6	52.3	296.3	1.4	ND	ND
2.06	19.1	75.2	394.0	2.0	ND	ND
2.21	14.8	65.1	441.4	3.1	ND	ND
2.36	13.6	65.6	480.4	3.0	ND	ND
2.51	15.8	65.0	410.7	2.6	ND	ND
2.67	17.8	84.0	472.2	3.0	ND	ND
2.82	15.5	73.5	473.2	2.5	ND	ND
3.11	10.0	NT	NT	NT	NT	NT
3.55	10.7	NT	NT	NT	NT	NT
3.88	9.2	56.0	606.3	3.9	ND	ND
4.09	9.8	NT	NT	NT	NT	NT
4.31	8.1	NT	NT	NT	NT	NT
4.52	7.0	NT	NT	NT	NT	NT
4.75	10.2	32.2	317.0	ND	ND	ND

Table B.56. Soil anions and gravimetric water content measurements for Site 11. Depth value is the midpoint of depth interval the measurement represents. ds = dry soil, pw = pore water, ND = non-detect (concentration level below the detection limit of 0.1 mg/L), NT = sample not taken since it consisted of bedrock.

Depth (m)	Source	Bulk Density (g/g)	Average Bulk Density (g/g)
0.46	Core	1.77	1.71
		1.65	
0.69		1.31	1.32
		1.33	
1.45		1.44	1.43
		1.41	
2.06		1.89	1.89
		1.88	
2.67		1.92	1.89
		1.87	
0.19	Pit	1.51	1.49
		1.47	
0.70		1.36	1.41
		1.47	
0.83		1.49	1.48
		1.46	
1.52		1.62	1.72
		1.81	
2.22		1.61	1.58
		1.56	

Table B.57. Bulk density measurements from soil core and pit from Site 11. Two measurements were taken for each depth and then averaged. Depth value is the midpoint of depth interval the measurement represents.

Depth (m)	Organic (% weight)	Sand (% weight)	Silt (% weight)	Clay (% weight)	Texture
0.46	2.9	62.7	24.0	13.3	sandy loam
0.84	3.8	31.9	41.8	26.3	loam
1.45	3.3	24.9	60.0	15.1	silty loam
2.06	2.4	49.7	34.6	15.7	loam
2.67	2.6	21.8	64.8	13.5	silty loam

Table B.58. Particle size analysis for Site 11. The textural classes were determined based on the USDA textural triangle (Soil Survey Staff 1999). Depth value is the midpoint of depth interval the measurement represents.

Depth (m)	Calcium Carbonate (% weight)
0.84	0.21
1.14	1.51
2.82	5.44

Table B.59. Calcium carbonate content measurements for Site 11. Depth value is the midpoint of depth interval the measurement represents.